The star formation history of elliptical galaxies

Louisa A. Nolan

Doctor of Philosophy

The University of Edinburgh

2001

This thesis is my own composition except where indicated in the text.

September 22, 2002

Abstract

The results of an investigation into the star formation history of elliptical galaxies, and the subsequent implications for the still controversial issue of their formation and evolution are presented. New, high signal-to-noise data and new, non-solar metallicity models motivate the re-investigation of elliptical galaxy formation with synthetic stellar population models, which has been difficult in the past because of uncertainties in the model spectra and the effects of age-metallicity degeneracy.

Three different groups of elliptical galaxies, covering a range of redshift and nuclear activity are investigated. The rest-frame optical spectra of a population of 24 low-redshift ($z \simeq 0.2$) AGN host galaxies, together with the high-quality rest-frame ultraviolet spectra of two high-redshift ($z \simeq 1.5$) mJy radio galaxies and ultraviolet-to-optical spectra of two low-redshift ($z < 0.1$) inactive galaxies are compared with a range of simple, near-instantaneous starburst stellar population model spectra from various authors. With the benefit of non-solar metallicity models, the attempt is made to reliably determine the ages and metallicities of the stellar populations of the observed galaxies via continuum fitting.

A simultaneous test of the ability of these models to accurately reproduce the spectra of real stellar populations is also presented. This is carried out both by testing the models' ability to recover the correct ages and metallicities of two well-studied F stars and the Sun, in the regimes where these stars dominate the integrated model flux, and by investigating the quality of the continuum fits to the observed galaxy spectra.

With high-quality data, and reliable model spectra, it is possible to lift age-metallicity degeneracy, and robustly constrain the ages and metallicities of the galaxies studied. Models with stellar populations of more than one age and / or metallicity have been constructed, and this has allowed composite galaxy populations to be disentangled.

The results are consistent with the existence of two classes of elliptical galaxies, one formed at high redshift, with predominantly passive evolution, and the other formed at lower redshift, from galaxy-galaxy merging, with associated star formation. The spectroscopic determination of the stellar content of the galaxies studied has enabled their epochs of star formation to be determined, and hence their formation routes.

The constraints imposed by the reliable identification of old stellar populations at known redshift favour a Λ-dominated cosmological model, and strongly reject an Einstein-de Sitter universe.

Acknowledgements

There are many people who I would like to thank for contributing to a fantastic four years in Edinburgh. The first are my mum and dad, for transmitting their enthusiasm for science to me, and for their continued support and encouragement.

I owe my supervisor, Jim Dunlop, a huge thanks for his help, both in the production of my thesis and in preparing me for the next step. I have greatly benefitted from his clarity of thinking, which has kept me motivated and making progress in the right direction. My thanks is also due to others I have worked with and learned from, in particular, Raul Jimenez and Alan Heavens.

Things wouldn't have been the same without the unique atmosphere of R7 (with apologies to Adrian Webster). I could write several pages about the experiences I have had in that office, which have often made me laugh until it hurt, but perhaps it's best I don't. So, thanks to Helen for female moral support and a shared interest in shiny things. Thanks to James for rides in the Beast and the plants. Thanks to Michael for his wit, his rock 'n' roll charm, and his rampant heterosexuality. And thanks to Ali, for the Loudness which has kept us amused for quite literally years, for the use of his library, and for agreeing with me. Thanks also to Rob, Big Tall Will and Ignas, both for their help in preparing my thesis, and for general all-round entertainment. I may have mentioned this before, but I love you all hundreds!

Thanks also to the non-astronomers at the R.O.E. who have made my life better: Ralph, for chocolate cake and banter, Horst and John Barrow, for being fantastic at keeping my computer running properly, and Liz Gibson, for being a goddess of efficiency.

Away from the Observatory, thanks to Pam for being the best flatmate ever for over three years! And, finally, of course, I'd like to thank everyone who I have been involved with through rugby, both at Edinburgh Uni and Watsonians. Rugby has been a huge part of my life in Edinburgh, and I have had some brilliant times, and met some fantastic people; particular mention is due to Lindsey, Sarah, Heather, Genny and Kate. Thanks to all of you

for the top laughs and unforgettable moments, both on the pitch and when out enjoying the legend which is Edinburgh's nightlife.

Edinburgh: October 1997 - December 2001. It's been fantastic.

Contents

List of Figures

List of Tables

Chapter 1

Introduction

1.1 Thesis outline

This thesis is the result of an investigation into the spectral determination of the ages and metallicities of elliptical galaxies, and the subsequent implications for theories of the formation and evolution of elliptical galaxies. The simultaneous determination of the ages and metallicities of real stellar populations has been controversial in the past, with investigations using the stellar population synthesis models of different authors often producing different results. Here, therefore, as well as attempting to place robust limits on the ages and metallicities of the component stellar populations of various high- and low-redshift elliptical galaxies, the ability of the models created by different authors to convincingly reproduce real stellar population spectra is also explored. New high signal-to-noise spectral data, together with new non-solar-metallicity stellar population models, motivate a re-investigation of this subject, and make a meaningful analysis possible.

In this thesis, the results of investigations into the ages and metallicities of three different groups of elliptical galaxies are presented. In Chapter 2, the ages of the dominant stellar populations of a sample of 24, $z \sim 0.2$, host galaxies of powerful active galactic nuclei (AGN) are determined from their rest-frame optical spectra. In Chapter 3, the main sequence (MS) time evolution of the solar-metallicity stellar population models of various authors are tested, by checking their calibration against a solar spectrum. In the light of the results of this test, the ages of two high-redshift ($z \simeq 1.5$) mJy radio galaxies, LBDS 53W091 and LBDS 53W069 are investigated, using high-quality rest-frame ultraviolet (UV) spectra. Chapter 4 extends

this work to non-solar-metallicity stellar population models. The ability of the models to recover the known ages and metallicities of two F stars, and thus the potential for lifting the well-known age-metallicity degeneracy present in stellar populations is investigated. F stars such as those considered in this chapter are expected to be the dominant stars in the stellar populations of the two high-redshift radio galaxies. Therefore, the two $z \simeq 1.5$ radio galaxies are revisited in the light of the F star analysis, and robust age limits are able to be placed upon their stellar populations. Chapter 5 returns to the low-redshift regime. High-quality UV-to-optical spectra are constructed for two $z < 0.01$ inactive elliptical galaxies, NGC 3605 and NGC 5018, and are then fitted with a wide range of models in an attempt to disentangle their component stellar populations. The implications for their formation processes are then discussed. This progression from low-redshift AGN host galaxies to high-redshift radio galaxies to low-redshift inactive galaxies, with increasing data quality, corresponds to an increasing ability to differentiate between the model sets of different authors. Finally, in Chapter 6, over-all conclusions are presented, together with suggestions for further work.

In this chapter, the background which lays the foundations for this work is presented. This includes the standard model of cosmology, a review of current theories of the formation and evolution of elliptical galaxies, and a discussion of stellar population synthesis.

1.2 Cosmology

In this section, the Robertson-Walker (RW) metric (Robertson, 1935; Walker, 1936) is derived, in order to define the time-dependent scale factor R(t), and its relationship with redshift (z). The relationship between redshift, the age of the Universe and the cosmological parameters, i.e. Hubble's constant, H_0, and the density parameters, Ω_m and Ω_Λ, are then derived from the expansion dynamics of the Universe.

1.2.1 The Robertson-Walker metric

The RW metric describes the geometry of the Universe. Its initial assumptions are that the Universe is statistically homogeneous (constant density) and isotropic (the same in all directions).

Once we have assumed that the Universe is isotropic, we may simplify our geometry, by using spherical polar co-ordinates, and working at constant radius.

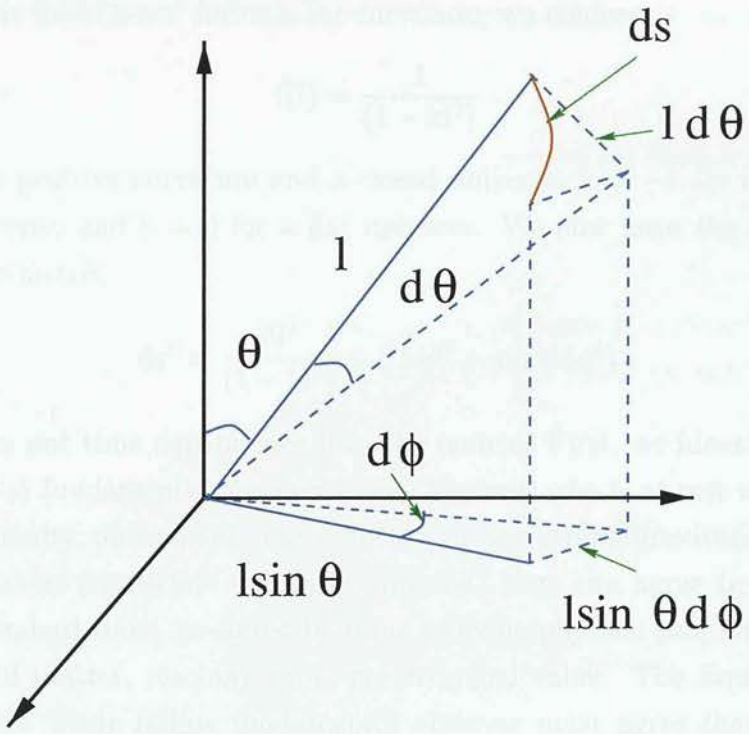

Figure 1.1: Sketch showing the geometry of a line element, ds, on the surface of a sphere, with surface area $4\pi l^2$.

By inspection of Figure 1.1, we see that the angular interval on the surface of the sphere, with l^2 = surface area / 4π, must be:

$$ds^2_{(l=const)} = l^2 d\theta^2 + l^2 \sin^2\theta d\phi^2 \tag{1.1}$$

However, we cannot assume that the geometry of space is flat, i.e. that l is the distance from the origin to the surface of the sphere, so we must include an extra term to allow for curved geometries. Hence,

$$ds^2 = f(l)dl^2 + l^2(d\theta^2 + \sin^2\theta d\phi^2) \tag{1.2}$$

so that $\sqrt{f(l)}dl$ is the proper distance between the points (l,θ,ϕ) and $(l+dl,\theta,\phi)$. Homogeneity implies that the curvature of space (whatever it is) must be the same everywhere. Therefore, in order to find out what form f(l) takes, we may reduce equation 1.2 to two dimensions, by choosing $\theta = \pi/2$. The metric on this surface is then

$$ds^2_{(\theta=\pi/2)} = f(l)dl^2 + l^2 d\phi^2 \tag{1.3}$$

with the metric tensor

$$g = \begin{pmatrix} f(l) & 0 \\ 0 & l^2 \end{pmatrix} \tag{1.4}$$

Putting this metric into Gauss' formula for curvature, we recover

$$f(l) = \frac{1}{(1 - kl^2)} \tag{1.5}$$

where $k = +1$ for positive curvature and a closed universe, $k = -1$ for negative curvature and an open universe, and $k = 0$ for a flat universe. We now have the expression for the spatial part of the metric

$$ds^2 = \frac{dl^2}{(1 - kl^2)} + l^2(d\theta^2 + \sin^2\theta d\phi^2) \tag{1.6}$$

the next step is to put time dependence into the metric. First, we identify a set of fundamental observers. A fundamental observer is any observer who is at rest with respect to the matter in their vicinity, and outside the influence of any strong gravitational fields. These fundamental observers can define a cosmic time, i.e., they can agree to synchronize their clocks at some standard time, measured by some evolving physical property of the Universe, e.g. the density of matter, reaching some pre-arranged value. The Equivalence Principle then says that each freely falling fundamental observer must agree that the proper time interval between two events, labelled in cosmic time, must look locally like special relativity.

Having identified a global time co-ordinate, we must next relate the space part of the fundamental observers' metric to spatial co-ordinates centred on us. Homogeneity and uniform expansion in the Universe means that the geometry of the Universe at any two epochs t and $t + \Delta t$ differ only by a scale factor. Therefore, we can define a scale length, R(t) via the spatial curvature

$$K(t) = \frac{k}{R(t)^2} \tag{1.7}$$

We then define a dimensionless co-ordinate, $r = l \,/\, R(t)$. This co-ordinate is constant in time, as are θ and ϕ. Therefore, (r, θ, ϕ) are co-moving co-ordinates, i.e. they move with the cosmic fluid. Using the definition of R(t), and requiring that for an object with constant (r, θ, ϕ), the interval is the proper time interval dt, we may now write the complete RW metric

$$d\tau^2 = dt^2 - \frac{R(t)^2}{c^2}\left(\frac{dr^2}{1 - kr^2} + r^2(d\theta^2 + \sin^2\theta d\phi^2)\right) \tag{1.8}$$

Now we have defined the scale factor, R(t), and its place in the RW metric, we may relate it to the redshift. This is necessary in order to relate redshift (which we are able to measure directly) to the cosmological parameters (which we cannot measure directly), as will be shown in Section 1.2.2.

Redshift, z, is defined from the shift in spectral lines emitted from a moving body

$$\frac{\nu_{\text{emit}}}{\nu_{\text{obs}}} \equiv 1 + z \tag{1.9}$$

As photons travel on null geodesics, with zero proper time, we see from the metric (equation 1.8), that for these photons

$$r = \int \frac{cdt}{R(t)} \tag{1.10}$$

where r is the co-moving distance. As the co-moving distance is constant, the value of the integral must remain constant, whatever the time at which a photon is emitted. This imposes the condition

$$\frac{dt_{\text{emit}}}{dt_{\text{obs}}} = \frac{R(t_{\text{emit}})}{R(t_{\text{obs}})} \tag{1.11}$$

This time-dilation obviously affects the frequency of light emitted from distant objects, which allows us to relate the scale factor, R(t), to redshift

$$\frac{\nu_{\text{emit}}}{\nu_{\text{obs}}} \equiv 1 + z = \frac{R(t_{\text{obs}})}{R(t_{\text{emit}})} \tag{1.12}$$

1.2.2 Expansion dynamics of the Universe

We now wish to find the equation of motion for R(t), the scale factor, so that we may find a relationship between observable redshift, and time.

This may be done via a quasi-Newtonian method. Consider a sphere about an arbitrary point, with radius, R(t)r. In Newtonian gravity, the motion of a point at the edge of the sphere will only be influenced by the internal mass of the sphere. We may therefore write down the equation for conservation of energy that arises (Friedmann's equation)

$$\frac{(\dot{R}r)^2}{2} - \frac{GM}{Rr} = \text{constant} \tag{1.13}$$

However, gravitation for mass shells at large distances is not Newtonian, although, as is stated in Birkoff's theorem, the gravitational field inside a uniform spherical body is always zero, even in general relativity. From the Einstein stress-energy tensor in general relativity, therefore, the constant of integration in Friedmann's equation may be calculated, and we have

$$\dot{R}^2 = \frac{8\pi G}{3}\rho R^2 - kc^2 + \frac{1}{3}\Lambda R^2 \tag{1.14}$$

Where Λ is the constant of integration which corresponds to the contribution from the vacuum energy density, ρ is the matter density, and we have assumed that contributions from radiation are negligible.

Next we wish to rewrite this equation in terms of the Hubble parameter, H, and the cosmological parameters Ω_m, $\Omega_\Lambda$and Ω_R. Hubble's law, v = Hl, relates recessional velocity to the proper distance between the observer and the receding object. We may rewrite this using the scale factor, R(t), and setting R(0) = 1

$$\mathrm{H}^2 = \left(\frac{\dot{\mathrm{R}}}{\mathrm{R}}\right)^2 = \left(\frac{\dot{\mathrm{z}}}{1+\mathrm{z}}\right)^2 \tag{1.15}$$

The critical density ρ_c, is defined as

$$\rho_\mathrm{c} = \frac{3\mathrm{H}^2}{8\pi\mathrm{G}} \tag{1.16}$$

We may then define the cosmological density parameters:

$$\Omega_\mathrm{m}(\mathrm{z}) = \frac{\rho(\mathrm{z})}{\rho_\mathrm{c}} = \frac{\mathrm{H}_0^2}{\mathrm{H}^2}\frac{\rho_0}{\rho_{\mathrm{c},0}}(1+\mathrm{z})^3 = \frac{\mathrm{H}_0^2}{\mathrm{H}^2}\Omega_{\mathrm{m},0}(1+\mathrm{z})^3 \tag{1.17}$$

$$\Omega_\Lambda(\mathrm{z}) = \frac{\Lambda}{3\mathrm{H}^2} = \frac{\mathrm{H}_0^2}{\mathrm{H}^2}\Omega_{\Lambda,0} \tag{1.18}$$

and

$$\Omega_\mathrm{R}(\mathrm{z}) = \frac{\mathrm{kc}^2}{\mathrm{H}^2\mathrm{R}(\mathrm{t})^2} = \frac{\mathrm{H}_0^2}{\mathrm{H}^2}\Omega_{\mathrm{R},0}(1+\mathrm{z})^2 \tag{1.19}$$

where the subscript 0 denotes the present-day value of a parameter. Putting these into equation 1.14, we have

$$\mathrm{H}^2 = \left(\frac{\dot{\mathrm{z}}}{1+\mathrm{z}}\right)^2 = \mathrm{H}_0^2\left[\Omega_\mathrm{m}(1+\mathrm{z})^3 + \Omega_\mathrm{R}(1+\mathrm{z})^2 + \Omega_\Lambda\right] \tag{1.20}$$

The subscript 0's have been dropped from Ω_m, $\Omega_\Lambda$and Ω_R; in the rest of this chapter, and the remaining chapters, these will denote the present-day values of the parameters. Equation 1.20 states the relationship between redshift, time, and the cosmological parameters which account for the components of the Universe (matter, vacuum energy) and it's geometry, and is the equation which will be used to relate the ages determined for stellar populations at known redshift to possible cosmologies in later chapters.

1.3 Formation and evolution of elliptical galaxies

1.3.1 Formation scenarios

One of the most controversial issues in astronomy today is the question of when massive elliptical galaxies first obtained sizes and masses similar to those seen at the present day.

Much evidence exists that the bulk of the stars in elliptical galaxies were formed at high redshift (e.g. Renzini, 1998), although this is still disputed by some (e.g. Franceschini et al. 1998; Kodama et al. 1999). In any case, the epoch of assembly of stellar populations into present-day ellipticals is currently the subject of much debate.

The simplest galaxy formation models have massive ellipticals forming in a single, rapid collapse, at high redshift, with a monolithic burst of star formation (e.g. Eggen et al. 1962; Larson 1974), followed by passive stellar evolution. Conversely, in hierarchical clustering models (e.g. White & Rees 1978; Kauffman et al. 1993), massive objects form from the assembly of smaller pieces and have additional star-formation associated with this merging. In hierarchical cold dark matter (CDM) cosmologies, where fluctuations in the primordial density field survive recombination only on very small scales, the first objects form from the nonlinear collapse are of small mass (Peacock, 1999). These small units then merge hierarchically to form progressively larger objects. In semi-analytical simulations of this process, this leads to the formation of most massive ellipticals at $z < 1$ through the merging of spiral galaxies. A space density of massive ellipticals that is lower by a factor of 2-3 at $z = 1$ than at the present day, is predicted for a flat universe with $\Omega_m = 1$ (Kauffmann 1996; Baugh, Cole & Frenk 1996). The merging process is expected to stimulate star formation, so in this scenario, elliptical galaxies contain young stellar populations, and a deficit of massive mature ellipticals is predicted at high redshift compared to passive evolution models.

In principle, therefore, it should be relatively easy to conduct an observational test of purely passive evolution. Passively evolving ellipticals in the redshift range $1 \lesssim z \lesssim 2$ are characterised by their very red colours ($R - K \gtrsim 5 - 6$, Daddi et al. 2000a), so large-scale surveys over this redshift range, with selection based on colour, should be able to determine the co-moving density of elliptical galaxies, and hence reject or accept pure luminosity evolution models. In practice, of course, things are not so straightforward. Firstly, extremely red, $R - K \gtrsim 5$, objects (EROs) may be starburst galaxies (e.g. Cimatti et al. 1998), rather than passively evolving ellipticals. However, several studies strongly suggest that ellipticals account for $\sim 70\%$ of EROs (Cimatti et al. 1999; Moriondo et al. 2000; Daddi et al. 2000b). Secondly, a statistically large survey of both field and cluster EROs is necessary, in order for a statistically fair test to be possible. Finally, the choice of colour threshold may lead to an under-counting of passively evolving ellipticals. The level of the colour threshold is determined by modelling the evolution of stellar populations. In this work, the stellar population models of several authors (Worthey 1994; Yi et al. 2000; Bruzual & Charlot 2001; Jimenez et al. 2001) are investigated, and it is the bluest models of Jimenez et al., which consistently result in the most reliable reproduction of real stellar population spectra. Therefore, studies based on

redder models, are potentially failing to detect the true number of galaxies at high redshift. In addition, the number count may also be underestimated because the presence of even a small fraction of young stars may make the over-all colour of a galaxy blue enough to drop out of the colour-selected sample. The well-known age-metallicity degeneracy (Worthey, 1994), which means that metal-poor galaxies are bluer than metal-rich galaxies of the same age, will also affect colour-selection. It is these uncertainties in the colour-modelling of real stellar populations which have motivated the spectral investigation of elliptical galaxies and stellar population models presented in this work.

Notwithstanding these uncertainties, results from recent wide-field surveys (Thompson et al. 1999; Daddi et al. 2000b) suggest that the surface density of EROs is in good agreement with the predictions of pure luminosity evolution models (Daddi et al., 2000a).

There is also evidence in support of the hierarchical formation scenario, both from surveys claiming a deficit of elliptical galaxies at $z \sim 1$ (e.g. Zepf 1997; Barger et al. 1999; Menanteau et al. 1999; Treu & Stiavelli 1999) and from numerical simulations of disk-disk mergers which result in elliptical galaxies with properties similar to those observed (Negroponte & White 1983; Barnes & Hernquist 1996). In addition, the behaviour of galaxies in the Local Group appears to be consistent with hierarchical structure formation, in which galaxies are formed before galaxy clusters. Studies of the relative velocity field in our neighbourhood suggest that Local Group galaxies are falling towards the Virgo cluster, and that the cluster is therefore still in the process of formation. As our galaxy contains old stars, it may be postulated that it is older than the group that is forming around it (Peebles, 1988). It should also be noted that, whereas the results of Daddi et al. (2000a) exclude the standard (Einstein-de Sitter universe) CDM hierarchical model, other CDM models are not rejected. For example, in a ΛCDM model, although structure still forms hierarchically, merging takes place at earlier epochs, and the number of ellipticals therefore falls less steeply with redshift (Daddi et al., 2000a).

Clearly, attempts to securely determine the formation scenario for elliptical galaxies require large-scale surveys plus number density predictions from semi-analytical hierarchical models for a variety of cosmologies plus accurate stellar population modelling.

1.3.2 The fundamental plane

It has been known for some time that elliptical galaxies have surface-brightness profiles which are well-described by de Vaucouleurs' law (de Vaucouleurs, 1948),

$$I(r) = I_0 \exp\left[-(r/r_0)^{1/4}\right] \tag{1.21}$$

where I(r) is the surface brightness of the galaxy at radius, r. r_0 and I_0 are the characteristic radius and surface brightness. It is more useful in observational work to use the effective radius, r_e, which contains half the light, and I_e, the surface brightness at this radius (or sometimes the mean surface brightness contained within this radius). I(r) may be integrated to give the luminosity, $L \propto I_0 r_0^2$. We also have a third observable, the central velocity dispersion, σ_v, i.e. the Doppler width of the spectral lines in the galaxy's centre. Empirically, it is found that these three observables are closely related, and define a plane in which elliptical galaxies lie. This is the fundamental plane, which relates luminosity, L, to the characteristic surface brightness and central velocity dispersion:

$$L \propto I_0^x \sigma_v^y \tag{1.22}$$

where (x,y) $\simeq$ (−0.7,3) (Dressler et al. 1987; Djorgovski & Davis 1987). This simply means that elliptical galaxies are self-gravitating systems, with approximately constant mass-to-light ratios.

According to the virial theorem, the condition for equilibrium of a collapsing sphere occurs when the sphere has collapsed by a factor of two from its maximum expansion. The sphere's kinetic energy, K, is at this point related to its potential energy, V, by V = − 2K. Assuming that elliptical galaxies may be modelled as virialized systems, they must then satisfy the Keplerian relation

$$\sigma_v^2 \propto \frac{M}{r_0}. \tag{1.23}$$

If we then have a weakly varying mass-to-light ratio, M/L (from the meaning of equation 1.22)

$$M/L \propto M^a. \tag{1.24}$$

Rewriting equations 1.23 and 1.24,

$$M \propto r_0 \sigma_v^2 \tag{1.25}$$

$$L \propto M^{1-a}, \tag{1.26}$$

and substituting these into the relationship

$$L \propto I_0 r_0^2, \tag{1.27}$$

we may then write the fundamental plane relationship in terms of observable quantities:

$$I_0 \propto \sigma^{2-2a} r_0^{-1-a}. \tag{1.28}$$

Projections of this relationship between observable quantities can be found in Chapters 5 and 6. As Busarello et al. (1997) concluded, the empirically determined existence of the fundamental plane may be consistently explained by the virial theorem.

There is a remarkably small scatter in the fundamental plane, which implies that elliptical galaxies are all made in very similar processes. The scatter which is observed may be explained by the variations in age and metallicity of the stellar populations of elliptical galaxies (Pahre et al. 1998; Forbes, et al. 1998). The precise slope of the fundamental plane depends on the systematic variation of the mass-to-light ratio with luminosity (Bender et al., 1992). Section 1.3.3 describes how the fundamental plane may be used as a tool in the determination of galaxy formation processes.

1.3.3 Boxy versus disky ellipticals

There are in fact two distinct classes of elliptical galaxies, which differ in their precise morphology, dynamics and stellar content (e.g. Faber et al. 1997; Genzel et al. 2001). 'Boxy' ellipticals, i.e. those with boxy isophotes, are massive luminous objects, which have very little rotational support, and are anisotropic. 'Disky' galaxies are less luminous, have greater rotational support and smaller radii (Bender et al. 1992; Kormendy & Bender 1996; Faber et al. 1997; Genzel et al. 2001).

These differences are expected to arise from differences in the precise formation process. Disky ellipticals are expected to form in the gas-rich, recent merging of spiral galaxies (Faber et al., 1997), whereas it has been suggested that boxy ellipticals form at high redshift, in gas-poor, dissipation-less mergers. (e.g. Binney & Petrou 1985; Nieto 1988; Nieto & Bender 1989; Bender et al. 1992). Boxy ellipticals will therefore look very similar to ellipticals formed in pure luminosity evolution models. It appears that different quantities of gas present during the formation processes lead to differences in the observed properties. (Kormendy & Bender 1996; Faber et al., 1997). The power-law surface-brightness profiles that are found in

the centres of disky galaxies plausibly arise from gas-rich, dissipative processes. Numerical simulations (Barnes & Hernquist 1991; Hernquist & Barnes 1991; Mihos & Hernquist 1994) have shown that angular momentum transfer and dissipation can rapidly transport much of the gas in merging galaxies to the centre of the merger remnant, where it may fuel starbursts. The central surface-brightness profiles of boxy ellipticals, which flatten off to form a 'core', are more difficult to explain in terms of dissipation-less merging. However, evidence that massive black holes reside in the centres of elliptical galaxies (Kormendy & Richstone 1995) may offer a solution. The black holes in merging galaxies may be able to scour out a core as a result of their decaying binary orbits (Faber et al. 1997). The question of how power-law galaxies would escape this scenario remains unanswered.

As a result of their differences, boxy ellipticals occupy different positions from disky ellipticals on the fundamental plane (Genzel et al., 2001). This makes the fundamental plane a useful tool in determining the formation processes of individual elliptical galaxies. Information from the fundamental plane, together with an exploration of star formation history, is therefore exploited in the investigations into galaxy formation processes in chapters 5 and 6.

1.4 Stellar population evolutionary synthesis models

1.4.1 Synthesizing stellar populations

The synthetic spectra of stellar populations are extremely useful tools in the analysis of the integrated spectra of galaxies at distances too great for their individual stars to be resolved. For several decades, therefore, groups have attempted to create synthetic stellar populations which model the spectral evolution of real stellar populations (e.g. Tinsley 1968; Renzini 1981; Guideroni & Rocca-Volmerange 1987; Worthey 1994). The principle is simple; the spectral energy distribution (SED) of a star evolves according to its initial mass and metallicity. If the initial mass distribution and metallicity of a stellar population is known, and spectral evolution of each individual star in this initial population may be modelled, the stellar spectra may be summed over the mass distribution at any point in time to give the integrated spectrum of the population at that age. The ingredients for a stellar population model are therefore: stellar evolutionary tracks; a library of stellar spectra; a method of calibrating the theoretical luminosity and effective temperature, $T_{\rm eff}$, determined from the evolutionary tracks, so that the appropriate atmosphere may be assigned to each star at each time-step in its evolution.

The initial conditions of the population are set by three input parameters, the initial mass function (IMF), the rate of star-formation and the chemical evolution. For the simple stellar population models (SSP) considered here, the stars are assumed to have all formed in an initial, instantaneous burst of star-formation, and the initial metallicity, Z, does not evolve.

1.4.2 Description of the models

Here, the main ingredients of the four stellar population models studied in this work are listed. The four sets of models are those of Jimenez et al (2001; J01), Yi et al. (2000; Y00), Bruzual & Charlot (2001; BC01) and Worthey (1994; W94)

Jimenez et al., 2001

The stellar interior library of the J01 models was computed using the latest version of the JMSTAR15 code (Jimenez et al. 1996, Jimenez & McDonald 1996). This uses the OPAL95 opacities (Iglesias & Rogers 1996) for stellar temperatures $\gtrsim$ 6000K, and Alexander's opacities for temperatures $<$ 6000K. The mixing-length theory of Baker & Temensvary (1966), modified to allow for the limit of optically thin convective elements (Mihalas 1978), was used for the treatment of convective energy transport. The model grid was calculated for a range of metallicities, $Z = 0.0002 - 0.1$, with solar metallicity, $Z_{\odot} = 0.2$, and the solar helium fraction, $Y_{\odot} = 0.28$. The mixing-length parameter, α, was calibrated by a comparison of the computed solar model with the observed effective temperature, T_{eff}, age, luminosity and radius of the Sun. In addition, a consistency check was carried out, using the position of the red giant branch (RGB) in globular clusters with known metallicity (Jimenez et al. 1996).

Stellar masses range from 0.1 to 120 $M_{\odot}$, with step size, $\Delta M = 0.05$, from 0.1 to 3 $M_{\odot}$, and $\Delta M = 1$ $M_{\odot}$ thereafter. The tracks were evolved all the way from the contracting Hyashi track to the planetary nebula (PN) phase, except for the most massive stars, where the evolution was followed until carbon ignition. All tracks were computed using solar-scaled abundances.

The stellar evolutionary tracks were computed using the boudary conditions set by the theoterical photospheric models calculated by J01. Therefore, for each calculated point on the track, the associated stellar spectrum was known, and there was no need to introduce the uncertainties which arise in calibrating real stellar spectra to theoretical isochrones.

Semi-convection arises as a natural consequence of this modelling method.

JMSTAR15 computes the whole evolution of star in a single run, including the helium core flash, through the thermally-pulsing asymptotic giant branch (TPAGB), ejecting a PN at the end. This is possible due to the adaptive mesh of grid points, which allows very rapid stages of evolution to be modelled in detail. The SSP code includes a semi-empirical algorithm for computing the evolution of the RGB, horizontal branch (HB) and asymptotic giant branch (AGB). This is more realistic than a purely numerical code, and faster, but allows the same degree of accuracy. The AGB was modelled as in Jørgensen (1991).

A semi-empirical algorithm was also used in the calculation of mass-loss. The fast computation of post-main sequence (post-MS) stages allowed several values of the mass-loss efficiency parameter, (η in Reimers' formula, Reimers 1975), and mixing-length parameter, α, to be investigated. A realistic mean value of η was then found by matching the observed HB mass distribution (Jimenez et al. 1995).

The stellar spectra were those of the Kurucz (1992) library of theoretical stellar atmosphere models for stars with $T_{eff} > 6000$ K. For cooler stars, theoretical photospheres wer computed by J01, using the improved (Helling et al. 1996) MARCS code (Gustafsson et al. 1975), which includes molecular opacities.

Bruzual & Charlot 1993; Bruzual 2000

The BC01 models are based on the Padova evolutionary tracks (Alongi et al. 1993; Bressan et al. 1993; Fagotto et al. 1994a,b,c; Girardi et al. 1996) which are described in detail by Charlot & Bruzual (1991). The tracks were computed for a range of metallicities, $Z = 0.0001$ to 0.1, $Z_{\odot} = 0.02$, and $Y = 2.5Z + 0.23$. The 32 initial stellar masses range from 0.6 to 120 $M_{\odot}$, with a power law IMF (Salpeter 1955).

Mild convective core overshoot (the inertia-produced penetrative motion of convective cells, Shaviv & Salpeter (1973), reaching beyond the convective core as defined by Schwarzchild (1906)) was introduced in stars with masses $> M_{\odot}$.

All stars with an initial mass < 7 $M_{\odot}$ were evolved from the zero-age main sequence (ZAMS) to the white dwarf (WD) cooling stage. The most massive stars were evolved to the supernova stage. An improvement in the BC01 models over the 1996 version was that an analytic prescrition for the post-AGB and TPAGB evolution of low to intermediate mass stars was added.

The synthetic stellar spectra are those from the library compiled by Lejeune et al. (1997, 1998). In this library, the O–K stellar spectra are the 1995 version of Kurucz' theoretical spectra, the M giants come from Bessel et al. (1989, 1991) and the M dwarfs from Allard & Hauschildt (1995). However, for the $Z_{\odot}$ models, the Pickles (1998) empirical atlas was used.

Six colours were used in the calibration of the empirical spectra to the theoretical evolutionary tracks, i.e. U–V, V–R, V–I, V–J, V–J and B–V. The spectrum assigned to each evolutionary stage is the one which most closely matches these colours. Although the empirical library contains stars with non-solar as well as solar metallicities, it was expected that matching these six colours would allow stars only of the appropriate metallicity to be assigned.

With the Padova track prescription, the fractional contribution to the bolometric light at ages > 1 Gyr from the RGB is ~ 40 %, and from the AGB it is ~ 10 %. Using this prescription results in an upturn in the UV flux for stellar populations at ages > 10 Gyr, due to flux contributions from post-AGB stars.

Yi et al., 2000

The Y00 models used in Chapter 3 of this thesis are those of Yi et al. (1997), updated specifically for comparison with the UV spectra of young ($1 - 5$ Gyr) populations typical of massive galaxies at high redshift. The stellar evolutionary tracks were computed using the Yale code, together with OPAL95 opacities. Yi et al. were only interested in the UV spectrum of populations with ages of 1 to 5 Gyr. Therefore, only masses in the range $0.4 - 2.2$ $M_{\odot}$ were included in the models, as these are expected to dominate the UV spectrum at these ages. Tracks for populations with $Z = 0.005$, 0.2 and 0.04 ($Z_{\odot} = 0.02$) were computed. The models include convective core overshoot, and a constant mass-loss efficiency parameter, η, of 0.7. The post-RGB prescription of Yi et al. (1997) was followed. However, the late stages of evolution have little effect on the Y00 integrated spectrum at young ages. The stellar spectra come from the Kurucz (1992) theoretical library.

Worthey, 1994

The isochrones on which the W94 models were based were an amalgamation of the stellar evolutionary isochrones of VandenBerg (VandenBerg 1985; VandenBerg & Laskarides 1987), plus the Revised Yale Isochrones (RYI, Green et al. 1987). The theoretical stellar atmospheres were again those of Kurucz (1992), together with M giant fluxes from Bessel et al.

(1989, 1991). Each point on the isochrones represent a parcel of stars, rather than a single star. Extrapolation in (Z,Y,age) plus linear interpolation in (log(Z),Y,log(age)) of the isochrones was carried out, to allow models with arbitrary age, Z and Y to be calculated. The helium fraction was related to the metallicity using $Y = 0.228 + 2.7Z$, and $Z_{\odot} = 0.0169$. The IMF is that of Salpeter (1955), with initial stellar masses > 0.6 $M_{\odot}$.

The VandenBerg isochrones are only evolved to the base of RGB, so the RYI were matched in log T_{eff} to the last point at the base of RGB. Consequently, the mass and composition agree between the two sets of isochrones, but the ages may be mis-matched.

The mass-loss efficiency parameter is, $\eta = 0.2$. The RYI have lifetimes for the stars near the tip of RGB increasing with increasing metallicity. This increases mass-loss, as it is at the RGB tip that the majority of mass-loss occurs. There are therefore $\sim$ 20% differences in the stellar lifetimes of the two sets of isochrones, although the metal-poor stars are better matched than those with high metallicities.

In the W94 models, the treatment of the HB, early AGB (EAGB) and TPAGB was schematic (Lattanzio 1991; Bedijn 1988), and therefore susceptible to systematic errors. EAGB lifetimes and the luminosities of TPAGB switch-on were extrapolated for $Z > Z_{\odot}$; the AGB was forced to start from HB temperature location and the HB itself was approximated to red clump near the giant branch, which is not a good approximation for metal-poor populations. In addition, post-AGB contributions were not included.

1.4.3 Comparison of the synthetic spectra

Most of the differences between synthetic stellar population models stem from differences in the treatment of post-MS evolution. The physics of post-MS stellar evolution (e.g. opacities, convection, nuclear rates) is not well-understood, which is why the late stages of evolution (HB, EAGB, TPAGB, PN, WD) are often either crude approximations or completely omitted in many codes. This has important consequences for the integrated spectra; the HB strongly influences the UV spectrum, contributions from the RGB and AGB dominate at infrared (IR) wavelengths, and post-AGB contributions are important at wavelengths less than 3000Å (W94).

In the young Y00 models, post-RGB contributions to the integrated flux are negligible. However, both these models and those of BC00 develop an increase in UV flux (UV upturn) at older ages and high metallicities as a result of their treatment of HB evolution. The schematic approach to the AGB of W94 leads to an AGB tip which is very bright. One of

the strengths of the J01 models is the adoption of a realistic, adjustable, mass-loss efficiency parameter which limits how far stars ascend the AGB. This prevents the prediction of overly red optical-IR colours in the first gigayear of evolution which occurs when a fixed value of η is adopted. Choice of the mass-loss efficiency parameter, which is associated with HB morphology, and hence the integrated UV flux, together with the effects of inclusion or non-inclusion of AGB and HB stars can lead to variations in colour of as much as 0.4 magnitudes (J01).

The luminosity function at the tip of the RGB is very sensitive to mass, and hence the mass-loss efficiency parameter and mass resolution. As visible light is dominated by contributions from RGB stars, even a slight error in the positioning of the RGB tip leads to an error in the visible integrated spectrum (and a potential error in the normalised UV flux of the Y00 models). As most mass-loss occurs in the last stage of the RGB, with luminous M giants most affected, an incorrect choice of mass-loss parameter also leads to inaccuracies in the integrated red light of old, Z-rich populations of the RGB, where M giants dominate. As the mass-loss efficiency parameter is dependent on both age and metallicity (Y00), the choice of a fixed value by all model authors except J01, introduces inaccuracies in the modelling.

There are $2-5$ times as many TPAGB stars in the Padova evolutionary prescription than in the W94 models, because of the long lifetimes adopted for these cool luminous stars in the Padova model. This reddens the BC01 spectrum. However, brighter V− and K−band light from the RGB and the red clump approximation to the HB in the W94 models results in a V−K colour which is ~ 0.2 magnitudes brighter for W94 than for BC01 models (Charlot, Worthey & Bressan 1996; CWB).

Difficulties in modelling opacities lead to significant uncertainties in theoretical spectral libraries, with cool stars and high metallicities most affected. In particular, metal-rich populations at most ages are dominated by M giants ($T_{eff} < 3900$ K), for which molecular opacities are important, and consequently their modelled stellar fluxes have always been uncertain. However, the latest MARCS code, used by J01, includes a detailed treatment of molecular opacities, and has substantially improved the accuracy of the modelled IR spectra of cool stars. As a result, IR absorption bands are stronger in the J01 models than in other models.

The use of empirical stellar spectra avoids the need for modelling opacities. However, the calibration of empirical spectra with theoretical isochrones can introduce even larger errors. W94 identifies a spread of 0.2 magnitudes in theoretical B−V stellar calibrations. Worthey himself notes that the B−V colour used in the calibration of the stellar spectra used in

the W94 models was systematically too red, and that U−V and J−K colours also have systematic defects.

Convective overshoot affects both the shape of the MS turn-off and the luminosity function. Overshooting allows more hydrogen from the stellar core to be burned while the star is on the MS, and MS lifetimes are consequently longer if overshoot is included in the models. Convective overshoot is not included in the W94 models, which means that, by a population age of 12 Gyr, the rate of stars leaving the MS is approximately 60 % less for the BC01 models than for the W94 models. No overshoot means that the MS progenitors of the subgiants consume less hydrogen, so more is available for the next evolutionary stage. Consequently, the W94 subgiant population is an order of magnitude greater than that of the BC01 models. With convective overshoot included in the models, the RGB lifetime becomes shorter, as there is less hydrogen available by the time stars reach this stage. Therefore, as overshooting increases, the visible (RGB-dominated) flux decreases (Y00). As giants dominate the blue-visual colour of old populations, W94 is redder in B−V colour than other models (CWB).

Variations in the choice of IMF and in Y affect the integrated spectra to the same order of magnitude as the uncertainties in the evolutionary models and stellar flux libraries (W94).

In summary, the major differences between the models arise from the underlying stellar evolution theory, in particular, the treatment of mass loss and convection, and from the modelling of cool and high-metallicity stellar fluxes.

The comparison of the models outlined above is that of a model-maker, where the models are deconstructed and indivual elements compared step-by-step. However, a different approach is taken in this thesis; it is the over-all ability of the various models to reproduce the spectra of real stellar populations which is checked by comparison with observational data.

Chapter 2

The ages of quasar host galaxies

2.1 Introduction

Determining the nature of the host galaxies of powerful active galactic nuclei (AGN) is of importance not only for improving our understanding of different manifestations of AGN activity, but also for exploring possible relationships between nuclear activity and the evolution of massive galaxies. The recent affirmation that black-hole mass appears approximately proportional to spheroid mass in nearby inactive galaxies (Magorrian et al., 1998) has further strengthened the motivation for exploring the link between active AGN and the dynamical and spectral properties of their hosts. In particular, investigations of this kind may assist in resolving whether or not nuclear activity represents a normal phase in the evolution of massive galaxies bulges (e.g. Lawrence 1999; Corbin 2000).

Over the last few years, improvements in imaging resolution offered by both space-based and ground-based optical/infrared telescopes have stimulated a great deal of research activity aimed at determining the basic structural parameters (i.e. luminosity, size and morphological type) of the hosts of radio-loud quasars, radio-quiet quasars, and lower-luminosity X-ray-selected and optically-selected AGN (e.g. Disney et al., 1995; Hutchings & Morris 1995; Bahcall et al., 1997; Hooper et al., 1997; McLure et al., 1999; Schade et al., 2000). However, relatively little corresponding effort has been invested in spectroscopic investigations of AGN hosts, despite the fact that this offers an independent way of classifying these galaxies, as well as a means of estimating the age of their stellar populations.

Related work in this field to date has focussed on the investigation of the hosts of matched

samples of radio-quiet quasars (RQQs), radio-loud quasars (RLQs) and radio galaxies (RGs) at relatively modest redshift (z = 0.2). Details of these samples can be found in Dunlop et al. (1993). The sub-samples of quasars (i.e. RQQs and RLQs) have been selected to be indistinguishable in terms of their two-dimensional distribution on the $V - z$ plane, while the sub-samples of radio-loud AGN (i.e. RLQs and RGs) have been selected to be indistinguishable in terms of their two-dimensional distribution on the $P_{5GHz} - z$ plane (as well as having indistinguishable spectral-index distributions). Deep infrared imaging of these samples (Dunlop et al., 1993; Taylor et al., 1996) has recently been complemented by deep WFPC2 HST optical imaging (McLure et al., 1999), the final results of which are reported by Dunlop et al., (2001). As well as demonstrating that, dynamically, the hosts of all three types of luminous AGN appear indistinguishable from normal ellipticals, this work has enabled crude deductions of spectral information on the host galaxies in the form of optical-infrared colours. However, broad-baseline colour information can clearly be most powerfully exploited if combined with detailed optical spectroscopy. Over the past few years, therefore, attempts have been made to complement the imaging studies with a programme of deep optical off-nuclear spectroscopy of this same sample of AGN.

Details of the observed samples, spectroscopic observations, and the basic properties of the observed off-nuclear spectra are given in Hughes et al. (2000). As discussed by Hughes et al. (2000), the key feature of this study (other than its size, depth, and sample control) is the endeavour to obtain spectra from positions further off-nucleus ($\simeq$ 5 arcsec) than previous workers, in an attempt to better minimize the need for accurate subtraction of contaminating nuclear light. This approach was made possible by deep infrared imaging data, which allows slit positions to be selected at $\simeq$ 5 arcsec off-nucleus , which still intercept the brighter isophotes of the host galaxies (slit positions are shown, superimposed on the infrared images, in Hughes et al., 2000).

Here, the results of attempting to fit the resulting off-nuclear spectra with evolutionary synthesis models of galaxy evolution are presented. The primary aim was to determine whether, in each host galaxy, the optical spectrum could be explained by the same model as the optical-infrared colour, and, if so, to derive an estimate of the age of the dynamically dominant stellar population. However, this study also offered the prospect of determining whether the hosts of different classes of AGN differ in terms of their more recent star-formation activity.

It is worth noting that the off-nuclear spectroscopy obviously does not enable us to say anything about the level of star-formation activity in the nucleus of a given host galaxy. Rather, any derived estimates of the level of star-formation activity refer to the region

probed by the observations $\simeq 5$ arcsec off-nucleus. However, given the large scalelengths of the hosts, their relatively modest redshift, and the fact that the spectra are derived from long-slit observations, it is reasonable to regard our conclusions as applying to fairly typical regions, still located well within the bulk of the host galaxies under investigation.

The layout of this chapter is as follows. In section 2.2, details of the adopted models, and how they have been fitted to the data are provided. The results are presented in section 2.3, along with detailed notes on the fitting of individual spectra. The implications of the model fits are then discussed in section 2.4, focussing on a comparison of the typical derived host-galaxy ages in the three AGN subsamples. Finally, the conclusions are summarized in section 2.5.

2.2 Spectral fitting.

The stellar population synthesis models adopted for age-dating the AGN host galaxy stellar populations are the solar metallicity, instantaneous starburst models of Jimenez et al. (2001). For each off-nuclear host galaxy optical spectrum, a fit is attempted by a combination of two single starburst components. For the first component, age is fitted as a free parameter, while for the second component the age is fixed at 0.1 Gyr, and the normalization relative to the first component is the only free parameter. This dual-component approach was adopted because single-age models are not able to adequately represent the data, and because it allows the age of the dynamically dominant component to be determined in a way which is not overly reliant on the level of ultraviolet flux which might be contributed either by a recent burst of star-formation, or by contamination of the slit by scattered light from the quasar nucleus. After experimentation it was found that the spectral shape of the blue light was better represented by the 0.1 Gyr-old (solar metallicity) model of Jimenez than by models of greater (intermediate) age (e.g. 1 Gyr). Moreover, the further addition of a third intermediate age component, $\simeq 1$ Gyr, did not significantly improve the quality of the fits achieved.

In general, these data are of insufficient quality to tell whether the component which dominates at $\lambda \simeq 3000$ Å really is due to young stars, or is produced by direct or scattered quasar light. However, while the origin of the blue light is obviously of some interest, it has little impact on the main results presented in this chapter, which refer to the age of the dynamically dominant stellar population which dominates the spectrum from longward of the 4000 Å break through to the near infrared. The robustness of the age determination of the

dominant population is demonstrated by comparing the results of the two stellar-population model fit with the results of a fit allowing for a nuclear contribution as well as the two stellar populations.

The model parameters determined were therefore the age of the dominant stellar population, which we can reasonably call the age of the galaxy, and the fraction, by (visible) baryonic mass, of the 0.1 Gyr component. For the fit including a nuclear contribution, the fraction of the total flux contributed by quasar light was a third parameter. The red end of each SED was further constrained by fitting $R - K$ colour simultaneously with the optical spectral energy distribution. The fitting process is described below.

First, the observed off-nuclear spectra were corrected for redshift and transformed to the rest frame. They were then rebinned to the spectral resolution of the model spectra. The rebinned flux is then the mean flux per unit wavelength in the new bin and the statistical error on each new bin is the standard error in this mean. The data were normalised to a mean flux per unit wavelength of unity across the wavelength range 5020 – 5500 Å.

The two-component model was built from the instantaneous-burst stellar-population synthesis model SEDs, so that

$$F_{\lambda,age,\alpha} = const(\alpha f_{\lambda,0.1} + (1-\alpha) f_{\lambda,age})$$

where $f_{\lambda,age}$ is the mean flux per unit wavelength in the bin centred on wavelength λ for a single burst model of *age* Gyr, α is the fraction by mass of the young (0.1 Gyr) component, and $F_{\lambda,age,\alpha}$ is then the new, mean twin stellar-population flux per unit wavelength in the bin centred on wavelength λ for a model of *age* Gyr. This composite spectrum was then normalised in the same way as the observed spectra.

A χ^2 fit was used to determine the age of the older stellar population and the mass-fraction, α, of the younger population, for each host galaxy in the sample. The whole parameter space was searched, with the best-fit values quoted being those parameter values at the point on the grid with the minimum calculated χ^2. The normalization of the model spectra was allowed to float during the fitting process, to allow the best-fitting continuum shape to be determined in an unbiased way.

The models were fitted across the observed (rest-frame) spectral range, within the wavelength ranges listed in Table 2.1. As a result of the optimisation of the instruments with which the objects were observed, some of the galaxy spectra contain a 'splice' region where the red and blue end of the spectrum have been observed separately and then joined together (see Hughes et al. (2000) for details). These splice regions, defined in Table 2.1, were masked

out of the fit in order to guard against the fitting procedure being dominated by data-points whose flux calibration was potentially less robust. The main emission lines, present due to nuclear light contamination or nebular emission from within the host, were also masked out, over the wavelength ranges given in Table 2.2.

The fit including a nuclear component was carried out in the same way, with the model flux in this case being

$$F_{\lambda,age,\alpha,\eta} = const(\alpha f_{\lambda,0.1} + (1-\alpha) f_{\lambda,age} + \eta f0054_{\lambda})$$

where η is the fraction contributed to the total model flux by the nucleus, and $f0054_{\lambda}$ is the observed flux of the nucleus of the radio quiet quasar 0054+144. α is the fraction by mass of the total stellar population contributed by the 0.1 Gyr population. The wavelength range of the observed nuclear flux of 0054+144 is 3890−6950 Å. This was extended to 3500−8500 Å by a smooth polynomial extrapolation over the wavelength ranges 3500−3890 Å and 6950−8500 Å in order to carry out the χ^2 fit across the full wavelength range of the observed off-nuclear spectra.

$R-K$ colour was fitted in both cases with a typical error of a few percent. The observed $R-K$ colours for the host galaxies are obtained from UKIRT and H_0images (McLure et al., 1999, Dunlop et al., 2001), and define the basic shape of the host galaxy SED out to $\lambda \simeq 2\mu m$. The composite model spectra were appropriately red-shifted before calculating the colour, so that they could be compared to the observed colours without introducing uncertainties in k-correction. The R band was simulated using the filter function, including system response and CCD quantum efficiency, for the HST WFPC2 F675W filter, and the K band was reproduced using the filter data for the IRCAM3 K Ocli filter at 77K combined with Mauna Kea atmosphere.

2.3 Results

The plots showing fits to individual spectra and χ^2 as a function of fitted age are shown in Figures 2.1 and 2.2. The plots for the two-component fit are presented in Figure 2.1, and those for the two stellar-component plus nuclear contribution are in Figure 2.2. In Figure 2.1 the rest-frame spectra are in the first column (green), with the best-fitting two-component model spectra (Jimenez et al., 2001) superimposed (black). The spectra of the single-aged old population (red) is given for comparison. In Figure 2.2, the fits allowing for an additional contribution to the flux from the nucleus are presented. In this case, the key is:

IAU name	Telescope	Wavelength range / Å	Masked splice region / Å
		Radio-loud quasars	
0137+012	M4M	3890–6950	
0736+017	M4M	3890–6950	
	WHT	3500–8000	6050–6150
1004+130	WHT	3500–8000	6050–6150
1020−103	M4M	3890–6950	
1217+023	WHT	3500–7500	6000–6100
2135−147	WHT	3500–8500	6000–6100
2141+175	WHT	3500–8500	6000–6100
2247+140	M4M	3890–6950	
	WHT	3500–7500	6050–6150
2349−014	WHT	3500–8300	6000–6100
		Radio-quiet quasars	
0054+144	M4M	3890–6950	
	WHT	3500–8000	6000–6100
0157+001	M4M	3890–6950	
	WHT	3500–8000	6050–6150
0204+292	WHT	3500–8000	6050–6150
0244+194	WHT	3500–8500	6000–6100
0923+201	WHT	3500–7000	
1549+203	WHT	3500–8000	6050–6150
1635+119	WHT	3500–7800	6000–6100
2215−037	WHT	3500–8500	6000–6100
2344+184	M4M	3890–6950	
	WHT	3500–8500	6000–6100
		Radio galaxies	
0230−027	WHT	3500–8500	6000–6100
0345+337	WHT	3500–8500	6000–6100
0917+459	WHT	3500–8500	6050–6150
1215−033	WHT	3500–7500	6000–6100
1330+022	M4M	3890–6950	
2141+279	M4M	3890–6950	

Table 2.1: Wavelength ranges of observed spectra, and splice regions which were excluded from the fitting process. All wavelengths are in the observed frame. M4M denotes the Mayall 4m Telescope at Kitt Peak, and WHT denotes the 4.2m William Herschel Telescope on La Palma (see Hughes et al. (2000) for observational details).

rest-frame spectra, green; best-fitting two-component spectra + nuclear flux contribution, black; best-fitting two-component model spectra, red; single-aged old population spectra, blue, dotted.

The second column of plots shows the χ^2 evolution with age for the dominant older population. The third column shows the best-fit χ^2 as a function of percentage young population, α, for fixed ages of the dominant component. The models have solar metallicity. The subscript η denotes results obtained by including the nuclear contribution.

Where there are two spectra of the same object, the spectrum given first is the one observed on the Mayall 4m Telescope, and the second is that observed using the William Herschel Telescope. The data for the following objects have been smoothed using a Hanning function: 2135+147 (RLQ), 2141+175 (RLQ), 0244+194 (RQQ), 0923+201 (RQQ), 1549+203 (RQQ), 2215-037 (RQQ), 0230-027 (RG) and 0345+337 (RG).

The results for each object are summarized below, under their IAU names, with alternative names given in parentheses. Objects are listed in order of increasing right ascension, within each AGN class (radio loud quasars, radio quiet quasars and radio galaxies). The telescopes with which the spectra were obtained are also noted; M4M denotes the Mayall 4m Telescope at Kitt Peak, and WHT denotes the 4.2m William Herschel Telescope on La Palma.

Figure 2.1: Model fits to the off-nuclear rest frame spectra, for each object, with the corresponding χ^2 plots. The rest-frame host-galaxy spectra are in the first column (green), with the best-fitting two-component model spectra (Jimenez et al., 2001) superimposed (black). The spectra of the single-aged old population (red) is given for comparison. The second column shows the χ^2 evolution with age for the dominant older population and the third column shows the best-fit χ^2 as a function of percentage young population, α, for fixed ages of the dominant component. All models have solar metallicity. Where there are two spectra of the same object, the spectrum given first is the one observed on the Mayall 4m Telescope, and the second is that observed using the William Herschel Telescope. The data for the following objects have been smoothed using a Hanning function: 2135+147 (RLQ), 2141+175 (RLQ), 0244+194 (RQQ), 0923+201 (RQQ), 1549+203 (RQQ), 2215−037 (RQQ), 0230−027 (RG) and 0345+337 (RG).

Radio Loud Quasars

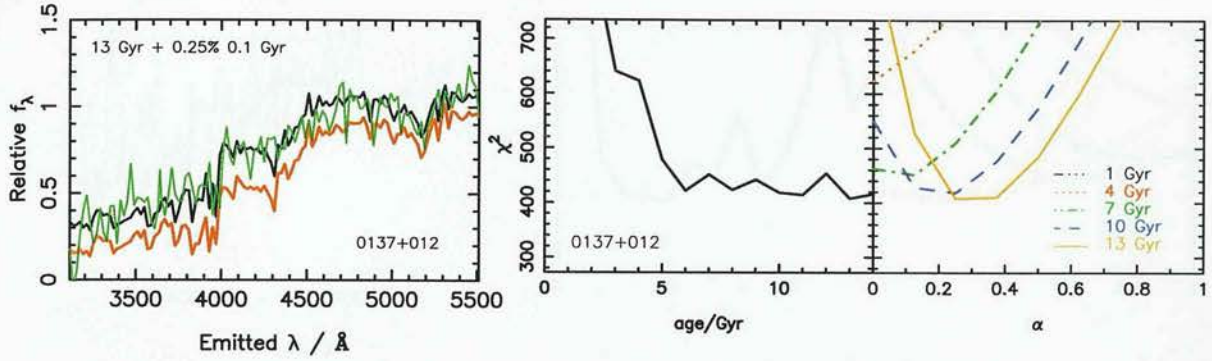

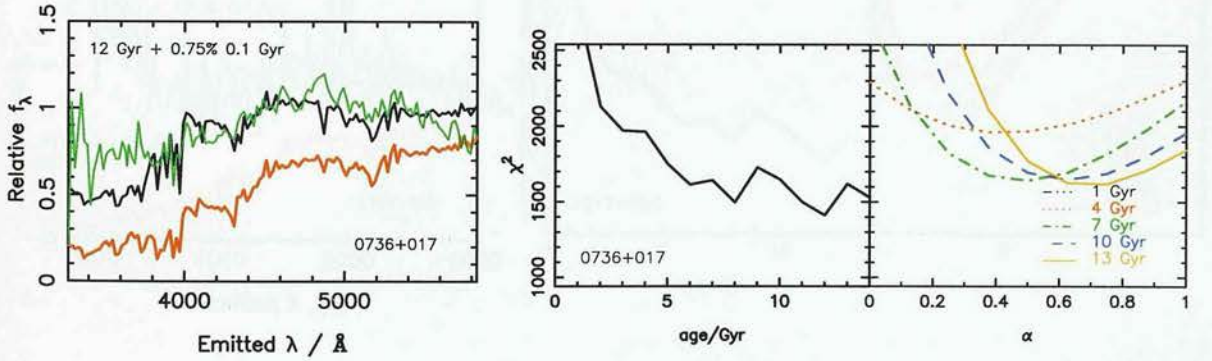

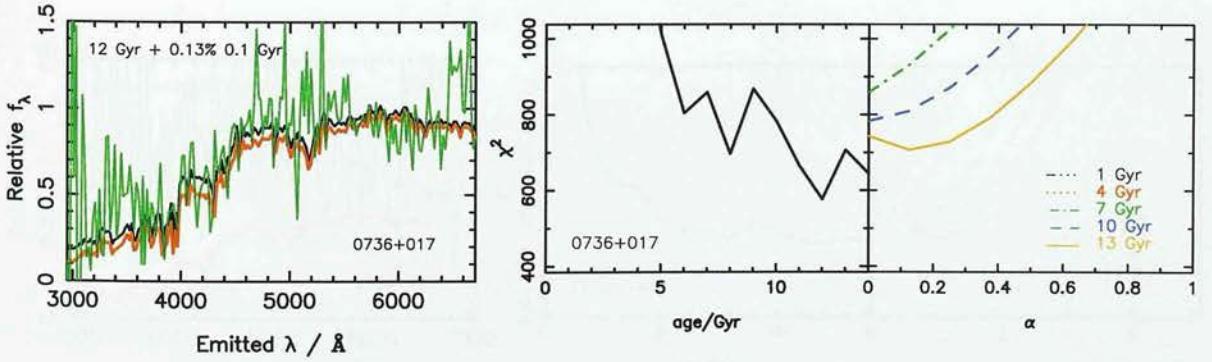

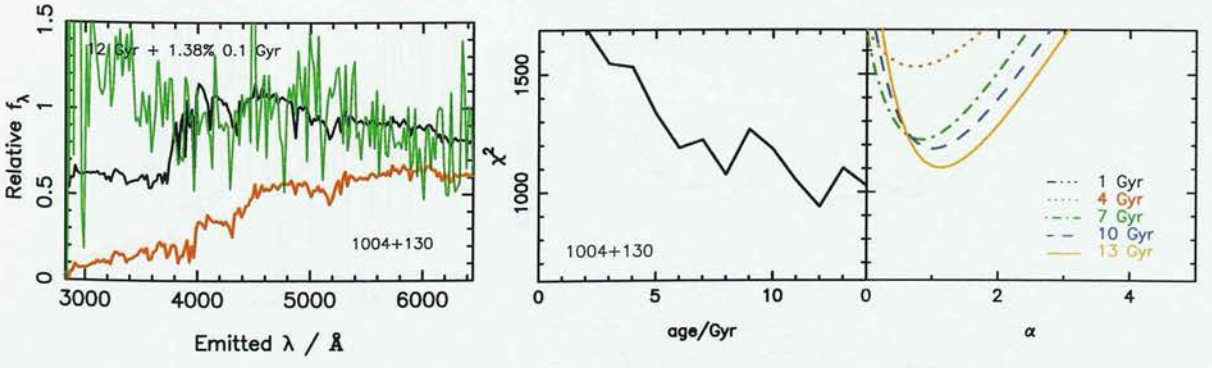

Radio Loud Quasars

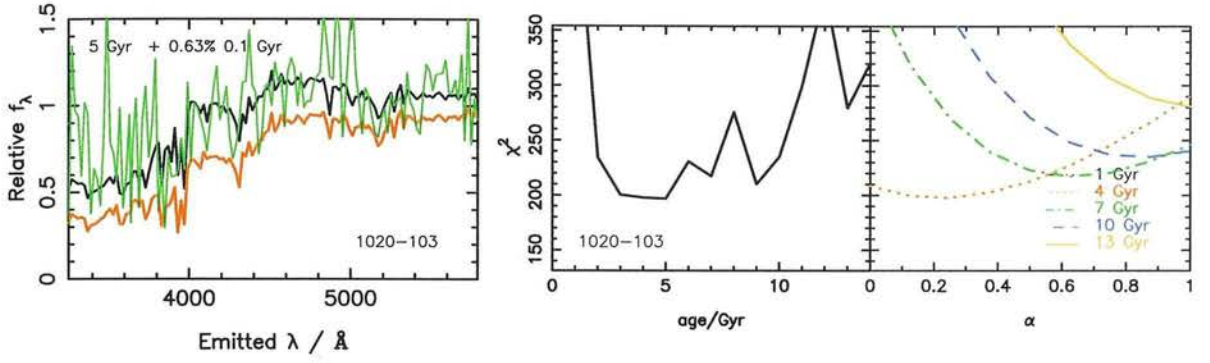

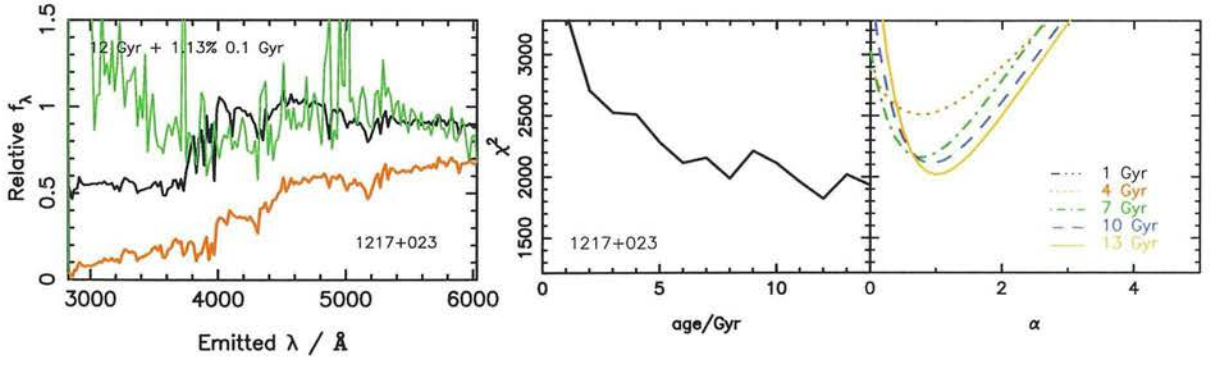

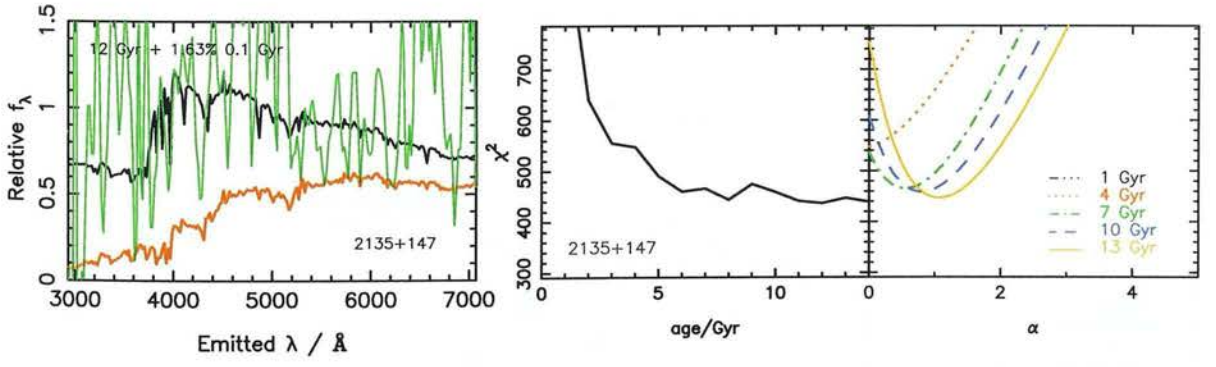

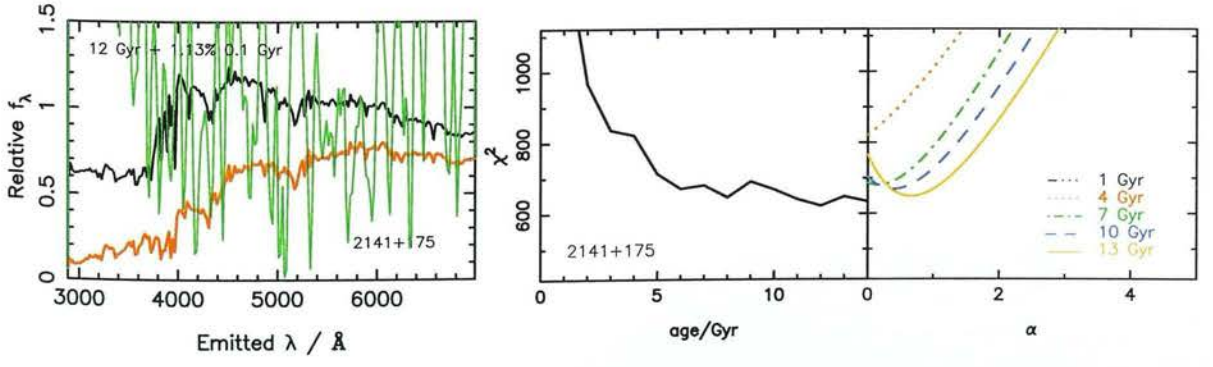

Radio Loud Quasars

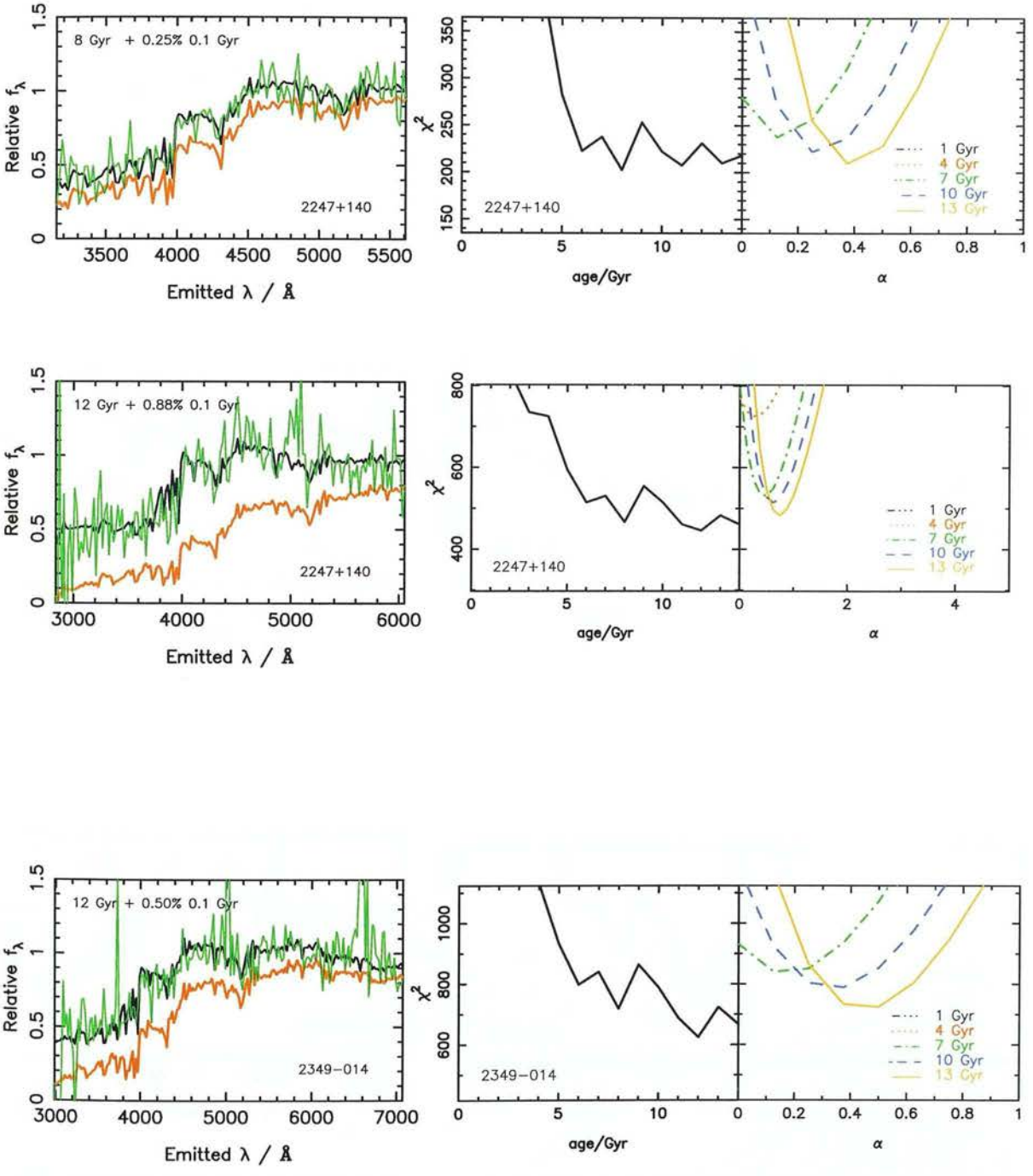

Radio Quiet Quasars

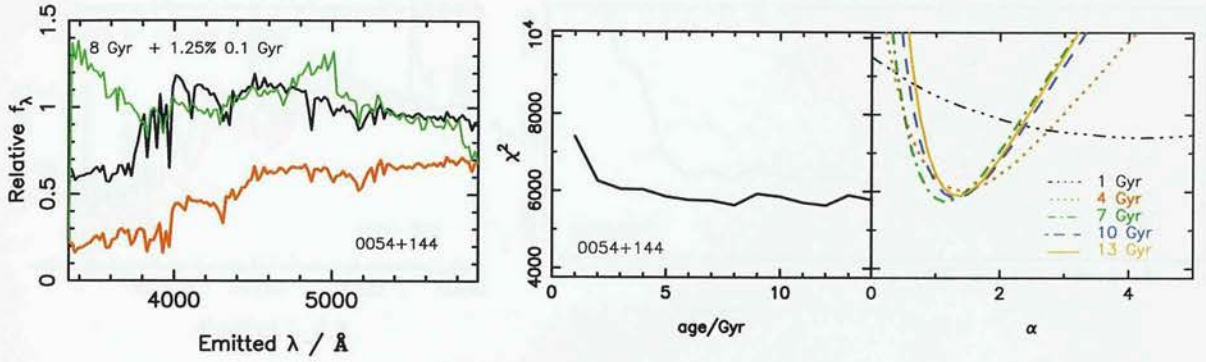

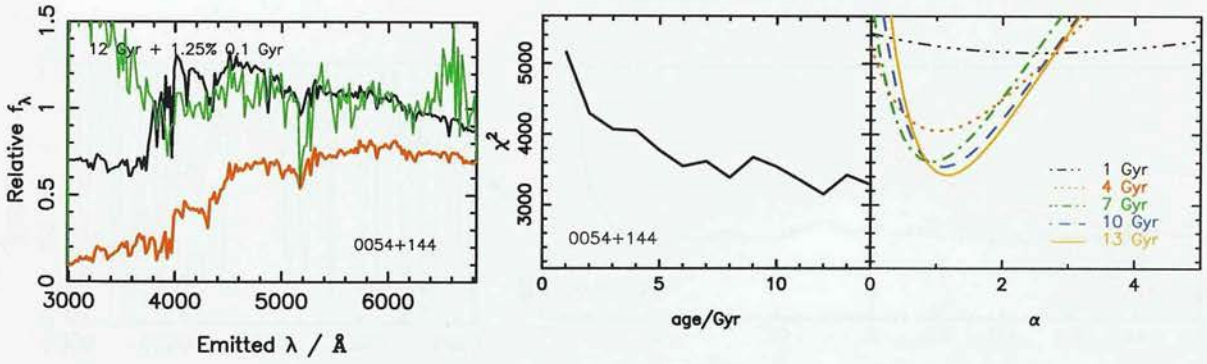

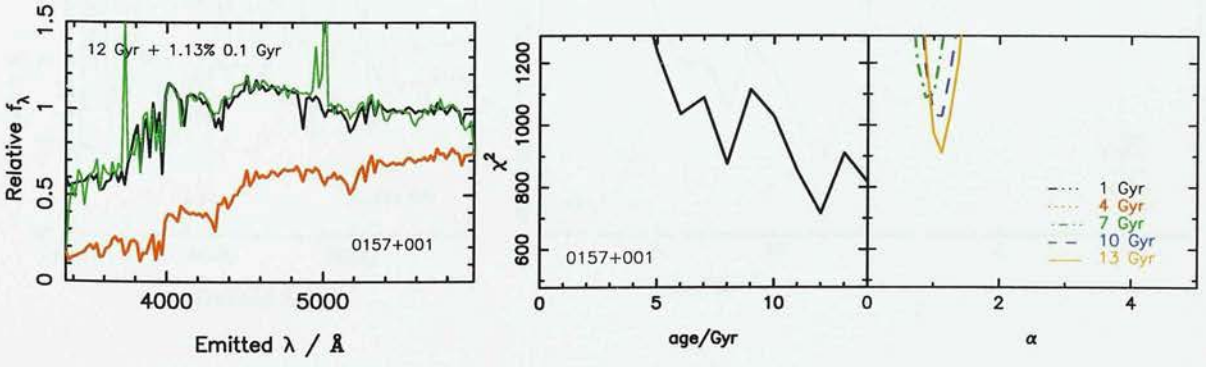

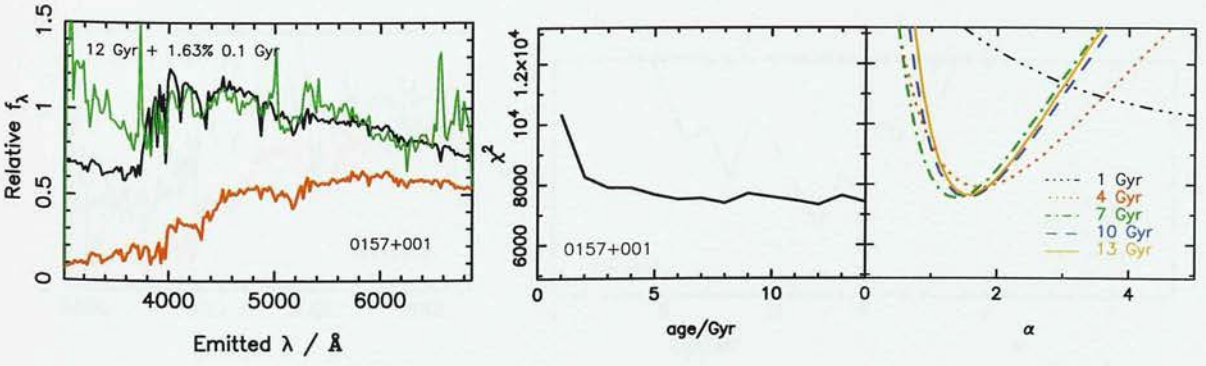

Radio Quiet Quasar

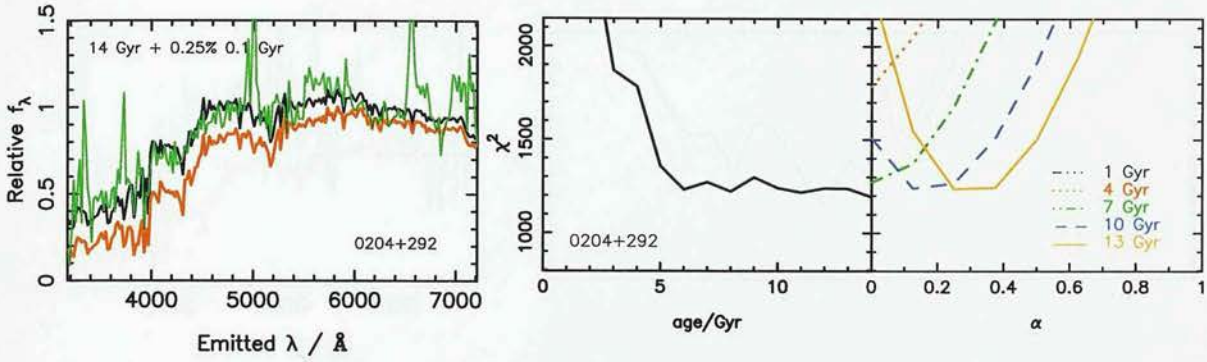

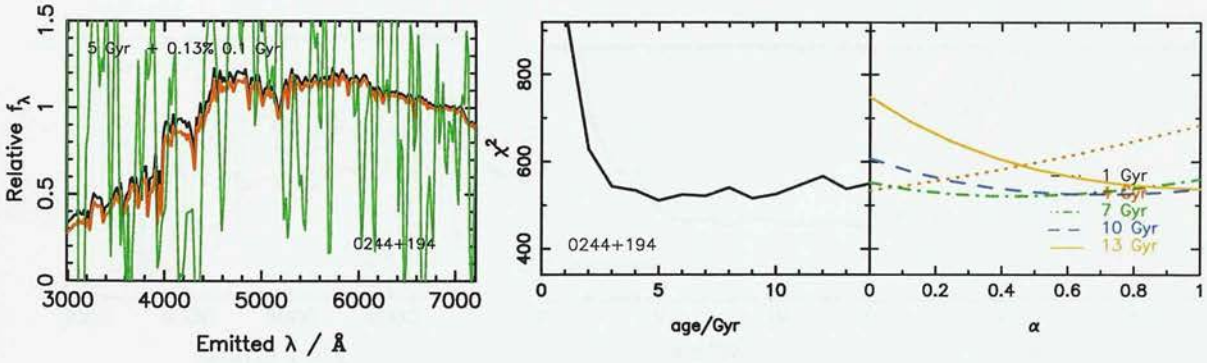

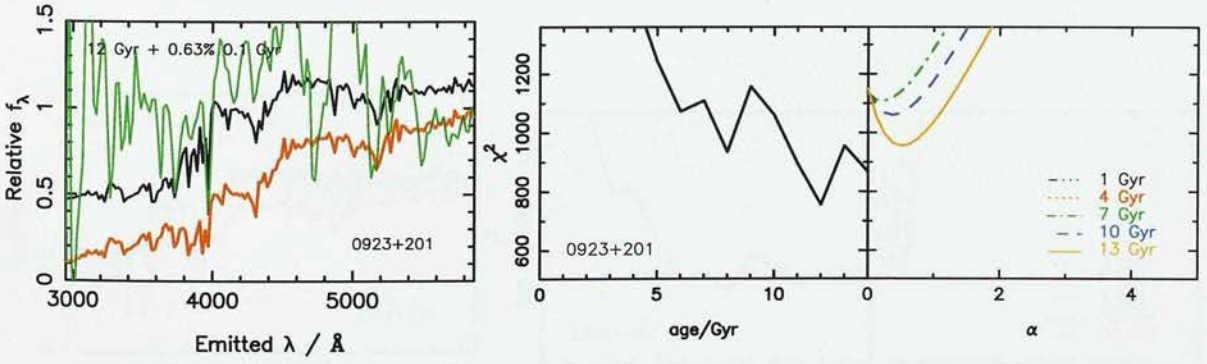

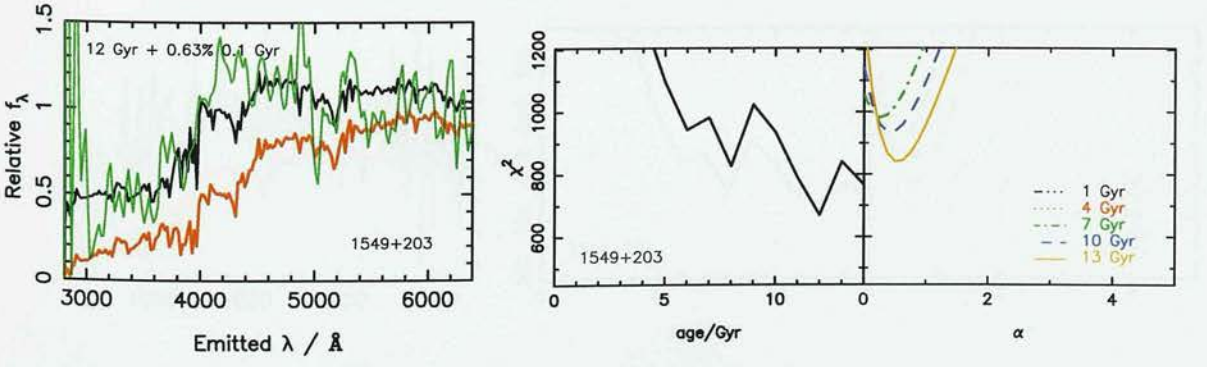

Radio Quiet Quasars

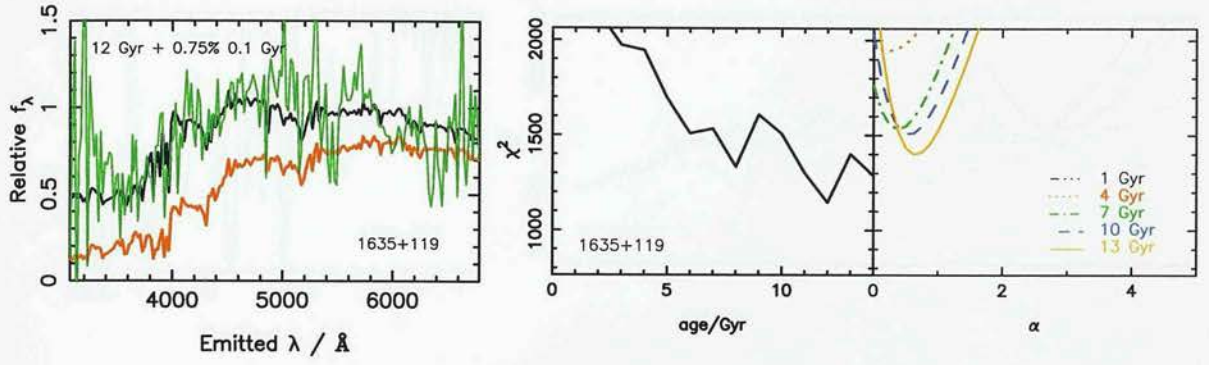

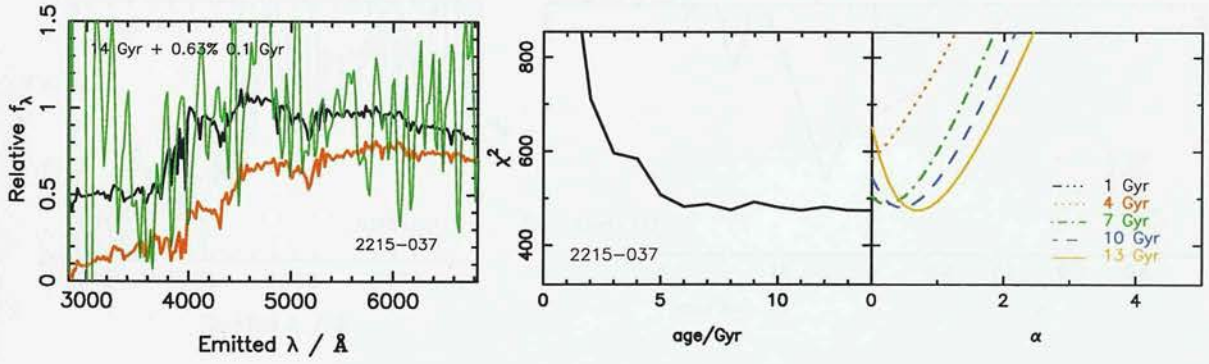

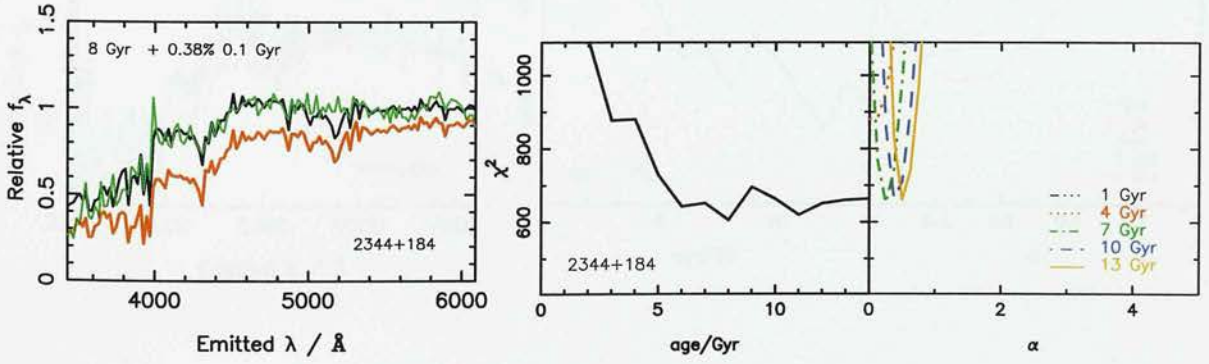

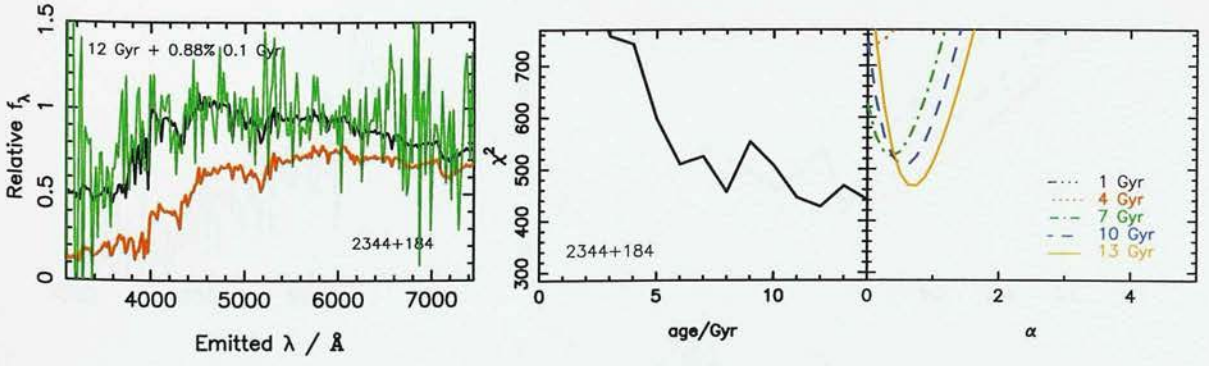

Radio Galaxies

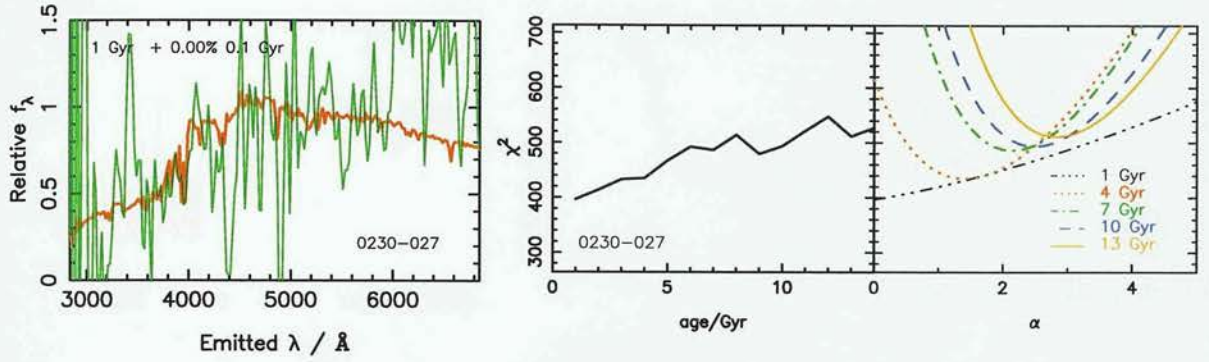

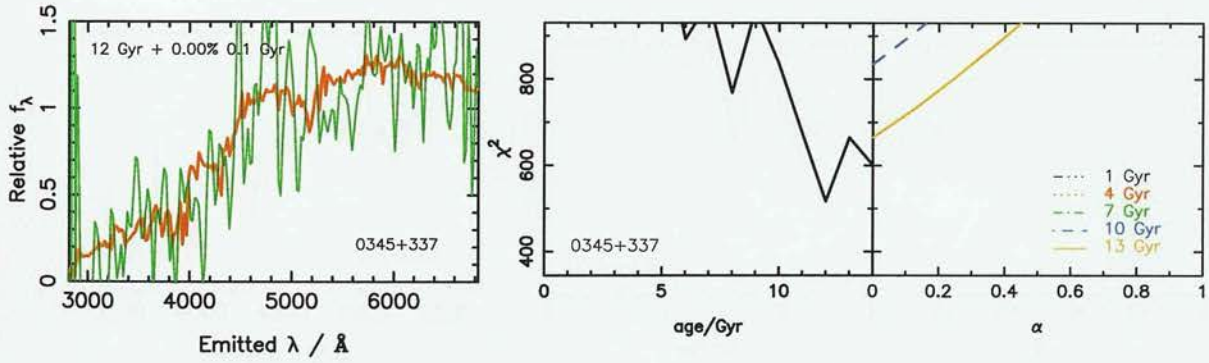

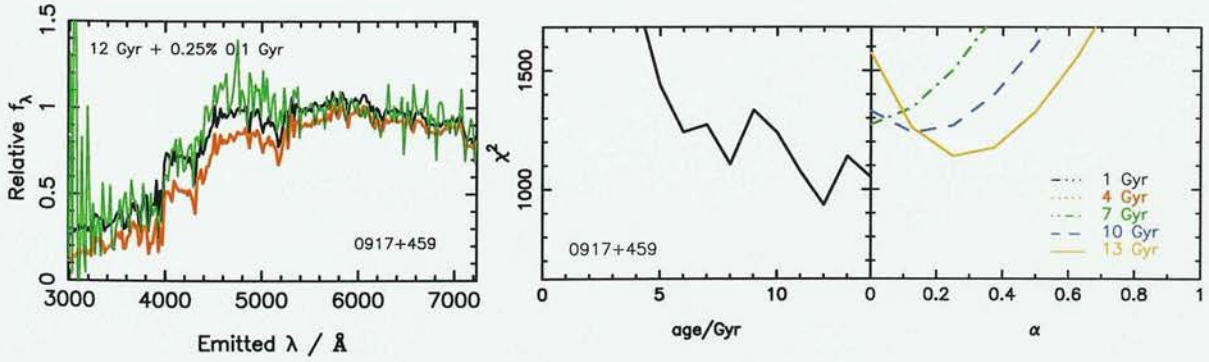

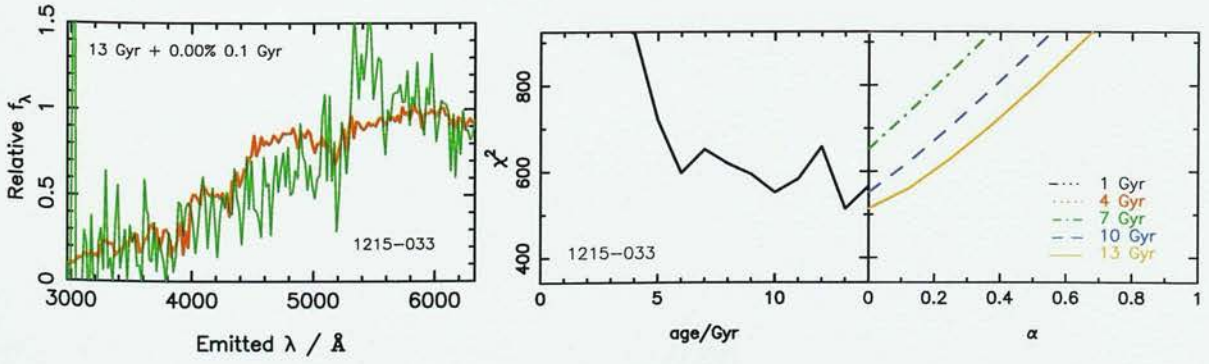

Radio Galaxies

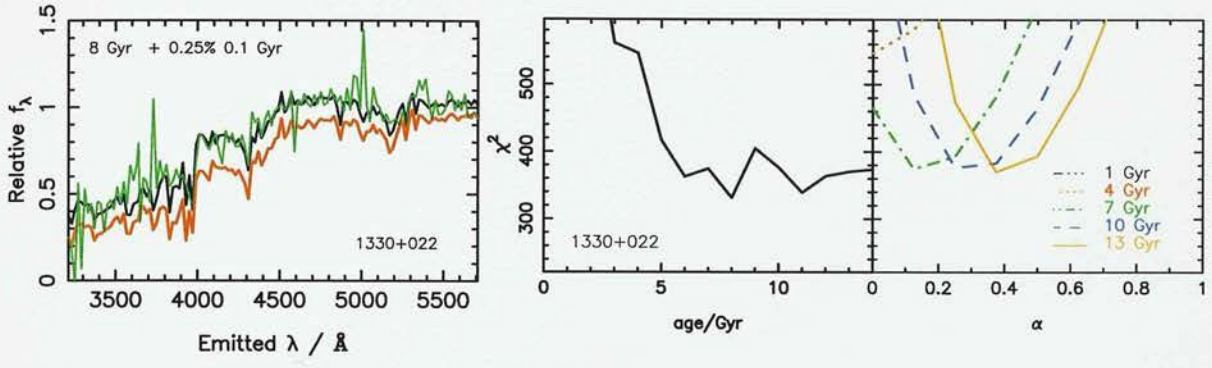

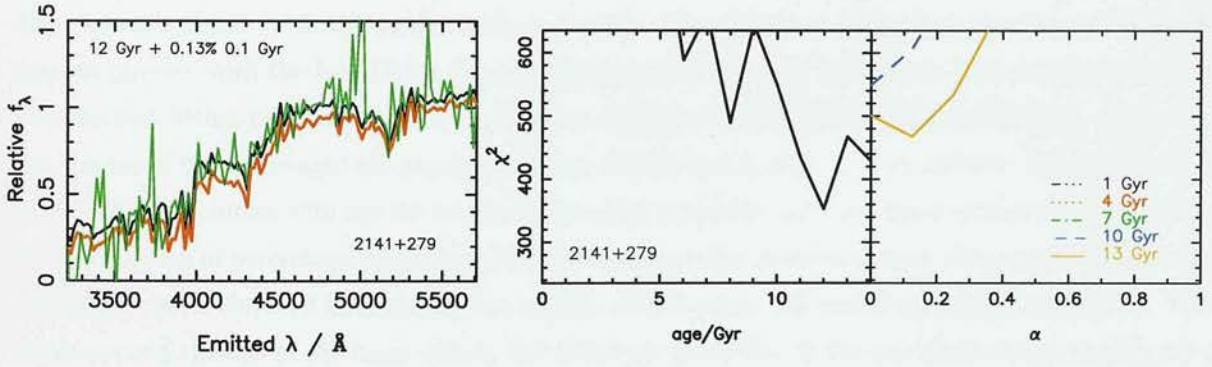

Figure 2.2: Model fits to the off-nuclear rest frame spectra, including the modelling of a nuclear contribution, for each object, with the corresponding χ^2 plots. The rest frame host galaxy spectra are in the first column (green), with the best-fitting two-component model flux plus the nuclear flux contribution (black) and the best-fitting two-component model spectra (Jimenez et al., 2001) superimposed (red). As in Fig 3, the spectra of the single-aged old population (blue, dotted line) is given for comparison. The second column shows the χ^2 evolution with age for the dominant older population and the third column shows the best-fit χ^2 as a function of percentage young population, α, for fixed ages of the dominant component. The subscript η denotes results obtained by including the nuclear contribution. All models have solar metallicity. Where there are two spectra of the same object, the spectrum given first is the one observed on the Mayall 4m Telescope, and the second is that observed using the William Herschel Telescope. The data for the following objects have been smoothed using a Hanning function: 2135+147 (RLQ), 2141+175 (RLQ), 0244+194 (RQQ), 0923+201 (RQQ), 1549+203 (RQQ), 2215−037 (RQQ), 0230−027 (RG) and 0345+337 (RG).

Radio Loud Quasars

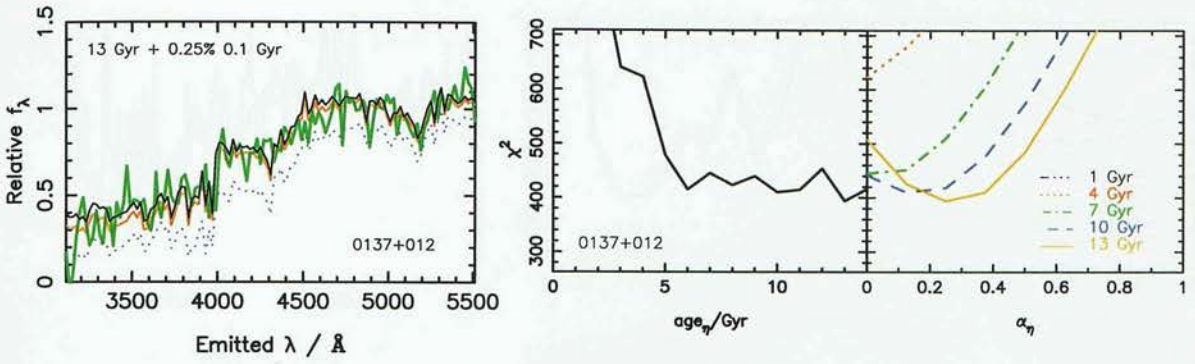

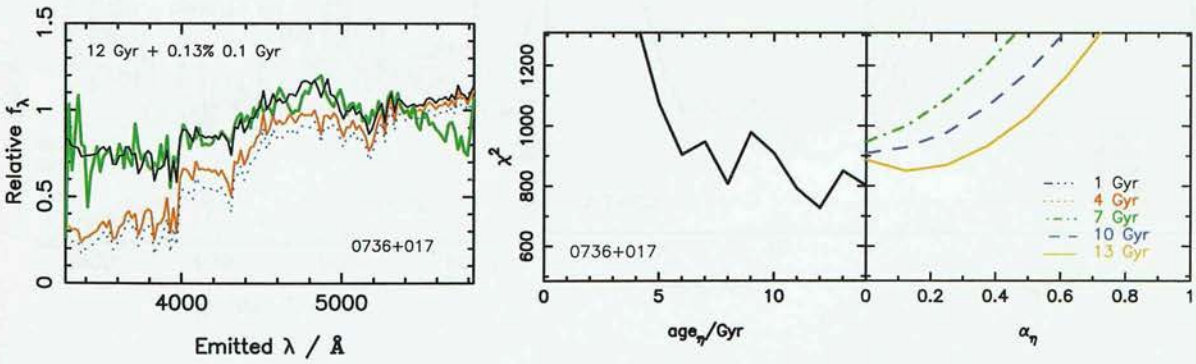

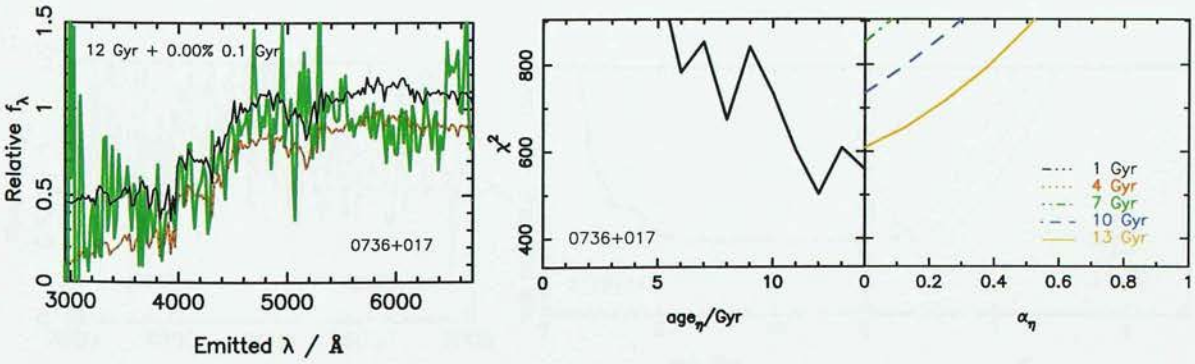

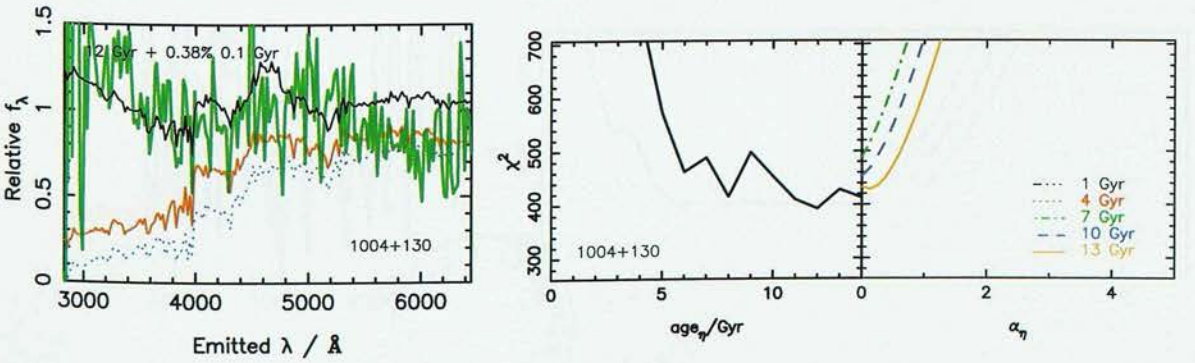

Radio Loud Quasars

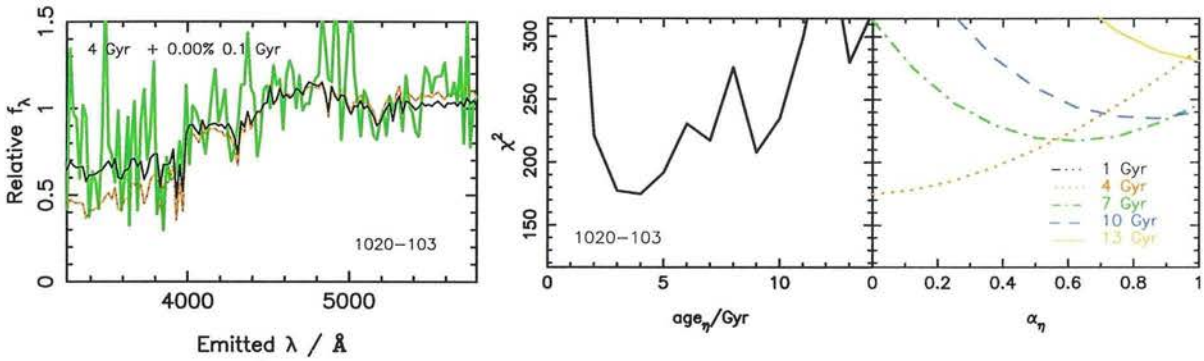

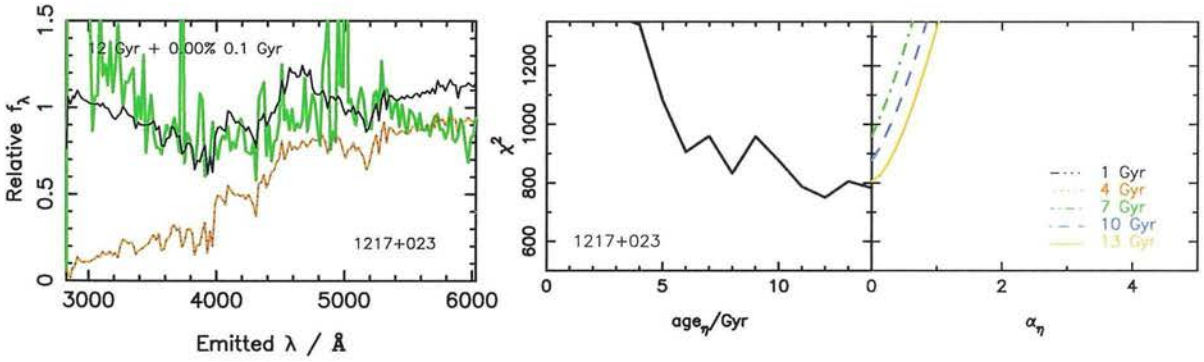

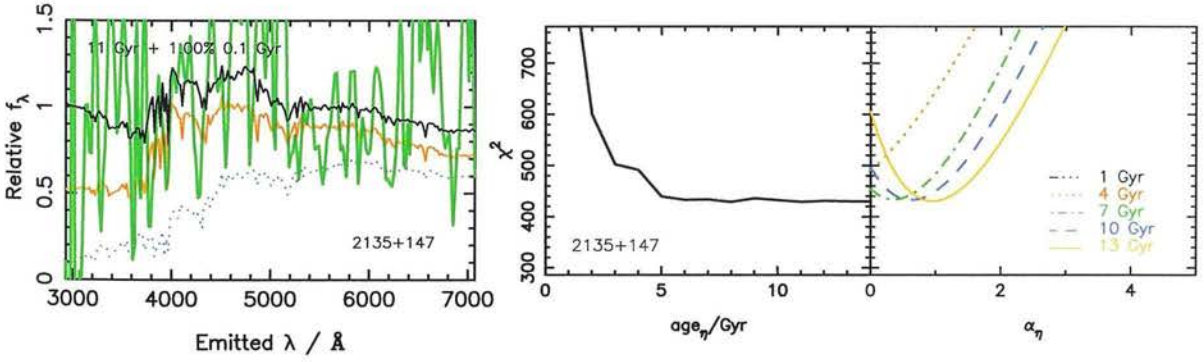

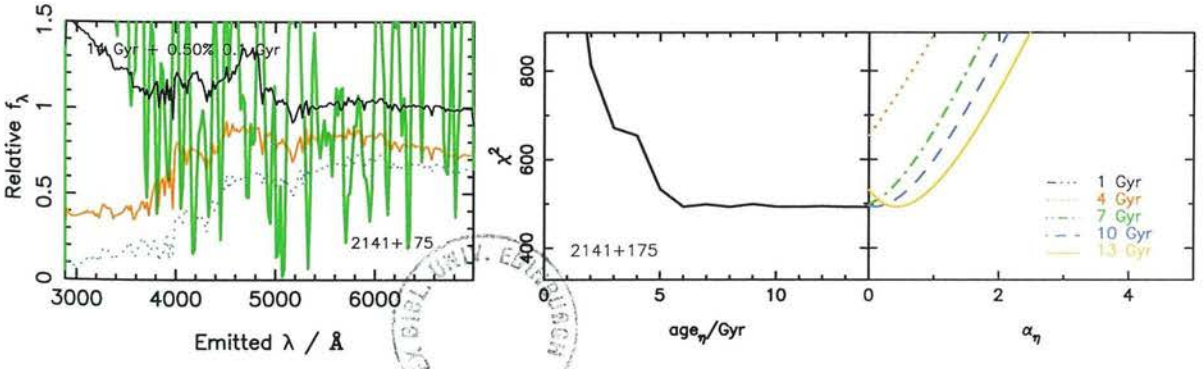

Radio Loud Quasars

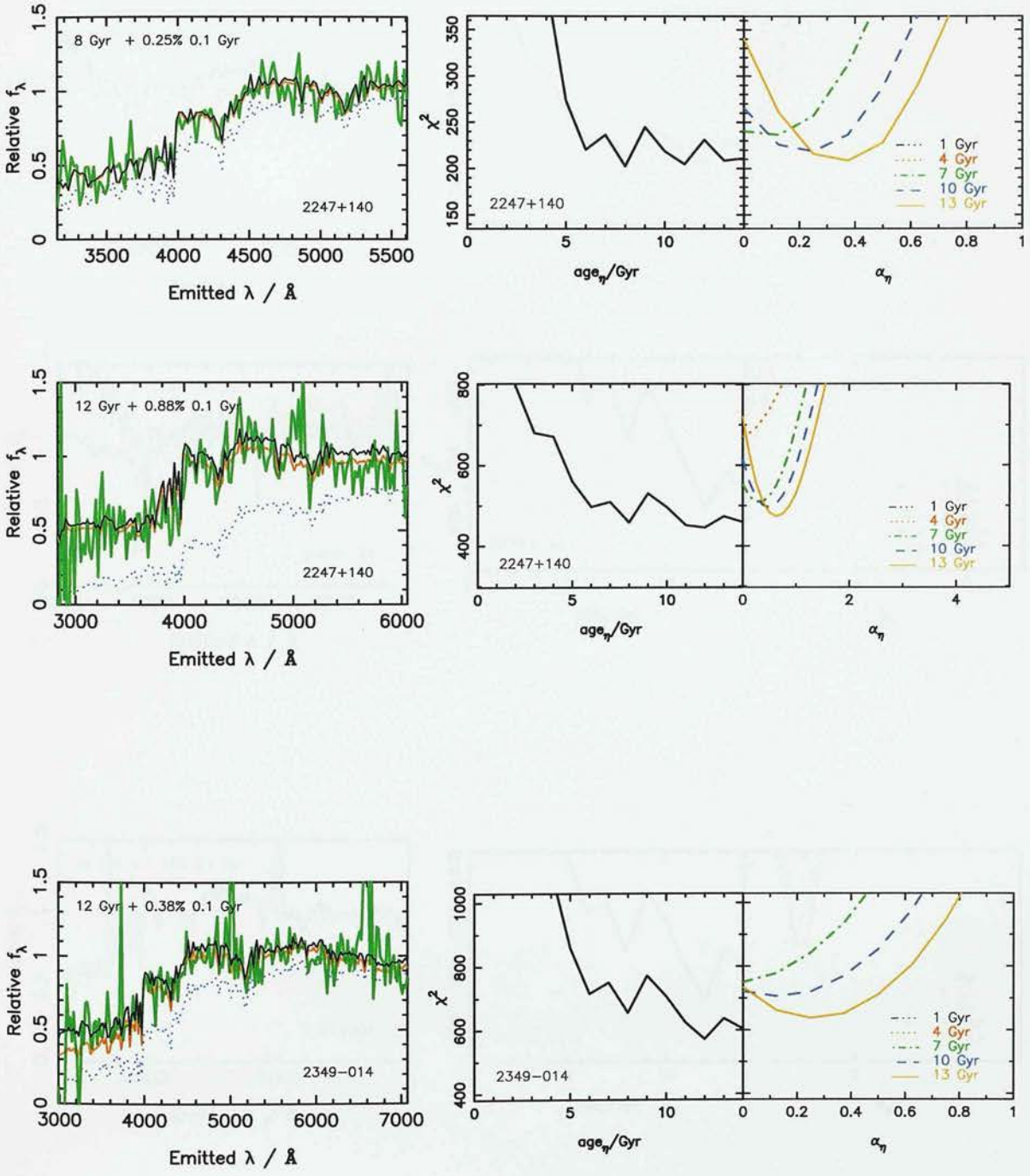

Radio Quiet Quasars

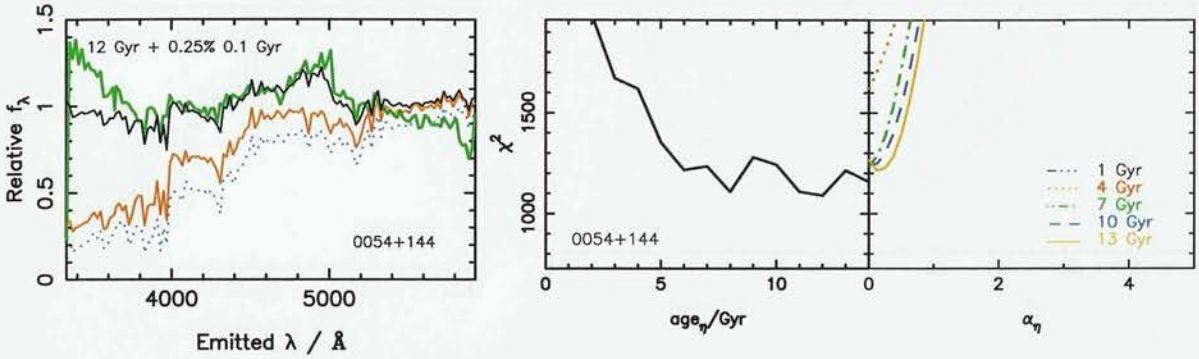

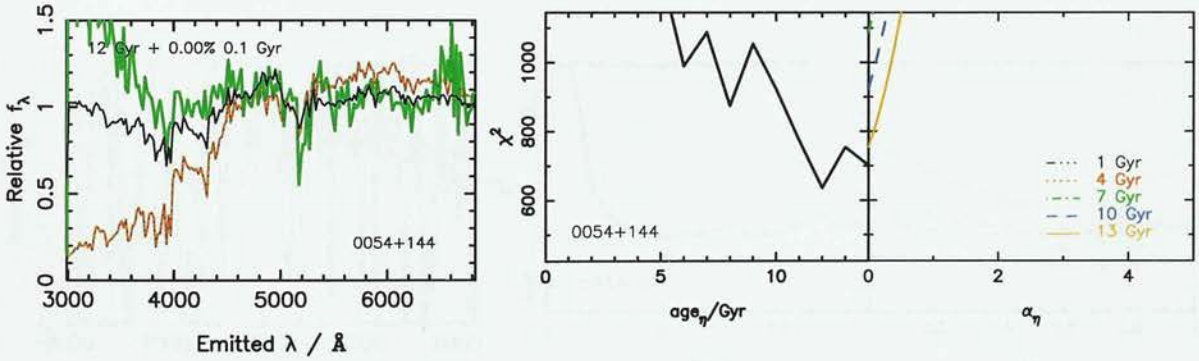

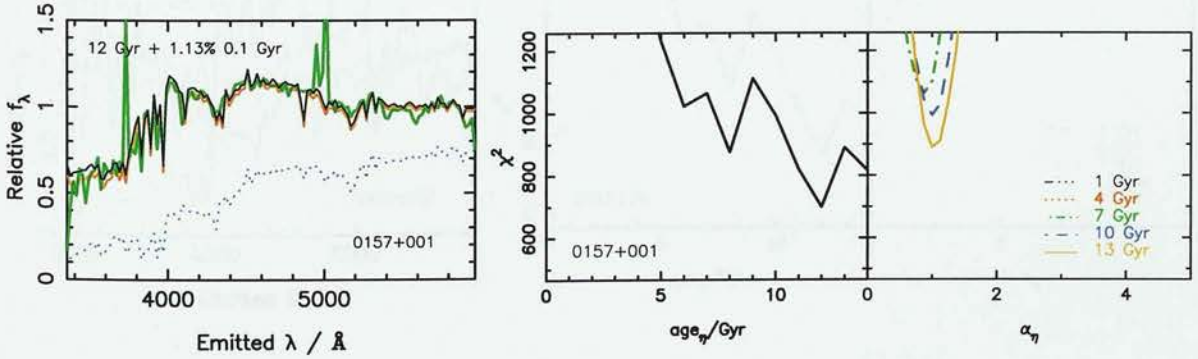

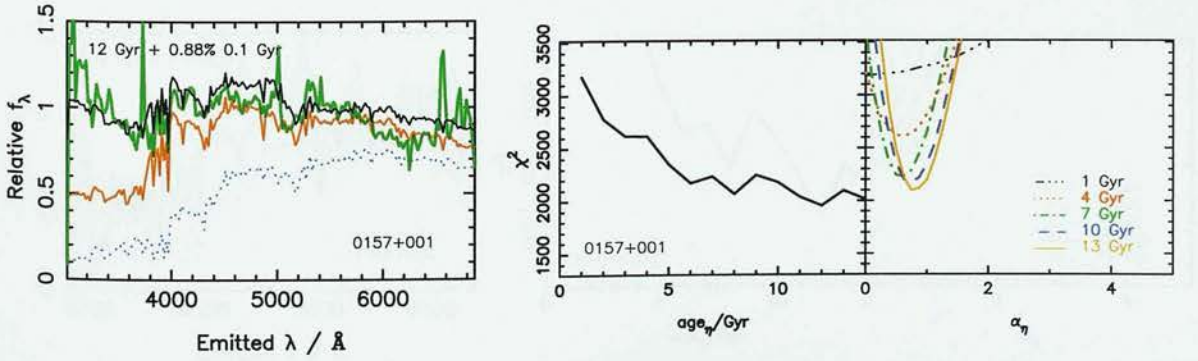

Radio Quiet Quasars

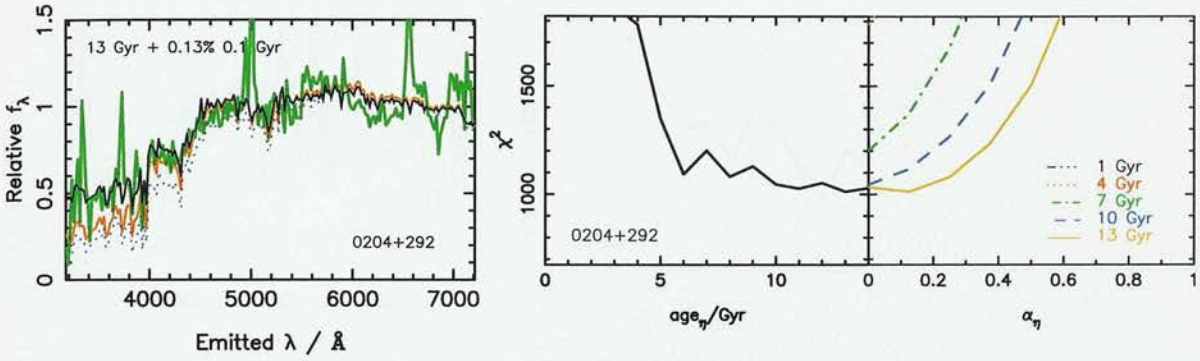

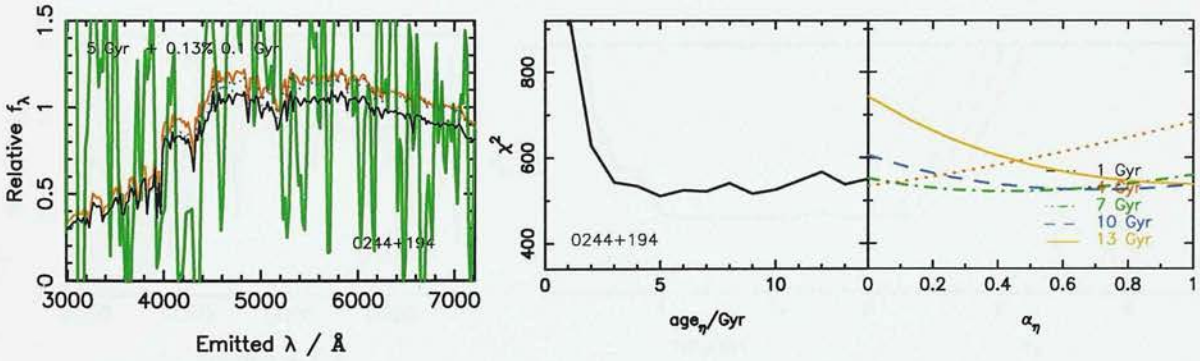

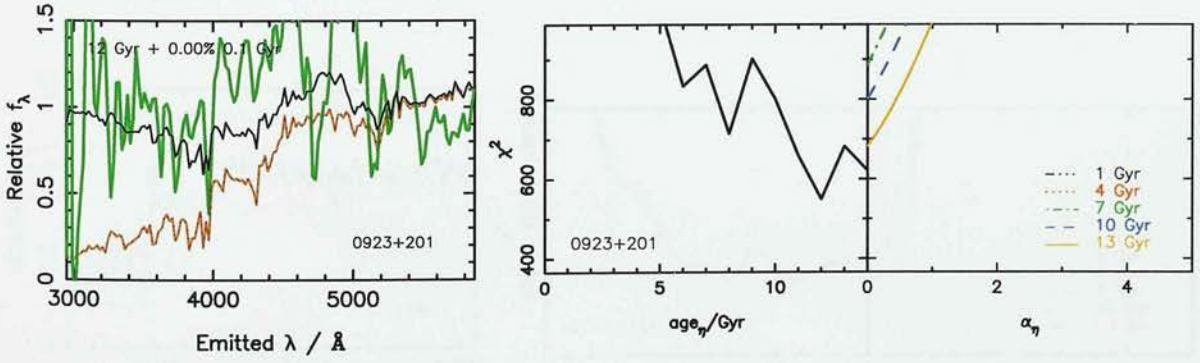

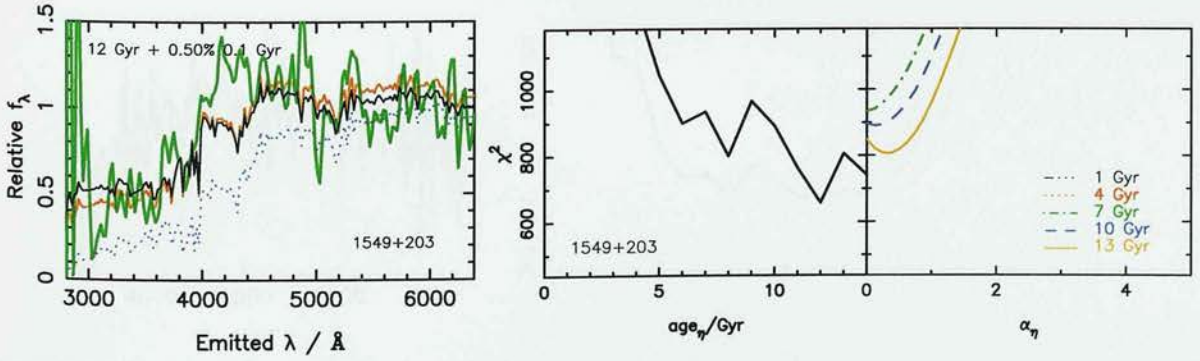

Radio Quiet Quasars

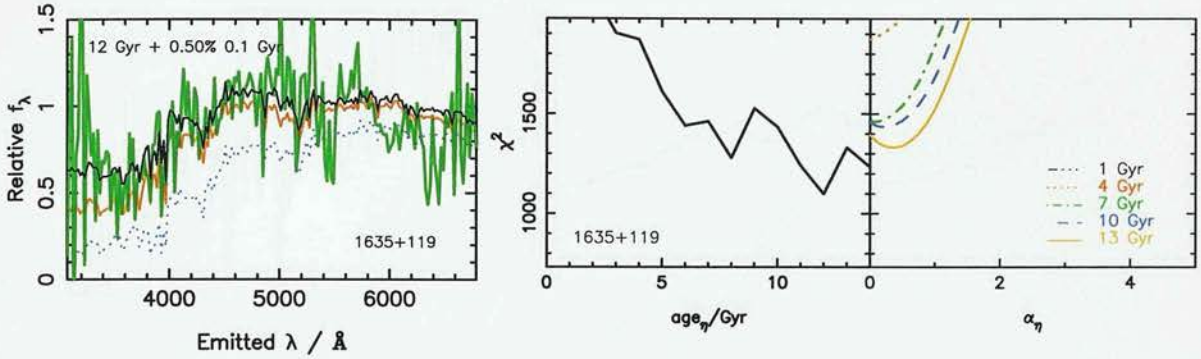

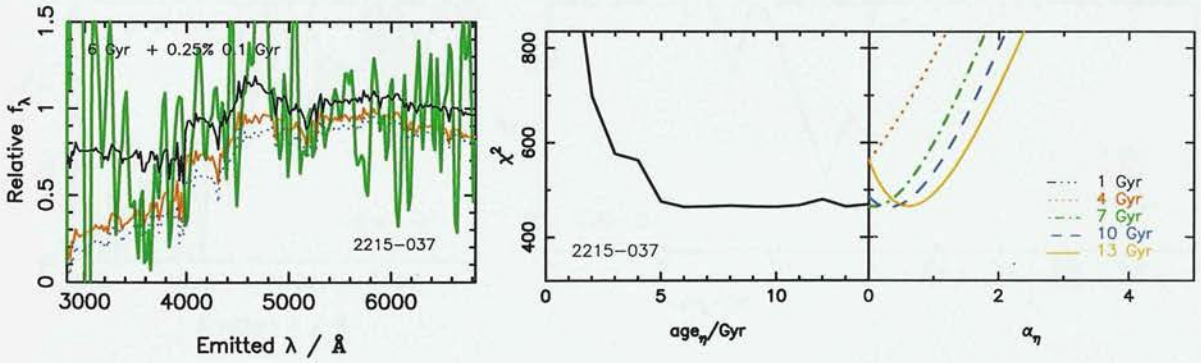

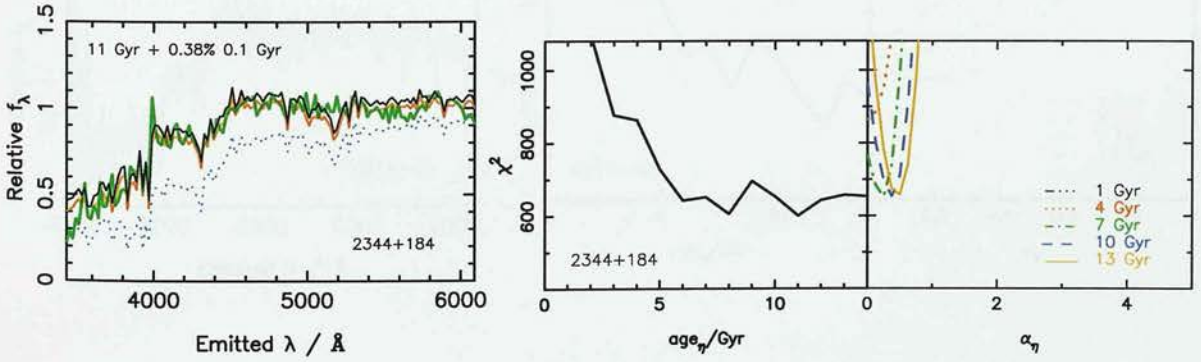

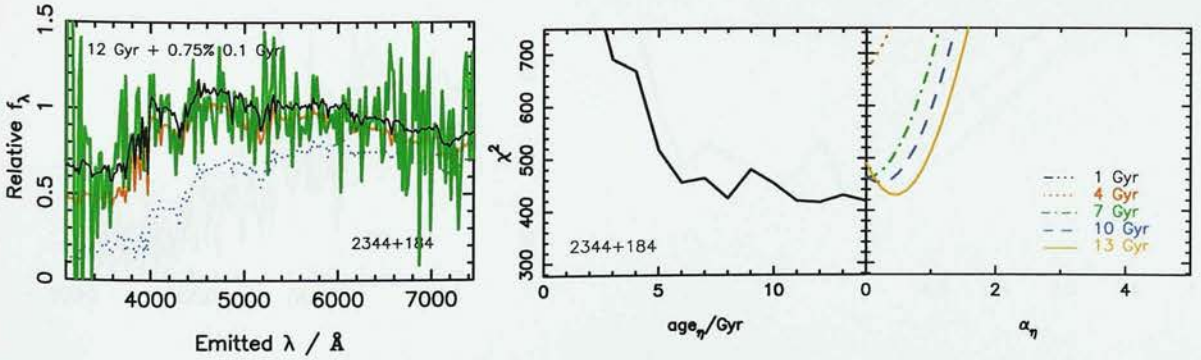

Radio Galaxies

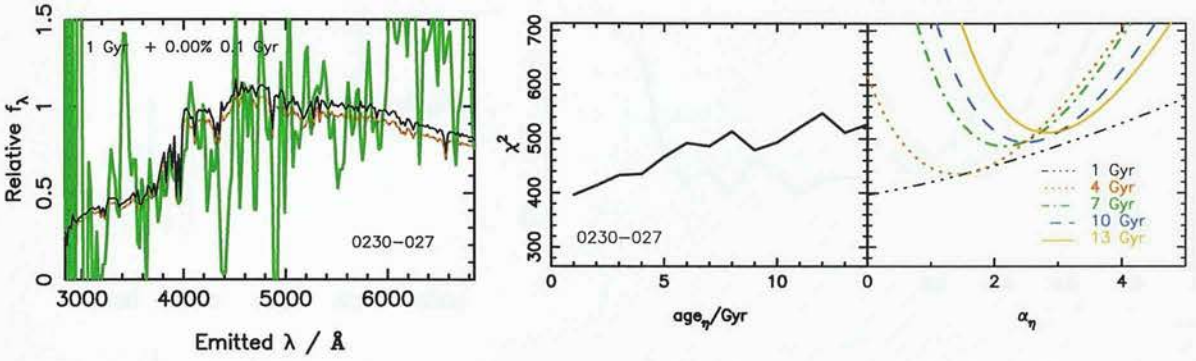

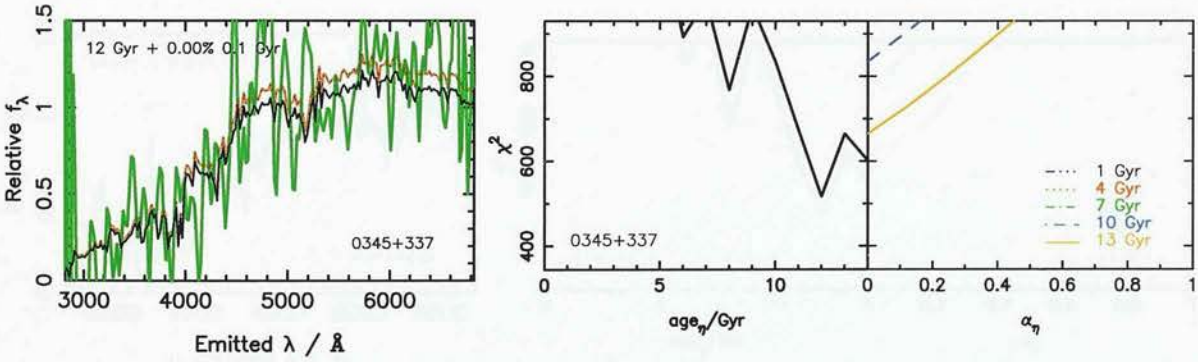

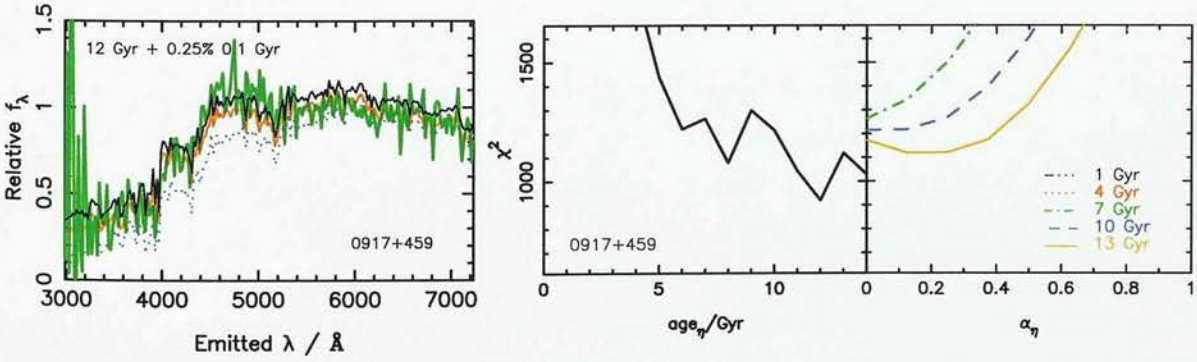

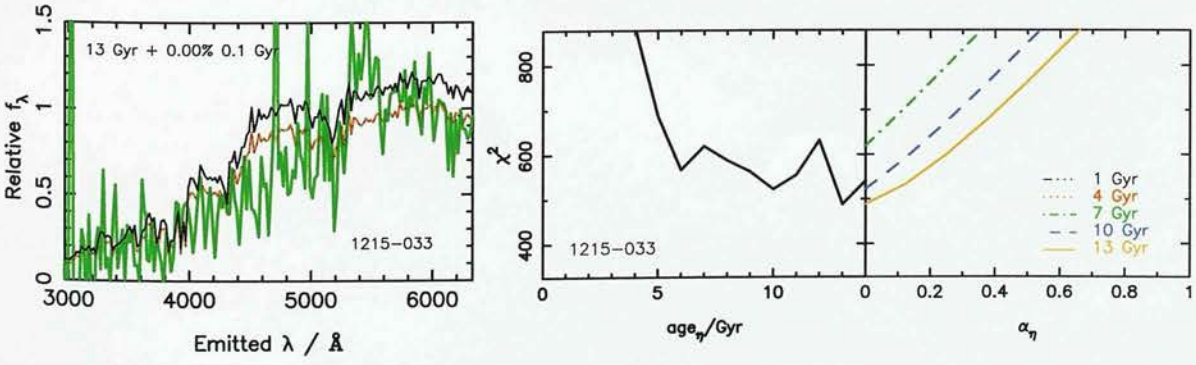

Radio Galaxies

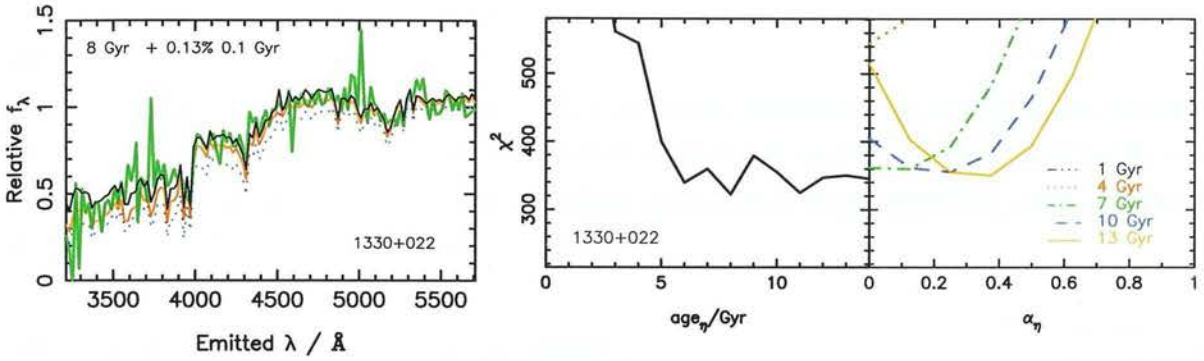

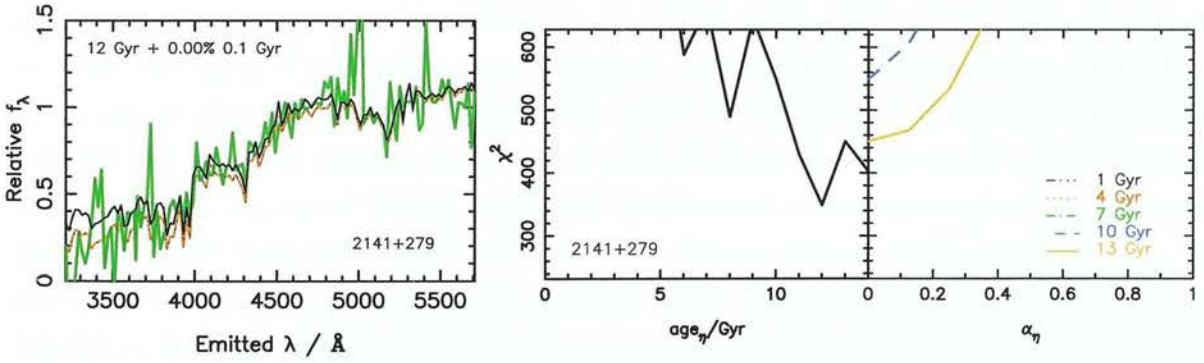

2.3.1 Notes on individual objects

Radio loud quasars

0137+012 (L1093) M4M

The models give a good fit at 13 Gyr, which is clearly improved by the inclusion of a small percentage (0.25%) of young stars. There is no significant nuclear contribution to the spectrum. HST imaging has shown that this host galaxy is a large elliptical, with a half-light radius $r_{1/2} = 13$ kpc (McLure et al., 1999).

0736+017 (S0736+01, OI061) M4M, WHT

0736+017 has been observed with both telescopes, and fits to the two observed spectra are in good agreement. Both indicate an age of 12 Gyr. The M4M spectrum requires a somewhat larger young blue population (0.75%) than the WHT spectrum (0.125%). This may be due to poorer seeing at Kitt Peak leading to slightly more nuclear contamination of the slit, or to the use of slightly different slit positions at the two telescopes. However, this difference between the observed spectra shortward of 4000 Å leaves the basic form of χ^2 versus age, and the best-fitting age of 12 Gyr unaffected. Inclusion of a nuclear component gives a much better fit to the blue end of the M4M spectrum, without changing the age estimation. The size of the fitted young populations are in much better agreement in this case. HST imaging has shown that morphologically this host galaxy is a large elliptical, with a half-light radius $r_{1/2} = 13$ kpc (McLure et al., 1999).

1004+130 (S1004+13, OL107.7, 4C13.41) WHT

The spectrum of this luminous quasar certainly appears to display significant nuclear contamination below the 4000 Å break. As a result a relatively large young population is required to attempt (not completely successfully) to reproduce the blue end of the spectrum . However, the models predict that the underlying stellar population is old (12 Gyr). Allowing a nuclear component to be fit reproduces the blue end of the spectrum much more successfully, without changing the best-fit age estimation. HST R-band imaging indicates the morphology of the host galaxy is dominated by a large ($r_{1/2} = 8$ kpc) spheroidal component, but subtraction of this best-fit model reveals two spiral-arm-type features on either side of the nucleus (McLure et al., 1999), which may be associated with the young stellar component required to explain the spectrum.

1020−103 (S1020−103, OL133) M4M
This object has the second bluest $R - K$ of this sample, which leads to a much younger inferred age than the majority of the rest of the sample (5 Gyr), despite the presence of a rather clear 4000 Å break in the optical spectrum. Ages greater than $\simeq$ 10 Gyr are rejected by Jimenez' models, primarily on the basis of $R - K$ colour. HST imaging has shown that this host has an elliptical morphology, and a half-light radius of $r_{1/2} = 7$ kpc. (Dunlop et al., 2001).

1217+023 (S1217+02, UM492) WHT
Nuclear contamination can again be seen bluewards of 4000 Å, with a correspondingly large young population prediction for the purely stellar population model, which still fails to account for the very steep rise towards 3000 Å. Hence, a large nuclear contribution is required to reproduce the blue end of the spectrum. The fit achieved by the models suggests that the dominant population is old, with a best-fit age of 12 Gyr. HST imaging has shown that this host has an elliptical morphology, and a half-light radius of $r_{1/2} = 11$ kpc. (Dunlop et al., 2001).

2135+147 (S2135−14, PHL1657) WHT
2135+147 has a very noisy spectrum, but a constrained fit has still been achieved, and an old population is preferred. 2135+147 requires a large α, even when a nuclear contribution is fitted. HST imaging has shown that this host has an elliptical morphology, and a half-light radius of $r_{1/2} = 12$ kpc. (Dunlop et al., 2001).

2141+175 (OX169) WHT
This is another noisy spectrum, which has a relatively large quasar light contribution. An old population is again indicated by the model fits. From optical and infrared imaging this object is known to be complex, but HST images indicate that it is dominated by a moderate sized ($r_{1/2} = 4$ kpc) elliptical component (see McLure et al. (1999) for further details).

2247+140 (PKS2247+14, 4C14.82) M4M, WHT
2247+140 has been observed with both telescopes. The model fitting indicates an old population is required by both spectra - although the two observations do not agree precisely, the general level of agreement is very good, the two χ^2 plots have a very similar form, and the difference in χ^2 between the alternative best-fitting ages of 8 Gyr and 12 Gyr is very small.

No significant nuclear contribution to the flux is present. HST imaging has shown that this host has an elliptical morphology, and a half-light radius of $r_{1/2} = 14$ kpc (Dunlop et al., 2001).

2349−014 (PKS2349−01, PB5564) WHT
This is a very good fit to a good-quality spectrum, showing an obvious improvement when the low-level young population is added. Jimenez' models clearly predict that the dominant population is old, with a well-constrained age of 12 Gyr. A very small nuclear contribution ($\eta = 0.050$) does not significantly change the results. HST imaging of this object strongly suggests that it is involved in a major interaction, with a massive tidal tail extending to the north of the galaxy. However, the dominant morphological component is a spheroid with a half-light radius of $r_{1/2} = 18$ kpc (McLure et al., 1999).

Radio quiet quasars

0054+144 (PHL909) M4M,WHT
There is evidence of relatively large contamination from nuclear emission in the spectrum of this luminous quasar taken on both telescopes, and the age is not well-constrained, although the fit to the WHT spectrum derived from the models again suggests an old age. The χ^2 plots serve to emphasize how similar the two spectra of this object actually are (as also discussed by Hughes et al., 2000). Inclusion of a nuclear component in the model better constrains the age and improves the goodness of the fit. HST imaging of this object has shown that, morphologically, it is undoubtedly an elliptical galaxy, with a half-light radius $r_{1/2} = 8$ kpc (McLure et al., 1999).

0157+001 (Mrk 1014) M4M,WHT
The age inferred from both the M4M and WHT spectrum of 0157+001 is again 12 Gyr. The apparently more nuclear-contaminated WHT spectrum does not give such a good fit, but 0157+001 is a complex object known to have extended regions of nebular emission, and the slit positions used for the two observations were not identical (Hughes et al., 2000). The age is much better constrained from the more passive M4M spectrum, to which Jimenez' models provide a very good fit. Again, it seems that the nuclear contamination does not have a great influence on the predicted age of the old population, although the fit to the WHT spectrum is greatly improved by including a nuclear component in the model. Despite

its apparent complexity in both ground-based and HST images, this host galaxy does again seem to be dominated by a large spheroidal component, of half-light radius $r_{1/2} = 8$ kpc (McLure et al., 1999).

0204+292 (3C59) WHT
Jimenez' models fit the spectrum of this object well, indicating an old underlying stellar population (> 6Gyr), with a best-fit age of 13 Gyr for the stellar population plus nuclear component model, and a very small young population. HST imaging has shown this galaxy to be an elliptical, with half-light radius $r_{1/2} = 9$ kpc (Dunlop et al., 2000).

0244+194 (MS 02448+19) WHT
The colour derived from the optical and infrared imaging of this host galaxy is rather blue ($(R-K)_{obs} = 2.34$) and this in part leads to a fairly young (5 Gyr) age prediction. However, the spectrum is very noisy, and, as indicated by the very flat χ^2 plot, the age is not strongly constrained. No nuclear flux contamination is fitted. HST imaging has shown this galaxy to have an elliptical morphology, with half-light radius $r_{1/2} = 9$ kpc (McLure et al., 1999).

0923+201 WHT
The spectrum of 0923+201 is noisy, and it also appears to have some nuclear contamination. The fit is therefore improved by inclusion of a nuclear component. An old age is strongly preferred by the form of the χ^2 / age plot, with a best-fit value of 12 Gyr. HST imaging has shown this galaxy to have an elliptical morphology, with half-light radius $r_{1/2} = 8$ kpc (McLure et al., 1999).

1549+203 (1E15498+203, LB906, MS 15498+20) WHT
This is a good fit, which is clearly improved by the addition of the younger population. The slope of the χ^2 / age plot strongly indicates an old dominant population, with a best-fit age of 12 Gyr. There is very little evidence of nuclear contamination. HST imaging has shown this galaxy to be a moderate-sized elliptical $r_{1/2} = 5$ kpc (Dunlop et al., 2001).

1635+119 (MC1635+119, MC2) WHT
This is another very successful fit. An old age (12 Gyr) is inferred. Again, HST imaging has shown this galaxy to be a moderate-sized elliptical $r_{1/2} = 6$ kpc (McLure et al., 1999).

Masked region / Å	Emission line
3720 – 3735	OII 3727
3860 – 3880	NeIII 3869
4840 – 5020	OIII 4959, OIII 5007, H_β 4861

Table 2.2: Rest frame emission lines masked out in the χ^2 fit.

2215−037 (MS 22152−03, EX2215−037) WHT
2215−037 has a noisy spectrum, to which an acceptable fit has nevertheless been possible. Jimenez' models suggest an old population, with a best-fitting age of 14 Gyr, but this age is not well constrained. This is the only object where the inclusion of a nuclear contribution to the fitted spectrum substantially changes the age predicted of the dominant stellar population. However, the χ^2 plots are very flat after an age of 5 Gyr, and the age is not strongly constrained in either case. HST imaging has shown this galaxy to have an elliptical morphology, with $r_{1/2} = 7$ kpc (Dunlop et al., 2000).

2344+184 (E2344+184) M4M,WHT
2344+184 has been observed with both telescopes, and the fits to both spectra are in good agreement – although, formally, two different ages are predicted. This is because the χ^2 / age plots are fairly flat after about 8 Gyr. The fits to both observations suggest an old dominant population, with a small young blue population improving the fit. There is no significant change in the predictions when a nuclear flux component is included in the model. HST imaging has shown this to be one of the few host galaxies in the current sample to be disc-dominated. However, the nuclear component is in fact sufficiently weak that this object should really be classified as a Seyfert galaxy rather than an RQQ (McLure et al., 1999).

Radio galaxies

0230−027 (PKS0230−027) WHT
0230−027 has a very noisy spectrum, and the colour of the host as derived from optical and infrared imaging is very blue ($(R-K)_{obs} = 2.09$). Consequently the best-fitting age derived using the models is 1 Gyr, with no younger component, but it is clear that little reliance can be placed on the accuracy of this result. Allowing for a contribution from quasar light does not improve the fit. HST imaging has shown this galaxy to have an elliptical morphology,

with $r_{1/2} = 8$ kpc (Dunlop et al., 2001).

0345+337 (3C93.1) WHT
0345+337 requires no young component or nuclear flux contribution at all, and an old age, of 12 Gyr, is clearly indicated by the models. HST imaging has shown this galaxy to be a large elliptical, with $r_{1/2} = 13$ kpc (Dunlop et al., 2001).

0917+459 (3C219, 3C219.0) WHT
This is an excellent fit, with an old age produced by the models (12 Gyr), together with a very small young population. HST imaging has shown this galaxy to be a large elliptical, with $r_{1/2} = 22$ kpc (Dunlop et al., 2001).

1215−033 WHT
Jimenez' models suggest that the population of 1215−033 is universally old (best-fit age, 13 Gyr), with no young component or nuclear contribution required. HST imaging has shown this galaxy to be a large elliptical, with $r_{1/2} = 9$ kpc (Dunlop et al., 2001).

1330+022 (3C287.1) M4M
An excellent fit to the data is produced by Jimenez' models, indicating that the dominant population is old, with a best-fit age of 8 Gyr. HST imaging has shown this galaxy to be a large elliptical, with $r_{1/2} = 16$ kpc (Dunlop et al., 2001).

2141+279 (3C436) M4M,WHT
This is another very successful, and well-constrained fit, with an inferred age of 12 Gyr. HST imaging has shown this galaxy to be a large elliptical, with $r_{1/2} = 21$ kpc (McLure et al., 1999).

2.3.2 Sample overview

The results illustrated in Figures 2.1 and 2.2 are summarised in Table 2.3. It should be noted that the 4000 Å break typical of evolved stellar populations is present in the majority of the observed spectra (see Figures 2.1 and 2.2, and Hughes et al., 2000), so we can be confident

in fitting stellar population models to the data. The plots clearly show that the addition of even a very small amount of secondary star formation to the simple, near-instantaneous star-burst models reproduces the blue end of the observed host galaxy spectra much more successfully (and in most cases very well) than does a single stellar population. Including a nuclear component further improves the fit to the blue end, especially for those spectra not well fit by purely stellar light. At the same time, the red end of the spectra, plus the observed $R - K$ colours generally require that the underlying stellar populations are old.

The most meaningful output from the model fitting is a constraint on the minimum age of the host galaxies, as listed in Table 2.3. Although the χ^2 plots show that often the best-fit age is not strongly constrained but the trend is clearly towards old ($\geq$ 8 Gyr) stellar populations. In general, young populations are strongly excluded.

The relatively poor quality of the fits ($\chi^2_\nu > 1.5$, see Table 2.3) is most likely a result of the simplifications used in modelling the spectra, i.e. the use of the same template nuclear spectrum for every host galaxy, fixing the age of the younger population at 0.1 Gyr for every galaxy, and the assumption that the host galaxies consist of two, simple, instantaneous starbust stellar populations. However, a more sophisticated treatment of the modelling would not be expected to significantly change the general result that the dominant populations in these host galaxies are old, as young stellar populations are in most cases strongly rejected.

The peaks and troughs in χ^2 as a function of model age appear to be the result of real features of the population evolution synthesis, rather than being due to, for example, poor sampling (Jimenez, private communication).

IAU name	Telescope	Best fit age/Gyr	Best fit age_η/Gyr	99.99% lower age limit/ Gyr	99.99% lower $age\,limit_\eta$/ Gyr	α	α_η	Reduced χ^2	Reduced $\chi^2{}_\eta$	$(R-K)_{fit}$	$(R-K)_{fit_\eta}$	$(R-K)_{obs}$	η	z
Radio-loud quasars														
0137+012	M4M	13	13	6.0	12.8	0.2	0.3	3.7	3.6	2.88	2.88	2.82	0.025	0.258
0736+017	M4M	12	12	11.8	11.8	0.7	0.1	12.0	6.2	2.69	2.89	3.16	0.250	0.191
	WHT	12	12	11.8	11.9	0.1	0.0	3.3	2.9	2.89	2.93		0.100	
1004+130	WHT	12	12	11.9	11.1	1.4	0.4	5.4	2.2	2.65	2.96	3.01	0.350	0.240
1020−103	M4M	5	4	2.7	2.7	0.6	0.0	1.7	1.5	2.33	2.29	2.29	0.125	0.197
1217+023	WHT	12	12	11.9	11.6	1.1	0.0	11.8	4.9	2.71	3.10	3.18	0.350	0.240
2135−147	WHT	12	11	7.7	4.9	1.6	1.0	2.2	2.2	2.50	2.50	2.49	0.175	0.200
2141+175	WHT	12	14	11.2	5.6	1.1	0.5	3.2	2.5	2.66	2.69	2.69	0.500	0.213
2247+140	M4M	8	8	7.6	7.6	0.3	0.3	1.8	1.8	2.77	2.77	2.81	0.000	0.237
	WHT	12	12	11.0	8.0	0.9	0.9	2.9	2.9	2.79	2.79		0.000	
2349−014	WHT	12	12	11.8	11.7	0.5	0.4	3.3	3.0	2.71	2.75	2.87	0.050	0.173
Radio-quiet quasars														
0054+144	M4M	8	12	7.9	11.2	1.3	0.3	46.9	9.1	2.32	2.78	3.12	0.400	0.171
	WHT	12	12	11.9	11.9	1.3	0.0	17.7	3.6	2.51	2.86		0.475	
0157+001	M4M	12	12	11.9	11.9	1.1	1.1	5.9	5.8	2.52	2.52	2.83	0.025	0.164
	WHT	12	12	11.9	11.8	1.6	0.9	41.0	10.9	2.41	2.58		0.250	
0204+292	WHT	14	13	13.7	11.0	0.2	0.1	6.3	5.4	2.47	2.45	2.49	0.125	0.109
0244+194	WHT	5	5	4.4	4.4	0.1	0.1	2.6	2.6	2.37	2.37	2.34	0.000	0.176
0923+201	WHT	12	12	11.9	11.9	0.6	0.0	5.6	4.0	2.72	2.92	3.24	0.375	0.190
1549+203	WHT	12	12	11.9	11.9	0.6	0.5	3.8	3.8	2.90	2.95	3.37	0.050	0.250
1635+119	WHT	12	12	11.9	11.9	0.7	0.5	6.7	6.4	2.57	2.63	3.27	0.100	0.146
2215−037	WHT	14	6	5.7	5.0	0.6	0.3	2.4	2.4	2.70	2.69	2.68	0.175	0.241
2344+184	M4M	8	11	7.7	7.8	0.4	0.4	4.8	4.9	2.43	2.57	2.51	0.025	0.138
	WHT	12	12	11.2	7.8	0.9	0.8	2.1	2.0	2.51	2.54		0.075	
Radio galaxies														
0230−027	WHT	1	1	1	1	0.0	0.0	2.0	2.0	2.02	2.02	2.08	0.000	0.230
0345+337	WHT	12	12	11.9	11.9	0.0	0.0	2.7	2.7	3.13	3.13	3.62	0.000	0.244
0917+459	WHT	12	12	11.9	11.9	0.2	0.3	4.7	4.6	2.79	2.79	3.42	0.025	0.174
1215−033	WHT	13	13	12.9	12.9	0.0	0.0	3.4	3.4	2.74	2.74	2.56	0.000	0.184
1330+022	M4M	8	8	7.7	7.6	0.3	0.1	2.9	2.8	2.70	2.74	2.79	0.050	0.215
2141+279	M4M	12	12	11.8	11.8	0.1	0.0	3.1	2.5	3.27	3.01	3.25	0.025	0.215

Table 2.3: Results from the simultaneous fitting to the AGN host sample of the two-component model spectra (using the solar metallicity models of Jimenez et al., 2001) and $R-K$ colour. α is the percentage young population, by mass. Results are also presented for the fits including the subtraction of a nuclear component from the observed spectrum. η is the fraction of nuclear flux subtracted, and the corresponding results are denoted by the subscript η.

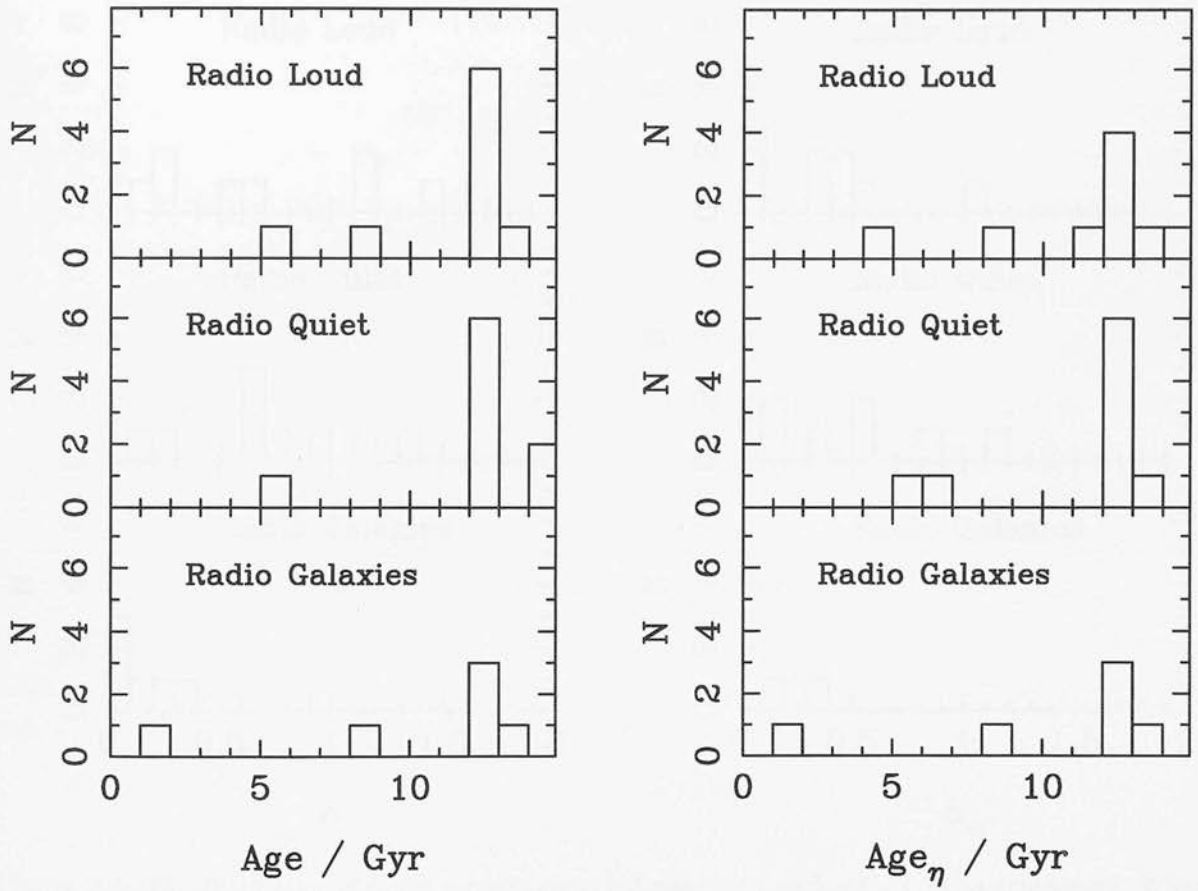

Figure 2.3: The age distribution of the dominant stellar populations of the sample host galaxies. These are the best-fitting results from Jimenez' solar metallicity models. On the left, results are shown for the fits to the data using a two-component model. The results on the right are those for the two-component model plus a nuclear contribution. The populations are predominantly old (12-14 Gyr) in both cases.

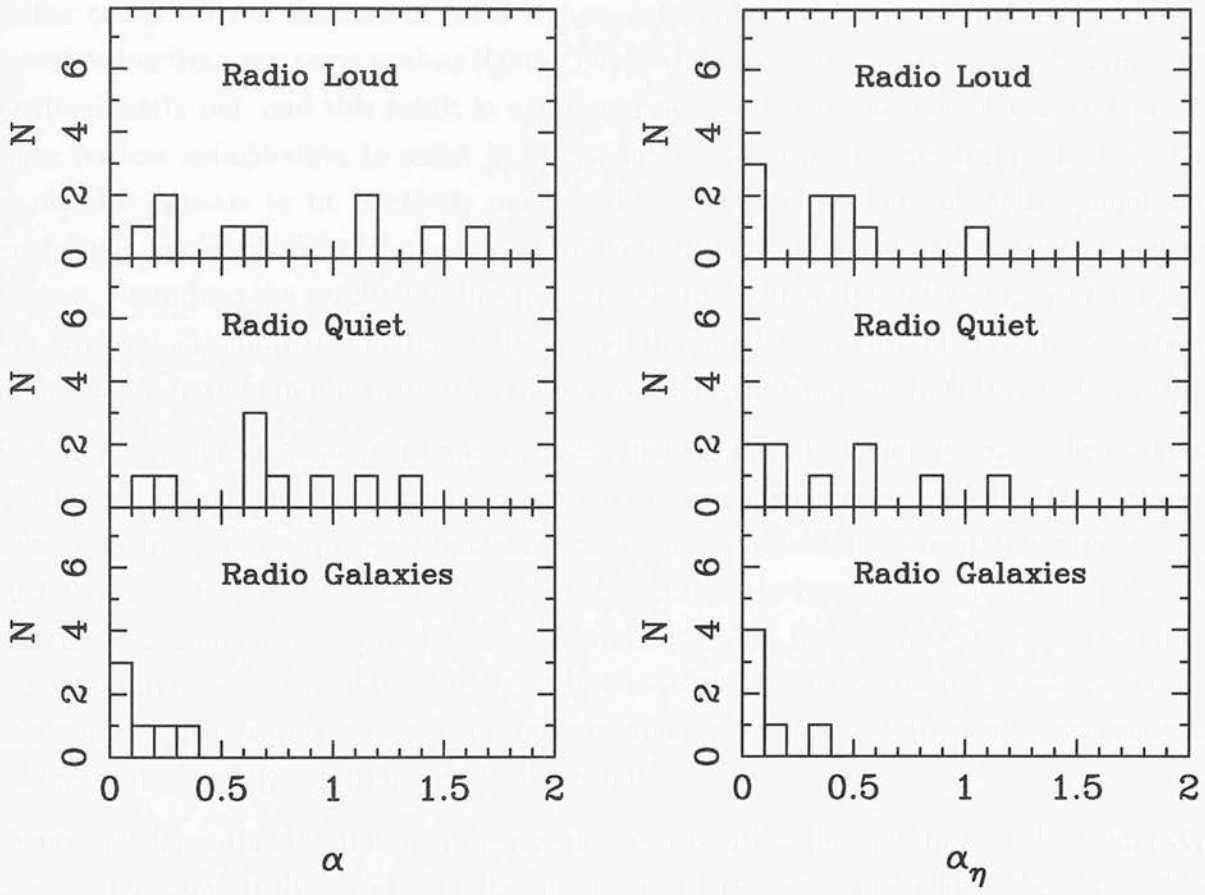

Figure 2.4: The distribution of α, the percentage contribution (by mass) of the 0.1 Gyr component. Where results have been obtained from two spectra for one object, the best-fitting result has been adopted. Again, the results on the left are for fits using the two-component model, and those on the right are for fits with the two-component model plus a nuclear contribution. Allowing for the possibility of a nuclear contribution means that a smaller α is required to fit the blue end of the spectrum, and the apparent difference between the radio galaxies and radio-loud and quiet quasars is reduced to a statistically insignificant level.

2.4 Discussion

Figure 2.3 shows the distribution of best-fit ages estimated using Jimenez' models. The left-hand panel shows the ages of the dominant stellar component which result from fitting the two-component (stars only) model, while the right-hand panel shows the ages of the dominant stellar component in the case of the 3 component model (i.e. two stellar components + a contribution from scattered nuclear light). The host galaxies of the AGN in each sample are predominantly old, and this result is unaffected by whether or not one chooses to include some nuclear contribution to assist in fitting the blue end of the spectrum. This general result also appears to be relatively unaffected by the precise choice of stellar population model; the models of Bruzual and Charlot (2001), fitted to the host galaxies with the same process, reproduce the results for Jimenez' models to within a typical accuracy of 1-3 Gyr. We have not attempted to fit the stellar population models of Yi et al. (2000), because of problems we have found in their MS rate of evolution (see Chapter 3, Nolan et al., 2001a).

Inclusion of a nuclear contribution in the 3-component models obviously raises the question of whether a young stellar population component is really necessary at all. Thus, the results of fitting a two-component model consisting of a single stellar population plus nuclear contribution were also explored. Such a model adequately reproduces the two-population-plus-nuclear-component results for the *redder* galaxies, but in fact the spectra of the bluest galaxies cannot be adequately reproduced by these models; the resulting serious increase in minimum χ^2 demonstrates that inclusion of a young population component is necessary to achieve a statistically acceptable fit to these data.

Figure 2.4 shows the distribution of percentage contribution (by mass), α, of the young (0.1 Gyr) component to the spectra of the hosts. The left-hand panel shows the values of α as derived from fitting the two-component (stars only) model, while the right-hand panel shows the values of α produced by the 3 component model (i.e. two stellar components + a contribution from scattered nuclear light).

Where two spectra of the same object have been obtained with alternative telescopes / instruments, the derived ages of the dominant stellar components are reproduced reassuringly well. There are, however, small discrepancies in the estimated percentage of young population present (see Table 2.3). This effect is suggestive that at least some of the blue light might be due to a scattered nuclear contribution, the strength of which would be highly dependent on the seeing at the time of observation, and on the precise repeatability of slit placement relative to the galaxy core. Interestingly, when a nuclear component is included with the stellar flux model, an even smaller percentage of 0.1 Gyr stellar population is re-

quired to fit the blue end of the spectra, and (more importantly) the difference in α between two spectra of the same object is generally reduced. This provides further support for the suggestion that some of the bluest quasar host spectra remain contaminated by quasar light at the shortest wavelengths, and indicates that the right-hand panel of Figure 2.4 provides a more realistic estimate of the level of on-going star-formation in the host galaxies. While this figure still appears to suggest that at least some quasar hosts display higher levels of ongoing star-formation activity than do radio galaxies, statistically this 'result' is not significant.

There are three galaxies which have very low age estimates, namely 0230−027, 0244+1944 and 1020−103. These objects have the bluest observed $R-K$ colours, so it may be expected that the fitted ages would be younger than the rest of the sample, and that these populations are genuinely young. As discussed above, it may be that these objects are bluer because of scattered nuclear light contaminating the host galaxy spectrum. However, it seems unlikely that their fitted ages are low simply because of this, because elsewhere in our sample, where two spectra have been obtained of the same object, the amount of nuclear contamination present does not significantly affect the age estimation (e.g. 0736+017 and 0157+001). Moreover, the inclusion of a nuclear component to the fit does not change the estimated age distribution of the host galaxies. If these ages are in error, then a more likely explanation, supported by the relative compactness of these particular host galaxies, is that nuclear and host contributions have been imperfectly separated in the K-band images, leading to an under-estimate of the near-infrared luminosity of the host. It should also be noted that, in this work, only solar metallicity models are considered. It is possible that a sub-solar metallicity model would provide a better fit at an older age.

The result of the three-component fitting process which also allows a contribution from scattered nuclear light is that there are in fact only 3 host galaxies in the sample for which there is evidence that $\alpha > 0.5$. One of these is the host of a radio-loud quasar (2135−147) but, as can be seen from Fig 4, this spectrum is one of the poorest (along with 0230−027, the only apparently young radio galaxy) in the entire dataset. The 2 convincing cases are both the hosts of radio-quiet quasars, namely 0157+001 and 2344+184.

Within the somewhat larger sample of 13 RQQs imaged with the HST by McLure et al. (1999) and Dunlop et al. (2001), 4 objects showed evidence for a disk component in addition to a bulge, namely 0052+251, 0157+001, 0257+024, and 2344+184. Since we do not possess spectra of 0052+251 and 0257+024 this means that there is a 1:1 correspondence between the objects identified on the basis of this spectroscopic study as having recent star-formation activity, and those which would be highlighted on the basis of HST imaging as possessing a significant disk component. This straightforward match clearly provides us with considerable

confidence that the spectral decomposition attempted here has been effective and robust. Finally, it should be noted that Canalizo & Stockton (2000), find evidence that 0157+001, which has the largest starburst component ($\alpha = 1.1$) based on this spectroscopic analysis, has recently undergone a strong interaction or merging event, which one would expect to give rise to an episode of star formation.

2.5 Conclusion

It may be concluded that the hosts of all three major classes of AGN contain predominantly old stellar populations ($\simeq$ 11 Gyr) by z $\simeq$ 0.2. This agrees well with the results of McLure et al. (1999), and Dunlop et al. (2001) who compare host galaxy morphologies, luminosities, scale lengths and colours in the same sample, and conclude that the hosts are, to first order, indistinguishable from 'normal' quiescent giant elliptical galaxies.

The best-fitting age of the dominant stellar population is *not* a function of AGN class. For the purely stellar models, the fitted percentage contribution of the blue component is, however, greater in the quasar hosts than in the radio galaxies; the median values are 0.6% for the 9 radio-loud quasars, 0.6% for the 9 radio-quiet quasars, and 0.05% for the 6 radio galaxies. However, when a nuclear component is included, the median values are 0.3% for the radio-loud quasars, 0.3% for the radio-quiet quasars, and 0.00% for the radio galaxies. Performing a Kolmogorov-Smirnov test on these results yields a probability greater than 0.2 that the percentage of young stellar population in host galaxies is in fact also not a function of AGN class.

These results strongly support the conclusion that the host galaxies of all three major classes of AGN are massive ellipticals, dominated by old stellar populations.

In the next chapter, the high-resolution spectra of two z $\simeq$ 1.5 mJy radio galaxies, LBDS 53W069 and 53W091 are investigated. The higher signal-to-noise data, together with the expectation that the stellar populations of these high-redshift galaxies are approximately coeval, allow a more detailed comparison of the ability of the stellar population models of different authors to reproduce real galaxy spectra than is possible with the lower signal-to-noise spectra presented in this chapter.

Chapter 3

The Sun, stellar-population models, and the age estimation of high-redshift galaxies

3.1 Introduction

In Chapter 2, the spectra of low-redshift host galaxies were studied. Here, the investigation proceeds to the high-resolution spectra of two $z \simeq 1.5$ mJy radio galaxies, LBDS 53W069 and 53W091. At such a redshift, the stellar populations of these red galaxies are expected to be approximately coeval, as a result of the time constraints imposed by the relative youth of the Universe at this epoch. This allows a more detailed comparison of the ability of the single stellar population models of different authors to reproduce real galaxy spectra than is possible with the lower signal-to-noise spectra of potentially more complex stellar systems presented in the preceeding chapter.

Astronomers have attempted to estimate the ages of high-redshift galaxies using broad-band optical-infrared photometry for over a decade now (e.g. Lilly 1988; Dunlop et al. 1989, Chambers & Charlot 1990). Unfortunately, however, the derived ages have been rendered virtually meaningless by disagreements between modellers over post main-sequence evolution (e.g. Charlot, Worthey & Bressan 1996), and by the extreme susceptibility of such relatively crude broad-band data to dust reddening, emission-line contamination etc.

In contrast, it has long been anticipated that relatively robust age constraints for high-redshift galaxies could be derived given rest-frame near-ultraviolet spectra of sufficient quality. This is because, for the potential ages of interest at z > 1 (i.e. ages < 5 Gyr), the ultraviolet light of a stellar population is expected to be dominated by stars close to the turn-off point of the 'well-understood' main sequence (MS) (*e.g.* Magris & Bruzual 1993).

With the advent of deep optical spectroscopy on 10-m class telescopes, it has now proved possible to put this technique into practice. In particular, Dunlop et al. (1996) were able to use a deep Keck spectrum of the z = 1.5 radio galaxy LBDS 53W091 to first confirm that its near-ultraviolet spectrum was indeed dominated by starlight, and then to extract an age constraint of > 3 Gyr based primarily on comparison with a main-sequence only model of an evolving stellar population. Spinrad et al. (1997) explored further the reliability of this age estimate, and confirmed that the best agreement between ages derived using alternative evolutionary synthesis models was obtained if fitting was confined to the detailed shape of the near-ultraviolet spectral energy distribution.

Not surprisingly, given its implications for cosmology (for $H_0 = 70 \mathrm{kms}^{-1}\mathrm{Mpc}^{-1}$, the age of an Einstein-de Sitter universe at $z = 1.5$ is only 2.3 Gyr), this result has been the subject of subsequent close scrutiny, and claims that 53W091 is in fact less than 2 Gyr old have been put forward by, for example, Bruzual & Magris (1997). However, Dunlop (1999) has argued that such young ages are only deduced using some models if the near-infrared photometry is also included in the fitting process, once again placing undesirable emphasis on the reliability of the modelling of post main-sequence evolution (a point previously also explored by Spinrad et al. 1997). Moreover, Dunlop (1999) has shown that, certainly for the slightly redder, z = 1.43 galaxy, 53W069, if fitting is confined to the Keck spectroscopic data (Dey et al. 2001), the models of Bruzual & Charlot (1993), Worthey (1994), and Jimenez et al. (2001) *all* lead to the conclusion that its stellar population is > 3 Gyr old (assuming solar metallicity).

Most recently, however, the reliability of even this near-ultraviolet spectroscopic age-dating has been called into question by Yi et al. (2000). Yi et al. (2000), claim to have derived a much younger age for 53W091, but also claim that this age is not due to differences in post-MS evolution, but rather to the fact that the spectrum produced by the main sequence in their models reddens much more rapidly than in the models of Jimenez et al. (2001). In support of their revised age estimates, Yi et al. cite the fact that their models can reproduce the spectrum of the Sun at an age of 5 Gyr, whereas the solar spectrum is not reproduced by the Jimenez et al. models until 8-10 Gyr. However, it is not clear why a stellar population should be expected to mimic the spectrum of the Sun at its current age ($\simeq$ 5 Gyr); even if the light from the stellar population is dominated by stars near the main-sequence turnoff

the Sun is not expected to leave the main sequence until an age of $\simeq$ 10 Gyr (Jorgensen 1991). Nevertheless, this claim has motivated an explicit check on the calibration of the main-sequence evolution of different evolutionary synthesis models of galaxy evolution.

The relatively low quality spectra of the $z \simeq 0.2$ AGN host galaxies of Chapter 1 did not allow a credible comparison of the model spectra of different authors. However, the high signal-to-noise data of the two high-redshift radio galaxies, together with the solar spectrum, allows this comparison to be undertaken. This is the main subject of this chapter. Three alternative and independent models of galaxy evolution, developed by Yi et al. (2000), Jimenez et al. (2001) and Worthey (1994), are investigated with respect to how rapidly they evolve to mimic the solar spectrum with and (more importantly) without inclusion of their post-MS components. The models are summarized in section 3.2, and the results of the comparison with the solar near-ultraviolet spectrum are presented in section 3.3. In section 3.4, these models are used (again with and without post-MS components) to check explicitly the extent to which the age estimates of 53W091 and 53W069 really are affected by different approaches to modelling post-MS evolution. The main remaining uncertainty is the impact of having to assume a value for the metallicity of the stellar population, and section 3.5 contains an exploration of whether, given near-ultraviolet data of sufficient quality, it may be possible to break the well-known age-metallicity degeneracy. Finally, the conclusions are summarized in section 3.6.

3.2 The models

3.2.1 The models

This study was motivated by the apparent disagreement reported by Yi et al. (2000) between their own models and those of Jimenez et al. (2001). The comparison of these models is possible because Sukyoung Yi has kindly provided his model SEDs up to an age of 5 Gyr (Yi, private communication). The predictions of a third, independent set of evolutionary synthesis models, are also compared; these are the models of Worthey (1994). The reason for this choice was that it is already known, from previous modelling of 53W091 (Dunlop et al. 1996, Spinrad et al. 1997), that the models of Worthey (1994) also appear to yield younger ages than those of Jimenez et al. (2001), but for reasons which were suspected to be due primarily to a different treatment of post-MS evolution (see Charlot et al. 1996).

Since the primary objective in this chapter is to check the calibration of MS evolution using

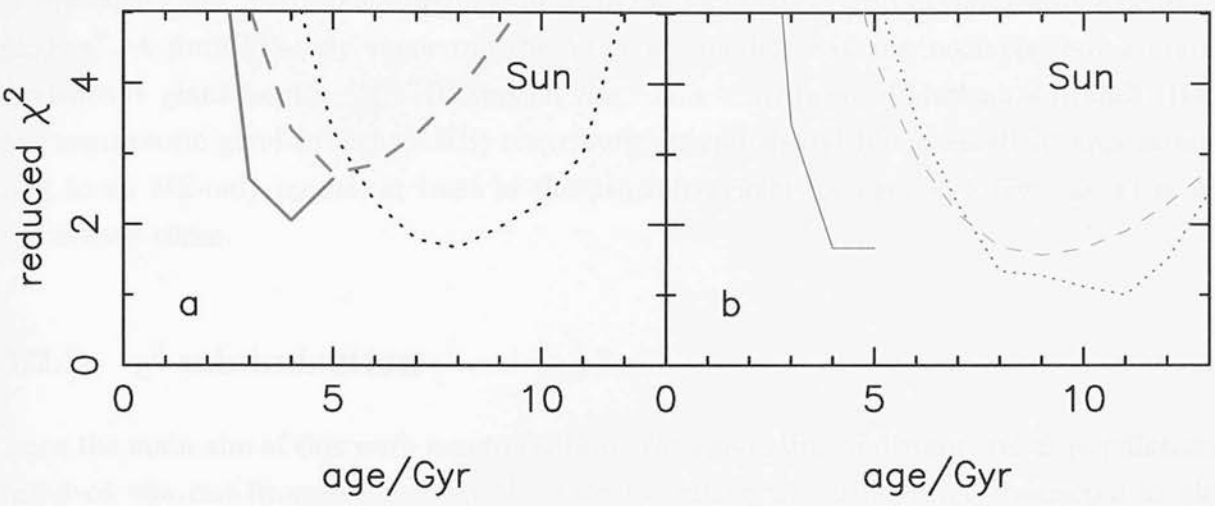

Figure 3.1: Reduced χ^2 as a function of age for the six different solar metallicity stellar population models fitted to the solar spectrum. On the left-hand panel are the results for the full stellar population models, and on the right-hand side are those for Worthey and Jimenez et al. main sequence (MS) only models and Yi et al. main sequence plus red giant branch (MSGB) models. Solid lines - Yi et al. (2000): dashed lines - Worthey (1994): dotted lines - Jimenez et al. (2001). The MS / MSGB models result in a better fit than the full models. The best-fit age of Yi et al.'s MSGB models differ from the best-fit ages of both Worthey's and Jimenez et al.'s MS only models by a factor of order two, implying a MS-turnoff age for the Sun of only 4-5 Gyr, compared with 9 or 11 Gyr implied by the MS-only models of Worthey and Jimenez et al. respectively.

the Sun, attention is confined to models which assume solar metallicity. However, it *is* important to remove any potential confusion introduced by different treatments of post-MS evolution, because it is hard to be sure that the UV spectrum of an instantaneous starburst really is completely dominated by MS stars in all the models beyond an age of 2-3 Gyr (and beyond 5 Gyr it is not expected to be).

This is because, although at young ages most stars have not yet evolved beyond the MS, and consequently post-MS evolutionary stages contribute only a small fraction to the integrated UV flux, at ages greater than a few gigayears, this is no longer true. However, MSTO stars occupy the highest luminosity and effective temperature point of the main sequence. They are, therefore, the hottest and brightest group of stars in a young stellar population and are expected to dominate the integrated UV flux of young populations, and also the integrated UV flux of any single-aged MS-only population.

Therefore, an MS-only version of the models of Jimenez et al. (2001) was constructed, together with an MS-only version of the models of Worthey (1994) (Worthey, private communication). In both the Jimenez and the Worthey models the isochrones have been cut off

at the same point (corresponding to point 55 in the Vandenberg grid in the case of Worthey's models). A pure MS-only version of the Yi et al. models was not available, but a main-sequence + giant branch (MSGB) version was. This is stripped of horizontal branch (HB) and asymptotic giant branch (AGB) contributions, and should be an excellent approximation to an MS-only model, at least in the near-ultraviolet for ages < 5 Gyr, as Yi et al. themselves claim.

3.2.2 χ^2 minimization

Since the main aim of this work was to calibrate the age-dating of distant stellar populations based on the rest-frame near-ultraviolet spectra, fitting was deliberately restricted to the spectral range $2000 - 4000$ Å. The best fit was determined by binning the data to the same spectral resolution as the model in question, and then varying the age and normalization as free parameters until χ^2 was minimized.

For the high-redshift galaxies 53W091 and 53W069, the error on each binned spectral data point was derived from propagation of the original errors in the Keck optical spectra (see Dunlop et al. 1996; Dey et al. 2001). In the case of the Sun, the theoretical spectrum of Kurucz is used, as the best available representation of the true solar SED, and a constant flux-density error is assumed (i.e. independent of wavelength), adjusted in size until reduced chi-squared (χ^2_ν) equalled unity for the very best fitting model. It is thus only possible to compare the relative (rather than absolute) ability of the different models to reproduce the solar ultraviolet spectrum as the age of each model is varied.

3.3 Comparison with the solar spectrum

3.3.1 Full models

Figure 3.1a presents reduced χ^2 as a function of age for each of the full stellar population models when age is varied in an attempt to best reproduce the solar spectrum. The models of Yi et al. predict the youngest age, indicating that the near-ultraviolet spectrum produced by these models best mimics that of the sun after an age of only 4 Gyr. The models of Worthey yield a best-fit age of 5 Gyr, while those of Jimenez et al. predict an age of 8 Gyr. From this plot it might appear that it is the models of Jimenez et al. that are most

unusual, but it is important to note that i) it is the models of Jimenez et al. which yield the best quality of fit to the solar spectrum, and ii) it is to be expected that the full stellar population models will *underestimate* the main-sequence turn-off (MSTO) age of the sun, because of the inclusion of post-MS stars. Moreover, from this plot it is completely unclear how much of the (substantial) difference between the derived best-fit ages can be attributed to differing contributions of post-MS stars to the model stellar population ultraviolet SEDs.

3.3.2 Main-sequence only models

For a meaningful comparison between stellar population synthesis models and the expected MS turn-off age of the sun, it should be ensured that the ultraviolet spectra produced by the models are completely MS dominated. Therefore, in Figure 3.1b, reduced χ^2 as a function of age is presented in an analogous way to Figure 3.1a, but this time using models, stripped as far as possible of post-MS contributions. This allows not only a sensible comparison with the Sun, but also makes it possible to assess the relative impact of post-MS contributions to the full model fits shown in Figure 3.1a.

This plot makes it clear that it is the models of Yi et al. that are unusual, and apparently in error by a factor of two in terms of rate of MS evolution. Stripped of HB and AGB contributions the predictions of the Yi et al. models are little changed, indicating a best-fit age of 4-5 Gyr. In contrast, stripped of post-MS evolution the models of Worthey and Jimenez et al. appear to be in good agreement not only with each other (9 Gyr and 11 Gyr respectively) but also with the generally accepted MS turnoff age of the Sun (10.5 Gyr - Jorgensen 1991).

It is hard to assess the likely impact on the predictions of the Yi et al. models if the GB was also removed, but the lack of any dramatic change upon removal of HB and AGB contributions does tend to support their own claim that their models are already highly MS dominated at ages < 5 Gyr. In contrast the contribution of post-MS stars in the models of Worthey must be relatively strong, even at 5 Gyr, because removal of HB + AGB moves the derived age from 5 to 7 Gyr, and subsequent removal of remaining post-MS stars completes the shift to 9 Gyr as shown in Figure 3.1b. This therefore backs up the suggestion made in Jimenez et al. (2001) that the main difference between the models of Jimenez et al. and Worthey lies in the strength of the AGB and RGB, but that the MS evolution in both models is very similar, and yields sensible values for the turn-off age of the Sun.

These results are tabulated in Table 3.1, and in Figure 3.2, the best-fit model spectra su-

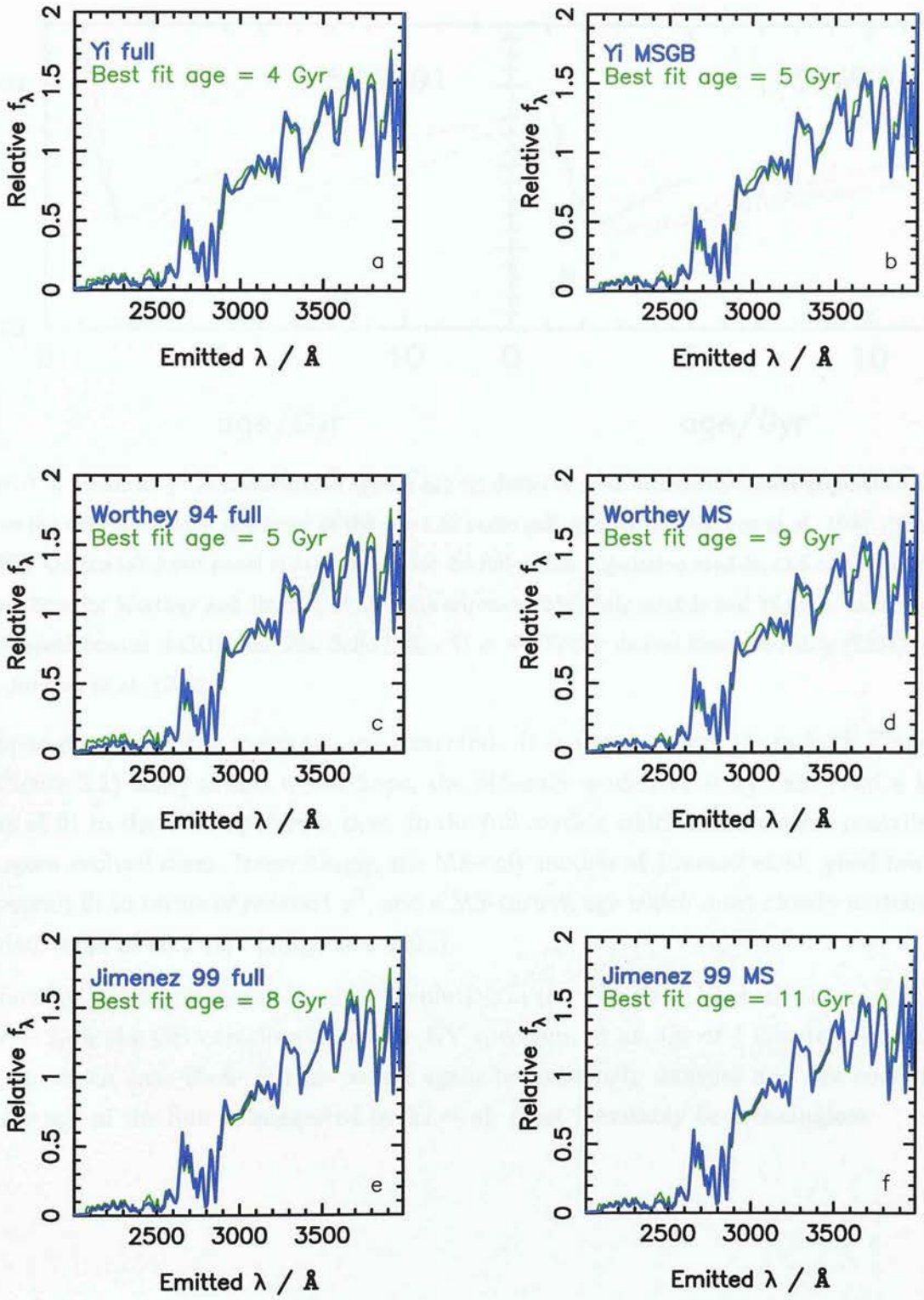

Figure 3.2: Best fits to the solar spectrum (blue lines) for the various solar metallicity models (green lines).

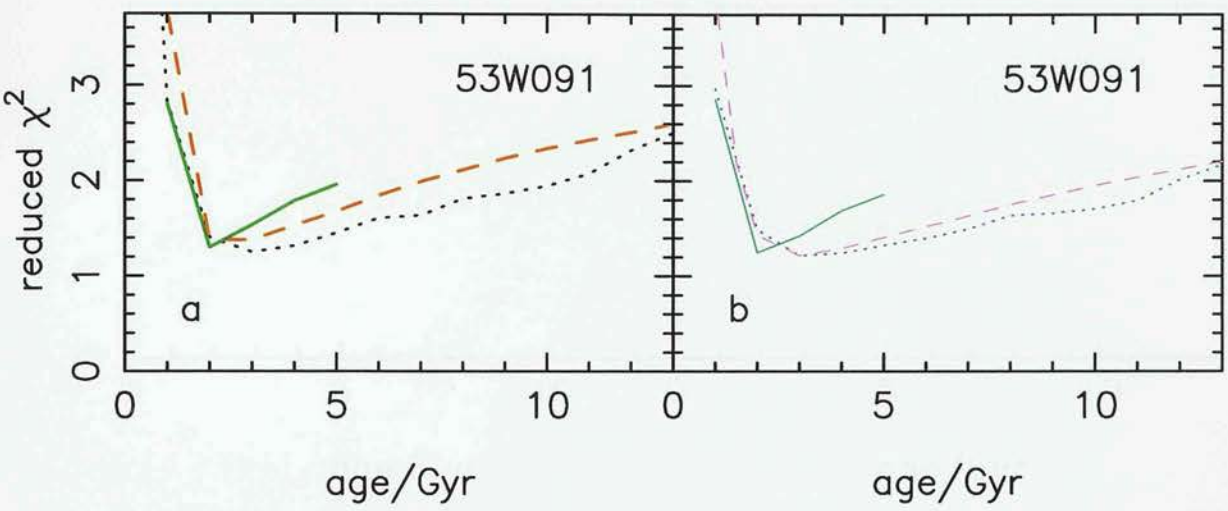

Figure 3.3: Reduced χ^2 as a function of age for the six different solar metallicity stellar population models fitted to the near-ultraviolet spectrum of the z = 1.55 radio galaxy 53W091 (Dunlop et al. 1996; Spinrad et al. 1997). On the left-hand panel are the results for the full stellar population models, and on the right-hand side are those for Worthey and Jimenez et al. main sequence (MS) only models and Yi et al. main sequence plus red giant branch (MSGB) models. Solid lines - Yi et al. (2000): dashed lines - Worthey (1994): dotted lines - Jimenez et al. (2001).

perimposed on the solar spectrum are presented. It is worth noting (from both Figure 3.2 and Figure 3.1) that, as one would hope, the MS-only models in every case yield a better *quality* of fit to the solar spectrum than do the full models which include some contribution from more evolved stars. Interestingly, the MS-only models of Jimenez et al. yield both the best overall fit in terms of reduced χ^2, and a MS-turnoff age which most closely matches the accepted value of 10.5 Gyr (Jorgensen 1991).

In summary, either the timescale of MS evolution in the models of Yi et al. is too short by a factor $\simeq 2$, or the GB contribution to the UV spectrum at an age of 4 Gyr is unexpectedly large, in which case these models would again be extremely unusual and the comparison with the age of the Sun as suggested by Yi et al. must inevitably be meaningless.

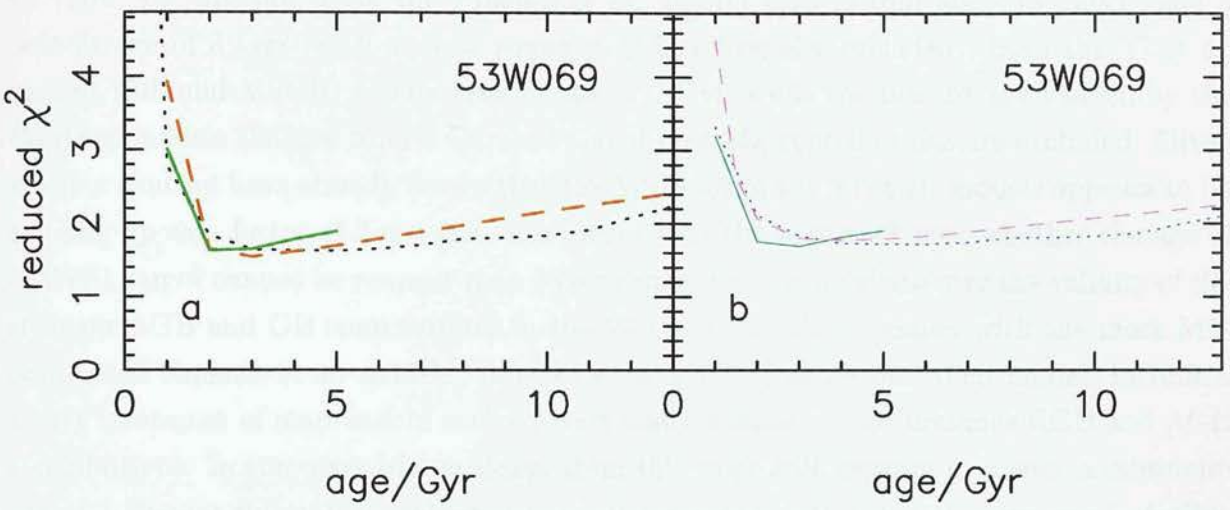

Figure 3.4: Reduced χ^2 as a function of age for the six different solar metallicity stellar population models fitted to the near-ultraviolet spectrum of the z = 1.43 radio galaxy 53W069 (Dunlop 1999; Dey et al. 2001). On the left-hand panel are the results for the full stellar population models, and on the right-hand side are those for Worthey and Jimenez et al. main sequence (MS) only models and Yi et al. main sequence plus red giant branch (MSGB) models. Solid lines - Yi et al. (2000): dashed lines - Worthey (1994): dotted lines - Jimenez et al. (2001).

3.4 Comparison with the spectra of red galaxies at z ≃ 1.5

3.4.1 LBDS 53W091

The age implications of the deep Keck optical spectrum of the red mJy radio galaxy 53W091 have already been discussed in some detail by Dunlop et al. (1996) and Spinrad et al. (1997). However it is interesting and important to revisit the age-determination of this object for a number of reasons. First, the models of Jimenez et al. have been updated in the intervening years. Second, the Yi et al. models did not exist in 1996/1997. Third, the MS-only versions of the Worthey models were only recently obtained. Finally, it is important to re-analyze this spectrum given the claims made by Bruzual & Magris (1997) and Yi et al. (2000) that the most recent models yield best-fit ages for the stellar population in 53W091 of less than 2 Gyr.

Therefore, in Figure 3.3 the results of fitting the same six models, as fitted to the Sun above, to the rest-frame near-ultraviolet SED of 53W091 are presented. The results, summarized

in Table 3.1, are that both the Jimenez et al. (2001) models (full and MS only) yield a best-fit age of 3 Gyr (with ages as young as 2 Gyr formally excluded), both the Yi et al. models (full and MSGB) yield a best fit age of 2 Gyr, while the best-fit age yielded by the Worthey models changes from 2 Gyr to 3 Gyr if post-MS contributions are excluded. Given the fact that we have already shown that the MS clock in the Yi et al. models appears to be running up to a factor of 2 too fast, this means that the argument over whether the age of 53W091 can or cannot be younger than 3 Gyr comes down to a debate over the validity of the stronger AGB and GB contributions in the Worthey models compared with the more MS-dominated Jimenez et al. models. Jimenez et al. (2000a) argue that their models include a better treatment of mass-loss in evolved stars which results in less luminous RGB and AGB contributions. In summary, the evidence from this work still appears to favour a minimum age of 3 Gyr for this galaxy, subject to remaining uncertainties over the impact of possible non-solar metallicity (see section 3.5). These uncertainties are addressed in Chapter 4.

3.4.2 LBDS 53W069

As discussed by Dunlop (1999), the Keck spectrum of the even redder mJy radio galaxy 53W069 ($z = 1.43$; Dey et al. 2001) appears to offer the best example discovered to date of a highly-evolved coeval stellar population at a redshift as high as $z \simeq 1.5$. Dunlop (1999) found, from a comparison of their near-ultraviolet SEDs, that 53W069 is significantly redder than 53W091, and that the SED of the latter galaxy can be decomposed into that of 53W069 plus a low-level blue component which is approximately flat in f_λ. It is therefore to be expected that model-fitting to the near-ultraviolet SED of 53W069 might yield even older age limits than those derived above for 53W091.

In Figure 3.4 the results of fitting the same six models as before to the near-ultraviolet SED of 53W069 are presented. The results can again be found in tabulated form in Table 3.1. In summary, for this object 5 out of the 6 models yield a minimum age > 3 Gyr, with only the Yi et al. full models allowing an age as young as 2 Gyr. Since these models appear flawed based on the solar comparison discussed in section 3.3, we conclude that it is extremely hard to escape the conclusion that, if solar metallicity is assumed, 53W069 is at least 3 Gyr old. For this object, the debate over whether the post-MS treatment of Jimenez et al. (2000a) is to be preferred over that of Worthey (1994) translates into an uncertainty over whether the best-fit age is in fact > 3 or > 4 Gyr (see Table 3.1).

For $H_0 = 70$ kms^{-1}Mpc^{-1}, the age of an Einstein-de Sitter Universe at $z = 1.43$ is only 2.5

object	model	age / Gyr	95.4% limits / Gyr	χ^2_ν
SUN	J Full	8	7.9 - 8.1	1.67
	J MS	11	10.8 - 11.1	1.00
	W Full	5	5.0 - 5.4	2.72
	W MS	9	8.8 - 9.3	1.57
	Y Full	4	3.9 - 4.1	2.06
	Y MSGB	4	> 3.9	1.67
	J 3Z	8	7.5 - 8.2	1.37
LBDS 53W091	J Full	3	2.9 - 3.4	1.25
	J MS	3	2.9 - 3.8	1.22
	W Full	2	1.9 - 3.1	1.38
	W MS	3	2.9 - 3.3	1.22
	Y Full	2	1.9 - 2.1	1.30
	Y MSGB	2	1.9 - 2.1	1.25
LBDS 53W069	J Full	5	2.9 - 6.0	1.63
	J MS	6	3.9 - 7.0	1.72
	W Full	3	2.8 - 3.4	1.54
	W MS	4	3.2 - 5.1	1.78
	Y Full	2	1.9 - 3.1	1.63
	Y MSGB	3	2.6 - 3.2	1.69

Table 3.1: A summary of the best fit ages and 95.4% confidence limits produced by fitting the 6 different models discussed in the text to the near-ultraviolet spectral energy distribution of i) the sun (see Figures 3.1 and 3.2), ii) the z = 1.55 galaxy 53W091 (see Figure 3.3), and iii) the z = 1.43 galaxy 53W069 (see Figure 3.4). In the case of the sun, the result of fitting the mixed metallicity model discussed in section 3.5 is also given (see Figure 3.5). The value of reduced χ^2 (χ^2_ν) is also given in each case, although in the case of the fits to the Sun, the values of reduced χ^2 can only be used to judge the relative quality of the alternative model fits. Abbreviations: J - Jimenez et al. (2001); W - Worthey (1994); Y - Yi et al. (2000).

Gyr. Therefore, given the apparently flawed nature of the Yi et al. models, we conclude that the only way that the age of 53W069 at z = 1.43 can be contained within an Einstein-de Sitter Universe is if varying the assumed metallicity from solar can in fact reduce the best-fit age to < 2.5 Gyr.

3.5 Breaking the age-metallicity degeneracy

The potential severity of the age-metallicity degeneracy was highlighted in the work of Worthey (1994), and acknowledged by Dunlop et al. (1996) in their original attempts to determine the age of 53W091. It might be expected that assuming a metallicity of twice solar for the entire stellar population results in the lower limit to the derived age of both 53W091 and 53W069 falling below 2.5 Gyr.

Spinrad et al. (1997) presented arguments that, even assuming these galaxies possess a high-metallicity core, adoption of a universally high metallicity is inappropriate when analyzing the integrated light from the central $\simeq$ 10 kpc of an elliptical galaxy (as sampled at z > 1 by the Keck spectroscopic slit). Moreover, both Jimenez et al. (2000b) and Yi et al. (2000) have now attempted to produce more realistic mixed metallicity models and have independently found that such mixed-metallicity models in fact yield very similar ages to simple *solar* metallicity models (despite the basic disagreement between model timescales detailed above). This appears to be true, even when the average metallicity is twice solar, simply because it is the low metallicity component which dominates the light shortward of 3000 Å (Jimenez et al. 2000b).

Ideally, however, we would like to be able to fit both metallicity mix and age to the data. The extent to which this is possible obviously depends both on the quality of the spectroscopic data available, and on the presence of (primarily) metallicity-dependent and age-dependent features within the available spectral range.

This approach is explored further in Chapter 4, but here, evidence is presented that the age-metallicity degeneracy can, at least in principle, be broken with data in the spectral range 2000 Å– 4000 Å, using the Sun, for which age and metallicity are already known, as a test case.

A mixed-metallicity model was constructed from the 0.2 $Z_{\odot}$, $Z_{\odot}$ and 2.5 $Z_{\odot}$ full models of Jimenez et al., with the relative contributions of the different metallicity models allowed to vary as free parameters. The ability of this mixed-metallicity model to reproduce the

metallicity and MSTO age of the sun is a test of the stellar population synthesis models' ability to break the age-metallicity degeneracy given data in this near-ultraviolet spectral range.

The solar spectrum was rebinned in the same way as for the solar-metallicity only fitting process. The mixed-metallicity model flux was built from the single-metallicity model SED's, so that

$$F_{3Z,\lambda,t} = X_{0.2\,z_\odot} f_{0.2\,z_\odot,\lambda,t} + X_{z_\odot} f_{z_\odot,\lambda,t} + X_{2.5\,z_\odot} f_{2.5\,z_\odot,\lambda,t}$$

where $F_{3Z,\lambda,t}$ is the mixed-metallicity flux per unit wavelength in the bin centred on wavelength λ at age t, $f_{Z,\lambda,t}$ is the flux per unit wavelength in the bin centred on wavelength λ of the model at age t, and metallicity Z, and X_Z is the fractional contribution to $F_{3Z,t}$ by $f_{Z,t}$.

A χ^2 fit was used to determine the best-fit age, total normalization, and values of $X_{0.2\,z_\odot}$, $X_{z_\odot}$ and $X_{2.5\,z_\odot}$.

In Figure 3.5 we show the results of this mixed-metallicity fitting procedure. Comparison of the left-hand plot with the dotted line in Figure 3.1a demonstrates the extent to which allowing metallicity to vary has weakened the constraint on age. However, the best-fit age is still 8 Gyr, as for the full solar-metallicity only models. Figure 3.5b shows the evolution of the fractional contributions to the flux of the different metallicity SED's. At the best-fit age of 8 Gyr, the flux is clearly completely dominated by the solar metallicity SED, as it should be. $X_{0.2\,z_\odot}$ is 0.01, $X_{z_\odot}$ is 0.99 and there is no contribution from the 2.5 $Z_\odot$ model. This gives a mean metallicity of 0.99 $Z_\odot$. In summary, given data of this (obviously excellent) quality, the mixed-metallicity model can return both the correct metallicity and the correct age to high accuracy (where here the correct age does not mean the turnoff age of the Sun, but rather the age of 8 Gyr which was returned using the full model with the correct metallicity).

3.6 Conclusion

In this chapter, a model-maker's comparison of different evolutionary synthesis models is not attempted. The debate over which model uses the most trustworthy components, such as isochrones, stellar atmospheres etc., is deliberately not entered into. Instead, the simple issue of whether the near-ultraviolet spectral energy distribution of the Sun is reproduced by

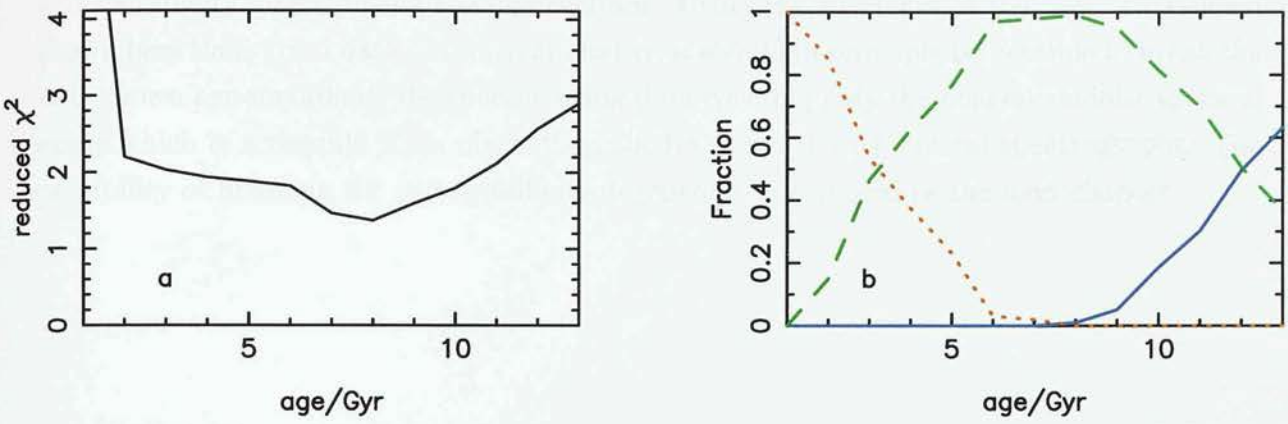

Figure 3.5: Left-hand side: reduced χ^2 as a function of age for the mixed-metallicity model (see §3.5 for details). The best-fit age is 8 Gyr, just as for the full solar-metallicity models of Jimenez et al. (2000). Right-hand side: fractional contributions to the mixed-metallicity model of the different metallicity components as a function of age, i.e. 0.2 $Z_\odot$ (solid line), $Z_\odot$ (dashed line) and 2.5 $Z_\odot$ (dotted line). The large contribution of the super-solar component at young ages, and the large contribution of the sub-solar component at large ages reflects the well-known age-metallicity degeneracy. However, at the best fit age of 8 Gyr, the mean metallicity is 0.99 $Z_\odot$, with the solar metallicity contribution completely dominating the model.

the main-sequence only components of three independent models at an age commensurate with current estimates of the MS-turnoff age of the Sun is addressed. This test was suggested by Yi et al. (2000), but in fact leads to the conclusion that the evolutionary timescale of the main sequence in the Yi et al. models is anomalous when compared with the either the models of Worthey (1994), Jimenez et al. (2001) or the current best estimate of the MS turn-off age of the Sun.

The issue of the extent to which varying contributions from post-MS phases of stellar evolution can affect the age estimation of galaxies at $z \simeq 1.5$ from rest-frame ultraviolet spectra has also been re-addressed. It is found that (assuming solar metallicity) the minimum age of the dominant stellar population in the the $z = 1.55$ radio galaxy 53W091 is 2 Gyr if one invokes the relatively strong AGB/RGB components included in the models of Worthey (1994), and 3 Gyr is one adopts the weaker post-MS contributions included in the models of Jimenez et al. (2001). In the case of the even redder $z = 1.43$ radio galaxy 53W069, these numbers become 3 Gyr and 4 Gyr respectively.

Finally, as stated above, these figures are derived on the assumption of approximately solar metallicity. Yi et al. (2000) and Jimenez et al. (2000b) have in fact shown that the age-metallicity degeneracy in a realistic mixed-metallicity population is probably not nearly as severe as previously feared. Nevertheless, ideally it is clearly desirable to determine both age

and metallicity directly from the observations. Using the spectrum of the Sun, it has been shown here that, given data of sufficient quality, it should in principle be possible to break the well-known age-metallicity degeneracy using data covering only the near-ultraviolet spectral range which is accessible when observing galaxies at $z > 1$ with optical spectrographs. The possibility of breaking the age-metallicity degeneracy is explored in the next chapter.

Chapter 4

F stars, metallicity, and the ages of red galaxies at z > 1

4.1 Introduction

In this chapter, the investigation into the ability of synthetic stellar population models to determine the ages of high-redshift elliptical galaxies, begun in Chapter 3, is continued. In an attempt to clarify the key issues, i.e. disagreements over the details of stellar evolution, and the well-known degeneracy between derived age and metallicity (Worthey 1994), both the extent to which various evolutionary synthesis models differ in their evolutionary predictions, and the extent to which rest-frame near-UV data may allow the age-metallicity degeneracy to be lifted are investigated. In Chapter 3, the time evolution of the solar-metallicity ($Z_{\odot}$) population synthesis models of Yi et al. (2000), Worthey (1994) and Jimenez et al. (2001) was checked, by comparing the ability of the main-sequence components of these models to reproduce the near-UV solar spectrum of the Sun at its anticipated main-sequence turn-off age. Here, the investigation is extended to non-solar metallicity models.

Therefore, this work explores whether, given data of sufficient quality, variable-metallicity models can extract the correct metallicity of a stellar population simply from fitting to the near-UV spectral region accessible through optical spectroscopy of high-redshift galaxies. This is done by fitting variable- and mixed-metallicity versions of the models of Jimenez et al. (2001, in preparation) to the HST ultraviolet spectra of two well-studied, non-solar metallicity, main sequence stars, kindly supplied by Sally Heap (Heap, private communica-

tion). These stars are HR 4683, an F4V star, with sub-solar metallicity, and HR 4688, an F8V star with super-solar metallicity (Edvardsson et al., 1993). The motivation for this is that the rest-frame near-UV spectra of the oldest known galaxies at $z \simeq 1.5$ (e.g. 53W091 and 53W069) mimic the spectra of main-sequence F stars (F5V - F9V; Dunlop 1999).

This is, of course, a rather one-sided test, but it is still potentially very instructive. Specifically, if the models cannot extract the correct metallicity from the high-quality near-UV data available for these F-stars, then it is probably safe to assume that breaking the age-metallicity degeneracy in high-redshift galaxies is currently impossible. Conversely, if the models can yield the correct metallicity for these F-stars, then that provides some hope that the age-metallicity degeneracy can be lifted in high-redshift galaxies given near-UV data of sufficient quality. However, such optimism must be tempered by the knowledge that the spectrum of a high-redshift galaxy is unlikely to be as clean as that of the test-case F-stars, given the obvious likelihood of a mixture of metallicities and ages in a substantial stellar population. Nevertheless, as is reported in this chapter, the results of fitting the new variable/mixed metallicity models of Jimenez et al. (2001, in preparation) to the near-UV spectra of the two F-stars are sufficiently encouraging to motivate the refitting of the Keck spectra of LBDS 53W091 and 53W069 with metallicity allowed to vary as a free parameter.

The layout of the chapter is as follows. In section 4.2, the models used are described, together with the procedure by which they have been fitted to the data. In section 4.3, the results of fitting both single (but variable) metallicity models, and mixed metallicity models (comprising a free mix of six different metallicities) to the HST near-UV spectra of the F stars are presented. Section 4.4 contains the results of fitting the same models to the optical (rest-frame near-UV) spectra of the $z \simeq 1.5$ galaxies LBDS 53W091 and 53W069, and a discussion of the extent to which such modelling allows the age-metallicity degeneracy to be lifted. Finally, as a check on whether the assumption of single burst models is appropriate, the spectra of these two galaxies are fitted using MOPED (Heavens et al., 2000), which allows the star formation history to be unconstrained. The conclusions, including revised constraints on the ages of these red galaxies, are summarized in section 4.5.

4.2 Models and model fitting

The stellar population evolutionary synthesis models utilised in this paper are the instantaneous starburst models of Jimenez et al. (2001, in preparation). The reliability and consistency of the solar metallicity ($Z_{\odot}= 0.02$) version of these models were confirmed by

Nolan et al. (2001a). We now also possess non-solar metallicity models, with metallicities of 0.01 $Z_{\odot}$, 0.2 $Z_{\odot}$, 0.5 $Z_{\odot}$, 1.5 $Z_{\odot}$and 2.5 $Z_{\odot}$.

This suite of six different metallicity models has been utilised in two ways. First, the results of simply fitting each of these six models in turn at all possible ages, to identify the best-fitting single value of metallicity, and the resulting inferred age are explored. Second, the six single-metallicity models were combined to produce a composite model in which mean metallicity is allowed to vary by varying the fractional contributions made by each of the six different metallicity components. The mixed-metallicity model was fitted to the spectra of the F stars, as well as the high redshift galaxies' spectra, to confirm that fitting this model allows the correct metallicity to be reclaimed.

4.2.1 Fitting single-metallicity models

The best fit was determined for each single-metallicity model (0.01 $Z_{\odot}$, 0.2 $Z_{\odot}$, 0.5 $Z_{\odot}$, $Z_{\odot}$, 1.5 $Z_{\odot}$and 2.5 $Z_{\odot}$) in the following way. First, the data were rebinned to the same spectral resolution as the models, with the new flux calculated as the mean flux per unit wavelength in the new bin. Both the rebinned and model fluxes were then normalised to a mean flux per unit wavelength of unity across the wavelength range $3000 - 3500$Å for the galaxy fits, and across the range $3000 - 3117$Å for the F-star fits (because of the shorter wavelength range of the F-star spectra). The model age and normalisation were then varied as free parameters until χ^2 was minimised.

In order to produce the contour plots for the single-metallicity fits in sections 4.3.1 and 4.4.1, the results were refined by carrying out two one-dimensional cubic spline interpolations, one for age, and one for metallicity, between the calculated points on the age-metallicity grid.

4.2.2 Fitting mixed-metallicity models

A mixed-metallicity model was constructed from the 0.01 $Z_{\odot}$, 0.2 $Z_{\odot}$, 0.5 $Z_{\odot}$, $Z_{\odot}$, 1.5 $Z_{\odot}$ and 2.5 $Z_{\odot}$ models of Jimenez *et al.* (2001, in preparation), with the relative contributions of the different metallicity models allowed as free parameters. In this section, it is assumed that all six populations were formed at the same time, so that the one other free parameter in the fit was the age of the complete population. This constraint is lifted in section 4.4.3, in order to explore what happens when the stellar populations are formed at arbitrary times.

The mixed-metallicity model flux was built from the unnormalised single-metallicity model

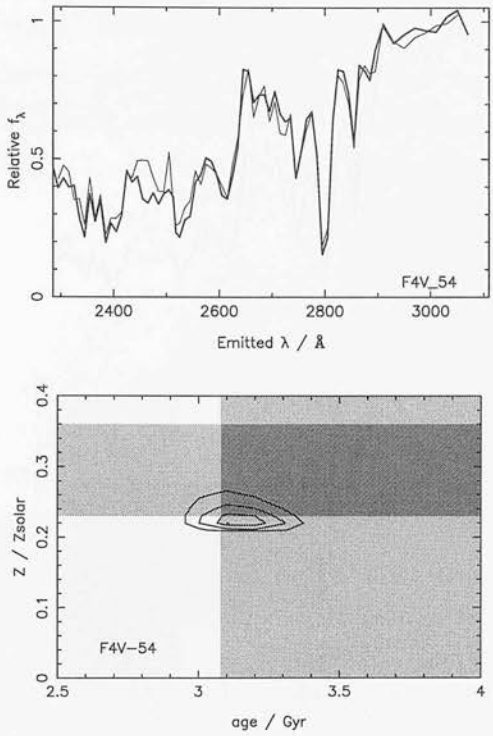

Figure 4.1: Top: the best-fitting, single-metallicity model (thin line, 0.2 $Z_\odot$ model at 3 Gyr, before interpolation of the results) to the spectrum of the F4V star, HR 4683 (thick line). Bottom: contours of constant reduced χ^2 (χ^2_ν) as a function of metallicity and age after interpolation. The contour levels contain 75%, 95% and 99.5% relative likelihood. The shaded regions represent the estimates of Edvardsson et al., with estimated errors ± 30% in age and ± 0.10 dex in metallicity. See §4.3.1 for discussion, and Table 4.1 for values of χ^2_ν.

fluxes, and then normalised to a mean flux per unit wavelength of unity across the wavelength range $3000 - 3117$Å, so that

$$\begin{aligned} F_{6Z,\lambda,t} \; = \; & \\ & const(\; X_{0.01\,z_\odot} f_{0.01\,z_\odot,\lambda,t} \; + \\ & X_{0.2\,z_\odot} f_{0.2\,z_\odot,\lambda,t} + X_{0.5\,z_\odot} f_{0.5\,z_\odot,\lambda,t} \; + \\ & X_{z_\odot} f_{z_\odot,\lambda,t} \; + \; X_{1.5\,z_\odot} f_{1.5\,z_\odot,\lambda,t} \; + \\ & X_{2.5\,z_\odot} f_{2.5\,z_\odot,\lambda,t} \;) \end{aligned} \tag{4.1}$$

where $F_{6Z,\lambda,t}$ is the mixed-metallicity model flux per unit wavelength in the bin centred on wavelength λ at age, t Gyr; $f_{Z,\lambda,t}$ is the flux per unit wavelength in the bin centred on wavelength λ of the single-metallicity model at age, t Gyr and metallicity Z, and X_Z is the

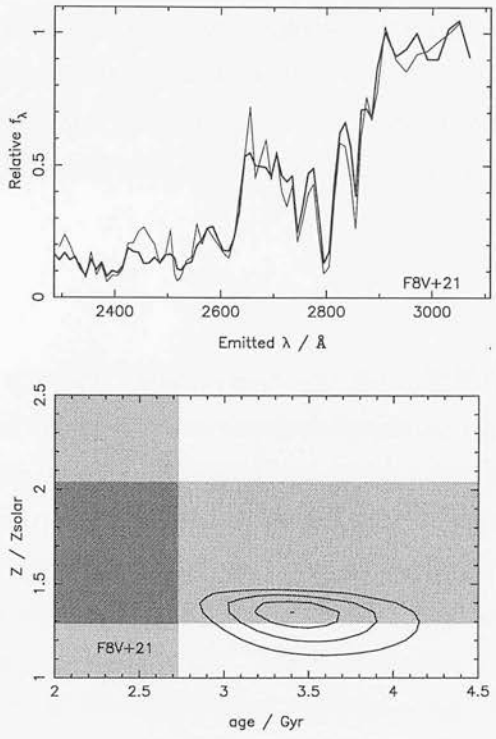

Figure 4.2: Top: the best-fitting, single-metallicity model (thin line, 1.5 $Z_\odot$ model at 3 Gyr, before interpolation of the results) to the spectrum of the F8V star, HR 4688 (thick line). Bottom: contours of constant χ^2_ν as a function of metallicity and age after interpolation. The contour levels contain 75%, 95% and 99.5% relative likelihood. The shaded regions represent the estimates of Edvardsson et al., with estimated errors ± 30% in age and ± 0.10 dex in metallicity. See §4.3.1 for discussion, and Table 4.1 for values of χ^2_ν.

fractional contribution (by mass) made by this single-metallicity model to the total model population.

A minimum-χ^2 fit was used to determine the best-fit age, total normalisation, and the values of $X_{0.01\,z_\odot}$, $X_{0.2\,z_\odot}$, $X_{0.5\,z_\odot}$, $X_{z_\odot}$, $X_{1.5\,z_\odot}$ and $X_{2.5\,z_\odot}$.

The whole parameter space was searched during the fitting process; the best fit values for the mixed-metallicity fits quoted in sections 4.3.2 and 4.4.2 and in Table 4.2 are therefore those parameter values which correspond to the point on the age-metallicity grid with the minimum calculated χ^2. However, for these mixed-metallicity, single-age fits, the same mean metallicity may be obtained from many different combinations of the component single-metallicity models. Therefore, in Figures 4.3, 4.4, 4.7 and 4.8, it is the marginalised distribution of mean metallicity that the relative likelihood contours represent.

The contour plots resulting from the six-metallicity fits to two of the objects, HR 4688 and LBDS 53W069, suggested that as good or better quality fits would be possible if a higher-

metallicity model was available in the mixed-model fit. Therefore, the 5 $Z_{\odot}$metallicity model of Jimenez et al. (2001) was obtained, and included in the mixed-metallicity model fits to these spectra in the same way as the other six metallicity models. In this way, the mixed-model has access to seven different single-metallicity models for these objects.

4.2.3 Errors

The errors on the binned spectral data points for the LBDS galaxies have been derived from the propagation of the original observational errors in the Keck optical spectroscopy (Dey et al., 2001, in preparation). Using these errors, statistically acceptable fits were achieved. For the F-star spectra, the error adopted for each rebinned data point was simply the standard error in the mean for that bin. For HR 4683 (the low-metallicity star), a formally acceptable fit was obtained using these errors. However, for HR 4688 (the high-metallicity star), this did not prove possible. While there are a number of reasons why this might occur (e.g. inadequacy of the super-solar models – e.g. Flynn, Kotoneva & Jimenez (2001), in preparation) uniform relaxation of the adopted errors was experimented with to see if this affected the parameter values yielded by the best-fitting models (see section 4.3).

The wavelength range $2400-2500$Å was excluded from the fits to all objects. When included, this region contributed $\sim 1/3$ of the total χ^2 when fitting to both the F stars and the high-redshift galaxies, indicating that the models are currently unable to account for the detailed spectral features in this wavelength region.

4.3 Comparison with F-star spectra

4.3.1 Single-metallicity models

In figures 4.1 and 4.2, the results of fitting each of the six single-metallicity models in turn to the HST spectra of the F stars HR 4683 and HR 4688 respectively are shown. The first plot in each figure shows the best-fitting model spectrum (before the interpolation of the results) superimposed on the observed near-UV stellar spectrum. The second plot shows contours of constant (interpolated) reduced χ^2 (χ^2_{ν}) as a function of metallicity and age. The contour levels contain 75%, 95% and 99.5% relative likelihood. The results are presented in Table 4.1.

object	$Z/Z_\odot$	Best fit age/Gyr	${\chi^2}_\nu$
F4V	0.01	13	11.2
	0.2	3	1.69
	0.22	3.1	0.96
	0.5	3	1.89
	1.0	1	3.09
	1.5	1	4.88
	2.5	0.7	5.93
F8V	0.01	13	46.0
	0.2	13	2.57
	0.5	11	2.40
	1.0	4	2.41
	1.35	3.4	2.01
	1.5	3	2.25
	2.5	1	2.58
LBDS 53W069	0.01	13	3.56
	0.2	13	1.55
	0.5	13	1.54
	1.0	5	1.69
	1.5	3	1.65
	2.15	2.4	1.47
	2.5	1	1.70
LBDS 53W091	0.01	9	4.84
	0.2	10	1.32
	0.5	10	1.38
	1.0	3	1.27
	1.10	2.3	1.18
	1.5	3	1.36
	2.5	1	1.42

Table 4.1: The results of fitting the near-ultraviolet spectra of the F-stars and the LBDS galaxies using the suite of six single-metallicity models. The results corresponding to the minimum interpolated χ^2_ν are also given. The best fitting models in the case of the F4V star and 53W091 are formally very acceptable fits. However, the best fitting single metallicity model to 53W069 is, at best, only marginally acceptable, while that to the F8V star is not formally acceptable without further relaxation of the assumed errors. This may reflect some problem with the reliability of the high-metallicity model atmospheres. The best fits for each of the single-metallicity models are given, together with the minimum χ^2found by interpolating the results.

Interpolating the results gives a minimum χ^2_ν corresponding to an age of 3.1 Gyr, with a metallicity of 0.22 $Z_\odot$ for the F4V star, HR 4683, and an age of 3.4 Gyr, with a metallicity of 1.35 $Z_\odot$for the F8V star, HR 4688.

Edvardsson et al. (1993) estimated the relative iron abundances ([Fe/H] = $Z/Z_{\odot}$, where $Z_{\odot} = 0.02$) of these two stars by fitting model stellar atmospheres to spectral lines observed at optical wavelengths. They estimated the uncertainty in the derived metallicities to be, at most, 0.10 dex. Based on these optical lines, they found the F4V star to have a metallicity of 0.29 $Z_{\odot}$, and the F8V star to have a metallicity of 1.62 $Z_{\odot}$. The metallicities yielded by the completely independent, near-UV model-fitting shown in figures 4.1 and 4.2 are therefore in very good agreement with those previously derived from optical indices; metallicities have been derived from the near-UV data which fall within the uncertainties in the optically-derived values (see figures 4.1 and 4.2).

Further confidence in the reliability of the age and metallicity estimates obtained from the model stellar population fits is provided by fitting the near-UV spectra of single atmosphere stellar models to the F-stars' spectra, using the process described above. Six single-atmosphere models, with the same metallicities as the population models used (i.e. 0.01 $Z_{\odot}$, 0.2 $Z_{\odot}$, 0.5 $Z_{\odot}$, $Z_{\odot}$, 1.5 $Z_{\odot}$and 2.5 $Z_{\odot}$) were fitted to the HST spectra. The best-fit single star model to the F4V star spectrum has a metallicity of 0.2 $Z_{\odot}$, and an age of 4 Gyr. For the F8V star, the best-fit single star model has an age of 1.5 Gyr, with a metallicity 1.5 $Z_{\odot}$. These results are in good agreement with the results from fitting the population models to the stellar spectra, and in excellent agreement with the optically-derived results of Edvardsson et. al.

Edvardsson et al. (1993) also derived ages for these stars from fits in the $T_{eff} - \log g$ plane to VandenBerg (1985) isochrones. They found an age of 4.4 Gyr for the F4 dwarf, HR 4683, and an age of 2.1 Gyr for the F8 dwarf, HR 4688. However, they pointed out that they expected the uncertainties in the relative ages of the stars in their sample to be $\sim 25\%$, and that the absolute errors may be larger. It should also be noted that the ages determined by Edvardsson and co-workers are the present ages of the stars, whereas fitting the stellar population models to the spectra should yield ages which correspond to the main-sequence lifetimes of the stars. For this reason it might be expected that the model-fitting should yield ages greater than those derived by Edvardsson and co-workers. However, the models include integration down the main-sequence, as well as post main-sequence contributions, both of which are likely to lead to an under-estimate of the true main-sequence turnoff age when fitted to the spectrum of a single star. Against this background, the level of agreement seen in figures 4.1 and 4.2 between the ages derived here, and those estimated by Edvardsson et al. is clearly acceptable.

More important than the exact values of the derived ages for single stars is the fact that the age appears to be well constrained despite the availability of six different metallicities at

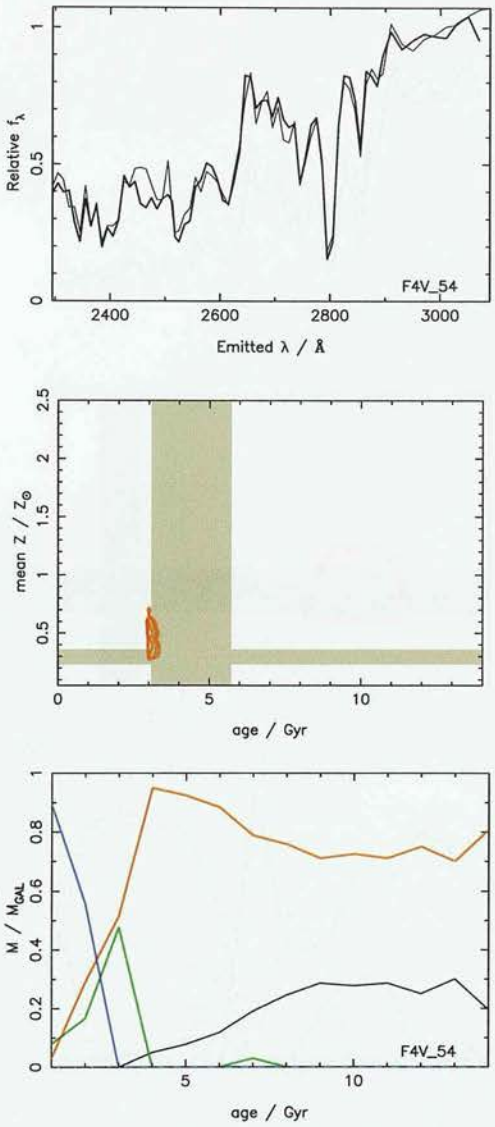

Figure 4.3: Top: the best-fitting, six-component, mixed-metallicity model (3 Gyr, 0.32 $Z_\odot$, thin line) to the spectrum of the F4V star, HR 4683 (thick line). Middle: contour plots of constant relative likelihood, for the marginalised distribution of mean metallicity with age. The contours contain 68.3%, 90% and 95.4% relative likelihood. The shaded regions in the likelihood plots represent the estimates of Edvardsson et al., with estimated errors ± 30% in age and ± 0.10 dex in metallicity. Bottom: fractional contributions (by mass) to the mixed metallicity model of the different metallicity components as a function of age , i.e. 0.01 $Z_\odot$ (black solid), 0.2 $Z_\odot$ (red solid), 0.5 $Z_\odot$ (green solid), $Z_\odot$ (blue solid), 1.5 $Z_\odot$ (black dashed) and 2.5 $Z_\odot$ (red dashed). See §4.3.2 for discussion, and Table 4.2 for values of χ^2_ν.

each age. These results therefore demonstrate that by fitting the single-metallicity models to the near-UV spectra of these F stars, it is apparently possible to break the age-metallicity degeneracy to the extent that uncertainty in age is < 1 Gyr.

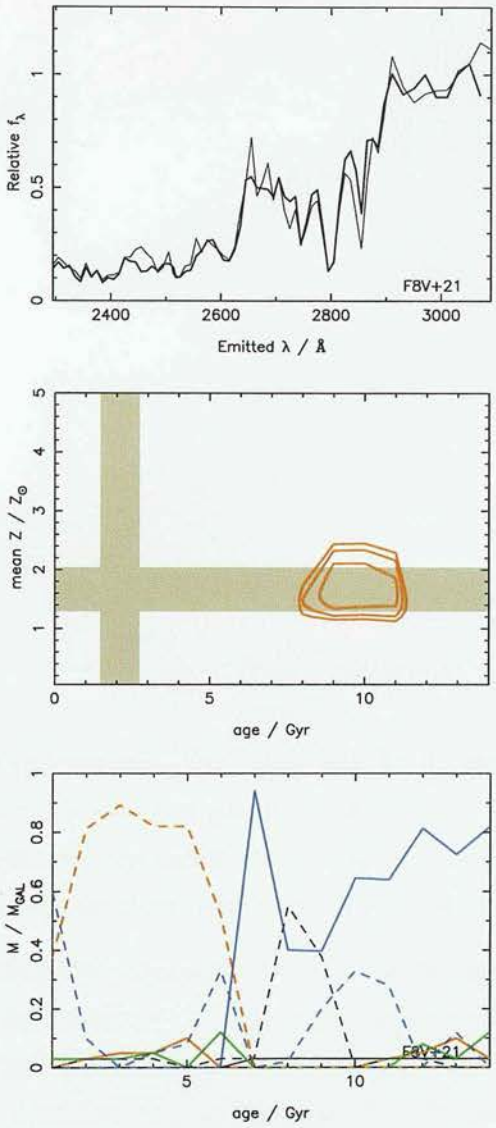

Figure 4.4: Top: the six-component, mixed-metallicity model (9 Gyr, 1.97 $Z_\odot$, thin line) fitted to the spectrum of the F8V star, HR 4688 (thick line), which lies closest to the parameters corresponding to the minimum interpolated χ^2_ν. Middle: contour plots of constant relative likelihood, for the marginalised distribution of mean metallicity with age. The contours contain 68.3%, 90% and 95.4% relative likelihood. The shaded regions in the likelihood plots represent the estimates of Edvardsson et al., with estimated errors ± 30% in age and ± 0.10 dex in metallicity. Bottom: fractional contributions (by mass) to the mixed metallicity model of the different metallicity components as a function of age , i.e. 0.01 $Z_\odot$ (black solid), 0.2 $Z_\odot$ (red solid), 0.5 $Z_\odot$ (green solid), $Z_\odot$ (blue solid), 1.5 $Z_\odot$ (black dashed), 2.5 $Z_\odot$ (red dashed) and 5.0 $Z_\odot$ (blue dashed). See §4.3.2 for discussion, and Table 4.2 for values of χ^2_ν.

4.3.2 Mixed-metallicity models

In figures 4.3 and 4.4, the results of fitting the mixed-metallicity model to the HST spectra of the F stars are shown. Again, each figure shows the best-fitting model (before interpolation

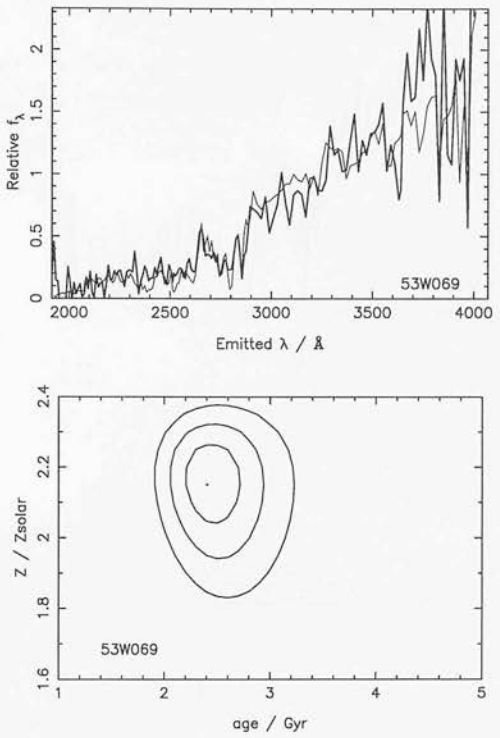

Figure 4.5: Top: the best fit single metallicity model (thin line, 1.5 $Z_\odot$ model at 3 Gyr, before interpolation of the results) to the spectrum of the z = 1.43 galaxy, LBDS 53W069 (thick line). Bottom: contours of constant χ^2_ν as a function of metallicity and age after interpolation. The contour levels represent 75%, 95% and 99.5% confidence. See §4.4.1 for discussion, and Table 4.1 for values of χ^2_ν.

of the results) superimposed on the observed near-UV stellar spectrum, followed by contour plots of constant relative likelihood as a function of mean metallicity and age. The contour levels contain 68.3%, 90% and 95.4% relative likelihood, for the marginalised distribution of mean metallicity with age. Also included this time is a third panel showing how the fractional contribution (by mass) of the six different metallicity components varies as a function of age. The results are tabulated in Table 4.2.

This time, the results predict a mean metallicity for the F4V star of 0.35 $Z_\odot$ at an age of 3 Gyr, while for the F8V star a mean metallicity of 1.97 $Z_\odot$, at an age of 9 Gyr, is predicted.

Fitting this type of mixed-metallicity model arguably provides a fairer test of ability to break the age-metallicity degeneracy. Once again it can be seen that the derived metallicities and ages are well-constrained, and, with the exception of the age of HR 4688 (which is perhaps unsurprising given the reasons discussed in Section 4.3.1), in excellent agreement with the completely independent, optically-based results of Edvardsson et al..

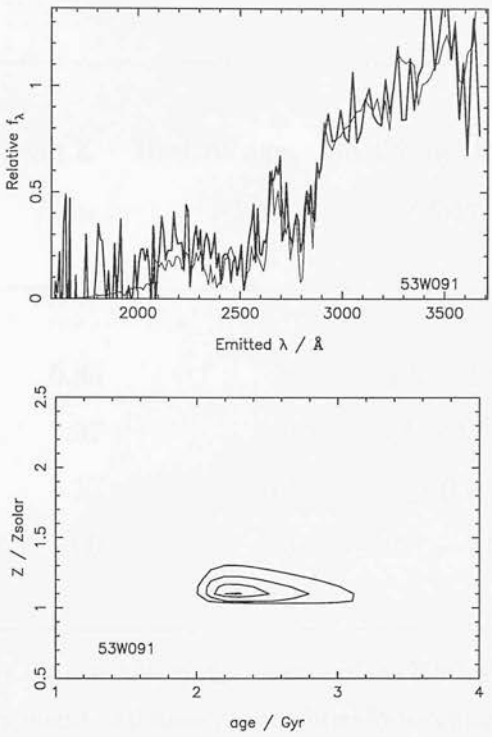

Figure 4.6: Top: the best fit single metallicity model (thin line, $Z_\odot$ model at 3 Gyr, before interpolation of the results) to the spectrum of the z = 1.55 galaxy, LBDS 53W091 (thick line).Bottom: contours of constant χ^2_ν as a function of metallicity and age after interpolation. The contour levels represent 75%, 95% and 99.5% confidence. See §4.4.1 for discussion, and Table 4.1 for values of χ^2_ν.

4.4 Red galaxies at z $\simeq$ 1.5

4.4.1 Single-metallicity models

In figures 4.5 and 4.6, results of fitting each of the six single-metallicity models in turn to the Keck spectra of the red mJy radio galaxies LBDS 53W069 (Dunlop 1999) and LBDS 53W091 (Dunlop et al. 1996; Spinrad et al. 1997) respectively are presented. The first plot in each figure shows the best-fitting model spectrum (before interpolating the results) superimposed on the rest-frame near-UV galaxy spectrum. The second plot shows contours of constant (interpolated) reduced χ^2 (χ^2_ν) as a function of metallicity and age. The contour levels represent 75%, 95% and 99.5% confidence. The results are presented in Table 4.1, including the ages and metallicities corresponding to the minimum χ^2_ν found by interpolation of the results. Following interpolation, an age of 2.4 Gyr, with a metallicity of 2.15 $Z_\odot$ is predicted for the galaxy LBDS 53W069 (z = 1.43) while LBDS 53W091 (z = 1.55) has a predicted metallicity of 1.10 $Z_\odot$, at an age of 2.3 Gyr.

object	mean Z / $Z_\odot$	Best fit age / Gyr	95.4% age limits / Gyr	χ^2_ν
F4V	0.35	3	$2.9 - 3.5$	1.76
F8V	1.97	9	$7.8 - 11.5$	1.66
53W069	4.17	13	≥ 9.0	1.30
53W091	1.00	3	$2.5 - 4.5$	1.31

Table 4.2: The results of fitting the near-ultraviolet spectra of the F-stars and the LBDS galaxies with the six-component, mixed-metallicity model. All these fits are formally acceptable, but it should be remembered that the errors used in the calculation of χ^2 for the F8V star are not absolute (see §4.2.3).

In both LBDS 53W069 and 53W091, age and metallicity have been simultaneously remarkably well-constrained (see figures 4.5 and 4.6), with a predicted age for 53W091 between 2.0 and 3.1 Gyr with 99.5% confidence, and for 53W069, between 2.0 and 3.2 Gyr at the same level of confidence. Thus, under the assumption of a single metallicity for the observed stellar populations in these galaxies, it is clear that allowing metallicity to vary as a free parameter does not alter the conclusion of Dunlop (1999), that both these galaxies are $\sim 3 - 4$ Gyr old, by any more than ~ 1 Gyr, even when, as in the case of LBDS 54W069, the predicted metallicity is more than twice the solar value.

The results confirm the validity of previous arguments in favour of assuming roughly solar metallicity when modelling LBDS 53W091 (Spinrad et al. 1997).

Below, the robustness of these results is investigated by fitting the mixed-metallicity model to the galaxy spectra.

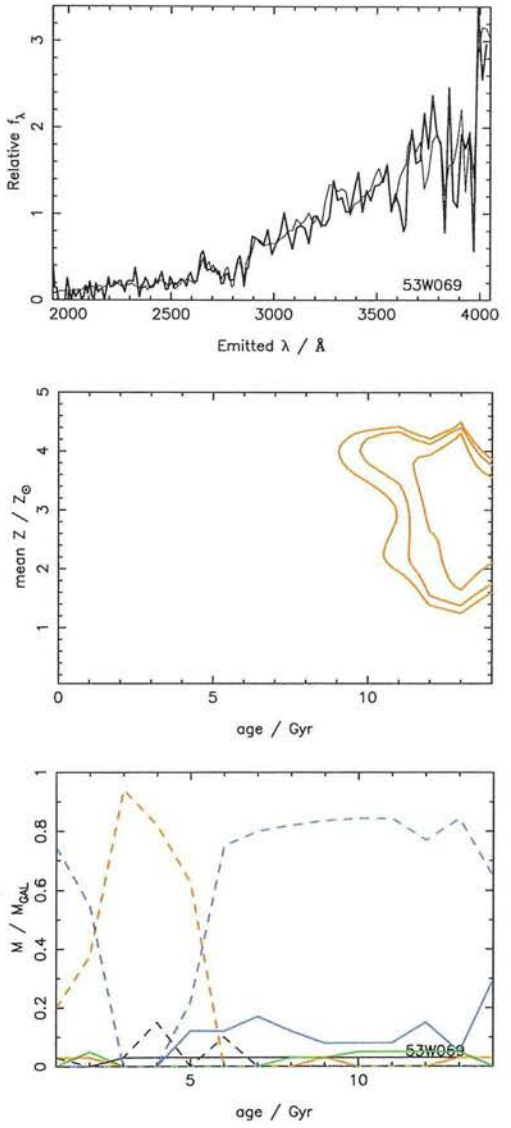

Figure 4.7: Top: the best-fitting, six-component, mixed-metallicity model (13 Gyr, 4.17 $Z_\odot$, thin line) to the spectrum of the high-redshift (z = 1.43) galaxy LBDS 53W069 (thick line). Middle: contour plots of constant relative likelihood, for the marginalised distribution of mean metallicity with age. The contours contain 68.3%, 90% and 95.4% relative likelihood. Bottom: fractional contributions (by mass) to the mixed-metallicity model of the different metallicity components as a function of age , i.e. 0.01 $Z_\odot$ (black solid), 0.2 $Z_\odot$ (red solid), 0.5 $Z_\odot$ (green solid), $Z_\odot$ (blue solid), 1.5 $Z_\odot$ (black dashed), 2.5 $Z_\odot$ (red dashed) and 5.0 $Z_\odot$ (blue dashed). See §4.4.2 for discussion, and Table 4.2 for values of χ^2_ν.

4.4.2 Mixed-metallicity models

In figures 4.7 and 4.8, the results of fitting the mixed-metallicity model to the Keck spectra of the LBDS galaxies are presented. As in figures 4.3 and 4.4, each figure shows the best-

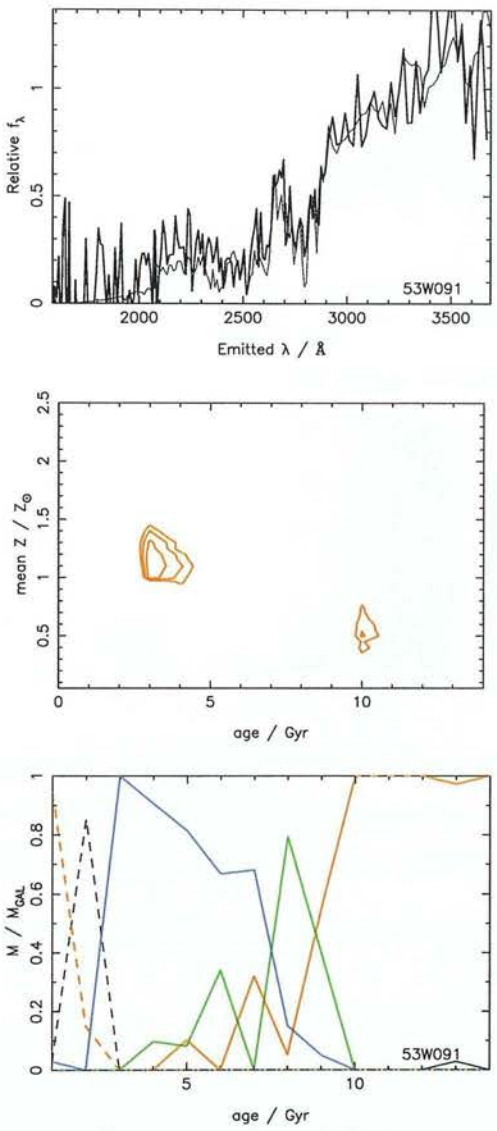

Figure 4.8: Top: the best-fitting, six-component, mixed-metallicity model (3 Gyr, $Z_\odot$, thin line) to the spectrum of the high-redshift (z = 1.55) galaxy LBDS 53W091 (thick line). Middle: contour plots of constant relative likelihood, for the marginalised distribution of mean metallicity with age. The contours contain 68.3%, 90% and 95.4% relative likelihood. Bottom: fractional contributions (by mass) to the mixed-metallicity model of the different metallicity components as a function of age , i.e. 0.01 $Z_\odot$ (black solid), 0.2 $Z_\odot$ (red solid), 0.5 $Z_\odot$ (green solid), $Z_\odot$ (blue solid), 1.5 $Z_\odot$ (black dashed) and 2.5 $Z_\odot$ (red dashed). See §4.4.2 for discussion, and Table 4.2 for values of χ^2_ν.

fitting model superimposed on the rest-frame near-UV spectrum, followed by contour plots of constant relative likelihood, for the marginalised mean metallicity, as a function of mean metallicity and age. The contours represent 68.3 %, 90 % and 95.4 % confidence levels. Again, a third panel is included showing how the fractional contribution (by mass) of the

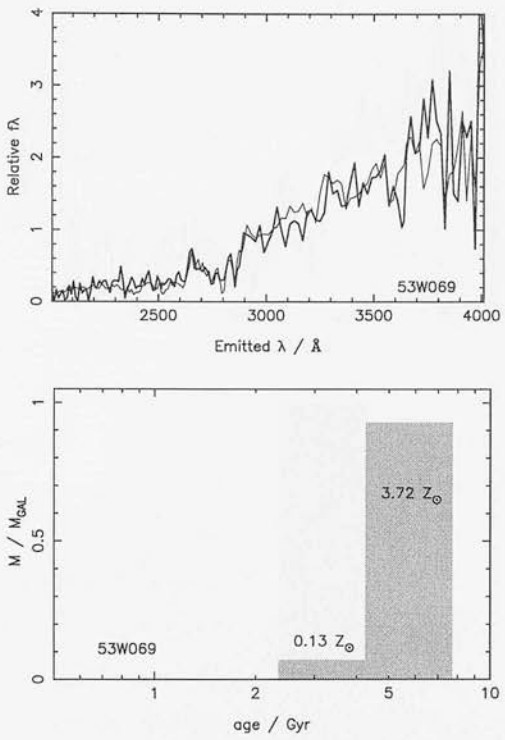

Figure 4.9: Top: best-fitting model (thick line) to the spectrum of LBDS 53W069 (thin line) predicted using MOPED (Heavens et al., 2000). Bottom: The predicted stellar population components. The population is dominated by the high metallicity component, with an age 4.25 – 7.72 Gyr.

six different metallicity components varies as a function of age. The results are presented in Table 4.2.

This time the best-fit mean metallicity of 53W069 is 4.17 $Z_{\odot}$. Only old ages are allowed, even at high metallicity. The third plot of figure 7 shows that the mixed-metallicity model is dominated by contributions from the highest metallicity (5.0 $Z_{\odot}$) model. This is a very different result from the single-metallicity fit, where the age is constrained at the 99.5 % level to between $\sim$ 1.9 – 3.2 Gyr, at less than half the metallicity here.

Despite the high value of best-fitting mass-weighted metallicity, the interesting thing is that the inferred age of LBDS 53W069 remains old. The second panel in Figure 7 demonstrates that while the age is constrained, ages $<$ 9 Gyr are prohibited at the 99.5% confidence level (the formal best-fit age is 13 Gyr). Such an high age at a redshift of 1.43 is not possible in currently-accepted cosmological models. This suggests that that there may be uncertainties in the old, highest-metallicity models, which is perhaps understandable given the difficulties still associated with the modelling of high-metallicity post-main sequence stellar atmospheres.

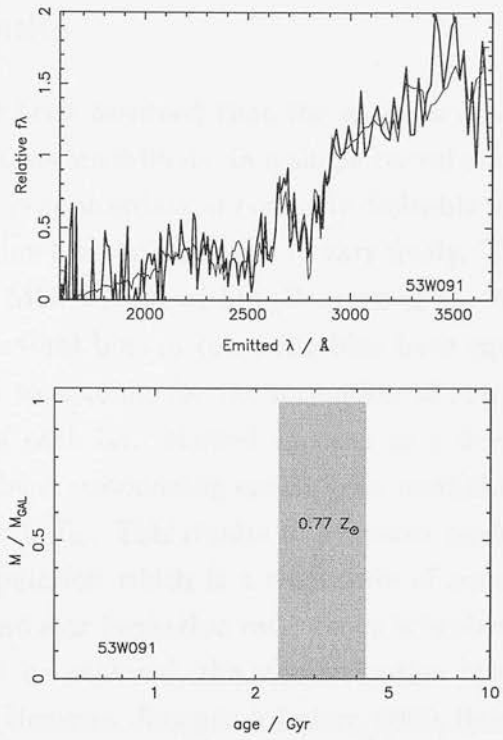

Figure 4.10: Top: best-fitting model (thick line) to the spectrum of LBDS 53W091 (thin line) predicted using MOPED (Heavens et al., 2000). Bottom: The predicted stellar population components. The population has negligible contributions from any component except the 0.77 $Z_{\odot}$ component, at an age of $2.35 - 4.25$ Gyr.

For 53W091, the mean metallicity derived from this mixed-metallicity modelling is very well constrained, and is in fact precisely solar. Not surprisingly, therefore, the best-fit age remains $\simeq$ 3 Gyr (c.f. Table 4.1), with ages $<$ 2.5 Gyr strongly excluded. The bottom panel of figure 8 shows that, at this age, the solar-metallicity component is completely dominant. While the second panel demonstrates the extent of the age-metallicity degeneracy, ages smaller than 2.5 Gyr can be formally rejected at the 95.4% confidence level.

Is these lower age limit on 53W091 robust, or are better fits possible at lower ages with even higher metallicities than those investigated? For this galaxy, the bottom plot in figure 8 shows that the highest metallicity component is only dominant at very young ages, where the statistical quality of the fit is completely unacceptable. A sufficient region of parameter space has been explored for the age limit $>$ 2.5 Gyr to be regarded as robust.

4.4.3 MOPED results

In all of the above, it has been assumed that the galaxies have formed the bulk of their stellar populations, of whatever metallicity, in a single coeval starburst. To check the extent to which this simplification is appropriate, it is clearly desirable to explore a larger parameter space, in which star formation history is allowed to vary freely. Therefore, the galaxy spectra has been refitted using the MOPED algorithm (Heavens et al., 2000). In this approach, star formation is divided into several bins in time; the bins have equal width in log space, and allow widths small enough to account for the formation of stars in giant molecular clouds (10^7 years). The height of each bin, allowed to float as a free parameter, represents the mass turned into stars at the corresponding epoch. The metallicity of each bin is allowed to take any value from 0.01 to 5 $Z_\odot$. This results in the most model-independent prescription for describing a stellar population which is a composite of simple stellar populations with arbitrary metallicity, age and star formation rate. Since it is obvious that a parameter space with 1000 variables cannot be explored, the star formation history is confined to 12 bins. With the help of MOPED (Heavens, Jimenez & Lahav, 2000, Reichardt, Jimenez & Heavens, 2001), this huge (24 dimensional) parameter space may be explored very efficiently, in only a few seconds.

Figures 4.9 and 4.10 show the best fitting value found searching the hyper-likelihood surface[1]. The results for 53W069 yield a population dominated by an old (4.25 – 7.72 Gyr), high-metallicity (3.72 $Z_\odot$) component, together with a small (7.0% by mass), younger component with a metallicity of 0.13 $Z_\odot$. For 53W091, an old component (2.35 – 4.25 Gyr) may be seen, with a metallicity of 0.77 $Z_\odot$ and negligible contributions from other populations, in good agreement with the previous findings. This, therefore, confirms that for both 53W091 and 53W069, the ages of the dominant populations remain old and apparently coeval, even when the star formation history is allowed to float freely. Unsurprisingly, therefore, the quality of the best fits achieved by MOPED are no better than those achieved with the single burst models explored in the earlier section of this paper.

[1]The hyper-likelihood surface is so large in this case that not all of it can be explored at once. Instead, 2000 random starting points are chosen, to find the global minimum, which is shown in figures 4.9 and 4.10, for 53W069 and 53W091 respectively.

4.5 Conclusion

The main conclusions of this work can be summarized as follows.

First, it has been demonstrated that, when fitted to high-quality, near-UV spectra of F stars, the synthetic near-UV spectra produced by the variable-metallicity models of Jimenez et al. (2001, in preparation) are sufficiently accurate to extract well-constrained estimates of metallicity in accord with the values determined from the study of well-established optical indices. This suggests that it should, in principle, be possible to break the age-metallicity degeneracy when fitting such models to high-quality optical spectra of high-redshift galaxies.

Second, fitting these variability-metallicity models to the Keck optical (rest-frame near-UV) spectrum of the red, $z \simeq 1.5$ galaxy 53W091 it is found to be dominated by a 3-Gyr stellar population of approximately solar metallicity, in good agreement with the original conclusions of Dunlop et al. (1996).

Third, the fit to the even redder $z \simeq 1.5$ galaxy 53W069 has been able to constrain the metallicity well, but the age has not been convincingly determined. Given the success of the fits to the other spectra, where the old, 5 $Z_{\odot}$ model does not make any significant contribution, this is most likely to represent some uncertainty in the very highest metallicity model at old ages. However, better quality UV data and / or the addition of rest-frame optical data may serve to resolve this problem.

The main finding of importance for cosmology is that, even after this exploration of the effects of varying metallicity, the best-bet age of the oldest known galaxies at $z \simeq 1.5$ remains 3 Gyr, with ages younger than 2 Gyr now more strongly excluded than before.

For $H_0 = 70 \mathrm{kms}^{-1}\mathrm{Mpc}^{-1}$ an Einstein-de Sitter universe is younger than 3 Gyr at $z \simeq 1.5$, and even the hard lower limit for coeval star formation of 2.0 Gyr translates into star-formation activity prior to $z = 8$. For a flat universe with $\Omega_m = 0.3$ and $\Omega_\Lambda = 0.7$, the best-bet age of 3 Gyr translates into $z = 5$, while the hard lower limit of > 2.0 Gyr translates into $z > 3$. The added flexibility in the star formation history investigated using the MOPED algorithm allows some later star formation, but the bulk of the stars ($> 90\%$) must still be formed at high redshift.

Our results therefore continue to argue strongly against an Einstein-de Sitter universe, and favour a Λ-dominated universe in which star formation in at least LBDS 53W091 is completed somewhere in the range $z = 3 - 5$. Such a conclusion is in accord with recent results from sub-mm surveys which suggest that star-formation activity in radio galaxies, and potentially all massive ellipticals is largely completed at $z > 3$ (Archibald et al. 2001; Dunlop 2001).

Following the success of this work in simultaneously determining the ages and metallicities of real stellar populations (with the possible exception of the age of LBDS 53W069), the main subject of the next chapter is an attempt to disentangle the potentially more complex stellar population components of two low-redshift, inactive elliptical galaxies, using very high quality UV-to-optical data.

Chapter 5

The star formation history of low redshift elliptical galaxies

5.1 Introduction

The formation of elliptical galaxies is a controversial subject. Although it is generally accepted that the bulk of their stars were formed at early epochs (e.g. Kauffman, Charlot & White, 1996, Zepf, 1997, Franceschini et al., 1998), when and how they were assembled to their present mass is still the subject of some debate. Empirical evidence exists both for the completion of formation processes at high redshift, $z \geq 2$ (Daddi et al., 2001a, Bender et al, 1992), followed by passive evolution, and for their formation from the merging of spiral galaxies at lower redshift, $z < 1$ (e.g Kauffman, 1996, Baugh, Cole & Frenk 1996, Baugh et al., 1998). Recent work (e.g. Kormendy & Bender, 1996, Genzel et al., 2001) suggests that two distinct classes of elliptical galaxies exist, which differ in their precise morphology, occupy distinct areas in the fundamental plane, and are the products of two different formation processes. *Disky* ellipticals have relatively small effective radii, intermediate masses and significant rotational support (Genzel et al., 2001). *Boxy* ellipticals are massive, luminous objects, with greater central velocity dispersions, large effective radii and 'boxy' isophotes.

It has been postulated that the disky elliptical galaxies are the product of disc-disc mergers at relatively low redshift ($z < 1$), whereas the formation of boxy ellipticals was completed at high redshift (Kormendy & Bender, 1996, Faber et al., 1997). Therefore, at the present epoch, giant, boxy ellipticals are expected to have relatively red colours as a result of their

purely passive evolution from an early epoch. However, one would expect star formation to be triggered by a merger event, and, consequently, the presence of relatively young, blue, stellar populations in disky ellipticals, if they are indeed produced by such an event. The age of the young population then indicates the epoch of the merger event.

Thus, the challenge is to determine the ages of the component stellar populations of elliptical galaxies, which may then provide clues to their formation history.

In this thesis, it has already been demonstrated that spectral synthesis models are able to successfully reproduce the rest-frame UV spectra of high-redshift massive elliptical galaxies, simultaneously determining age and metallicity (Z) (Chapters 3 and 4, Nolan et al., 2001a and 2001b). We now wish to determine whether, if high-quality spectral data across a wide enough wavelength range are available, the stellar population components of low-redshift elliptical galaxies may be disentangled. Low-redshift elliptical galaxies are potentially more complex systems than those at high redshift, if they have undergone one or more bursts of star formation, subsequent to the initial burst which produced their original populations. In addition, whereas the rest-frame UV flux of high-redshift elliptical galaxies is dominated by contributions from main sequence (MS) stars, which are relatively well-understood, at longer wavelengths, and ages $\gtrsim 5$ Gyr, post-main sequence contributions, over which there is still much uncertainty (e.g Charlot, Worthey & Bressan, 1996), become important. Here, therefore, the ability of spectral synthesis models from various authors to reproduce these post-MS contributions is also tested.

In this work, archived data has been used to produce high-quality ultraviolet (UV) to optical spectra for the two low-redshift ($z < 0.01$) elliptical galaxies, NGC 3605 and NGC 5018. We attempt to place limits on the ages and metallicities of the dominant stellar population components of these galaxies, by comparing their spectral energy densities (SEDs) with synthetic stellar population spectra. In Section 5.2, we discuss how the UV-to-optical spectra of the low-redshift galaxies were constructed. The model-fitting process is described in Section 5.3, and the results are presented and discussed in Section 5.4, together with the results of fitting the galaxy spectra with the MOPED algorithm (Heavens et al., 2000), which requires no initial assumption about the form of the star formation history. These results are discussed in Section 5.5, together with the potential for spectroscopic determination of the position of elliptical galaxies on the fundamental plane. Conclusions are presented in Section 5.6.

author	metallicities (Z / $Z_{\odot}$)	age range / Gyr
Jimenez et al., 2001	0.01, 0.20, 0.50, 1.00, 1.50, 2.50, 5.00	0.01 – 14.0
Bruzual and Charlot, 2001	0.005, 0.02, 0.20, 0.40, 1.00, 2.50, 5.00	0.1 – 19.8
Worthey, 1994	0.592, 1.00, 1.78, 3.16	1.0 – 14.0

Table 5.1: Table of stellar population evolutionary synthesis models used in this work, their metallicities with respect to solar metallicity ($Z_{\odot}$ = 0.02 for the Jimenez et al. (2001) and Bruzual & Charlot (2001) models; $Z_{\odot}$= 0.0169 for the Worthey (1994) models) and the age ranges covered.

5.2 The data

NGC 3605 is an elliptical galaxy at a redshift of 0.002228, and a non-interacting companion to NGC 3607. $M_B = -18.48$ (Schweizer & Seitzer, 1992). The UV spectrum (2250 – 4750 Å, Ponder et al., 1998) was observed using the Faint Object Spectrograph on the Hubble Space Telescope. The optical spectrum (3481 – 7375 Å, Jansen et al., 2000) was observed with the FAST spectrograph at the F. L. Whipple Observatory's 1.5m Tillinghast telescope. The two spectra were normalised to unity in the wavelength overlap region, and spliced.

NGC 5018 is a giant elliptical at z = 0.009320. The UV spectrum for this galaxy (2250 – 4750 Å, Ponder et al., 1998) was also observed using the Faint Object Spectrograph on the Hubble Space Telescope. The optical spectrum (3700 – 8000 Å, Bica & Alloin, 1987a) was observed using the Boller and Chivens spectrograph at the ESO 1.52m telescope at La Silla. The infrared (IR) spectrum (6300 – 9700 Å, Bica & Alloin, 1987b) was also observed with the Boller and Chivens spectrograph, on the ESO 2.2m telescope at La Silla. Therefore, the UV-to-IR spectrum, combined as for NGC 3605, has a total wavelength range 2215 – 9670 Å. $M_B = -22.22$ (Schweizer & Seitzer, 1992). NGC 5018 is a companion to the spiral galaxy NGC 5022, and both an optical (Schweizer & Seitzer, 1992) and an HI (Kim et al. 1988) bridge to this galaxy have been observed.

5.3 Models and fitting

In this work, three sets of instantaneous starburst evolutionary synthesis models with a range of metallicities were utilised. The models are those of Jimenez et al. (2001, in preparation, hereafter J01), Bruzual and Charlot (2001, in preparation, hereafter BC01) and Worthey (1994, hereafter W94); their metallicities, and the age ranges covered are listed in Table 5.1. J01 and BC01 assume a solar metallicity ($Z_{\odot}$) of 0.02, whereas W94 has $Z_{\odot} = 0.0169$

Each set of models was fitted to the near-UV-to-optical spectra of NGC 3605 and NGC 5018 in three ways. Firstly, each single-metallicity model was fitted individually, with age and normalisation allowed as free parameters. Secondly, a composite, mixed-metallicity model was fitted, as in Chapter 3, although in this case, seven J01 and BC01 metallicities were available, and four W94 metallicities. The normalisation and fractional contribution by mass of each metallicity were allowed to vary freely, and the component populations were assumed to be coeval. Thirdly, a two-component model was fitted. In this case, both the age and the metallicity of each component was allowed to vary freely. The best fit in each case was determined by a minimum χ^2 test. Finally, the galaxy spectra were fitted using the MOPED algorithm (Heavens et al., 2000), which allows the initial assumptions about the star formation history to be unconstrained.

For each fit, the observed spectra were first rebinned to the wavelength resolution of the model spectra, with the re-binned flux taking the value of the mean flux per unit wavelength in each new bin. The error adopted for each binned data point was the standard error on the mean value of the flux in each bin, relaxed by a constant multiplicative factor which allows the best-fit two population model for each galaxy to have a reduced χ^2 (χ^2_{ν}) of approximately unity. The χ^2 values quoted here are therefore relative rather than absolute values. The entire available wavelength range for each observed galaxy (i.e. 2235 – 7350 Å for NGC 3605, and 2215 – 9670 Å for NGC 5018) was included in the fits.

To produce the contour plots of constant relative likelihood presented in Figures 5.2, 5.3, 5.5 and 5.6, the errors were further relaxed by a constant multiplicative factor of two. This does not affect the best-fit parameters, but it should be noted that the contour levels are of relative, rather than absolute, likelihood. For the mixed-metallicity, single-age fits, the same mean metallicity may be obtained from many different combinations of the component single-metallicity models. Therefore, in Figures 5.2 and 5.5, it is the marginalised distribution of mean metallicity that the relative likelihood contours represent.

5.3.1 Single-metallicity model fits

Each available single-metallicity instantaneous starburst model, for each of the three sets of models, was fitted individually to the two galaxy spectra. Both the model and the observed spectra were normalised to a mean flux per unit wavelength of unity across the wavelength range 5020 – 5500 Å. The model age and normalisation were then varied as free parameters, and the best-fitting age for each metallicity was found by a χ^2 minimisation.

5.3.2 Coeval, mixed-metallicity model fits

For each set of models, a mixed-metallicity model was constructed, with the relative contribution by mass of each different metallicity component allowed to vary freely. In this model, it was assumed that all the component populations were formed at the same time, and the age of the total population was an additional free parameter. The models were built from the unnormalised fluxes of the single-metallicity models, so that the relative fraction of each single-metallicity model flux contributing to the total population is equivalent to its fractional contribution by mass. After the fractional addition, the mixed-metallicity population was normalised to a mean flux per unit wavelength of unity in the wavelength range 5020 – 5500 Å. The combined population is defined as:

$$F_{NZ,\lambda,t} = const \sum_{i=1}^{N} X_{Z_i} f_{Z_i,\lambda,t}$$

where $F_{NZ,\lambda,t}$ is the mixed, N-metallicity model flux per unit wavelength in the bin centered on wavelength λ at age, t Gyr (N is seven for J00 and BC01 and four for W94); $f_{Z_i,\lambda,t}$ is the flux per unit wavelength λ at age, t Gyr, for the single metallicity model with $Z = Z_i$, where $i = 1, N$, and X_{Z_i} is the fractional contribution (by mass) of the model with $Z = Z_i$ to the total population.

The best-fitting age, normalisation and the value of each X_{Z_i} were determined by χ^2 minimisation. The entire parameter space of the seven-dimensional age-metallicity hyper-cube was searched, so that the best fits quoted in the following sections are those parameter values which correspond to the point on the age-metallicity grid with the minimum χ^2.

5.3.3 Two population fits

Finally, a two-population model was constructed, where age, metallicity and fractional contribution by mass in each component were allowed to vary as free parameters, in order to determine whether more than one episode of star formation has occurred. We have

$$F_{2pop,\lambda} = const(X_i f_{Z_i,\lambda,t_i} + X_j f_{Z_j,\lambda,t_j})$$

Here, $F_{2pop,\lambda,t}$ is the model flux per unit wavelength in the bin centered on wavelength λ which is the sum of the two single-metallicity model fluxes (per unit wavelength in the bin centered on wavelength λ), f_{Z_i,λ,t_i} and f_{Z_j,λ,t_j}, which have metallicities and ages, Z_i, t_i Gyr, and Z_j, t_j Gyr, respectively. The fractional contributions of the two components, X_i and X_j, are allowed to vary freely, and again, normalisation to a mean flux of unity in the wavelength range $5020 - 5500$ Å was carried out after the addition of the two unnormalised fluxes.

A minimum-χ^2 fit was used to determine the best-fit values of X_i, Z_i, t_i, X_j, Z_j and t_j. Again, the whole parameter space was searched, with the best-fitting parameter values corresponding to the point on the age_i-age_j-Z_i-Z_j grid with the minimum calculated χ^2.

5.4 Results

5.4.1 NGC 3605

Single-metallicity model fits

The results of the single-metallicity fits to the spectrum of NGC 3605 are listed in Table 5.2. Figure 5.1 shows the best-fitting spectrum for each model set, superimposed on the observed spectrum. Even the best-fit relative minimum χ^2_ν values are several times unity, which suggests that this galaxy is not well-modelled by a single population. The best-fit parameters for the J01 and BC01 models are very similar. They are both old and metal-poor, i.e. 13 Gyr, $Z = 0.5\ Z_\odot$, and 13.75 Gyr, $Z = 0.4\ Z_\odot$ respectively. However, for the W94 models, the best fit is achieved by a younger (3 Gyr) solar metallicity model. As none of the single-metallicity, single-age models, of any author, are able to achieve a good fit to the spectrum of NGC 3605, it is not possible to produce meaningful estimates of the errors associated with these results. Consequently, it is also not possible to produce meaningful plots of the contours of constant relative likelihood for this set of model fits.

Model	Z / $Z_\odot$	Age / Gyr	Minimum χ^2_ν
NGC 3605			
Jimenez et al., 2001	0.01	13.0	184.9
	0.20	14.0	7.4
	0.50	13.0	4.5
	1.00	6.0	5.1
	1.50	6.0	4.6
	2.50	2.0	6.3
	5.00	2.0	10.7
Bruzual & Charlot, 2000	0.005	18.8	280.0
	0.02	14.8	158.8
	0.20	19.8	7.5
	0.40	13.8	3.1
	1.00	3.8	4.0
	2.50	1.6	4.4
	5.00	3.8	4.6
Worthey, 1994	0.059	8.0	4.3
	1.00	3.0	4.0
	1.78	2.0	4.4
	3.16	2.0	8.0
NGC 5018			
Jimenez et al., 2001	0.01	13.0	186.6
	0.20	14.0	52.0
	0.50	12.0	34.0
	1.00	12.0	9.3
	1.50	12.0	2.9
	2.50	5.0	2.8
	5.00	4.0	9.3
Bruzual & Charlot, 2000	0.005	19.8	232.2
	0.02	19.8	161.5
	0.20	19.8	21.3
	0.40	19.8	2.3
	1.00	8.8	2.3
	2.50	2.8	3.8
	5.00	1.0	22.3
Worthey, 1994	0.059	14.0	3.1
	1.00	9.0	2.2
	1.78	4.0	3.4
	3.16	2.0	4.6

Table 5.2: The results of fitting the near-UV-to-optical spectra of the two low-redshift galaxies with each set of single-metallicity models individually. For each model, the parameters quoted are those values on the age-metallicity grid which correspond to the minimum calculated χ^2. See § 5.4 for discussion.

	Mean Z / $Z_\odot$	Age / Gyr	Minimum χ^2_ν
NGC 3605			
Jimenez et al., 2001	2.55	4.0	1.2
Bruzual & Charlot, 2000	2.50	2.8	1.6
Worthey, 1994	2.66	2.0	3.1
NGC 5018			
Jimenez et al., 2001	1.95	10.0	1.0
Bruzual & Charlot, 2000	1.10	19.8	1.1
Worthey, 1994	1.12	13.0	1.8

Table 5.3: The results of fitting the near-UV-to-optical spectra of the two low-redshift galaxies with the single-age, mixed-metallicity models. For each model, the parameters quoted are those values on the age-metallicity hyper-cube which correspond to the minimum calculated χ^2. See § 5.4 for discussion.

Coeval, mixed-metallicity model fits

Table 5.3 lists the results for the mixed-metallicity, coeval population model fits. The corresponding plots are presented in Figure 5.2. All the models have a better quality of fit than the corresponding single-metallicity models, with the BC01 and J01 models capable of a better fit than the W94 models. In contrast to the single-metallicity fits, all the models here find a best-fit age which is young (2 - 4 Gyr) and high metallicity ($Z \simeq 2.5\ Z_\odot$). The blue end of the spectrum is better reproduced in all cases when a mix of metallicities is allowed.It should be remembered that neither the very low nor the very high metallicity options are available for W94 models, which may account for the poorer fit to the spectrum of NGC 3605 by this model set.

Two population fits

The results for the two-population model fits to the spectrum of NGC 3605 are presented in Table 5.4 and Figure 5.3. Allowing two differently-aged populations results in a better

	Z / $Z_\odot$	Age / Gyr	M / M_{gal}	Minimum χ^2_ν
NGC 3605				
Jimenez et al., 2001	5.00	2.0	0.88	1.0
	0.01	14.0	0.12	
Bruzual & Charlot, 2000	2.50	2.8	0.98	1.4
	0.005	2.3	0.02	
Worthey, 1994	3.16	3.0	0.92	1.8
	1.00	1.0	0.08	
NGC 5018				
Jimenez et al., 2001	2.50	12.0	0.78	1.0
	1.00	4.0	0.22	
Bruzual & Charlot, 2000	0.40	19.8	0.77	1.2
	2.50	19.8	0.23	
Worthey, 1994	0.592	13.0	0.80	1.8
	3.16	14.0	0.20	

Table 5.4: The results of fitting the near-UV-to-optical spectra of the two low-redshift galaxies with the two-component model. For each model, the parameters quoted are those values on the age-metallicity grid which correspond to the minimum calculated χ^2. The age and metallicity of each of the two-component populations are given, for the best fitting combination for each model set. M / M_{gal}, the fractional contribution, by mass, to the total population made by each component is shown in column 4. See § 5.4 for discussion.

fit to the observed spectrum for all the model sets, although, despite this, it is evident from the corresponding contour plots that it has not been possible here to place realistic limits on the best-fit parameters. This version of the W94 models have a substantially better quality of best fit than the best-fitting W94 coeval mixed-Z population, with a 3 Gyr, Z = 3.16 $Z_\odot$ population dominating, and some younger (1 Gyr), poorer-metallicity (Z = $Z_\odot$) component. BC01 manages a better fit than for the mixed-metallicity, single-age model, even though the

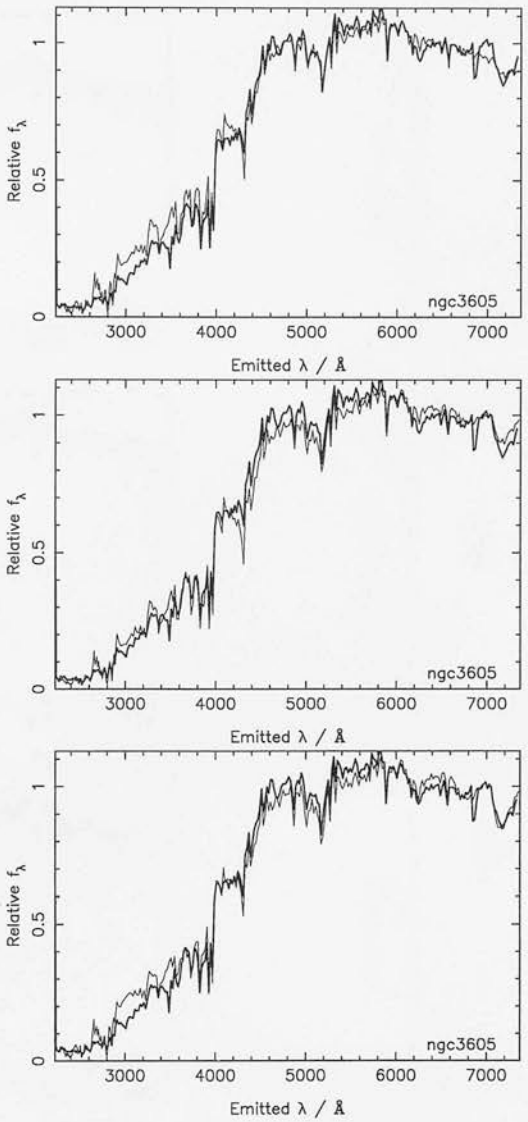

Figure 5.1: The best-fitting single-metallicity models (thin black line) superimposed over the spectrum of NGC 3605 (thick black line). Top: J01 - 13 Gyr, Z = 0.5 $Z_\odot$; middle: BC01 - 13.75 Gyr, Z = 0.4 $Z_\odot$; bottom: W94 - 3 Gyr, Z = $Z_\odot$. See § 5.4.1 for discussion.

two populations determined in the fit differ by only $\sim$ 0.5 Gyr in age. Not surprisingly, then, the dominant (98% by mass) population has the same age and metallicity as the coeval, mixed-metallicity best-fit model, i.e. 2.75 Gyr and Z = 2.5 $Z_\odot$. The fit is marginally poorer than for this model, as a mix of only two metallicities is allowed here. The J01 model set results in the best over-all fit, from a young (2 Gyr), metal-rich (Z = 5.0 $Z_\odot$) dominant population, together with a 12% by mass contribution from an old (14 Gyr), metal-poor (Z = 0.01 $Z_\odot$) component. For the J01 and W94 best-fit models, the low-metallicity population dominates at wavelengths less than $\simeq$ 2800 Å. The two populations of the BC01 fit, however,

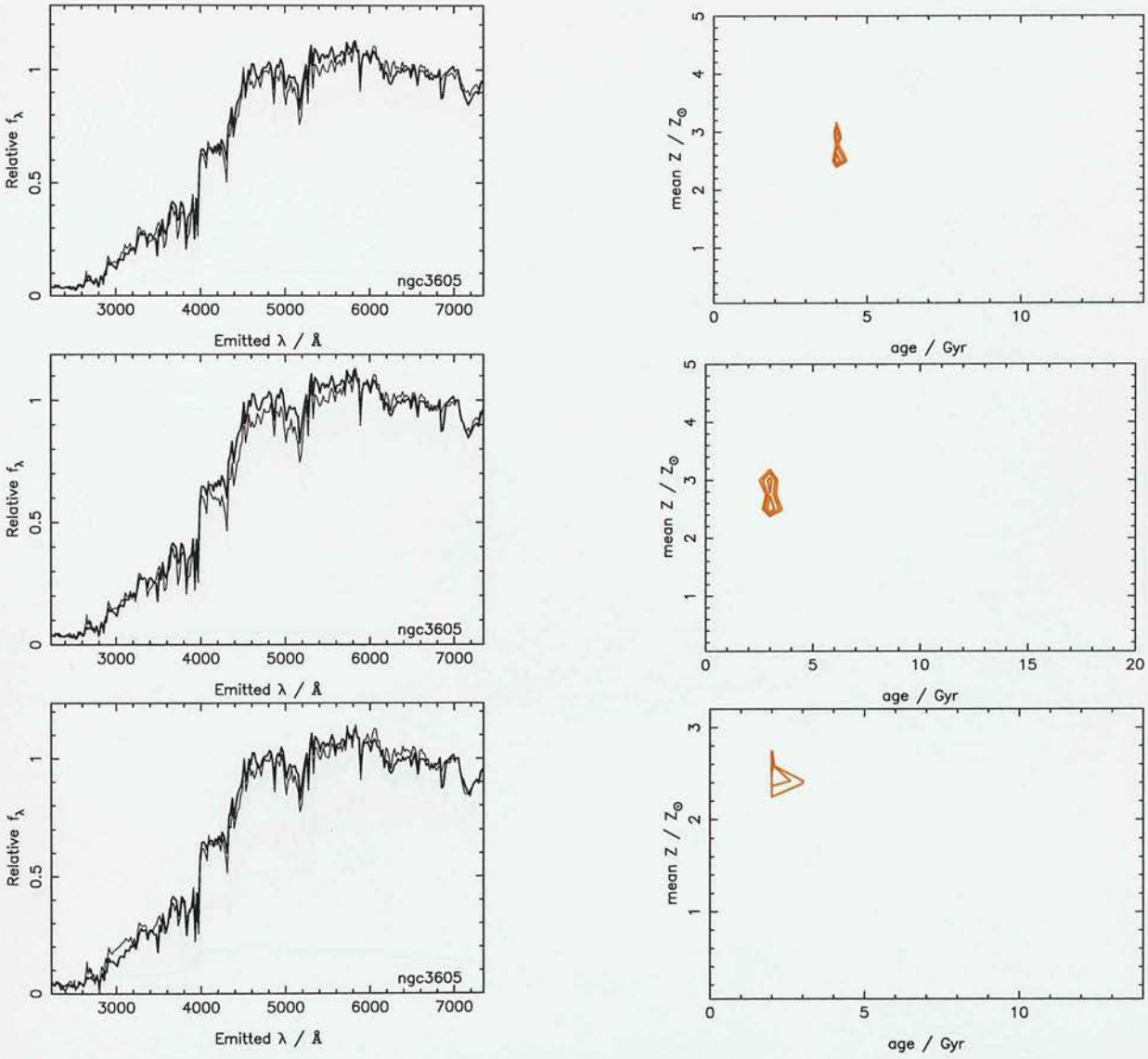

Figure 5.2: Left: the best-fitting mixed-metallicity, coeval models (thin black line) superimposed over the observed spectrum of NGC 3605 (thick black line). Top: J01 - 4 Gyr, mean Z = 2.55 $Z_\odot$; middle: BC01 - 2.75 Gyr, mean Z = 2.50 $Z_\odot$; bottom: W94 - 2 Gyr, mean Z = 2.66 $Z_\odot$. Right: contour plots of constant relative likelihood, for the marginalised distribution of mean metallicity with age. The contours contain 68.3%, 90% and 95.4% relative likelihood. See § 5.4.1 for discussion.

contribute roughly the same amount of flux at these wavelengths (see Figure 5.3).

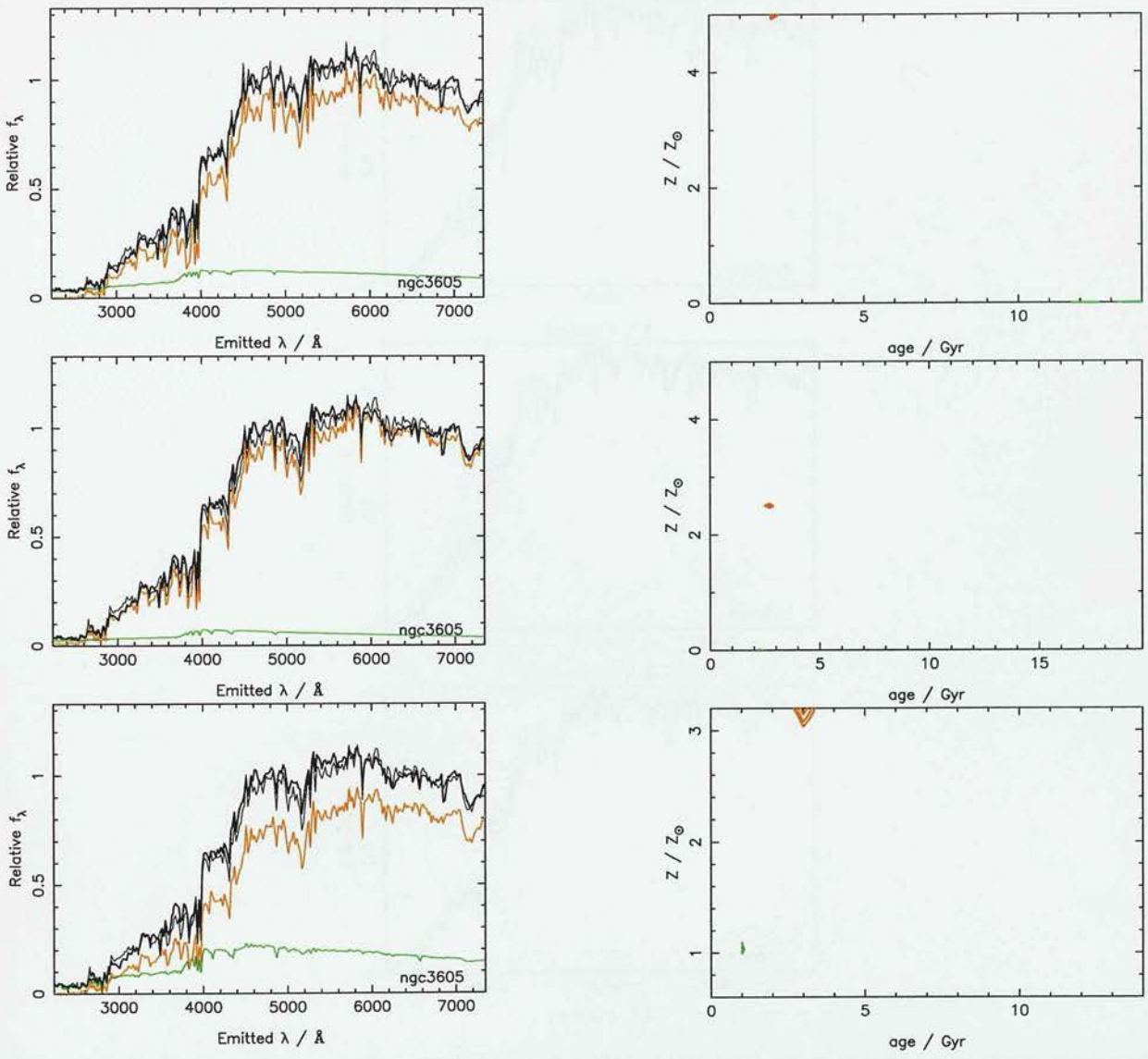

Figure 5.3: Left: the best-fitting two-component models (thin black line) superimposed over the spectrum of NGC 3605 (thick black line). The two component populations are also shown; the dominant population (p1) is in red, and the lesser population (p2) is in green. Top: J01, p1 - 2 Gyr, Z = 5.00 $Z_\odot$, p2 - 14 Gyr, Z = 0.01 $Z_\odot$; middle: BC01, p1 - 2.75 Gyr, Z = 2.5 $Z_\odot$, p2 - 2.30 Gyr, Z = 0.005 $Z_\odot$; bottom: W94, p1 - 3 Gyr, Z = 3.16 $Z_\odot$, p2 - 1 Gyr, Z = $Z_\odot$. Right: contour plots of constant relative likelihood. The contours contain 68.3%, 90% and 95.4% relative likelihood. The dominant population contours are in red, and the secondary population contours are green. See § 5.4.1 for discussion.

5.4.2 NGC 5018

Single-metallicity model fits

The results of the single-population fits to the spectrum of NGC 5018 are presented in Table 5.2. Figure 5.4 shows the observed spectrum, with the best-fit model spectra superimposed.

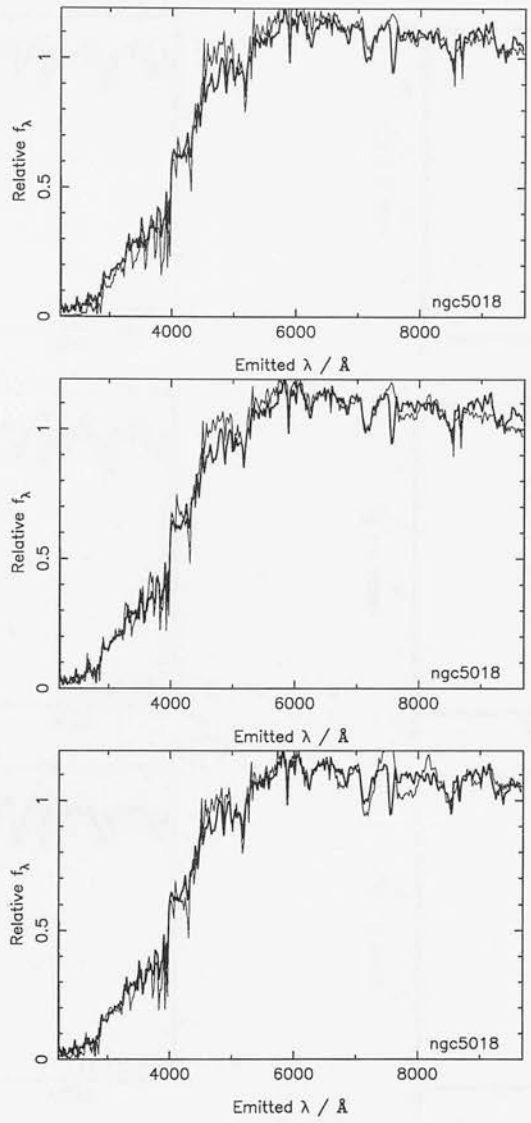

Figure 5.4: The best-fitting single-metallicity models (thin black line) super-imposed over the spectrum of NGC 5018 (thick black line). Top: J01 - 5 Gyr, Z = 2.50 $Z_\odot$; middle: BC01 - 8.75 Gyr, Z = $Z_\odot$; bottom: W94 - 9 Gyr, Z = $Z_\odot$. Right: contour plots of constant reduced χ^2. See § 5.4.2 for discussion.

As for NGC 3605, all of the single-metallicity models result in a minimum χ^2_ν of at least twice unity, from which we may infer that NGC 5018 does not consist of a single, simple stellar population. Again, as none of the single-metallicity, single-age models, of any author, are able to achieve a good fit to this spectrum, it is not possible to produce meaningful estimates of the errors associated with these results, or to produce meaningful plots of the contours of constant relative likelihood for this set of model fits. The BC01 and W94 model sets both find a best-fit with solar metallicity (solar metallicity for the Worthey models is 0.0169, and for the BC01 and J01 models it is 0.02), and an age of $\simeq$ 9 Gyr, with a similar quality of

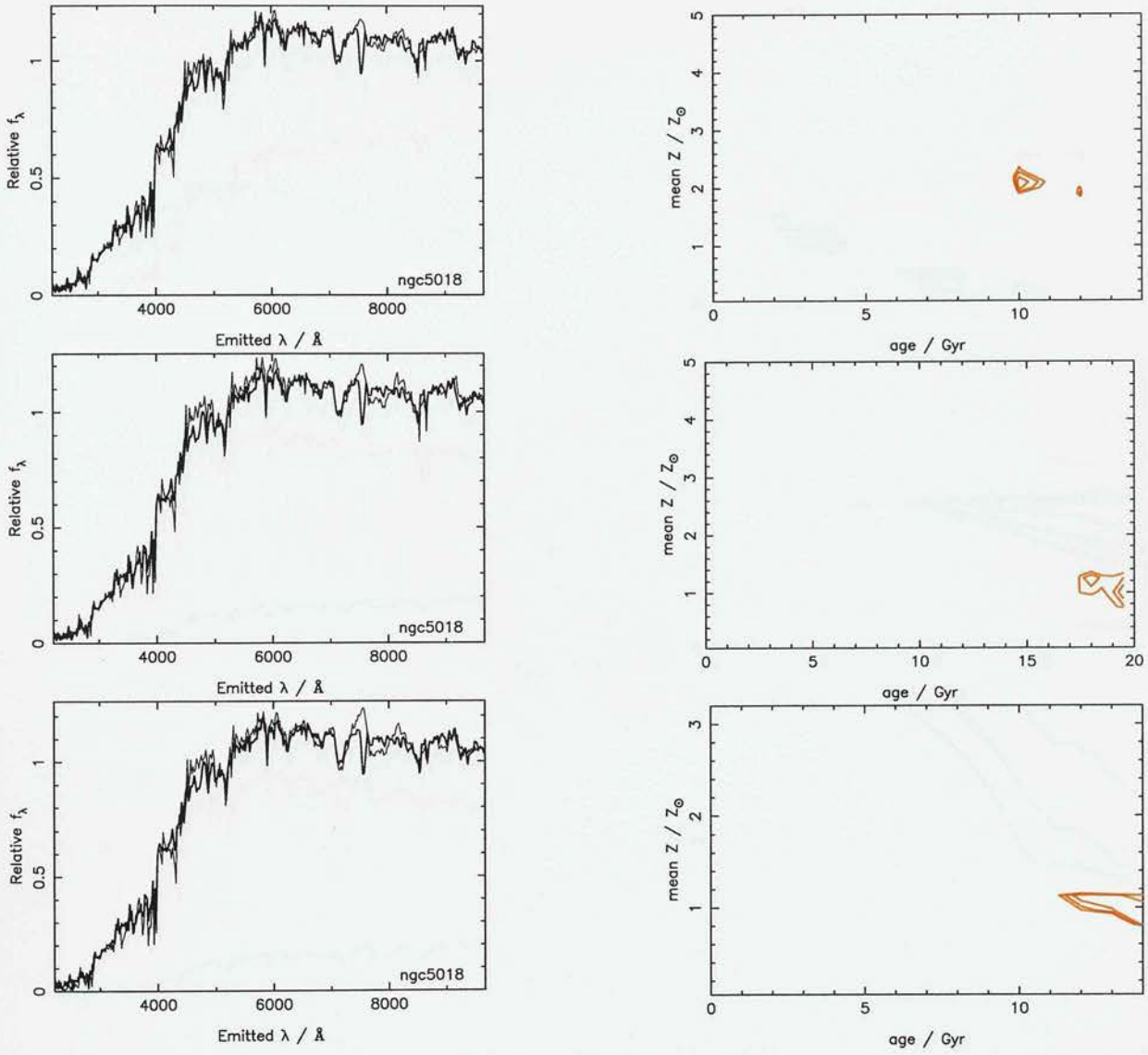

Figure 5.5: Left: the best-fitting mixed-metallicity, coeval models (thin black line) superimposed over the spectrum of NGC 5018 (thick black line). Top: J01 - 10 Gyr, mean Z = 1.95 $Z_\odot$; middle: BC01 - 19.75 Gyr, mean Z = 1.10 $Z_\odot$; bottom: W94 - 13 Gyr, mean Z = 1.12 $Z_\odot$. Right: contour plots of constant relative likelihood, for the marginalised distribution of mean metallicity with age. The contours contain 68.3%, 90% and 95.4% relative likelihood. See § 5.4.2 for discussion.

fit. The J01 model set results in the poorest fit for the single-metallicity, single-age models. The best-fit model is only 5 Gyr, and has a high (Z = 2.5 $Z_\odot$) metallicity. This does not allow the flux at wavelengths $\leq$ 2800 Å to be well-reproduced.

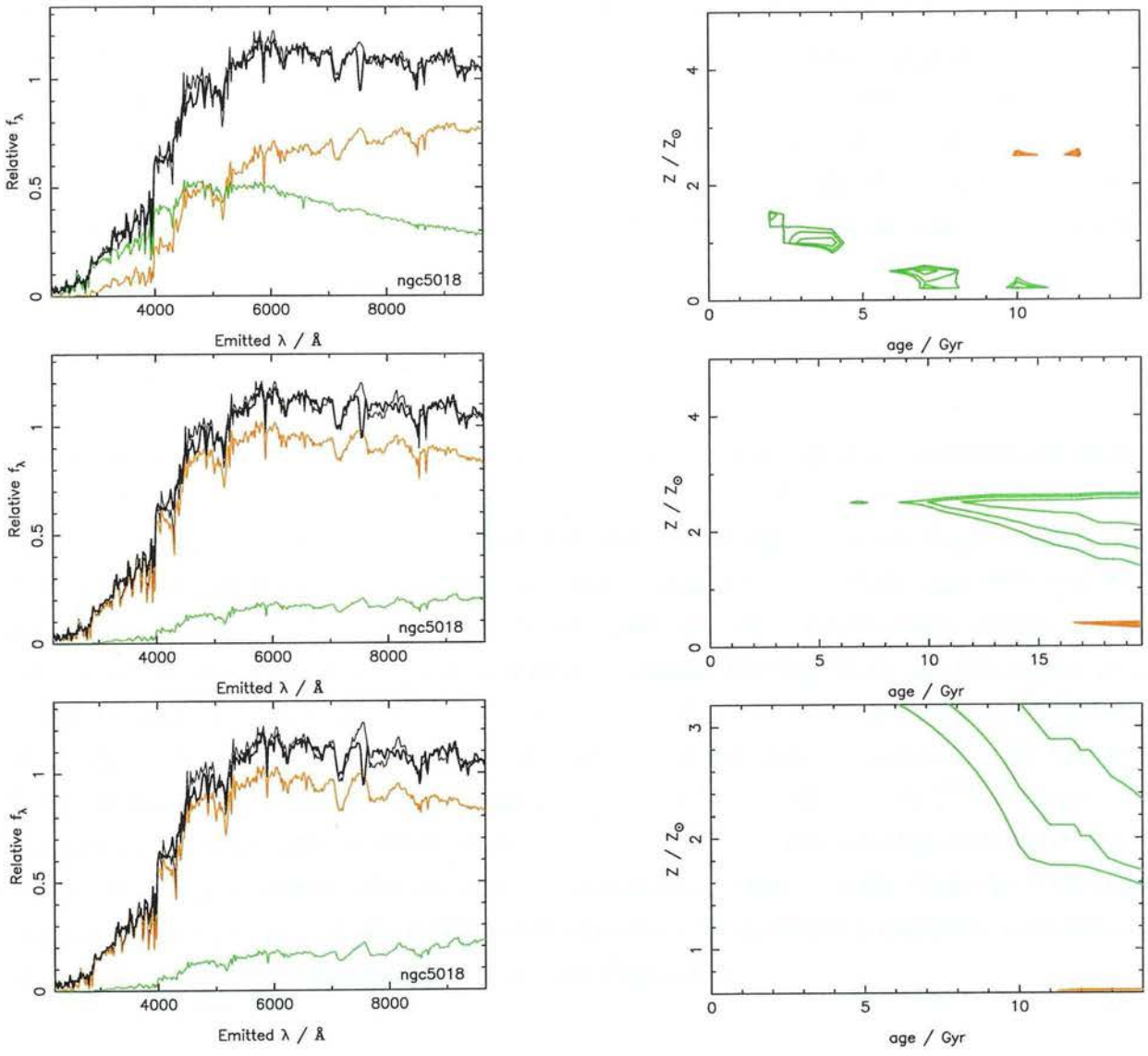

Figure 5.6: Left: the best-fitting two-component models (thin black line) superimposed over the spectrum of NGC 5018 (thick black line). The two component populations are also shown; the dominant population (p1) is in red, and the lesser population (p2) is in green. Left: Top: J01, p1 - 12 Gyr, Z = 2.50 $Z_\odot$, p2 - 4 Gyr, Z = $Z_\odot$; middle: BC01, p1 - 19.75 Gyr, Z = 0.40 $Z_\odot$, p2 - 19.75 Gyr, Z = 2.50 $Z_\odot$; bottom: W94, p1 - 13 Gyr, Z = 0.592 $Z_\odot$, p2 - 14 Gyr, Z = 3.16 $Z_\odot$. Right: contour plots of constant relative likelihood. The contours contain 68.3%, 90% and 95.4% relative likelihood. The dominant population contours are in red, and the secondary population contours are green. See § 5.4.2 for discussion.

Coeval, mixed-metallicity model fits

Table 5.3 lists the results of the mixed-Z, coeval population model fits to the spectrum of NGC 5018. The corresponding plots are presented in Figure 5.5. With several metallicities

allowed to contribute, the BC01 and W94 model sets now both fit an old stellar population, although the mean metallicity still remains at approximately solar metallicity. The J01 models fit best at 10 Gyr, with a 12 Gyr model possible at the 90% relative likelihood level, and a mean metallicity which is twice the solar value. The blue end of the spectrum is much better reproduced with a mix of metallicities allowed. This best-fit model has a minimum χ^2_ν value of unity, which means that the quality of the fit is as good as that of the best-fit two-population model.

Two population fits

The results of the two-population fit to the spectrum of NGC 5018 are presented in Table 5.4 and Figure 5.6. For the BC01 and W94 models, the results are very similar to the mixed-metallicity, coeval model fit results. For these model sets, both the fitted populations are old - of the same age for BC01 and differing by only 1 Gyr for W94 - and with roughly solar mean metallicity. The quality of the fits, therefore, are unsurprisingly similar to the quality of the mixed-metallicity, coeval model fit results. For the BC01 models, which fit a coeval population, even when this is not enforced, the fit is, as one might expect, marginally worse than when seven metallicities are available. The J00 best-fit model is quite different from the other two. Although the dominant population is still old (12 Gyr, 77% by mass), in contrast to the other two model set results, at Z = 2.5 $Z_\odot$, it has a higher metallicity than the secondary population. The secondary population is much younger than the dominant population (4 Gyr, $Z_\odot$). It should be noted that the 10 Gyr coeval population is contained within the 90% relative likelihood contour (see Figure 5.6).

5.4.3 MOPED results

The spectra of NGC 3605 and NGC 5018 were refitted with the MOPED algorithm (Heavens et al., 2000, Reichardt et al., 2001). MOPED, as described in Chapter 4, § 4.4.3, allows the star-formation history to vary freely, so that the total population is not restricted simply to one or two episodes of star formation. Figures 5.7 and 5.8 show the best-fitting results of searching the 24-dimensional parameter space.

The results for NGC 3605 are dominated by two high-metallicity populations (Z = 3.72 $Z_\odot$, and Z = 4.10 $Z_\odot$), with ages in the two bins spanning 1.5 - 4 Gyr. These two components account for 86% by mass of the total population. This is in fair agreement with the young, metal-rich, dominant populations fitted by the two-population models in § 5.4. However,

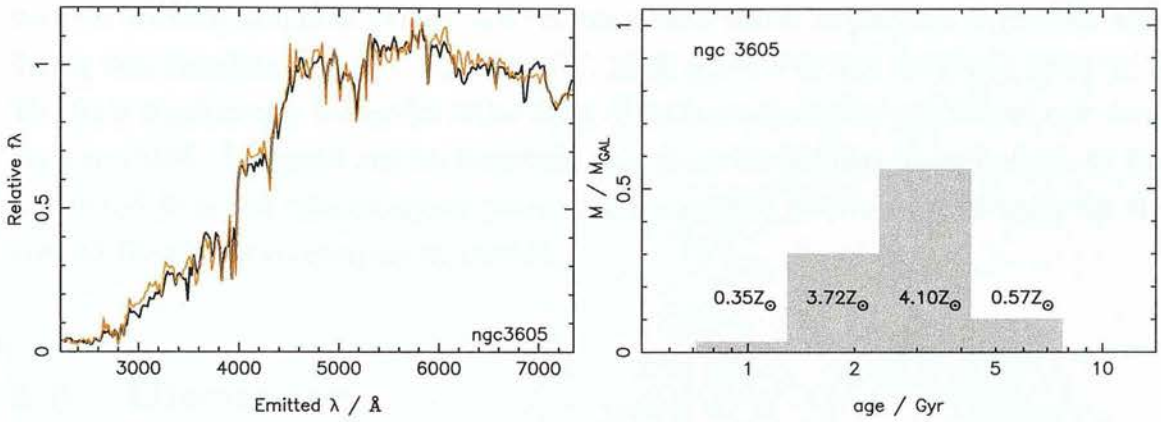

Figure 5.7: Left: best-fitting model (thin line) to the spectrum of NGC 3605 (thick line) predicted using MOPED (Heavens et al., 2000). Right: The predicted stellar population components. See § 5.4.3 for discussion.

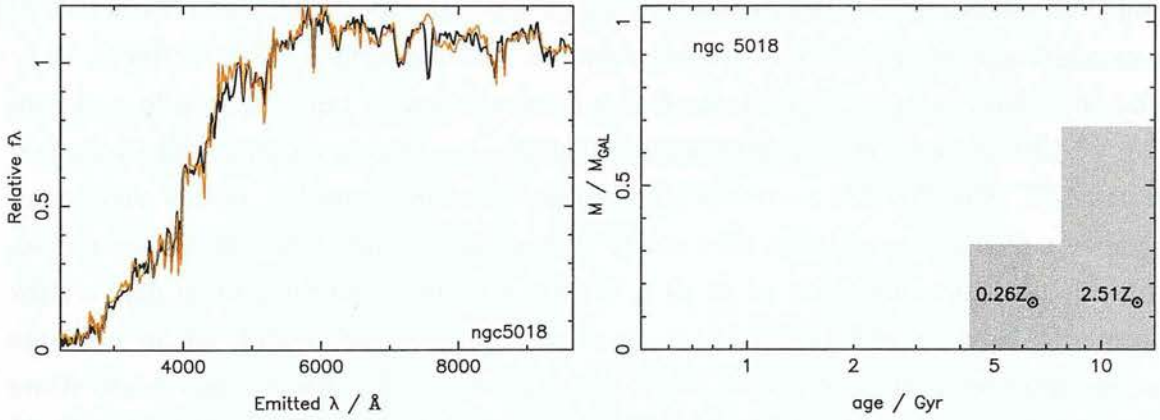

Figure 5.8: Left: best-fitting model (thin line) to the spectrum of NGC 5018 (thick line) predicted using MOPED (Heavens et al., 2000). Right: The predicted stellar population components. See § 5.4.3 for discussion.

although the secondary population of the two-component model fits for the J01 and BC01 models is old and very metal-poor; MOPED finds two other smaller populations, in the bins centred on 1 Gyr and 5.6 Gyr, with metallicities Z = 0.35 $Z_\odot$and Z = 0.57 $Z_\odot$ respectively.

For NGC 5018, the stellar population parameters determined by MOPED consist of a Z = 0.26 $Z_\odot$ component, with an age lying in the bin centred on 5.5 Gyr, and a second component with a metallicity of Z = 2.51 $Z_\odot$ and an age = 8 − 14 Gyr. The relative proportions by mass of these two populations are 32% and 68% respectively. This result is in excellent agreement with the best-fit two-population model of the J01 model set.

The unrestricted star-formation history permitted by the MOPED algorithm, together with its ability to allow the metallicity to vary freely, has enabled a better quality of fit to the

two low-redshift elliptical galaxy spectra than that which is possible with even the best-fitting two-population model, i.e. for NGC 3605, $\chi^2_\nu = 0.6$, and for NGC 5018, $\chi^2_\nu = 0.9$. The fit is significantly better for NGC 3605 when more than two episodes of star formation are permitted. It should not be forgotten that these are relative values of χ^2_ν, as they are calculated from the relaxed errors, which are normalised to give a χ^2_ν of unity for the best over-all fit of the two-component models.

5.5 Discussion

5.5.1 Lifting the age-metallicity degeneracy

In this work, model fits to long-baseline spectra have enabled the age-metallicity degeneracy to be lifted. Figure 5.9 demonstrates the improvement possible in the simultaneous determination of both age and metallicity when a wide wavelength range is used. The left-hand plot shows the contours of constant relative likelihood (68.3%, 90% and 95.4%) for a mixed-metallicity, coeval, J01 model fit to the optical-only spectrum of NGC 3605. The parameters are not well constrained, and the degeneracy of age with metallicity, in which a young model with a high metallicity has as good a quality of fit as an older, more metal-poor model, is apparent in the slope of the contours. However, if the UV data is included, the results are much better constrained. The right-hand plot shows contours of the same constant relative likelihood for the coeval, mixed-metallicity, J01 model fit to the optical-plus-UV spectrum of NGC 3605. In this case, the age-metallicity degeneracy has all but disappeared, and we are left with a neatly-constrained set of parameters. This clearly demonstrates the power of the long-baseline fit in determining age and metallicity.

5.5.2 Age and metallicity determination

The W94 model set results in the poorest fits for both NGC 3605 and NGC 5018. This may be as a consequence of the limited range of metallicities available in this work, and because post-main sequence (post-MS) contributions to the integrated light of these models are treated in a less sophisticated manner than for the other two model sets. It has already been established in this thesis that the W94 models are, for the same metallicity, redder at a younger age than the J01 model set (Chapter 3, Nolan et al., 2001a). This effect is particularly apparent in the mixed-metallicity model fits to the spectrum of NGC 3605.

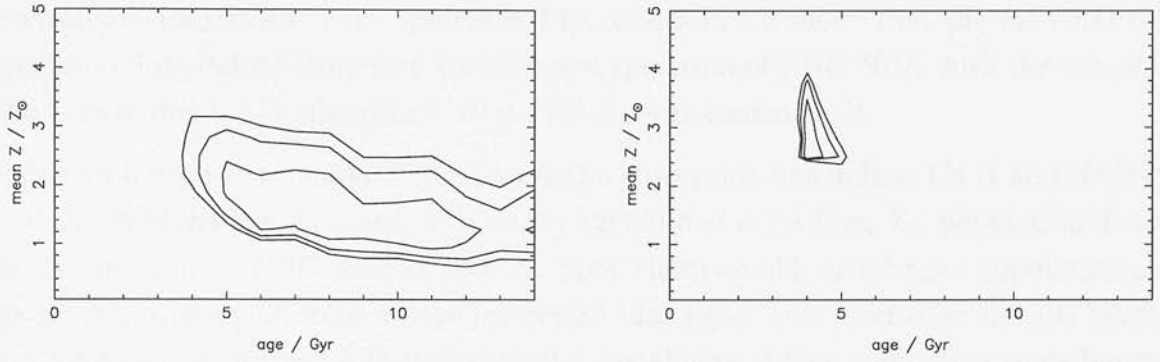

Figure 5.9: Left: contour plots of constant relative likelihood, for the marginalised distribution of mean metallicity with age. The contours contain 68.3%, 90% and 95.4% relative likelihood for the coeval, mixed-metallicity, J01 model fit to the optical-only spectrum of NGC 3605. Right: contour plots of the same constant relative likelihood for the coeval, mixed-metallicity, J01 model fit to the optical-plus-UV spectrum of NGC 3605. See § 5.5.1 for discussion.

Although a similar mean metallicity is determined by each model set, the W94 best-fit age is half that of the J01 best-fit age. The J01 fit is of a substantially better quality.

The best-fit parameters determined by BC01 and W94 mixed-metallicity and two-population fits are in good agreement, given the limited range of W94 models. The BC01 models are consistently capable of a better fit than the W94 models. However, the best possible composite-population fits to the spectra of both low-redshift galaxies are the result of fitting the bluer J01 model set.

All the models are in agreement that NGC 3605 has a predominantly young ($2 - 3$ Gyr), metal-rich ($Z \geq 2.5\ Z_{\odot}$) stellar population. The MOPED results are consistent with this, but find a more complex star formation history for this galaxy than can be investigated with the simple combination of single stellar population models, and it is this model which produces the best over-all fit.

For the redder spectrum of NGC 5018, all the models agree that the major stellar population is old ($\geq$ 12 Gyr). However, whilst the BC01 and W94 models predict that total stellar population is roughly coeval, with a mean metallicity $\sim$ solar, the J01 two-component models identify a substantial ($\sim$ 25% by mass) 4 Gyr secondary population, and a dominant older population, with a metallicity 2.5 times $Z_{\odot}$. Although this fit has a lower minimum χ^2_{ν} than the best-fitting BC01 and W94 models, it has the same minimum χ^2_{ν} value as the best-fitting coeval J01 model. The subsequent uncertainty over which version of the J01 composite model fits is more believable is alleviated by the MOPED result. This is in remarkable agreement

with the two-population J01 results, and, with a minimum χ^2_ν of 0.9, results in the best over-all fit. Inspection of the spectra in Figures 5.6 to 5.8 shows that the MOPED best-fit spectrum does indeed reproduce the observed spectrum of NGC 5018, with the exception of the feature due to sky absorption at $\sim$ 7500 Å, very convincingly.

Using an independent method (comparing the absorption line indices Ca II and Hδ/λ4045), and the W94 models, Leonardi & Worthey (2000) find a 2.8 Gyr, $Z_\odot$ population dominant in the spectrum of NGC 5018 at 4000 Å. They claim an old, metal-poor population cannot be contributing significantly to the integrated blue light. Our results for the J01 model fits are consistent with this. Although the solar metallicity, 4 Gyr population contributes only 22% of the total mass of the galaxy, at wavelengths $\leq$ 4500 Å, it dominates the integrated flux. This strengthens the argument for the presence of a young stellar population in NGC 5018, although neither the BC01 or W94 models identify it in the fit to the UV – optical spectrum.

Schweizer and Seitzer (1992), determined heuristic merger ages (HMA) for both these low-redshift galaxies, using a simple two-burst model of evolving stellar populations, and varying both the Hubble type of the pre-merger galaxies, and the gas-to-star conversion efficiency. The input stellar population models are the 1991 versions of Charlot and Bruzual's models, from which UBV colour residuals are constructed, which are then compared with the observed UBV colour residuals. For NGC 3605, they determine a merger age of between 7.4 and 9.4 Gyr, depending on the model used, with an age of 7.8 Gyr predicted using the 'most representative' model of disk-disk collisions. However, only solar metallicity models were considered in this work. We have a wider range of metallicities available, and, as one would expect, our predicted age is less than 7.4 Gyr, as the best-fit metallicity of the dominant component is super-solar. For NGC 5018, Schweizer and Seitzer find a 'most representative' age of 3.8 Gyr. Ages between 3.4 and 7.3 Gyr are predicted by various other versions of their models. The J01 model set best-fit two-population parameters identify a younger population with solar metallicity, and, as one would therefore hope, this younger population, which, if it formed as the result of a merger interaction, determines the epoch of that interaction, has an age of 4 Gyr, in good agreement with the results of Schweizer and Seitzer.

It should be remembered that the minimum χ^2 values discussed in this work are relative values, not absolute. Hence, a minimum χ^2_ν of unity does not imply a perfect fit, nor even, necessarily, a formally acceptable fit. There are well-known difficulties in modelling post-MS stellar spectra, which become more important at longer wavelengths, and ages $\gtrsim$5 Gyr (Magris & Bruzual, 1993, Dunlop et al., 1996, Spinrad et al., 1997). These probably contribute to the relatively poor fits by the BC01 and, in particular, the W94 composite

model fits. Also, as suggested in Chapter 4, these uncertainties may well be more significant in higher-metallicity model stellar atmospheres, which play a significant part in this work. Inspection of the contour plots of Figure 5.3 suggests that, in the case of the J01 fit to the spectrum of NGC 3605, a better solution, with a metallicity greater than 0.10, may be possible.

The χ^2 fits to the spectra of NGC 3605 and NGC 5018 are sensitive to the shape of the error spectrum. In order to place realistic limits on the parameters determined in these fits, the estimated error in the flux needs to be re-investigated. One would hope that the best-fit values would not change, but one might expect there to be more models available with a closer-to-best fit than are found in this work. The normalisation of the spectra would also benefit from a further investigation. Splicing together the various spectral regions may not have removed differences in the relative normalisation of the regions. Normalisation of the different regions independently, using a polynomial normalisation factor, may achieve a better quality of fit. Again, one would also hope that this would lead to more realistic limits on the parameters determined in the fit. It is unlikely, however, that the consideration of dust extinction would significantly improve the fit or alter the contour plots; the MOPED algorithm includes a dust parameter, but finds an insignificant contribution in both galaxies. This is corroborated by the findings of Buson et al., (2001), who, using deep HST imaging of NGC 5018, find that the UV flux of this galaxy is only marginally affected by internal extinction due to dust.

It is encouraging that, despite the uncertainties in the modelling and the differences between the models, the multiple component spectral fits, with three different model sets, plus the MOPED fits, are in good agreement regarding the age of the dominant populations of these galaxies.

5.5.3 Mergers and the fundamental plane

Figure 5.9 shows projections in the fundamental plane of the observed properties of NGC 3605 (Faber et al., 1989 and Faber et al., 1997) and NGC 5018 (Faber et al., 1989 and Scorza et al., 1998), together with a population of giant boxy ellipticals, and intermediate mass, disky ellipticals (Bender et al., 1992, and Faber et al., 1997) for comparison. The two galaxy populations occupy different positions in the fundamental plane. Giant, boxy ellipticals tend to be more massive, more luminous and have higher central velocity dispersions than the intermediate disky ellipticals. Mean values of the effective surface brightness, μ_e, effective

	Giant boxy ellipticals	Disky ellipticals / lenticulars
r_e / kpc	5.80 ± 1.70	1.76 ± 1.75
μ_e (K / mag)	17.07 ± 0.68	16.47 ± 1.00
σ_0 / kms^{-1}	238 ± 1	157 ± 2

Table 5.5: Mean properties of the galaxy samples plotted in Figure 5.9. The limits shown are the standard deviation of the sample. r_e is the effective half-light radius for the whole galaxy; μ_e is the mean surface brightness in the K band, within r_e, calculated from the B band value using $(B-K) = 3.9$ (Genzel et al., 2001); σ_0 is the central velocity dispersion. All data are taken from Bender et al. (1992), Faber et al. (1997) and Faber et al. (1989). All parameters are calaculated for a cosmology with $H_0 = 65$ kms^{-1}Mpc^{-1} and $\Omega_m = 0.3$. See § 5.5 for discussion.

Galaxy	r_e / kpc	μ_e (K / mag)	σ_0 / kms^{-1}
NGC 3605	2.1	18.0	103
NGC 5018	4.7	16.8	223

Table 5.6: Observed properties of NGC 3605 and NGC 5018: σ_0 is the central velocity dispersion; μ_e, the effective surface brightness in the K band, is calculated from the mean surface brightness within the effective half-light radius (r_e) in the B band, using $(B-K) = 3.9$ (Genzel et al., 2001). r_e for NGC 5018 is from Scorza et al. (1998), r_e for NGC 3605 is from Faber et al. (1997), and μ_e and σ_0 for both galaxies is from Faber et al. (1989). All parameters are calaculated for a cosmology with $H_0 = 65$ kms^{-1}Mpc^{-1} and $\Omega_m = 0.3$. See § 5.5 for discussion.

radius, r_e, and central velocity dispersion, σ, for the two galaxy populations are listed in Table 5.5, and the corresponding values for NGC 3605 and NGC 5018 are listed in Table 5.6. All the parameters are calaculated for a cosmology with $H_0 = 65$ kms^{-1}Mpc^{-1} and $\Omega_m = 0.3$.

In a study of the isophotes of NGC 3605, Michard and Marchal (1994) claim that this galaxy is a boxy elliptical. However, Faber et al. (1997) detect a surface brightness profile which, although it is boxy at large radii ($> 2''$), is disky in the inner regions of the galaxy, and its

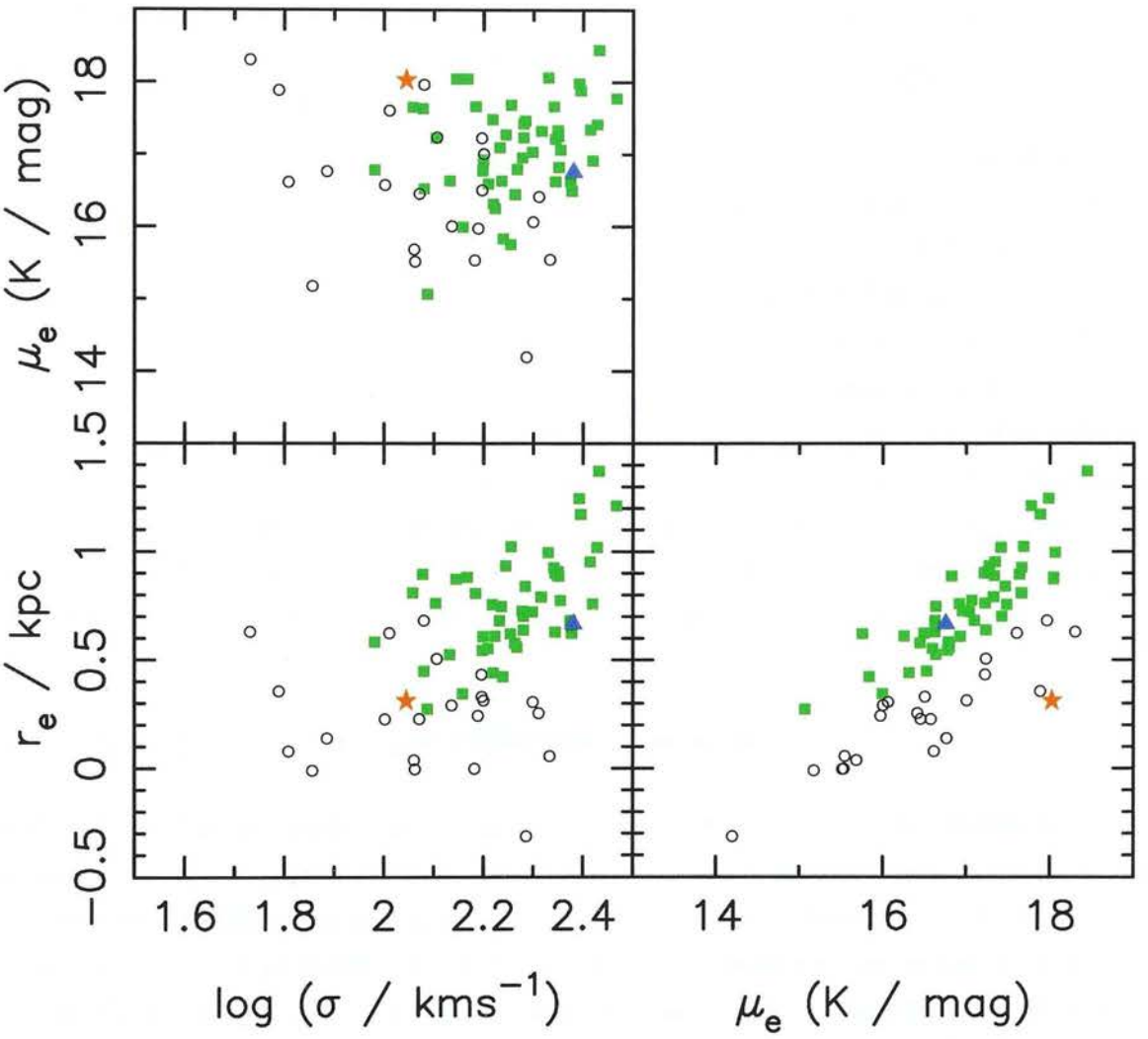

Figure 5.10: Projections of the fundamental plane. Green squares: giant, boxy ellipticals (from Bender et al., 1992, and Faber et al., 1997); black circles: intermediate mass, disky ellipticals (from Bender et al., 1992, and Faber et al., 1997); red star: NGC 3605 (from Faber et al., 1989 and Faber et al., 1997); blue triangle: NGC 5018 (from Faber et al., 1989 and Scorza et al., 1998). All parameters are calaculated for a cosmology with $H_0 = 65$ kms^{-1}Mpc^{-1} and $\Omega_m = 0.3$. See § 5.5 for discussion.

position on the fundamental plane places it unequivocally in the population of disky ellipticals. The spectroscopic determination of the ages of the constituent populations of NGC 3605 is consistent with the theory that this galaxy is indeed the product of a galaxy-galaxy merger. A small detectable old population is dominated by a much younger population, whose formation was most likely triggered by a major merger event.

NGC 5018, a shell galaxy, looks more ambiguous. Its effective radius, central velocity dispersion and relatively low μ_e suggest that it belongs with the giant boxy population. At

the same time, NGC 5018 appears to contain a fairly substantial young population (22% by mass). One might expect this young population to have been triggered by a merger event. However, NGC 5018 is a near companion to the spiral galaxy NGC 5022, and there is evidence of an on-going interaction between these two galaxies: an optical bridge has been detected between them (Schweizer and Seitzer, 1992), together with an HI bridge (Kim et al. 1988). Kim et al. conclude that the HI interaction between NGC 5018 and NGC 5022 is current, but Malin & Hadley infer from the deeply embedded dust lane in NGC 5018 that interactions between the two galaxies have occurred more than once in their history. Simulations indicate that shell structure resulting from a weak interaction between galaxies may survive for a few Gyr (Reduzzi et el., 1996). Therefore, although extra blue light from the shells and bridge mimics a post-merger galaxy, it is more likely that NGC 5018 consists of a predominantly mature central population, which has evolved passively, together with younger shells which are a product of mass transfer or accretion. The position of NGC 5018 in the fundamental plane favours this scenario over that of a major merger event.

5.5.4 Comparison of the different model sets

The motivation for this work, was, in part, to compare the ability of the different model sets to reproduce observed galaxy spectra. On examination of the results of the single-metallicity fits to the two low-redshift galaxy spectra, one might, naively, conclude that the BC01 model set most accurately reproduces real stellar populations. However, the errors were adjusted to give a minimum χ^2_ν of unity for the very best fit of any of the models fitted as described in Section 5.3 (which for both NGC 3605 and NGC 5018 were the two-population fits of the J01 model set). Therefore, although it is difficult to state exactly what value of χ^2_ν constitutes a formally good fit, all of the single-age, single-metallicity fits, by all of the model sets, have an unnaceptable quality of fit in comparison with the best over-all fit; even the very best BC01 single-age, single-metallicity results have a χ^2_ν of more than twice unity for NGC 5018 and more than three times unity for NGC 3605. When more flexibility in the star-forming history is allowed, the J01 model set have a significantly improved quality of fit, and consistently produce the best fits.

Additional confirmation of the strength of the J01 model set comes from their ability to disentangle the intermediate-age stellar population of NGC 5018 from the dominant older population. This is the only model set which is able to reproduce from continuum fitting the results which Leonardi & Worthey (2000) obtain from fitting absorption line indices. Not even Worthey's own models manage this in the continuum fits.

On this evidence, it is fair to say that, of the model sets considered here, the J01 models most convincingly reproduce the UV-to-optical continua of real stellar populations.

5.6 Conclusions

Neither NGC 3605 nor NGC 5018 are the result of purely passive star-forming histories. We find that NGC 3605 is most likely the result of a major merger event, but that NGC 5018 is essentially a giant, boxy, old elliptical, with an additional young stellar population, possibly resulting from its interaction with the companion galaxy, NGC 5022.

The spectral fitting is capable of disentangling the component populations, and the agreement between different models in the ages of the dominant populations of the galaxies, together with the results from independent studies (Schweizer and Seitzer, 1992, Leonardi and Worthey, 2000) encourages confidence in our results. An old, metal-poor population is necessary in addition to the younger component in order to convincingly fit the observed UV flux of NGC 3605. In NGC 5018, the younger population dominates the blue end of the spectrum, until wavelengths > 5000 Å, where the flux from the old component begins to dominate. Clearly, where multiple stellar populations are present, a wide wavelength range must be avaiable if the full star formation history of low redshift ellipticals like NGC 3605 and NGC 5018 is to be determined.

For a universe with $\Omega_m = 0.3$, $\Omega_\Lambda = 0.7$ and $H_0 = 65$ kms^{-1}Mpc^{-1}, the redshift at which NGC 3605 was assembled to its present state is $z_{merg} = 0.2$, if the formation of the stars in the 2 Gyr population is assumed to have been triggered by this event. This is in agreement with hierarchical structure formation scenarios in which merging events take place predominantly at $z < 1$. For NGC 5018, assuming that the age of older population indicates the age of the mature population of the underlying giant, boxy galaxy, then, for the same cosmology, an age of 12 Gyr implies a redshift of formation, $z_f = 2.8$. This is consistent with results from sub-mm studies which suggest massive elliptical galaxies have completed their star forming activity by $z \simeq 3$ (Archibald et al., 2001, Dunlop, 2001).

In conclusion, the spectroscopic disentanglement of the component populations of elliptical galaxies is possible, and is a useful tool in the investigation of elliptical galaxy formation and evolution. We are able to determine the formation scenarios of these galaxies, and hence their general position in the fundamental plane using this method. Further work on the relative normalisation of the different regions of the combined spectra, and on the error

estimation, would improve the reliability of the age and metallicity determinations. It has also been possible to distinguish between the different model set's abilities to reproduce real stellar population spectra; the Jimenez et al. (2001) models consistently achieve the best quality of fit when a realistic, multi-component population is fitted to the observed data.

Chapter 6

Conclusions

6.1 The evolutionary history of massive elliptical galaxies

6.1.1 Are high-redshift red galaxies the progenitors of low-redshift massive ellipticals?

The determination of the ages of the stellar populations in the elliptical galaxies studied in this work, together with the position of these galaxies in the fundamental plane, lead to some important conclusions about the formation history of elliptical galaxies. If elliptical galaxies are indeed the result of monolithic collapse at high redshift (e.g. Daddi et al., 2001a, Bender et al, 1992), and their subsequent evolution is predominantly passive, then high-redshift massive elliptical galaxies are likely to be the progenitors of low-redshift ellipticals. In this case the following should be true:

- both the high-redshift galaxies and their low-redshift counterparts should have formed at similar epochs;
- if they have undergone no dynamical evolution, the high-redshift galaxies should occupy the same position in the fundamental plane as their low-redshift counterparts.

galaxy	age / Gyr	z	z_f
53W091	3	1.55	4.5
NGC 5018	12	0.0022	2.8
	4		0.3
NGC 3605	2	0.0093	0.2
	14		9.8
AGN host galaxies	11	0.2	6.5

Table 6.1: Table of formation redshifts (z_f) for the stellar populations of the galaxies studied in Chapters 4 and 5. The ages are the best-fit ages determined in those chapters, and $H_0 = 65$ kms^{-1}Mpc^{-1}, $\Omega_m = 0.3$, $\Omega_\Lambda = 0.7$ is assumed. The first row for each NGC galaxy lists the results for their dominant stellar populations. The second row lists the results for their secondary population.

In Table 6.1, the redshifts of formation (z_f) for the stellar populations in the elliptical galaxies studied in this work are presented, for a cosmology with $H_0 = 65$ kms^{-1}Mpc^{-1}, $\Omega_m = 0.3$ and $\Omega_\Lambda = 0.7$. The ages are the best-fit ages that have been determined for the populations in these galaxies. For the high-redshift galaxy, LBDS 53W091, z_f lies within the redshift range $3 < z < 5$, in agreement with recent results from sub-millimetre surveys (Archibald et al., 2001, Dunlop, 2001) which suggest that radio galaxies, and potentially all massive elliptical galaxies, have completed their star formation activity by $z \gtrsim 3$. The massive, mature galaxy, NGC 5018, has a redshift of formation that lies at the lower limit of this range; for this cosmology, LBDS 53W091 and NGC 5018 have a similar epoch of formation. This is strong evidence in favour of NGC 5018 as a low-redshift counterpart to galaxies like the two high-redshift LBDS galaxies. Examination of the fundamental plane projections in Figure 6.1 are consistent with this suggestion. The effective half-light radius, r_e, and the central velocity dispersion, σ_0, are very similar for the LBDS galaxies and NGC 5018. Their K−band mean surface brightnesses (within r_e), μ_e, show a greater discrepancy. However, μ_e is strongly affected by stellar evolution; hence, as the ages of the populations of the LBDS galaxies and NGC 5018 differ, one might expect that μ_e for these galaxies would differ.

NGC 3605 looks very different from the LBDS galaxies and NGC 5018. In the fundamental plane (Figure 6.1), it lies securely with the population of disky, intermediate mass ellipticals. Although it has a small population of old stars, the bulk of its stars (88 % by mass) are

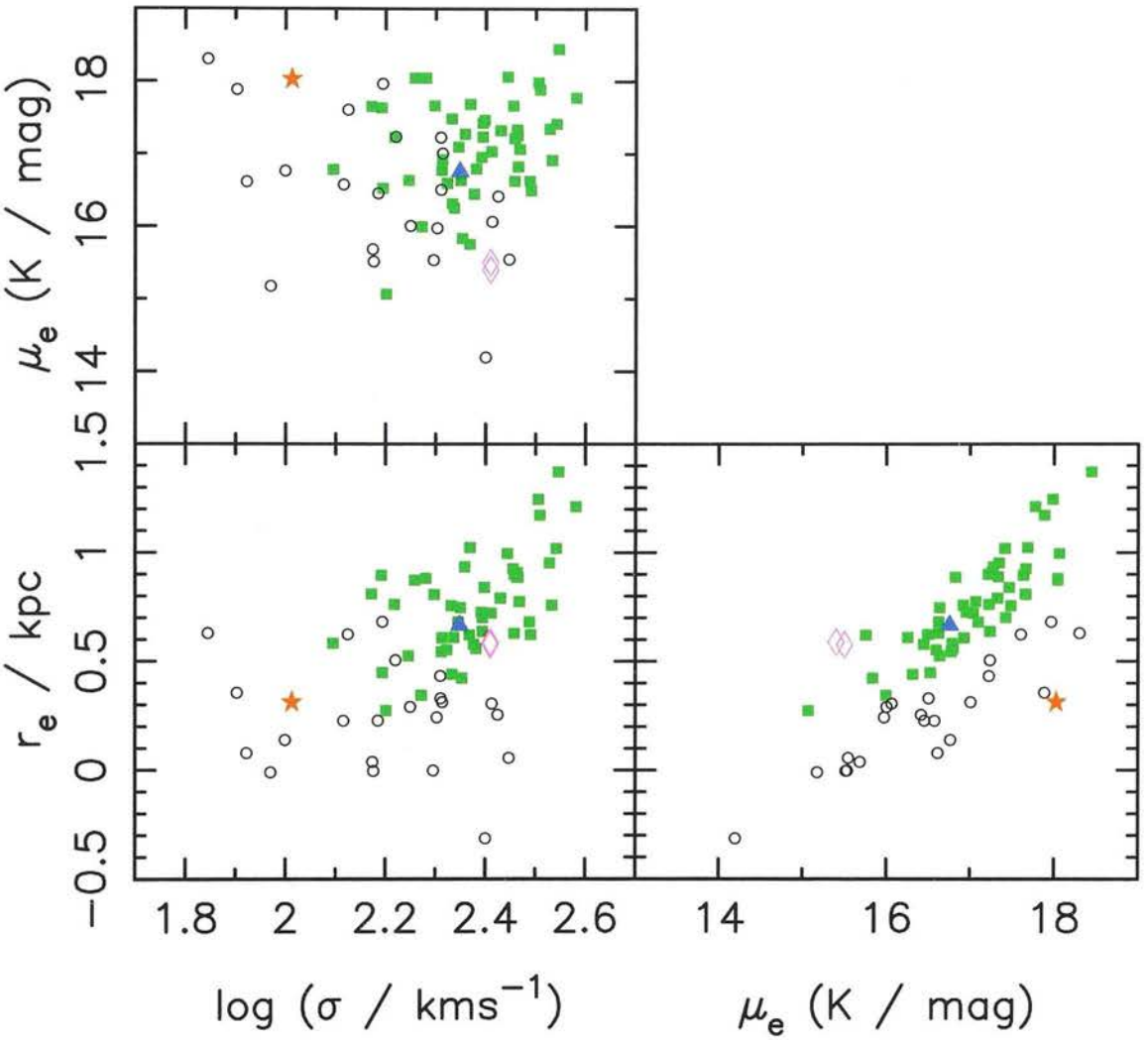

Figure 6.1: Projections of the fundamental plane, as in Chapter 5, but with the high-redshift LBDS galaxies in addition. Green squares: giant, boxy ellipticals (from Bender et al., 1992, and Faber et al., 1997); black circles: intermediate mass, disky ellipticals (from Bender et al., 1992, and Faber et al., 1997); red star: NGC 3605 (from Faber et al., 1989 and Faber et al., 1997); blue triangle: NGC 5018 (from Faber et al., 1989 and Scorza et al., 1998): magenta diamond; LBDS 53W069 and LBDS 53W091 (Dunlop, 1999, Peacock et al., 1998). All parameters are calculated for a cosmology with $H_0 = 65$ kms^{-1}Mpc^{-1}, $\Omega_m = 0.3$ and $\Omega_\Lambda = 0.7$.

young (2 Gyr), and must therefore have been formed at low redshift ($z \sim 0.2$). The small size and low central velocity dispersion of this galaxy suggest that it cannot have evolved from massive galaxies like LBDS 53W091 and LBDS 53W091. Instead, this galaxy is likely to have followed a different evolutionary path, undergoing one or more merger events, most recently at a redshift ~ 0.2. The underlying population of very old (14 Gyr) stars is identified in the two-component fit of Chapter 5, however, it should be noted that this population is

not identified with the unrestricted star formation model allowed by the MOPED fit.

In conclusion, there is evidence for the existence of two different evolutionary processes leading to the formation of elliptical galaxies. The evidence from low-redshift, 'boxy', old ellipticals, such as NGC 5018, and high-redshift ellipticals, such as LBDS 53W091 and LBDS 53W069, is consistent with formation from the single collapse of the high density peaks of the mass distribution at early epochs, and completion of assembly at high redshift ($z \gtrsim 3$). Their subsequent evolution is predominantly passive. 'Disky' ellipticals, like NGC 3605, differ from old, massive ellipticals in their stellar content, their precise morphology and their dynamics. These have most likely been assembled to their present state at lower redshift ($z < 1$), from merger interactions between spiral galaxies. The precise evolutionary path followed by an elliptical galaxy may be identified from its star formation history, determined from the fitting of stellar population evolutionary synthesis model spectra to high-quality data across a wide wavelength range. This work has successfully demonstrated the power of this method by simultaneously determining both the age and metallicity of the component stellar populations of a variety of elliptical galaxies.

6.1.2 Constraining cosmological parameters

Constraints on the cosmological parameters, H_0, Ω_m and Ω_Λ are possible from the age determination of stellar populations at known redshift, as the Universe has to be at least as old as these populations at the corresponding redshifts. Figure 6.2, therefore, presents cosmologies with $\Omega_m + \Omega_\Lambda = 1$, permitted by the stellar populations of the galaxies studied. i.e. an LBDS-like galaxy of 3 Gyr at $z = 1.5$, a typical AGN host galaxy from Chapter 2, with an age of 11 Gyr at a redshift of 0.2, the 14 Gyr secondary population of NGC 3605 ($z = 0.00932$) and the dominant, 12 Gyr population of NGC 5018 ($z = 0.00223$). Cosmologies to the upper right of the lines are excluded, as, in these regions, the Universe would be too young to contain populations at these ages. In this plot, no time has been allowed for the actual formation of the stars, so these should be considered upper boundaries.

The 11 Gyr stellar population of the typical AGN host galaxy and the 14 Gyr secondary population of NGC 3605 impose the severest restrictions on the cosmological parameters. Interestingly, the limits imposed by these two populations are very similar. Dunlop et al. (2001) find strong evidence from the position of the AGN host galaxy population on the photometric projection of the fundamental plane ($r_e - \mu_e$) that these host galaxies belong to the class of old, boxy ellipticals. It is, therefore, perhaps unsurprising that the limits set

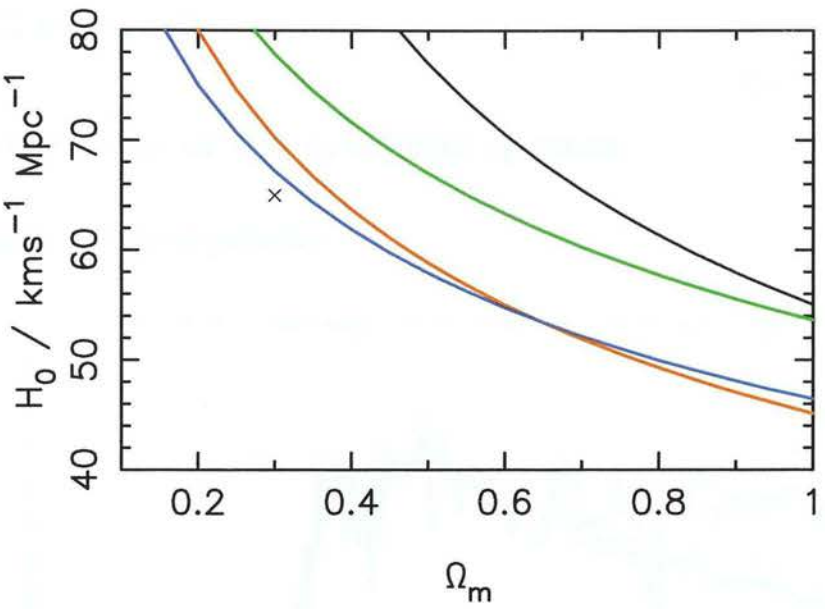

Figure 6.2: Lines of constant age in various cosmologies, where $\Omega_m + \Omega_\Lambda = 1$. The black line represents cosmologies where the Universe has an age of 3 Gyr at z = 1.5; red; cosmologies where the Universe is 11 Gyr at z = 0.2; green; cosmologies where the Universe is 12 Gyr at z = 0.0022, and blue; an age for the Universe of 14 Gyr at z = 0.00932. The ages are those determined for the stellar populations of the LBDS galaxies, the AGN host galaxies, NGC 5018 and NGC 3605 in Chapters 2, 4 and 5 (without time allowed for the actual formation of stars). For NGC 5018 and NGC 3605, these are the ages of the older stellar populations. Cosmologies to the upper right of the lines are therefore excluded, as, in these regions, the Universe would be younger than the ages of the stellar populations at the corresponding redshifts. The cross marks the point with $H_0 = 65$ kms^{-1}Mpc^{-1}, $\Omega_m = 0.3$ and $\Omega_\Lambda = 0.7$, which is permitted by all the stellar population ages.

by the dominant AGN host galaxy population and an old, z $\sim$ 0.01 population should be similar.

An Einstein-de Sitter Universe is only allowable if H_0 is very small (< 45 kms^{-1}Mpc^{-1}), but 'Cosmology 2001', the current favourite model, with $H_0 = 65$ kms^{-1}Mpc^{-1}, $\Omega_m = 0.3$ and $\Omega_\Lambda = 0.7$ is permitted by all the stellar population ages, with $\gtrsim$0.5 Gyr allowed for star formation.

6.2 Further work

6.2.1 Further tests of the synthetic spectra

The low-redshift elliptical galaxies

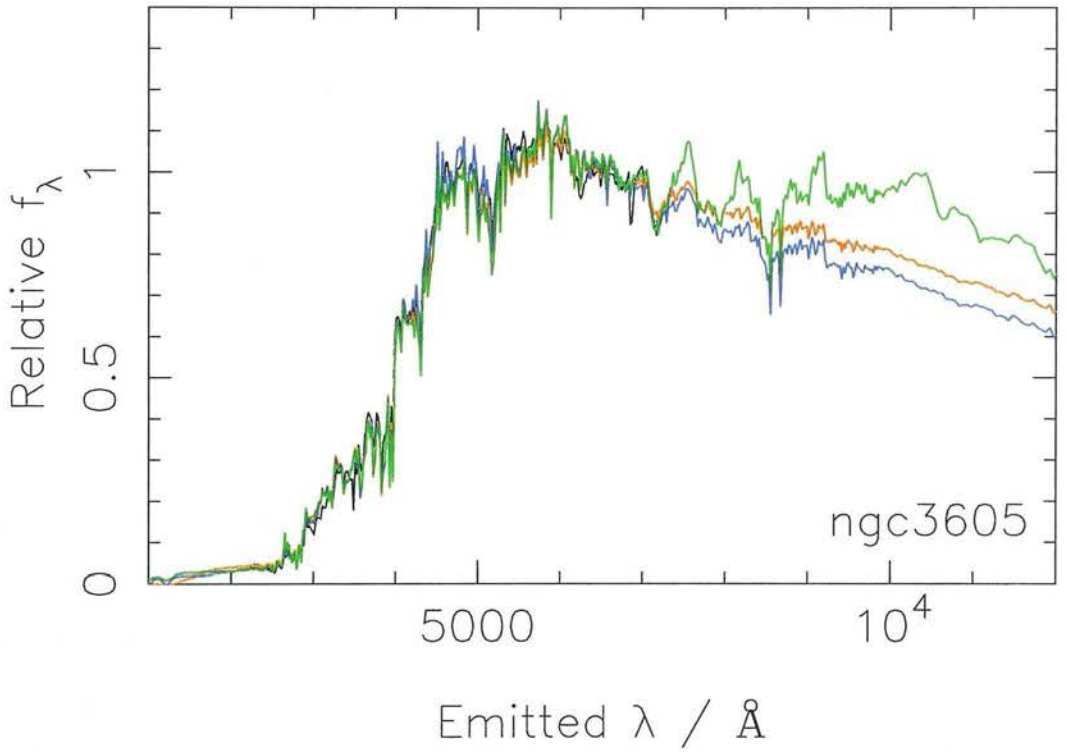

Figure 6.3: black - observed spectrum of NGC 3605; red - J01 coeval, mixed-metallicity model at 4 Gyr, and a mean metallicity of 0.051; blue - J01 two-population model, p1: 2 Gyr, Z = 0.1, p2: 14 Gyr, Z = 0.0002; green - BC01 two-population model, p1: 2.75 Gyr, Z = 0.05, p2: 2.30 Gyr, Z = 0.0001

The Jimenez et al. (2001, J01 hereafter) model spectra have consistently resulted in a better quality of fit to the galaxy spectra considered in this work than models by other authors. However, the difference in the quality of fit between the Bruzual and Charlot (2001) models (BC01 hereafter) and the J01 models has not always been large, even when the best-fit parameters differ fairly significantly. In addition, for the spectrum of NGC 5018, the same quality of fit is achieved by a (J01) 10 Gyr, mixed metallicity model as for a (J01) 12 Gyr, 5 $Z_\odot$ plus 25 % by mass 4 Gyr, $Z_\odot$ model.

In Figures 6.3 and 6.4, therefore, the model spectra are extended beyond the observed spectra of NGC 3605 and NGC 5018, in order to determine whether observations at longer or shorter

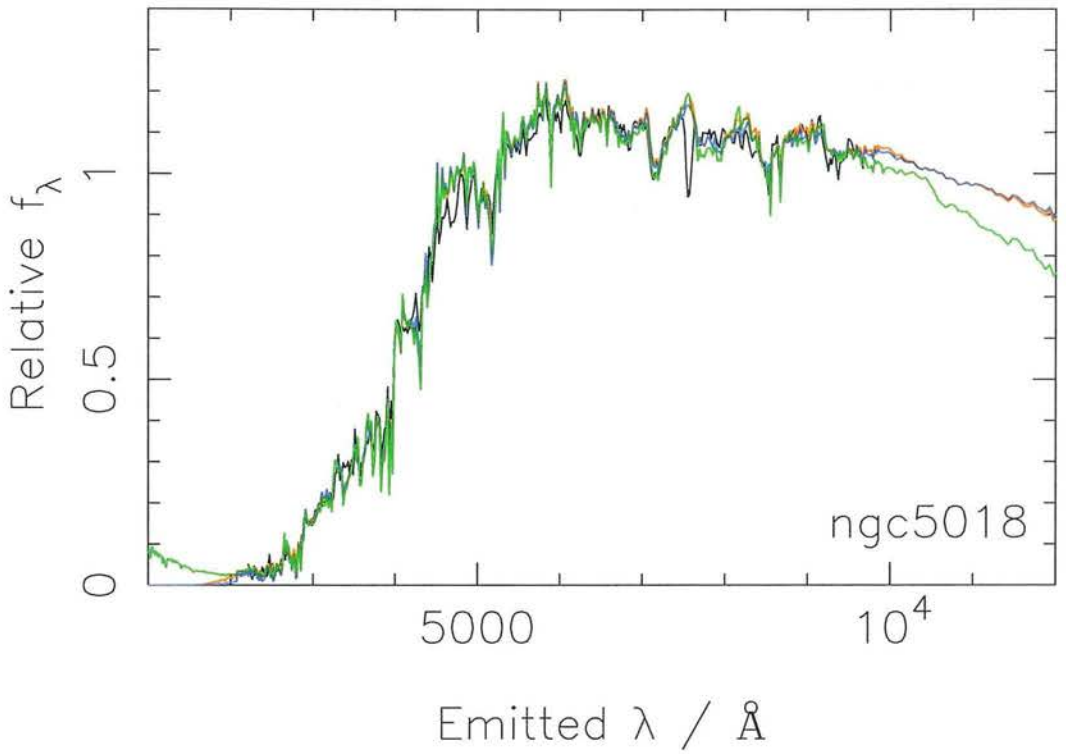

Figure 6.4: black - observed spectrum of NGC 5018; red - J01 coeval, mixed-metallicity model at 10 Gyr, and a mean metallicity of 0.039; blue - J01 two-population model, p1: 12 Gyr, Z = 0.05, p2: 4 Gyr, Z = 0.02; green - BC01 coeval, mixed-metallicity model at 19.75 Gyr, and a mean metallicity of 0.022

wavelengths would conclusively rule out any of the models.

The observed spectrum of NGC 3605 is presented in Figure 6.3, with the top three best-fitting models superimposed. The three models are easily differentiable at wavelengths > 7000 Å, which was the upper limit of the data available in this work. The BC01, two-population model is much redder than either of the J01 models, and the bluest model is in fact the best-fit over-all J01 two-population model. Hence, an infrared spectrum for this galaxy would assist in an even more robust determination of its star formation history.

For the spectrum of NGC 5018 (Figure 6.4), extending the spectra does not result in an easy distinction between the two, equally well-fitting, J01 models, although the best-fit BC01 model clearly differs from the J01 models at both very short ($\lambda < 2000$ Å) wavelengths, and very long ($\lambda \gtrsim 10^4$ Å) wavelengths, where enhanced contributions to the flux from giant branch stars are clearly evident. The two J01 models are not, however, identical, so perhaps the best hope for deciding which one is the 'true' best-fit lies with the re-consideration of the errors and normalisation discussed in Chapter 5.

Clearly, given the significant differences between the J01 and BC01 models at longer wave-

lengths, J band spectroscopy (for example with UIST at UKIRT) of NGC 3605 and NGC 5018 would provide conclusive evidence as to which author's model set has been best able to reproduce both the over-all continuum shape and the individual features of real stellar populations over a wide range of wavelengths.

The z $\sim$ 1.5 radio galaxies

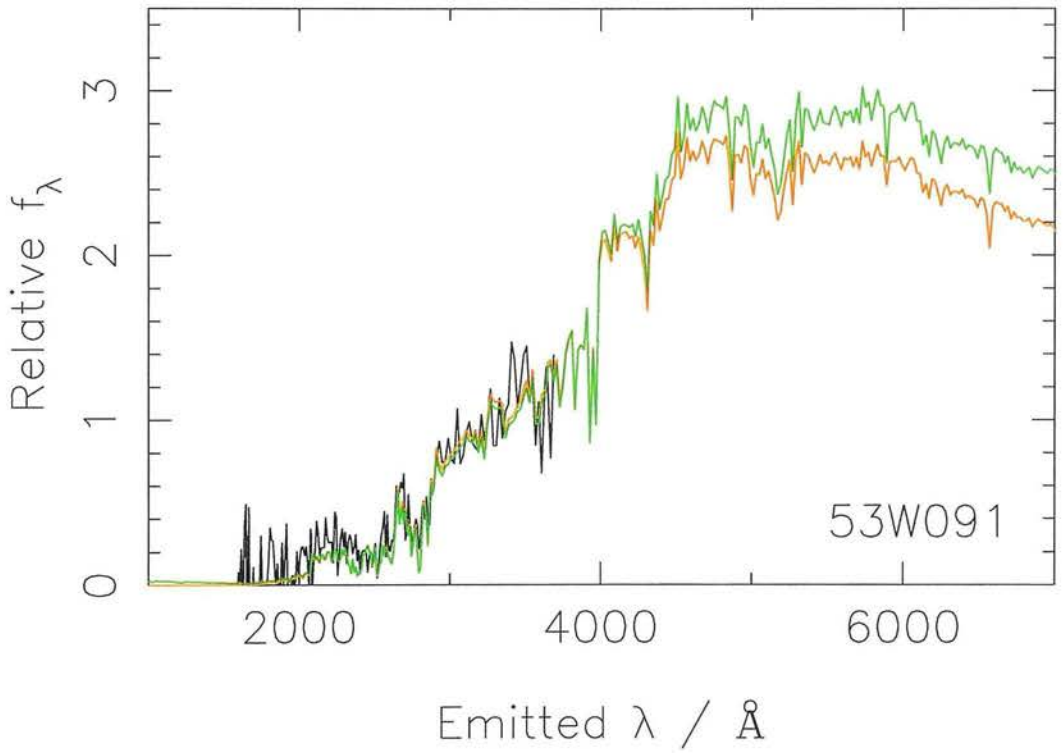

Figure 6.5: black - observed spectrum of LBDS 53W091; red - J01 coeval, mixed-metallicity model at 3 Gyr, and a mean metallicity of $Z_\odot$; green - BC01 coeval, mixed-metallicity model at 1.9 Gyr, and a mean metallicity of 1.1 $Z_\odot$.

In Figure 6.5, the rest-frame UV Keck spectrum of LBDS 53W091 is shown, with the best-fitting coeval, mixed-metallicity models of J01 and BC01, extended into the rest-frame optical wavelength region, superimposed. The 3 Gyr fit by the J01 models achieves a better quality of fit than the BC01, 1.9 Gyr, model ($\chi^2_\nu = 1.3$ for the J01 model, and $\chi^2_\nu = 1.4$ for the BC01 model). However, at these wavelengths, the differences between the models are much more significant. Because at high-redshift, red galaxies such as LBDS 53W091 are expected to be highly coeval, a situation which would be difficult to find in low-redshift galaxies, infrared spectroscopy e.g. from NIRSPEC at the Keck telescope of LBDS 53W091, enabling

a comparison of the two models with high-quality rest-frame optical data, offers the best way to decide which model of galaxy evolution is best able to reproduce the SED of a single stellar population at an age of 2-5 Gyr.

The results from Chapter 5 indicate that further investigation of LBDS 53W069 is necessary in order to determine its age more convincingly - the best-fit age achieved by the J01, coeval, mixed-metallicity models is 13 Gyr, which would imply some fairly exotic cosmology. Additional information provided by an optical spectrum would enable a more robust, and, one would hope, more plausible, age-determination for this object.

Finally, rest-frame optical data for the two high-redshift galaxies, LBDS 53W091 and LBDS 53W069, with their presumed coeval stellar populations, together with their now well-studied ages and metallicities, present us with the best opportunity to check the ability of single stellar population models to convincingly reproduce optical absorption features, e.g. the 4000 Å break, H_γ and Mg_b.

6.2.2 Extremely red objects at high redshift

This chapter has shown that studies of the ages and metallicities of passively evolving elliptical galaxies in the redshift range $1 < z < 2.5$, such as LBDS 53W069 and LBDS 53W091, can provide important clues to the still controversial questions of the formation and evolution of elliptical galaxies. For example, when was the epoch of star formation for these galaxies completed? Are these high-redshift, mature, elliptical galaxies consistent with formation from the single collapse of high-density peaks in the mass distribution in the early Universe, or did high-redshift merging events take place? If so, when did the epoch of merging end? Are these galaxies indeed the progenitors of low-redshift boxy elliptical galaxies? What is the relationship between their metallicity and other physical properties such as age, mass, luminosity and also environment?

A study of the ages and metallicities of a large population (~ 20) of extremely red objects (EROs), similar to the two LBDS galaxies, characterised by their very red colours ($R - K > 5$) and in the redshift range $1 < z < 2.5$, would allow the above questions to be tackled. High resolution optical (rest-frame UV) spectra for such a population may be obtained with the VLT. Using the proven ability of the continuum fitting method to simultaneously determine the age and metallicity of these objects, together with confidence in the choice of stellar population evolutionary synthesis model, robust constraints on the ages and metallicities of these galaxies may be imposed. With the ages confidently determined for a large number of

objects at a range of redshifts, the epoch of star formation for this class of galaxies may be determined, and the consequent implications for galaxy formation deduced.

References

Allard F. & Hauschildt P.H., 1995, ApJ, 445, 433

Alongi M., Bertelli G., Bressan A., Chiosi C., Fagotto F., Greggio L., Nasi E., 1993, A&AS, 97, 851

Archibald, E., Dunlop, J.S., Hughes, D.H., Rawlings, S., Eales, S.A., Ivison, R.J., 2001, MNRAS, in press (astro-ph/0002083)

Bahcall J.N., Kirhakos S., Saxe D.H., Schneider D.P., 1997, ApJ, 479, 642

Baker N., & Temensvary S., 1966, in: Tables of Convective Stellar Models

Barger A.J., Cowie L.L., Smail I., Ivison R.J., Blain A.W., Kneib J.-P., 1999, AJ, 117, 2656

Barnes J. & Hernquist L., 1991, ApJ, 370L, 65

Baugh C.M., Cole S., Frenk C.S., 1996, MNRAS, 283, 1361

Baugh C.M., Cole S., Frenk C.S., Lacey C.G., 1998 ApJ, 498, 504

Bedijn P.J., 1988, A&A, 205, 105

Bender R., Burstein D., Faber S. M., 1992, ApJ, 399, 462

Bertola F., Pizzella A., Persic M., Salucci Paolo., 1993, A&A, 280, 409

Bessell M.S., Brett J.M., Wood P.R., Scholz M., 1989, A&AS, 77, 1

Bessell M.S., Brett J.M., Wood P.R., Scholz M., 1991, A&AS, 89, 335

Bica E., Alloin D., 1987a, A&AS, 70, 28

Bica E., Alloin D., 1987b, A&A, 186, 49

Binney J. & Petrou M., 1985, MNRAS, 214, 449

Bressan A., Fagotto F., Bertelli G., Chiosi C., 1993, A&AS, 100, 647

Bruzual G.A., 2000, in: Proceedings of the XI Canary Islands Winter School of Astrophysics on Galaxies at High Redshift, eds I. Perez-Fournon, M. Balcells, and F. Sanchez (astro-ph/0011094)

Bruzual G.A., Charlot S., 1993, ApJ, 405, 538

Bruzual G.A., Charlot S., 2001, in preparation

Bruzual G., Magris G.C., 1997, The Ultraviolet Universe at Low and High Redshift : Probing the Progress of Galaxy Evolution, College Park, MD, edited by William H. Waller et al., New York, American Institute of Physics. Also AIP Conference Proceedings, v.408., p.291

Burkert A., Naab T., 2000, AAS, 197, 5605

Busarello G., Capaccioli M., Capozziello S., Longo G., Puddu, 1997, A&A, 320, 415

Buson L. M., Bertola F., Cappellari M., Burstein D., 2000, ASP Conf. Series, Ed. J.G.

Funes, S.J. Corsini, E.M. Corsini

Canalizo G., Stockton A., 2000, AJ, 120, 1750

Chambers K.C., Charlot S., 1990, ApJ, 348, L1

Charlot S., Bruzual G.A., 1991, ApJ, 367, 126

Charlot S., Worthey G., Bressan A., 1996, ApJ, 457, 626

Cimatti A., Andreani P., Rottgering H., Tilanus R., 1998, Nature, 392, 895

Corbin M.R., 2000, ApJ, 536L, 73

Daddi E., Cimatti A., Renziz A., 2000a, A&A, 362L, 45

Daddi E., Cimatti A., Pozzetti L., Hoekstra H., Rttgering H.J.A., Renzini A., Zamorani G., Mannucci F., 2000, SPIE, 4005, 45

de Vaucouleurs G., 1948, Ann. d'Ap, 11, 247

Dey A., et al. 2001, ApJ, in preparation

Disney M.J. et al., 1995, Nat, 376, 150

Djorgovski S. & Davis M., 1987, ApJ, 313, 59

Dressler A., Lynden-Bell D., Burstein D., Davies R.L., Faber S.M., Terlevich R, Wegner G., 1987, ApJ, 313, 42

Dunlop, J.S., 1999, In 'The Most Distant Radio Galaxies', KNAW Colloguium Amsterdam,

p.71, eds. Rottgering, H.J.A., Best, P., Lehnert, M.D., Kluwer

Dunlop, J.S., 1999, Astronomical Society of the Pacific Conference Series Volume 193, ed.s A.J. Bunker & W.J.M. van Breugel

Dunlop J.S., 2000, In: 'The Hy-Redshift Universe: Galaxy Formation and Evolution at High Redshift', ASP Conf. Ser., Vol 193, eds. A.J. Bunker & W.J.M. van Breugel, in press, (astro-ph/9912380)

Dunlop J.S., Guiderdoni B., Rocca-Volmerange B., Peacock J.A., Longair M.S., 1989, MNRAS, 240, 257

Dunlop J.S., McLure R.J., Kukula M.J., Baum S.A., O'Dea C.P., Hughes D.H., 2001, MNRAS, in press (astro-ph/0108397)

Dunlop J.S., 2001, 'Sub-mm clues to elliptical galaxy formation',In: Deep Millimetre Surveys, eds. Lowenthal, J. & Hughes, D.H., World Scientific, in press (astro-ph/0011077)

Dunlop J., Peacock J., Spinrad H., Dey A., Jimenez R., Stern D., Windhorst R., 1996, Nature, 381, 581

Dunlop J.S., Taylor G.L., Hughes D.H., Robson E.I., 1993, MNRAS, 264, 455

Edvardsson B., Andersen J., Gustafsson B., Lambert D.L., Nissen P.E., Tomkin J., 1993, A. & A. 275, 101

Eggen O.J., Lynden-Bell D., Sandage A.R., 1962, ApJ, 136, 748

Faber S. M., Wegner G., Burstein D., Davies, R.L., Dressler A., Lynden-Bell, D., Terlevich R. J., 1989, ApJS, 69, 763

Faber S. M., Tremaine S., Ajhar E.A., Byun Y-I., Dressler A., Gebhardt K., Grillmair C.,

Kormendy J., Lauer T.R., Richstone D., 1997, AJ, 114, 1365

Fagotto F., Bressan A., Bertelli G., Chiosi C., 1994a, A&AS, 100, 647

Fagotto F., Bressan A., Bertelli G., Chiosi C., 1994b, A&AS, 104, 265

Fagotto F., Bressan A., Bertelli G., Chiosi C., 1994c, A&AS, 105, 29

Forbes D.A., Ponman T.J., Brown R.J.N., 1998, ApJ, 508L, 43

Franceschini A., Silva L., Fasano G., Granato L., Bressan A., Arnouts S., Danese L., 1998, ApJ, 506, 600

Genzel R., Tacconi, L.J., Rigopoulou D., Lutz, D., Tecza M., 2001 astro-ph/0106032

Girardi L., Bressan A., Chiosi C., Bertelli G., Nasi E., 1996, A&AS, 117, 113

Green E.M., Demarque P., King C.R., 1987, in: the Revised Yale Isochrones and Luminosity Functions, New Haven: Yale Observatory, 1987

Guideroni B., & Rocca-Volmerange B., 1987, A&A, 186, 1

Gustafsson B., Bell R.A., Eriksson K., Nordlund A., 1975, A%A 42, 407

Heavens A.F., Jimenez R., Lahav O., 2000, MNRAS, 317, 965

Helling C., Jørgensen U.G., Plez B., Johnson H.R., 1996, A&A, 315, 194

Hernquist L. & Barnes J., 1991, Natur., 354, 210

Hooper E.J., Impey C.D., Foltz C.B., 1997, ApJ, 480, L95

Hughes D. H., Kukula M.J., Dunlop J.S., Boroson T., 2000, MNRAS, in press

Hutchings J.B., Morris S.C., 1995, AJ, 109, 1541

Iglesis C.A., & Rogers F.J., 1996, ApJ, 464, 943

Jansen R.A., Fabricant D., Franx M., Caldwell N., 2000, ApJS, 126, 331

Jimenez R., Jørgensen U.G., Thejll P., MacDonald J., 1995, MNRAS, 275, 1245

Jimenez R., & McDonald J., 1996, MNRAS, 283, 721

Jimenez R., Thejll P., Jørgensen U.G., MacDonald J., Pagel B., 1996, MNRAS, 283, 721

Jimenez R., Dunlop J.S., Peacock J.A., Padoan P., MacDonald J., Jørgensen U.G., 2000a, MNRAS, in press

Jimenez R., Padoan P., Dunlop J.S., Bowen D.V., Juvela M., Matteucci F., 2000b, ApJ, 532, 152

Jimenez R., Padoan P., Matteucci F., Heavens A.F., 1998, MNRAS, 299, 123

Jimenez R. et al., 2001, in preparation

Jørgensen, U.G., 1991, A&A, 246, 118

Kauffman G., Charlot S., White S.D.M., 1996, MNRAS, 283L, 117

Kauffman G., White S.D.M., Guideroni B., 1993, MNRAS, 264, 201

Kim D.-W., Jura M., Guhathakurta P., Knapp G.R., van Gorkom, J.H., 1988, ApJ, 330, 684

Kodama T., Bower R.G., Bell E.F., 1999, MNRAS, 306, 561

Kormendy D. & Richstone D., 1995, ARA&A, 33, 581

Kormendy J., Bender R., 1996, ApJ, 464L, 119

Kurucz R., 1992, in: The Stellar Populations in Galaxies, ed. B Barbuy, A Renzini, 225

Larson R., 1974, MNRAS, 173, 671

Lattanzio J.C., 1991, ApJS, 76, 215

Lawrence A., 1999, AdSpR, 23, 1167

Lejeune T., Cuisinier F., Buser R., 1997, A&AS, 125, 229

Lejeune T., Cuisinier F., Buser R., 1998, A&AS, 130, 65

Leonardi A.J., Worthey G., 2000, ApJ, 534, 650

Lilly S.J., 1988, ApJ, 333, 161

Magorrian J., et al., 1998, AJ, 115, 2285

Magris G.C., Bruzual G.B., 1993, ApJ, 417, 102

Malin D.F., Hadley B., 1997, Pub. Astro. Soc. of Aus., 14, 52

McLure R.J., Kukula M.J., Dunlop J.S., Baum S.A., O'Dea C.P., Hughes D.H., 1999, MN-

RAS, in press, (astro-ph/9809030)

Menanteau F., Ellis R.S., Abraham R.G., Barger A.J., Cowie L.L., 1999, MNRAS, 309, 208

Michard R., Marchal J., 1994, A&AS, 105, 481

Mihalas D., 1978, in: Stellar Atmospheres, San Francisco: W.H. Freeman, 1978

Mihos J.C. & Hernquist L., 1994, ApJ, 437L, 47

Nieto J.-L., 1988, Bol. Acad. Nac. Cine. Cordoba,58, 239

Nieto J.-L., & Bender R., 1989, A&A, 215, 266

Nolan L.A., Dunlop J.S., Jimenez R., 2001a, MNRAS, 323, 385

Nolan L.A., Dunlop J.S., Jimenez R., Heavens A.F., 2001b, submitted to MNRAS (astro-ph/0103450)

Pahre M.A., de Carvalho R.R., Djorgovski S.G., 1998, AJ, 116, 1606

Peacock J.A., Jimenez R., Dunlop J.S., Waddington I., Spinrad H., Stern D., Dey A., Windhorst R. A., 1998, MNRAS, 296, 1089

Peacock J.A., 1999, 'Cosmological Physics', Cambridge University Press

Peebles P.J.E., 1988, ApJ, 332, 17

Peterson R.C., Dalle Ore C.M., Kurucz R.L., 1993, ApJ, 404, 333

Pickles A.J., 1998, PASP, 110, 863

Ponder J. M., Burstein D., O'Connell R. W., Rose J.A., Frogel J.A., Wu C.-C., Crenshaw D.M., Rieke M.J., Tripicco M., 1998, AJ, 116, 2297

Reduzzi L., Longhetti M., Rampazzo R., 1996, MNRAS, 282, 149

Reichardt C., Jimenez R. & Heavens A.F., 2001, submitted, MNRAS (astro-ph/0101074)

Reimers D., 1975, Mem. Soc. Roy. Sci. Liége, 8,369

Renzini A., 1981, Ann. Phys. Fr., 6, 87

Renzini A., 1981, in: Colors and Poulations of Glaxies - Paris 1981, 1981, 76

Renzini A., 1998, in 'When and How do Bulges Form and Evolve?', ed. C.M. Carollo, H.C. Ferguson, R.F.G. Wyse (Cambridge University Press)

Robertson H.P., 1935, Proc. N.A.S., 15, 822

Rogers F.J., & Iglesias C A., 1992, ApJS, 79, 507

Salpeter E.E, 1955, ApJ, 121, 161

Schade, D.J., Boyle, B.J., Letawsky, M., 2000, MNRAS, in press

Schade D., Lilly S.J., Crampton D., Ellis R.S., Le Fevre O., Hammer F., Brinchmann J., Abraham R., Colless M., Glazebrook K., Tresse L., Broadhurst T., 1999, ApJ, 525, 31

Schwarzschild K., 1906, Gøttingen Nachr., 41

Schweizer F., Seitzer P., 1992, AJ, 104, 1039

Scorza C., Bender R., Winkelmann C., Capaccioli M., Macchetto D.F., 1998, A&AS, 131, 265

Shaviv G., and Salpeter E., 1973, ApJ, 184, 191

Spinrad H., Dey A., Stern D., Dunlop J.S., Peacock J.,

Jimenez R., Windhorst R., 1997, ApJ, 484, 581

Taylor G.T., Dunlop J.S., Hughes D.H., Robson E.I., 1996, MNRAS, 283, 930

Thompson D., et al. 1999, ApJ, 523, 100

Tinsley B, 1968, ApJ, 160, 811

Treu T. $ Stiavelli M., 1999, ApJ, 524, L27

VandenBerg D.A., 1985, ApJS 58, 711

VandenBerg D.A., & Laskarides P.G., 1987, ApJS, 64, 103

Walker A.G., 1936, Proc. London Math. Soc., 42, 90

White S. & Rees M., 1978, MNRAS, 183,341

Worthey G., 1994, ApJS, 95, 107

Yi S., Demarque P., Oemler A. Jr., 1997, ApJ, 486, 201

Yi S., Brown T.M., Heap S., Hubeny I., Landsman W., Lanz T., Sweigart A., 2000, ApJ, 533, 670

Zepf S.E., 1997, in: The Nature of Elliptical Galaxies; 2nd Stromlo Symposium. ASP Conference Series; Vol. 116; ed. M. Arnaboldi; G. S. Da Costa; and P. Saha, p.489

Mon. Not. R. Astron. Soc. **323**, 308–330 (2001)

The ages of quasar host galaxies

L. A. Nolan,[1★] J. S. Dunlop,[1] M. J. Kukula,[1] D. H. Hughes,[1,2] T. Boroson[3] and R. Jimenez[1†]

[1]*Institute for Astronomy, University of Edinburgh, Blackford Hill, Edinburgh EH9 3HJ*
[2]*INOAE, Apartado Postal 51 y 216, 72000, Puebla, Pue., Mexico*
[3]*NOAO, PO Box 26732, Tucson, AZ 85726-6732, USA*

Accepted 2000 October 25. Received 2000 October 25; in original form 2000 January 20

ABSTRACT

We present the results of fitting deep off-nuclear optical spectra of radio-quiet quasars, radio-loud quasars and radio galaxies at $z \simeq 0.2$ with evolutionary synthesis models of galaxy evolution. Our aim was to determine the age of the dynamically dominant stellar populations in the host galaxies of these three classes of powerful active galactic nuclei (AGN). Some of our spectra display residual nuclear contamination at the shortest wavelengths, but the detailed quality of the fits longward of the 4000-Å break provides unequivocal proof, if further proof were needed, that quasars lie in massive galaxies with (at least at $z \simeq 0.2$) evolved stellar populations. By fitting a two-component model we have separated the very blue (starburst and/or AGN contamination) from the redder underlying spectral energy distribution, and find that the hosts of all three classes of AGN are dominated by old stars of age 8–14 Gyr. If the blue component is attributed to young stars, we find that, at most, 1 per cent of the visible baryonic mass of these galaxies is involved in star formation activity at the epoch of observation, at least over the region sampled by our spectroscopic observations. These results strongly support the conclusion reached by McLure et al. that the host galaxies of luminous quasars are massive ellipticals which have formed by the epoch of peak quasar activity at $z \simeq 2.5$.

Key words: galaxies: active – galaxies: evolution – quasars: general – galaxies: stellar content.

1 INTRODUCTION

Determining the nature of the host galaxies of powerful active galactic nuclei (AGN) is of importance not only for improving our understanding of different manifestations of AGN activity, but also for exploring possible relationships between nuclear activity and the evolution of massive galaxies. The recent affirmation that black hole mass appears approximately proportional to spheroid mass in nearby inactive galaxies (Maggorian et al. 1998) has further strengthened the motivation for exploring the link between AGN and the dynamical and spectral properties of their hosts.

Over the last few years, improvements in imaging resolution offered by both space- and ground-based optical–infrared telescopes have stimulated a great deal of research activity aimed at determining the basic structural parameters (i.e. luminosity, size and morphological type) of the hosts of radio-loud quasars, radio-quiet quasars and lower-luminosity X-ray-selected and optically selected AGN (e.g. Disney et al. 1995; Hutchings & Morris 1995; Bahcall et al. 1997; Hooper, Impey & Foltz 1997; McLure et al. 1999; Schade, Boyle & Letawsky 2000). However, relatively little corresponding effort has been invested in spectroscopic investigations of AGN hosts, despite the fact that this offers an independent way of classifying these galaxies, and a means of estimating the age of their stellar populations.

Our own work in this field to date has focused on the investigation of the hosts of matched samples of radio-quiet quasars (RQQs), radio-loud quasars (RLQs) and radio galaxies (RGs) at relatively modest redshift ($z = 0.2$). Details of these samples can be found in Dunlop et al. (1993). In brief, the subsamples of quasars (i.e. RQQs and RLQs) have been selected to be indistinguishable in terms of their two-dimensional distribution on the V–z plane, while the subsamples of radio-loud AGN (i.e. RLQs and RGs) have been selected to be indistinguishable in terms of their two-dimensional distribution on the $P_{5\,\mathrm{GHz}}$–z plane (and having indistinguishable spectral-index distributions). Deep infrared imaging of these samples (Dunlop et al. 1993; Taylor et al. 1996) has recently been complemented by deep WFPC2 *Hubble Space Telescope* (*HST*) optical imaging (McLure et al. 1999), the final results of which are reported by Dunlop et al. (2001). In addition to demonstrating that, dynamically, the hosts of all three types of luminous AGN appear indistinguishable from normal ellipticals, this work has enabled us to deduce crude spectral

★E-mail: lan@roe.ac.uk
†Present address: Physics and Astronomy Department, Rutgers University, Piscataway, NJ 08854–8019, USA.

information on the host galaxies in the form of optical–infrared colours. However, broad-baseline colour information can clearly be most powerfully exploited if combined with detailed optical spectroscopy. Over the past few years we have therefore attempted to complement our imaging studies with a programme of deep optical off-nuclear spectroscopy of this same sample of AGN.

Details of the observed samples, spectroscopic observations and the basic properties of the observed off-nuclear spectra are given in a companion paper (Hughes et al. 2000). As discussed by Hughes et al. (2000), the key feature of this study (other than its size, depth and sample control) is that we have endeavoured to obtain spectra from positions further off-nucleus ($\simeq$5 arcsec) than previous workers, in an attempt to better minimize the need for accurate subtraction of contaminating nuclear light. This approach was made possible by our deep infrared imaging data, which allowed us to select slit positions $\simeq$5 arcsec off-nucleus, which still intercepted the brighter isophotes of the host galaxies [slit positions are shown, superimposed on the infrared images, in Hughes et al. (2000)].

In this paper we present the results of attempting to fit the resulting off-nuclear spectra with evolutionary synthesis models of galaxy evolution. Our primary aim was to determine whether, in each host galaxy, the optical spectrum could be explained by the same model as the optical–infrared colour, and, if so, to derive an estimate of the age of the dynamically dominant stellar population. However, this study also offered the prospect of determining whether the hosts of different classes of AGN differ in terms of their more recent star formation activity.

It is worth noting that our off-nuclear spectroscopy obviously does not enable us to say anything concerning the level of star formation activity in the nucleus of a given host galaxy. Rather, any derived estimates of the level of star formation activity refer to the region probed by our observations $\simeq$5 arcsec off-nucleus. However, given the large scalelengths of the hosts, their relatively modest redshift, and the fact that our spectra are derived from long-slit observations, it is reasonable to regard our conclusions as applying to fairly typical regions, still located well within the bulk of the host galaxies under investigation.

The layout of this paper is as follows. In Section 2 we provide details of the adopted models, and how they have been fitted to the data. The results are presented in Section 3, along with detailed notes on the fitting of individual spectra. The implications of the model fits are then discussed in Section 4, focusing on a comparison of the typical derived host-galaxy ages in the three AGN subsamples. Finally, our conclusions are summarized in Section 5. The detailed model fits, along with corresponding chi-squared plots are presented in Appendix A.

2 SPECTRAL FITTING

The stellar population synthesis models adopted for age-dating the AGN host galaxy stellar populations are the solar metallicity, instantaneous starburst models of Jimenez et al. (2001). We have endeavoured to fit each off-nuclear host galaxy optical spectrum by a combination of two single starburst components. For the first component, age is fitted as a free parameter, while for the second component the age is fixed at 0.1 Gyr, and the normalization relative to the first component is the only free parameter. This dual-component approach was adopted because single-age models are not able to adequately represent the data, and because it allows the age of the dynamically dominant component to be determined in a way that is not overly reliant on the level of ultraviolet flux which might be contributed either by a recent burst of star formation, or by contamination of the slit by scattered light from the quasar nucleus. After experimentation it was found that the spectral shape of the blue light was better represented by the 0.1-Gyr-old (solar metallicity) model of Jimenez than by models of greater (intermediate) age (e.g. 1 Gyr). Moreover, the further addition of a third intermediate age component, $\simeq$1 Gyr, did not significantly improve the quality of the fits achieved.

In general, our data are of insufficient quality to tell whether the component that dominates at $\lambda \simeq 3000$ Å is caused really by young stars, or whether it is produced by direct or scattered quasar light. However, while the origin of the blue light is obviously of some interest, it has little impact on the main results presented in this paper, which refer to the age of the dynamically dominant stellar population that dominates the spectrum from longward of the 4000-Å break through to the near-infrared. The robustness of the age determination of the dominant population is demonstrated by comparing the results of the two stellar-population model fits with the results of a fit allowing for a nuclear contribution in addition to the two stellar populations.

The model parameters determined were therefore the age of the dominant stellar population, which we can reasonably call the age of the galaxy, and the fraction, by (visible) baryonic mass, of the 0.1-Gyr component. For the fit including a nuclear contribution, the fraction of the total flux contributed by quasar light was a third parameter. The red end of each SED was further constrained by

Table 1. Wavelength ranges of observed spectra, and splice regions which were excluded from the fitting process. All wavelengths are in the observed frame. M4M denotes the Mayall 4-m telescope at Kitt Peak, and WHT denotes the 4.2-m William Herschel Telescope on La Palma (see Hughes et al. (2000) for observational details).

IAU name	Telescope	Wavelength range (Å)	Masked splice region (Å)
		Radio-loud quasars	
0137+012	M4M	3890–6950	
0736+017	M4M	3890–6950	
	WHT	3500–8000	6050–6150
1004+130	WHT	3500–8000	6050–6150
1020−103	M4M	3890–6950	
1217+023	WHT	3500–7500	6000–6100
2135−147	WHT	3500–8500	6000–6100
2141+175	WHT	3500–8500	6000–6100
2247+140	M4M	3890–6950	
	WHT	3500–7500	6050–6150
2349−014	WHT	3500–8300	6000–6100
		Radio-quiet quasars	
0054+144	M4M	3890–6950	
	WHT	3500–8000	6000–6100
0157+001	M4M	3890–6950	
	WHT	3500–8000	6050–6150
0204+292	WHT	3500–8000	6050–6150
0244+194	WHT	3500–8500	6000–6100
0923+201	WHT	3500–7000	
1549+203	WHT	3500–8000	6050–6150
1635+119	WHT	3500–7800	6000–6100
2215−037	WHT	3500–8500	6000–6100
2344+184	M4M	3890–6950	
	WHT	3500–8500	6000–6100
		Radio galaxies	
0230−027	WHT	3500–8500	6000–6100
0345+337	WHT	3500–8500	6000–6100
0917+459	WHT	3500–8500	6050–6150
1215−033	WHT	3500–7500	6000–6100
1330+022	M4M	3890–6950	
2141+279	M4M	3890–6950	

fitting $R-K$ colour simultaneously with the optical spectral energy distribution. The fitting process is described below.

First, the observed off-nuclear spectra were corrected for redshift and transformed to the rest frame. They were then rebinned to the spectral resolution of the model spectra. The rebinned flux is then the mean flux per unit wavelength in the new bin and the statistical error on each new bin is the standard error in this mean. The data were normalized to a mean flux per unit wavelength of unity across the wavelength range 5020–5500 Å.

The two-component model was built from the instantaneous-burst stellar-population synthesis model (SEDs), so that

$$F_{\lambda,age,\alpha} = \text{constant} \times [\alpha f_{\lambda,0.1} + (1-\alpha) f_{\lambda,age}],$$

where $f_{\lambda,age}$ is the mean flux per unit wavelength in the bin centred on wavelength λ for a single-burst model of *age* Gyr, α is the fraction by mass of the young (0.1-Gyr) component, and $F_{\lambda,age,\alpha}$ is then the new, mean twin stellar-population flux per unit wavelength in the bin centred on wavelength λ for a model of *age* Gyr. This composite spectrum was then normalized in the same way as the observed spectra.

A χ^2 fit was used to determine the age of the older stellar population and the mass fraction, α, of the younger population, for each host galaxy in the sample. The whole parameter space was searched, with the best-fitting values quoted being those parameter values at the point on the grid with the minimum calculated χ^2. The normalization of the model spectra was allowed to float during the fitting process, to allow the best-fitting continuum shape to be determined in an unbiased way.

The models were fitted across the observed (rest-frame) spectral range, within the wavelength ranges listed in Table 1. As a result of the optimization of the instruments with which the objects were observed, some of the galaxy spectra contain a 'splice' region where the red and blue end of the spectrum have been observed separately and then joined together [see Hughes et al. (2000) for details]. These splice regions, defined in Table 1, were masked out of the fit in order to guard against the fitting procedure being dominated by data points the flux calibration of which was potentially less robust. The main emission lines, present because of nuclear light contamination or nebular emission from within the host, were also masked out, over the wavelength ranges given in Table 2.

The fit including a nuclear component was carried out in the same way, with the model flux in this case being

$$F_{\lambda,age,\alpha,\eta} = \text{constant} \times (\alpha f_{\lambda,0.1} + (1-\alpha) f_{\lambda,age} + \eta f0054_{\lambda}),$$

where η is the fraction contributed to the total model flux by the nucleus, and $f0054_{\lambda}$ is the observed flux of the nucleus of the radio-quiet quasar 0054+144. α is the fraction by mass of the total stellar population contributed by the 0.1-Gyr population. The wavelength range of the observed nuclear flux of 0054+144 is 3890–6950 Å. This was extended to 3500–8500 Å by smooth extrapolation over the wavelength ranges 3500–3890 and 6950–8500 Å in order to carry out the χ^2 fit across the full wavelength range of the observed off-nuclear spectra.

$R-K$ colour was fitted in both cases with a typical error of a few per cent. The observed $R-K$ colours for the host galaxies are obtained from *UKIRT* and *HST* images (McLure et al. 1999; Dunlop et al. 2001), and define the basic shape of the host galaxy SED out to $\lambda \simeq 2\,\mu m$. The composite model spectra were appropriately redshifted before calculating the colour, so that they could be compared with the observed colours without introducing uncertainties in k-correction. The R-band was simulated using the filter function, including system response and CCD quantum efficiency, for the *HST* WFPC2 F675W filter, and the K-band was reproduced using the filter data for the IRCAM3 K Ocli filter at 77 K combined with Mauna Kea atmosphere.

Table 2. Rest frame emission lines masked out in the χ^2 fit.

Masked region (Å)	Emission line
3720–3735	O II 3727
3860–3880	Ne III 3869
4840–5020	O III 4959, O III 5007, Hβ 4861

3 RESULTS

The plots showing fits to individual spectra and χ^2 as a function of fitted age are given in Appendix A. The plots for the two-component fit are presented in Fig. A1, and those for the two stellar-component plus nuclear contribution are in Fig. A2. The results for each object are summarized below, under their IAU names, with alternative names given in parentheses. Objects are listed in order of increasing right ascension, within each AGN class (radio-loud quasars, radio-quiet quasars and radio galaxies). The telescopes with which the spectra were obtained are also noted; M4M denotes the Mayall 4-m telescope at Kitt Peak and WHT denotes the 4.2-m William Herschel Telescope on La Palma. Where there are two spectra, the first plot is for the spectrum observed with the Mayall 4-m telescope, and the second is for the spectrum taken with the William Herschel Telescope.

3.1 Notes on individual objects

3.1.1 Radio-loud quasars

0137+012 (L1093) M4M. The models give a good fit at 13 Gyr, which is clearly improved by the inclusion of a small percentage (0.25 per cent) of young stars. There is no significant nuclear contribution to the spectrum. *HST* imaging has shown that this host galaxy is a large elliptical, with a half-light radius $r_e = 13$ kpc (McLure et al. 1999).

0736+017 (S0736+01, OI 061) M4M, WHT. 0736+017 has been observed with both telescopes, and fits to the two observed spectra are in good agreement. Both indicate an age of 12 Gyr. The M4M spectrum requires a somewhat larger young blue population (0.75 per cent) than the WHT spectrum (0.125 per cent). This may be caused by poorer seeing at Kitt Peak leading to slightly more nuclear contamination of the slit, or to the use of slightly different slit positions at the two telescopes. However, this difference between the observed spectra shortward of 4000 Åleaves the basic form of χ^2 versus age, and the best-fitting age of 12 Gyr unaffected. Inclusion of a nuclear component gives a much better fit to the blue end of the M4M spectrum, without changing the age estimation. The size of the fitted young populations are in much better agreement in this case. *HST* imaging has shown that morphologically this host galaxy is a large elliptical, with a half-light radius $r_e = 13$ kpc (McLure et al. 1999).

1004+130 (S1004+13, OL 107.7, 4C 13.41) WHT. The spectrum of this luminous quasar certainly appears to display significant nuclear contamination below the 4000-Å break. As a result a relatively large young population is required to attempt (not completely successfully) to reproduce the blue end of the spectrum. However, the models predict that the underlying stellar population is old (12 Gyr). Allowing a nuclear component to be fitted reproduces the blue end of the spectrum much more

successfully, without changing the best-fitting age estimation. *HST R*-band imaging indicates the morphology of the host galaxy is dominated by a large ($r_e = 8$ kpc) spheroidal component, but subtraction of this best-fitting model reveals two spiral-arm-type features on either side of the nucleus (McLure et al. 1999), which may be associated with the young stellar component required to explain the spectrum.

1020−103 (S1020−103, OL 133) M4M. This object has the second bluest $R - K$ of this sample, which leads to a much younger inferred age than the majority of the rest of the sample (5 Gyr), despite the presence of a rather clear 4000-Å break in the optical spectrum. Ages greater than $\simeq$10 Gyr are rejected by Jimenez' models, primarily on the basis of $R - K$ colour. *HST* imaging has shown that this host has an elliptical morphology, and a half-light radius of $r_e = 7$ kpc (Dunlop et al. 2001).

1217+023 (S1217+02, UM 492) WHT. Nuclear contamination can again be seen bluewards of 4000 Å, with a correspondingly large young population prediction for the purely stellar population model, which still fails to account for the very steep rise towards 3000 Å. Hence, a large nuclear contribution is required to reproduce the blue end of the spectrum. The fit achieved by the models suggests that the dominant population is old, with a best-fitting age of 12 Gyr. *HST* imaging has shown that this host has an elliptical morphology, and a half-light radius of $r_e = 11$ kpc (Dunlop et al. 2001).

2135+147 (S2135−14, PHL 1657) WHT. 2135+147 has a very noisy spectrum, but a constrained fit has still been achieved, and an old population is preferred. 2135+147 requires a large α, even when a nuclear contribution is fitted. *HST* imaging has shown that this host has an elliptical morphology, and a half-light radius of $r_e = 12$ kpc (Dunlop et al. 2001).

2141+175 (OX 169) WHT. This is another noisy spectrum, which has a relatively large quasar light contribution. An old population is again indicated by the model fits. From optical and infrared imaging this object is known to be complex, but *HST* images indicate that it is dominated by a moderate sized ($r_e = 4$ kpc) elliptical component [see McLure et al. (1999) for further details].

2247+140 (PKS 2247+14, 4C 14.82) M4M, WHT. 2247+140 has been observed with both telescopes. The model fitting indicates an old population is required by both spectra – although the two observations do not agree precisely, the general level of agreement is very good, the two χ^2 plots have a very similar form, and the difference in χ^2 between the alternative best-fitting ages of 8 and 12 Gyr is very small. No significant nuclear contribution to the flux is present. *HST* imaging has shown that this host has an elliptical morphology, and a half-light radius of $r_e = 14$ kpc (Dunlop et al. 2001).

2349−014 (PKS 2349−01, PB 5564) WHT. This is a very good fit to a good-quality spectrum, showing an obvious improvement when the low-level young population is added. Jimenez' models clearly predict that the dominant population is old, with a well-constrained age of 12 Gyr. A very small nuclear contribution ($\eta = 0.050$) does not significantly change the results. *HST* imaging of this object strongly suggests that it is involved in a major interaction, with a massive tidal tail extending to the north of the galaxy. However, the dominant morphological component is a spheroid with a half-light radius of $r_e = 18$ kpc (McLure et al. 1999).

3.1.2 *Radio-quiet quasars*

0054+144 (PHL 909) M4M, WHT. There is evidence of relatively large contamination from nuclear emission in the spectrum of this luminous quasar taken on both telescopes, and the age is not well-constrained, although the fit to the WHT spectrum derived from the models again suggests an old age. The χ^2 plots serve to emphasize how similar the two spectra of this object actually are (as also discussed by Hughes et al. 2000). Inclusion of a nuclear component in the model better constrains the age and improves the goodness of the fit. *HST* imaging of this object has shown that, morphologically, it is undoubtedly an elliptical galaxy, with a half-light radius of $r_e = 8$ kpc (McLure et al. 1999).

0157+001 (Mrk 1014) M4M, WHT. The age inferred from both the M4M and WHT spectrum of 0157+001 is again 12 Gyr. The apparently more nuclear-contaminated WHT spectrum does not give such a good fit, but 0157+001 is a complex object known to have extended regions of nebular emission, and the slit positions used for the two observations were not identical (Hughes et al. 2000). The age is much better constrained from the more passive M4M spectrum, to which Jimenez' models provide a very good fit. Again, it seems that the nuclear contamination does not have a great influence on the predicted age of the old population, although the fit to the WHT spectrum is greatly improved by including a nuclear component in the model. Despite its apparent complexity in both ground-based and *HST* images, this host galaxy does again seem to be dominated by a large spheroidal component, of half-light radius $r_e = 8$ kpc (McLure et al. 1999).

0204+292 (3C 59) WHT. Jimenez' models fit the spectrum of this object well, indicating an old underlying stellar population (>6 Gyr), with a best-fitting age of 13 Gyr for the stellar population plus nuclear component model, and a very small young population. *HST* imaging has shown this galaxy to be an elliptical, with a half-light radius of $r_e = 9$ kpc (Dunlop et al. 2001).

0244+194 (MS 02448+19) WHT. The colour derived from the optical and infrared imaging of this host galaxy is rather blue [$(R - K)_{obs} = 2.34$] and this in part leads to a fairly young (5 Gyr) age prediction. However, the spectrum is very noisy, and, as indicated by the very flat χ^2 plot, the age is not strongly constrained. No nuclear flux contamination is fitted. *HST* imaging has shown this galaxy to have an elliptical morphology, with a half-light radius of $r_e = 9$ kpc (McLure et al. 1999).

0923+201 WHT. The spectrum of 0923+201 is noisy, and it also appears to have some nuclear contamination. The fit is therefore improved by inclusion of a nuclear component. An old age is strongly preferred by the form of the χ^2/age plot, with a best-fitting value of 12 Gyr. *HST* imaging has shown this galaxy to have an elliptical morphology, with a half-light radius of $r_e =$ 8 kpc (McLure et al. 1999).

1549+203 (1E 15498+203, LB 906, MS 15498+20) WHT. This is a good fit, which is clearly improved by the addition of the younger population. The slope of the χ^2/age plot strongly indicates an old dominant population, with a best-fitting age of 12 Gyr. There is very little evidence of nuclear contamination. *HST* imaging has shown this galaxy to be a moderate-sized elliptical with $r_e = 5$ kpc (Dunlop et al. 2001).

1635+119 (MC1635+119, MC2) WHT. This is another very successful fit. An old age (12 Gyr) is inferred. Again, *HST* imaging has shown this galaxy to be a moderate-sized elliptical with $r_e = 6$ kpc (McLure et al. 1999).

2215−037 (MS 22152−03, EX 2215−037) WHT. 2215−037 has a noisy spectrum, to which an acceptable fit has nevertheless been possible. Jimenez' models suggest an old population, with a best-fitting age of 14 Gyr, but this age is not well constrained. This is the only object where the inclusion of a nuclear contribution to the fitted spectrum substantially changes the age predicted of the

Table 3. Results from the simultaneous fitting to the AGN host sample of the two-component model spectra (using the solar metallicity models of Jimenez et al. 2000) and $R-K$ colour. α is the percentage young population, by mass. Results are also presented for the fits including the subtraction of a nuclear component from the observed spectrum. η is the fraction of nuclear flux subtracted, and the corresponding results are denoted by the subscript η.

IAU name	Telescope	Best fit age/Gyr	Best fit age$_\eta$/Gyr	α	α_η	Reduced χ^2	Reduced $\chi^2{}_\eta$	$(R-K)_{fit}$	$(R-K)_{fit_\eta}$	$(R-K)_{obs}$	η	z
						Radio-loud quasars						
0137+012	M4M	13	13	0.2	0.3	3.7	3.6	2.88	2.88	2.82	0.025	0.258
0736+017	M4M	12	12	0.7	0.1	12.0	6.2	2.69	2.89	3.16	0.250	0.191
	WHT	12	12	0.1	0.0	3.3	2.9	2.89	2.93		0.100	
1004+130	WHT	12	12	1.4	0.4	5.4	2.2	2.65	2.96	3.01	0.350	0.240
1020−103	M4M	5	4	0.6	0.0	1.7	1.5	2.33	2.29	2.29	0.125	0.197
1217+023	WHT	12	12	1.1	0.0	11.8	4.9	2.71	3.10	3.18	0.350	0.240
2135−147	WHT	12	11	1.6	1.0	2.2	2.2	2.50	2.50	2.49	0.175	0.200
2141+175	WHT	12	14	1.1	0.5	3.2	2.5	2.66	2.69	2.69	0.500	0.213
2247+140	M4M	8	8	0.3	0.3	1.8	1.8	2.77	2.77	2.81	0.000	0.237
	WHT	12	12	0.9	0.9	2.9	2.9	2.79	2.79		0.000	
2349−014	WHT	12	12	0.5	0.4	3.3	3.0	2.71	2.75	2.87	0.050	0.173
						Radio-quiet quasars						
0054+144	M4M	8	12	1.3	0.3	46.9	9.1	2.32	2.78	3.12	0.400	0.171
	WHT	12	12	1.3	0.0	17.7	3.6	2.51	2.86		0.475	
0157+001	M4M	12	12	1.1	1.1	5.9	5.8	2.52	2.52	2.83	0.025	0.164
	WHT	12	12	1.6	0.9	41.0	10.9	2.41	2.58		0.250	
0204+292	WHT	14	13	0.2	0.1	6.3	5.4	2.47	2.45	2.49	0.125	0.109
0244+194	WHT	5	5	0.1	0.1	2.6	2.6	2.37	2.37	2.34	0.000	0.176
0923+201	WHT	12	12	0.6	0.0	5.6	4.0	2.72	2.92	3.24	0.375	0.190
1549+203	WHT	12	12	0.6	0.5	3.8	3.8	2.90	2.95	3.37	0.050	0.250
1635+119	WHT	12	12	0.7	0.5	6.7	6.4	2.57	2.63	3.27	0.100	0.146
2215−037	WHT	14	6	0.6	0.3	2.4	2.4	2.70	2.69	2.68	0.175	0.241
2344+184	M4M	8	11	0.4	0.4	4.8	4.9	2.43	2.57	2.51	0.025	0.138
	WHT	12	12	0.9	0.8	2.1	2.0	2.51	2.54		0.075	
						Radio galaxies						
0230−027	WHT	1	1	0.0	0.0	2.0	2.0	2.02	2.02	2.08	0.000	0.230
0345+337	WHT	12	12	0.0	0.0	2.7	2.7	3.13	3.13	3.62	0.000	0.244
0917+459	WHT	12	12	0.2	0.3	4.7	4.6	2.79	2.79	3.42	0.025	0.174
1215−033	WHT	13	13	0.0	0.0	3.4	3.4	2.74	2.74	2.56	0.000	0.184
1330+022	M4M	8	8	0.3	0.1	2.9	2.8	2.70	2.74	2.79	0.050	0.215
2141+279	M4M	12	12	0.1	0.0	3.1	2.5	3.27	3.01	3.25	0.025	0.215

dominant stellar population. However, the χ^2 plots are very flat after an age of 5 Gyr, and the age is not strongly constrained in either case. *HST* imaging has shown this galaxy to have an elliptical morphology, with $r_e = 7$ kpc (Dunlop et al. 2001).

2344+184 (E2344+184) M4M, WHT. 2344+184 has been observed with both telescopes, and the fits to both spectra are in good agreement – although, formally, two different ages are predicted. This is because the χ^2/age plots are fairly flat after about 8 Gyr. The fits to both observations suggest an old dominant population, with a small young blue population improving the fit. There is no significant change in the predictions when a nuclear flux component is included in the model. *HST* imaging has shown this to be one of the few host galaxies in the current sample to be disc-dominated. However, the nuclear component is in fact sufficiently weak that this object should really be classified as a Seyfert galaxy rather than an RQQ (McLure et al. 1999).

3.1.3 *Radio galaxies*

0230−027 (PKS 0230−027) WHT. 0230−027 has a very noisy spectrum, and the colour of the host as derived from optical and infrared imaging is very blue [$(R-K)_{obs} = 2.09$]. Consequently, the best-fitting age derived using the models is 1 Gyr, with no younger component, but it is clear that little reliance can be placed on the accuracy of this result. Allowing for a contribution from quasar light does not improve the fit. *HST* imaging has shown this galaxy to have an elliptical morphology, with $r_e = 8$ kpc (Dunlop et al. 2001).

0345+337 (3C 93.1) WHT. 0345+337 requires no young component or nuclear flux contribution at all, and an old age, of 12 Gyr, is clearly indicated by the models. *HST* imaging has shown this galaxy to be a large elliptical, with $r_e = 13$ kpc (McLure et al. 1999).

0917+459 (3C 219, 3C 219.0) WHT. This is an excellent fit, with an old age produced by the models (12 Gyr), together with a very small young population. *HST* imaging has shown this galaxy to be a large elliptical, with $r_e = 11$ kpc (McLure et al. 1999).

1215−033 WHT. Jimenez' models suggest that the population of 1215−033 is universally old (best-fitting age, 13 Gyr), with no young component or nuclear contribution required. *HST* imaging has shown this galaxy to be a large elliptical, with $r_e = 9$ kpc (Dunlop et al. 2001).

1330+022 (3C 287.1) M4M. An excellent fit to the data is produced by Jimenez' models, indicating that the dominant population is old, with a best-fitting age of 8 Gyr. *HST* imaging has shown this galaxy to be a large elliptical, with $r_e = 16$ kpc (Dunlop et al. 2001).

2141+279 (3C 436) M4M, WHT. This is another very successful, and well-constrained fit, with an inferred age of 12 Gyr. *HST* imaging has shown this galaxy to be a large elliptical, with $r_e = 21$ kpc (McLure et al. 1999).

3.2 Sample overview

The results illustrated in Appendix A are summarized in Table 3. It should be noted that the 4000-Å break typical of evolved stellar populations is present in the majority of the observed spectra (see

Appendix A and Hughes et al. 2000), so we can be confident in fitting stellar population models to the data. The plots clearly show that the addition of even a very small amount of secondary star formation to the simple, near-instantaneous starburst models reproduces the blue end of the observed host galaxy spectra much more successfully (and in most cases very well) than does a single stellar population. Including a nuclear component further improves the fit to the blue end, especially for those spectra not well fitted by purely stellar light. At the same time, the red end of the spectra, plus the observed $R - K$ colours generally require that the underlying stellar populations are old.

The most meaningful output from the model fitting is a constraint on the minimum age of the host galaxies; the χ^2 plots show that often the best-fitting age is not strongly constrained but the trend is clearly towards old ($\geq$8 Gyr) stellar populations. In general, young populations are strongly excluded.

The peaks and troughs in χ^2 as a function of model age appear to be the result of real features of the population evolution synthesis, rather than owing to, for example, poor sampling (Jimenez, private communication).

4 DISCUSSION

Fig. 1 shows the distribution of best-fitting ages estimated using Jimenez' models. The left-hand panel shows the ages of the dominant stellar component that result from fitting the two-component (stars only) model, while the right-hand panel shows the ages of the dominant stellar component in the case of the three-component model (i.e. two stellar components + a contribution from scattered nuclear light). The host galaxies of the AGN in each sample are predominantly old, and this result is unaffected by whether or not one chooses to include some nuclear contribution to assist in fitting the blue end of the spectrum. This general result also appears to be relatively unaffected by the precise choice of stellar population model; the models of Bruzual & Charlot (in preparation), fitted to the host galaxies with the same process, reproduce the results for Jimenez' models to within a typical accuracy of 1–3 Gyr. We have not attempted to fit the stellar population models of Yi et al. (2000), because of problems we have found in their main-sequence (MS) rate of evolution (Nolan, Dunlop & Jimenez 2001).

Inclusion of a nuclear contribution in the three-component models obviously raises the question of whether a young stellar population component is really necessary at all. We thus also explored the results of fitting a two-component model consisting of a single stellar population plus nuclear contribution. Such a model adequately reproduces the two-population-plus-nuclear-component results for the *redder* galaxies, but in fact the spectra of the bluest galaxies cannot be adequately reproduced by these models; the resulting serious increase in minimum χ^2 demonstrates that inclusion of a young population component is necessary to achieve a statistically acceptable fit to these data.

Fig. 2 shows the distribution of percentage contribution (by mass), α, of the young (0.1 Gyr) component to the spectra of the hosts. The left-hand panel shows the values of α as derived from fitting the two-component (stars only) model, while the right-hand panel shows the values of α produced by the three-component model (i.e. two stellar components + a contribution from scattered nuclear light).

Where two spectra of the same object have been obtained with alternative telescopes/instruments, the derived ages of the dominant stellar components are reproduced reassuringly well. There are, however, small discrepancies in the estimated

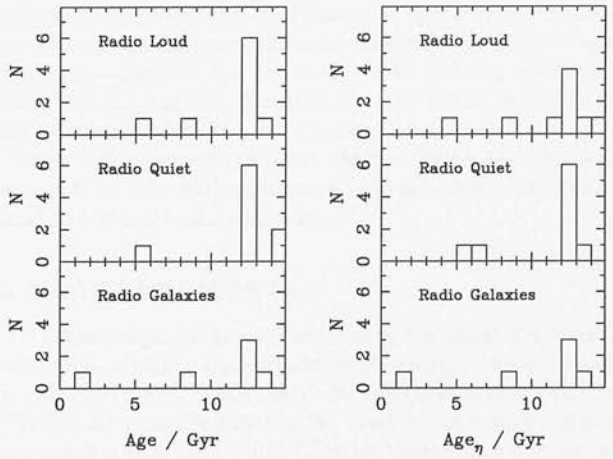

Figure 1. The age distribution of the dominant stellar populations of the sample host galaxies. These are the best-fitting results from Jimenez' solar metallicity models. On the left, results are shown for the fits to the data using a two-component model. The results on the right are those for the two-component model plus a nuclear contribution. The populations are predominantly old (12–14 Gyr) in both cases.

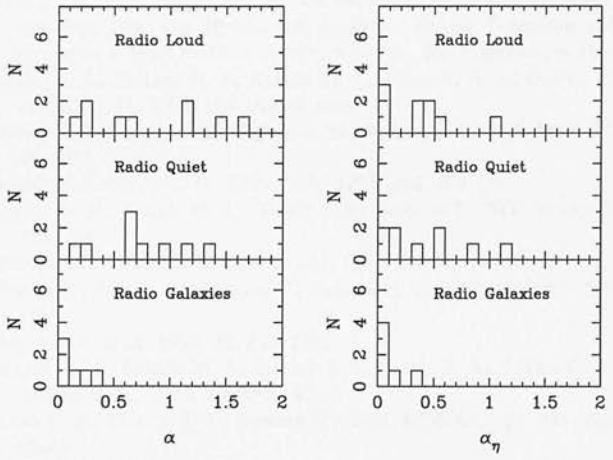

Figure 2. The distribution of α, the percentage contribution (by mass) of the 0.1-Gyr component. Where results have been obtained from two spectra for one object, the best-fitting result has been adopted. Again, the results on the left are for fits using the two-component model, and those on the right are for fits with the two-component model plus a nuclear contribution. Allowing for the possibility of a nuclear contribution means that a smaller α is required to fit the blue end of the spectrum, and the apparent difference between the radio galaxies and radio-loud and quiet quasars is reduced to a statistically insignificant level.

percentage of young population present (see Table 3). This effect is suggestive that at least some of the blue light might be caused by a scattered nuclear contribution, the strength of which would be highly dependent on the seeing at the time of observation, and on the precise repeatability of slit placement relative to the galaxy core. Interestingly, when a nuclear component is included with the stellar flux model, an even smaller percentage of 0.1-Gyr stellar population is required to fit the blue end of the spectra, and (more importantly) the difference in α between two spectra of the same object is generally reduced. This provides further support for the suggestion that some of the bluest quasar host spectra remain contaminated by quasar light at the shortest wavelengths, and indicates that the right-hand panel of Fig. 2 provides a more realistic estimate of the level of on-going star formation in the host galaxies. While this

figure still appears to suggest that at least some quasar hosts display higher levels of ongoing star formation activity than do radio galaxies, statistically this 'result' is not significant.

There are three galaxies that have very low age estimates, namely 0230-027, 0244+1944 and 1020−103. These objects have the bluest observed $R-K$ colours, so it may be expected that the fitted ages would be younger than the rest of the sample, and that these populations are genuinely young. As discussed above, it may be that these objects are bluer because of scattered nuclear light contaminating the host galaxy spectrum. However, it seems unlikely that their fitted ages are low simply because of this, because elsewhere in our sample, where two spectra have been obtained of the same object, the amount of nuclear contamination present does not significantly affect the age estimation (e.g. 0736+017 and 0157+001). Moreover, the inclusion of a nuclear component to the fit does not change the estimated age distribution of the host galaxies. If these ages are in error, then a more likely explanation, supported by the relative compactness of these particular host galaxies, is that nuclear and host contributions have been imperfectly separated in the *K*-band images, leading to an underestimate of the near-infrared luminosity of the host.

The result of the three-component fitting process that also allows a contribution from scattered nuclear light is that there are in fact only three host galaxies in the sample for which there is evidence that $\alpha > 0.5$. One of these is the host of a radio-loud quasar (2135−147) but, as can be seen from Fig. A2, this spectrum is one of the poorest (along with 0230−027, the only apparently young radio galaxy) in the entire data set. The two convincing cases are both the hosts of radio-quiet quasars, namely 0157+001 and 2344+184.

Within the somewhat larger sample of 13 RQQs imaged with the *HST* by McLure et al. (1999) and Dunlop et al. (2001), four objects showed evidence for a disc component in addition to a bulge, namely 0052+251, 0157+001, 0257+024 and 2344+184. Since we do not possess spectra of 0052+251 and 0257+024 this means that there is a 1:1 correspondence between the objects that we have identified on the basis of this spectroscopic study as having recent star formation activity, and those which would be highlighted on the basis of *HST* imaging as possessing a significant disc component. This straightforward match clearly provides us with considerable confidence that the spectral decomposition attempted here has been effective and robust. Finally, we note that it is almost certainly significant that 0157+001, which has the largest starburst component ($\alpha = 1.1$) based on this spectroscopic analysis, is also the only *IRAS* source in the sample.

5 CONCLUSIONS

We conclude that the hosts of all three major classes of AGN contain predominantly old stellar populations ($\simeq$11 Gyr) by $z \simeq 0.2$. This agrees well with the results of McLure et al. (1999) and Dunlop et al. (2001) who compare host galaxy morphologies, luminosities, scalelengths and colours in the same sample, and conclude that the hosts are, to first order, indistinguishable from 'normal' quiescent giant elliptical galaxies.

The best-fitting age of the dominant stellar population is *not* a function of AGN class. For the purely stellar models, the fitted percentage contribution of the blue component is, however, greater in the quasar hosts than in the radio galaxies; the median values are 0.6 per cent for the nine radio-loud quasars, 0.6 per cent for the nine radio-quiet quasars and 0.05 per cent for the six radio galaxies. However, when a nuclear component is included, the median values are 0.3 per cent for the radio-loud quasars, 0.3 per cent for the radio-quiet quasars and 0.00 per cent for the radio galaxies. Performing a Kolmogorov–Smirnov test on these results yields a probability greater than 0.2 that the percentage of young stellar population in host galaxies is in fact also not a function of AGN class.

These results strongly support the conclusion that the host galaxies of all three major classes of AGN are massive ellipticals, dominated by old stellar populations.

ACKNOWLEDGMENTS

LAN acknowledges the support provided by the award of a PPARC Studentship. MJK and DHH acknowledge the support provided by the award of PPARC PDRAs, while RJ acknowledges the award of a PPARC Advanced Fellowship. We thank an anonymous referee for perceptive comments which helped to clarify the robustness of our results and improved the clarity of the paper.

REFERENCES

Bahcall J. N., Kirhakos S., Saxe D. H., Schneider D. P., 1997, ApJ, 479, 642
Disney M. J. et al., 1995, Nat, 376, 150
Dunlop J. S., 2000, in Bunke A., Jr., van Breugel W. J. M., eds, ASP Conf. Ser. Vol. 193, The Hy-Redshift Universe: Galaxy Formation and Evolution at High Redshift. Astron. Soc. Pac., San Francisco, p. 133
Dunlop J. S., McLure R. J., Kukula M. J., Baum S. A., O'Dea C. P., Hughes D. H., 2001, MNRAS, in press
Dunlop J. S., Taylor G. L., Hughes D. H., Robson E. I., 1993, MNRAS, 264, 455
Hooper E. J., Impey C. D., Foltz C. B., 1997, ApJ, 480, L95
Hughes D. H., Kukula M. J., Dunlop J. S., Boroson T., 2000, MNRAS, 316, 204
Hutchings J. B., Morris S. C., 1995, AJ, 109, 1541
Jimenez R., Padoan P., Matteucci F., Heavens A. F., 1998, MNRAS, 299, 123
Magorrian J. et al., 1998, AJ, 115, 2285
McLure R. J., Kukula M. J., Dunlop J. S., Baum S. A., O'Dea C. P., Hughes D. H., 1999, MNRAS, 308, 377
Nolan L. A., Dunlop J. S., Jimenez R., 2001, MNRAS, 323, 385 (this issue)
Schade D. J., Boyle B. J., Letawsky M., 2000, MNRAS, 315, 498
Taylor G. T., Dunlop J. S., Hughes D. H., Robson E. I., 1996, MNRAS, 283, 930
Yi S., Brown T. M., Heap S., Hubeny I., Landsman W., Lanz T., Sweigart A., 2000, ApJ, 633, 670

APPENDIX A: SPECTRA AND χ^2 PLOTS

The fits for all the off-nuclear spectra are given. In Fig. A1, the rest frame spectra are in the first column (light grey), with the best-fitting two-component model spectra (Jimenez et al. 2000) superimposed (black). The spectra of the single-aged old population (mid-grey) is given for comparison. In Fig. A2, the fits allowing for an additional contribution to the flux from the nucleus are presented. The key is the same as in A1, with the additional dotted line representing the best-fitting two-component model flux plus the nuclear flux contribution.

The second column of plots shows the χ^2 evolution with age for the dominant older population. The third column shows the best-fitting χ^2 as a function of percentage young population, α, for fixed ages of the dominant component. The models have solar metallicity. The subscript η denotes results obtained by including the nuclear contribution.

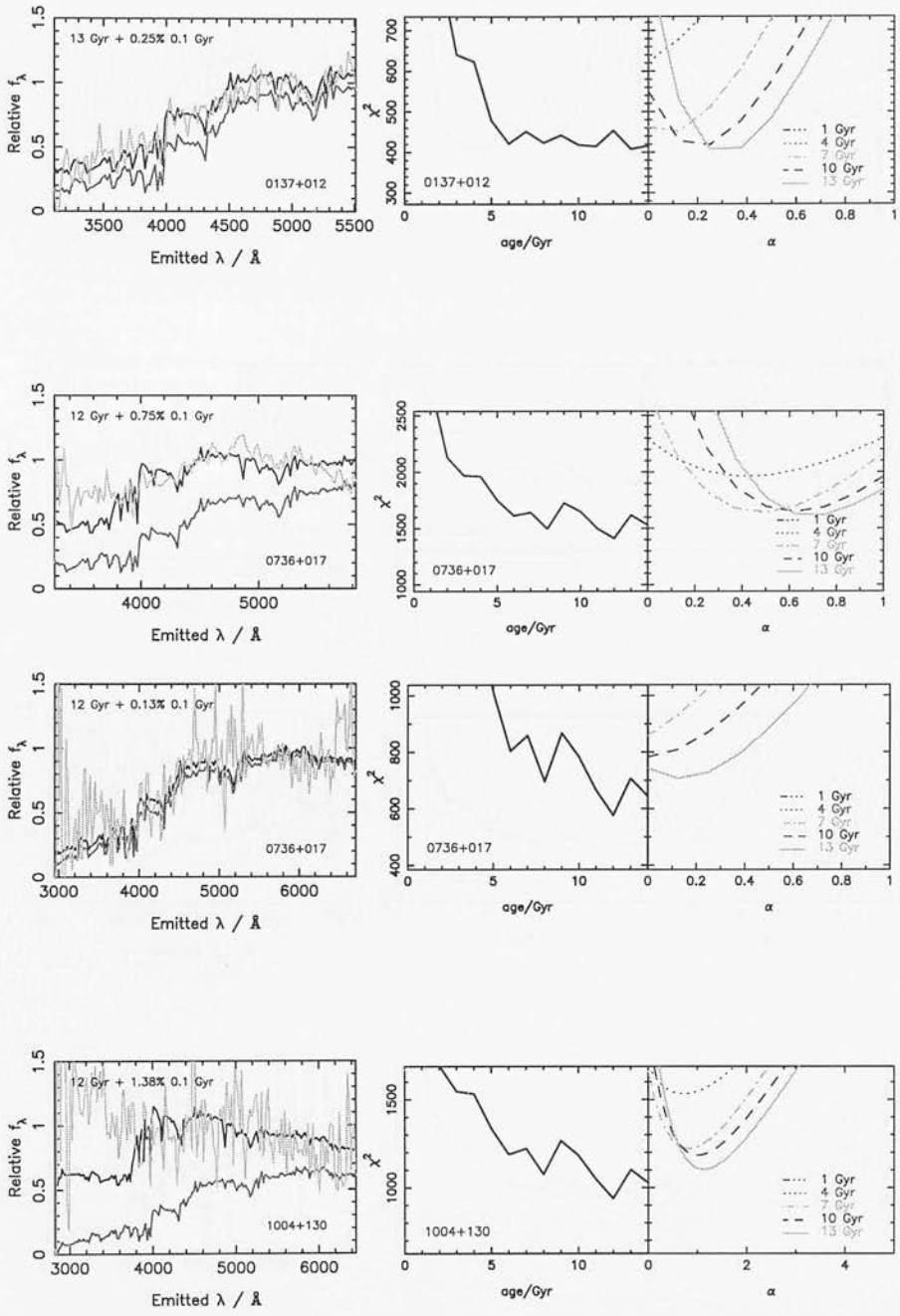

Figure A1. Model fits to the off-nuclear rest frame spectra, for each object, with the corresponding χ^2 plots. The rest-frame host-galaxy spectra are in the first column (lightest grey), with the best-fitting two-component model spectra (Jimenez et al. 2000) superimposed (black). The spectra of the single-aged old population (mid-grey, lowest line) is given for comparison. The second column shows the χ^2 evolution with age for the dominant older population and the third column shows the best-fitting χ^2 as a function of percentage young population, α, for fixed ages of the dominant component. All models have solar metallicity. Where there are two spectra of the same object, the spectrum given first is that observed on the Mayall 4-m telescope, and the second is that observed using the William Herschel Telescope. The data for the following objects have been smoothed using a Hanning function: 2135+147 (RLQ), 2141+175 (RLQ), 0244+194 (RQQ), 0923+201 (RQQ), 1549+203 (RQQ), 2215−037 (RQQ), 0230−027 (RG) and 0345+337 (RG).

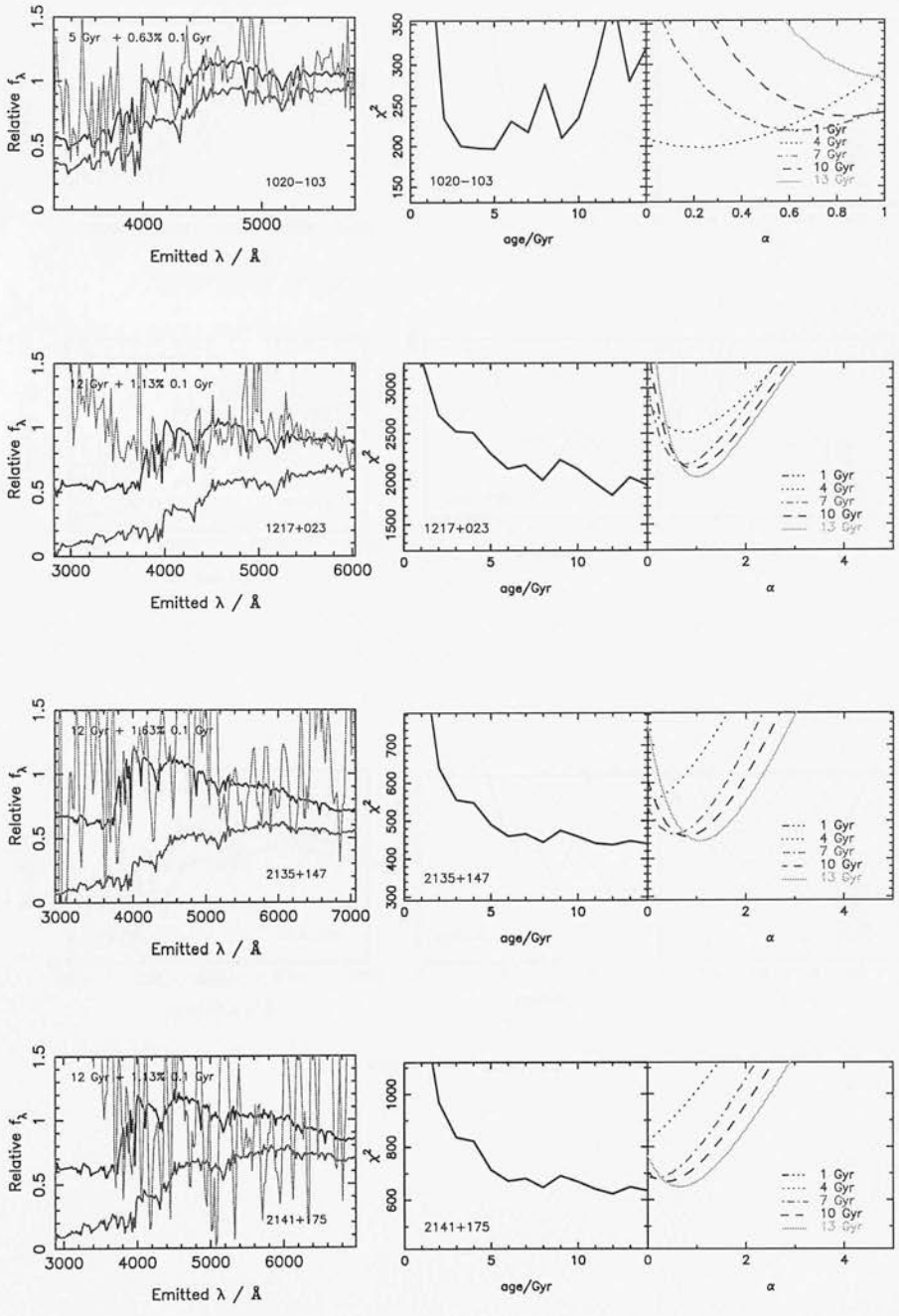

Figure A1 – *continued*

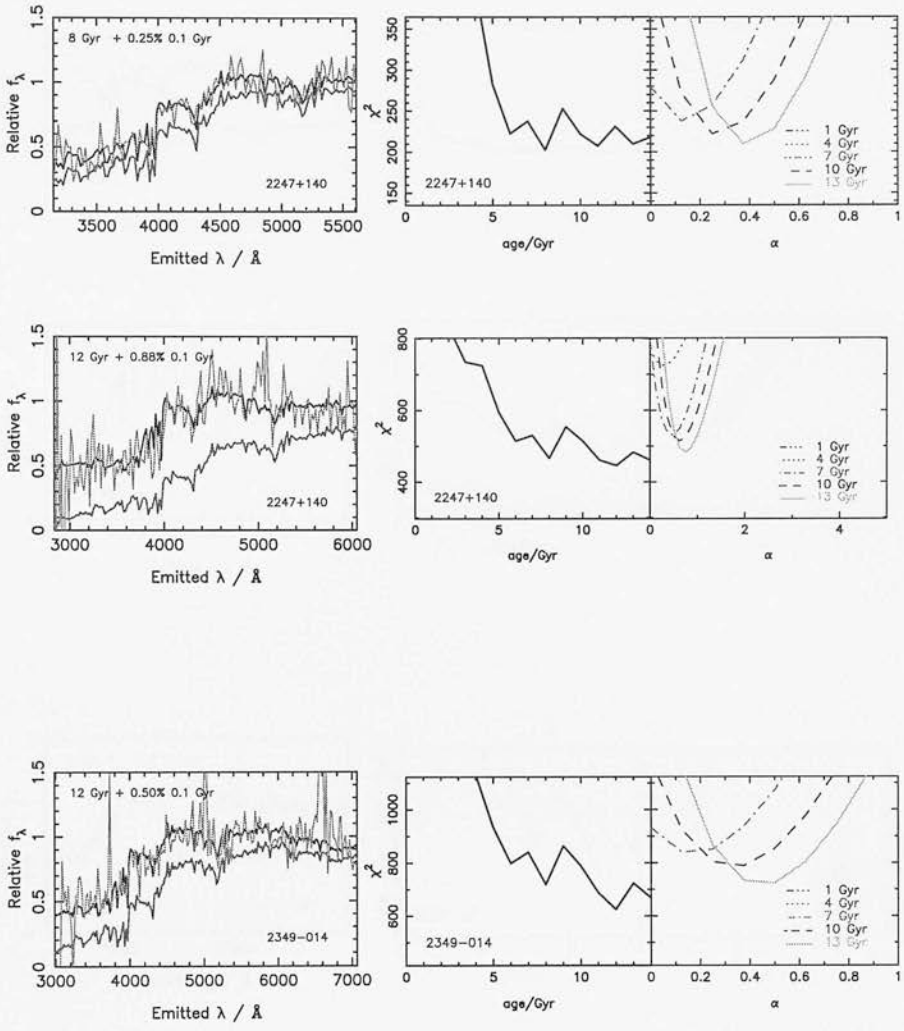

Figure A1 – *continued*

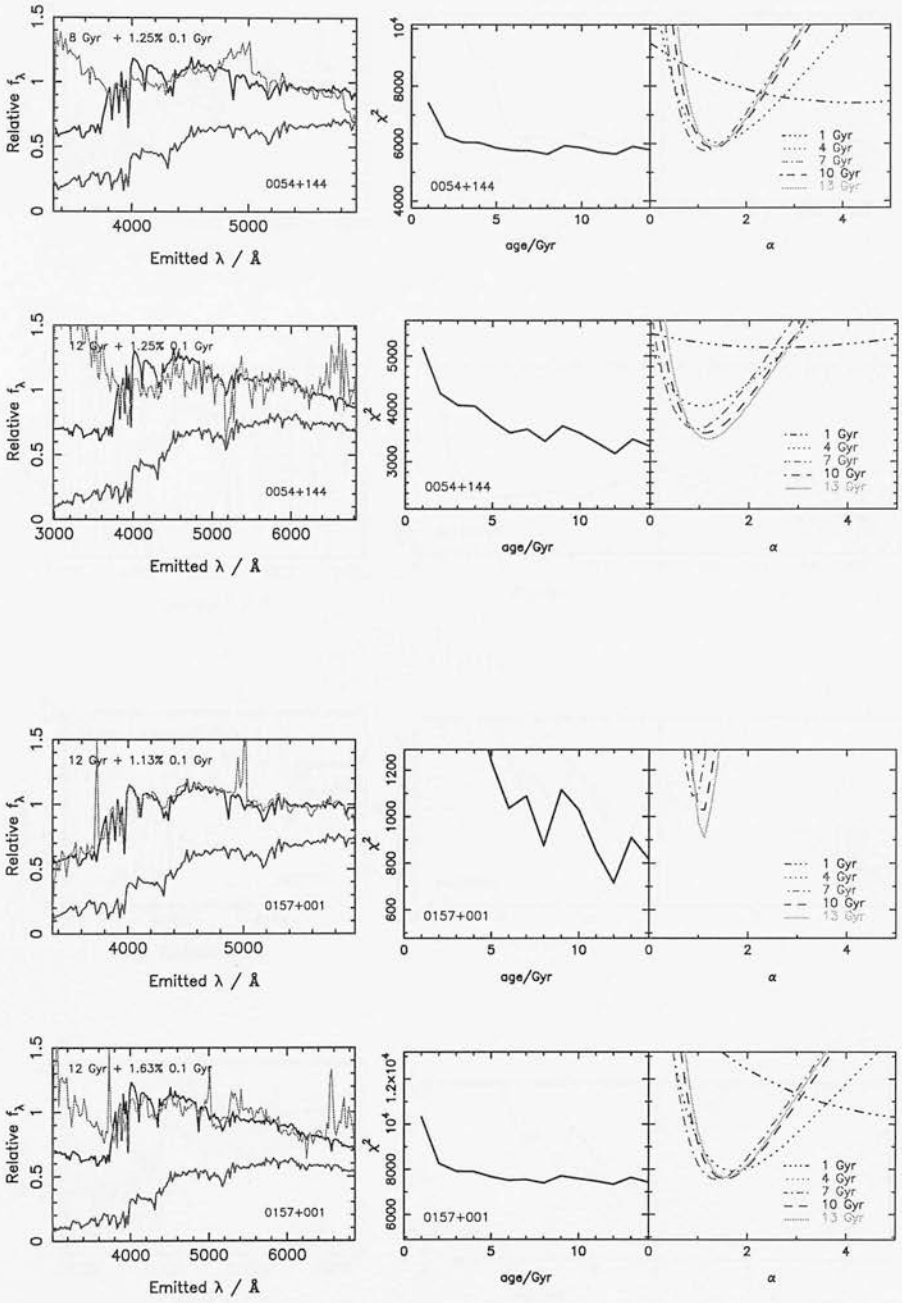

Figure A1 – *continued*

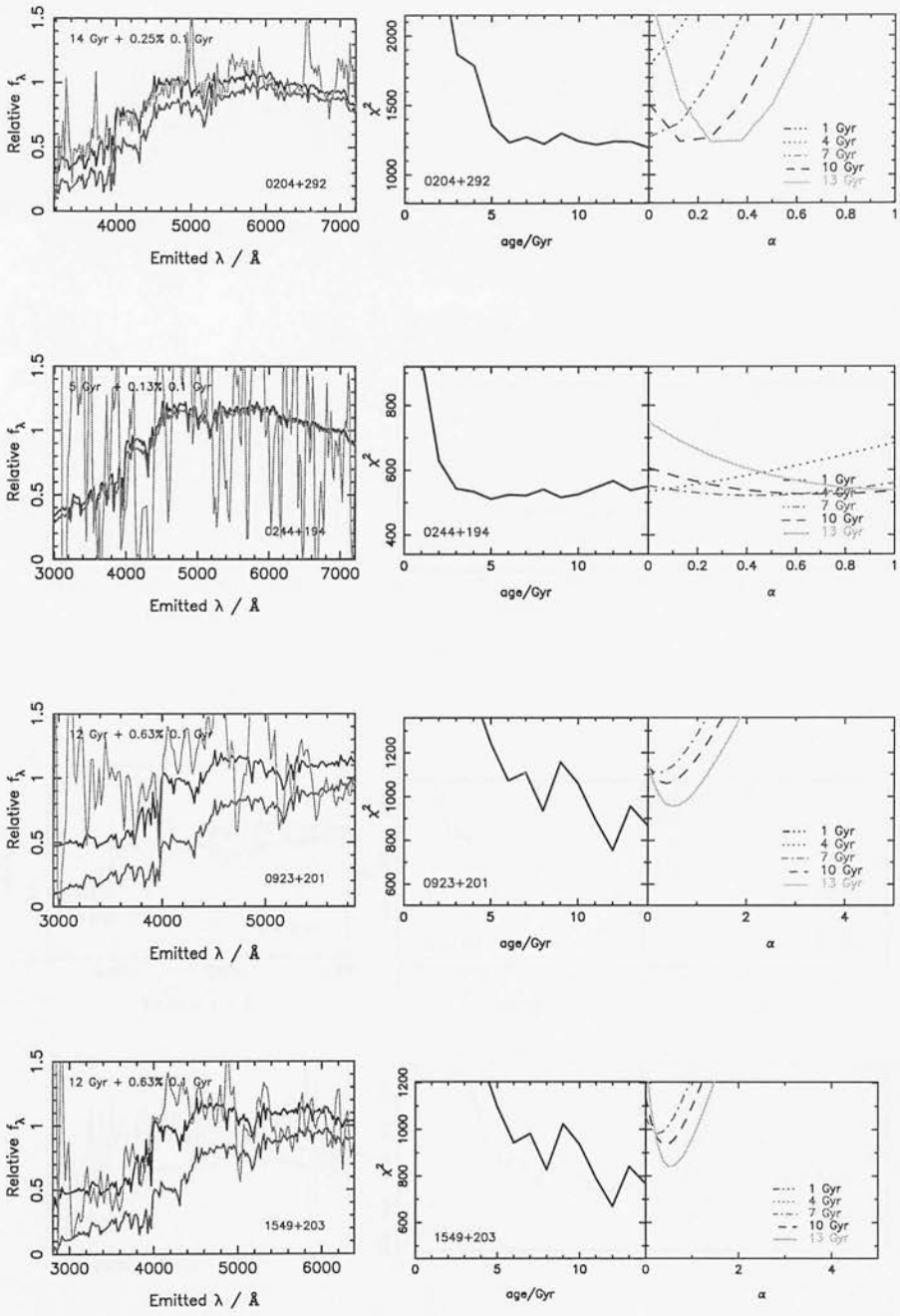

Figure A1 – *continued*

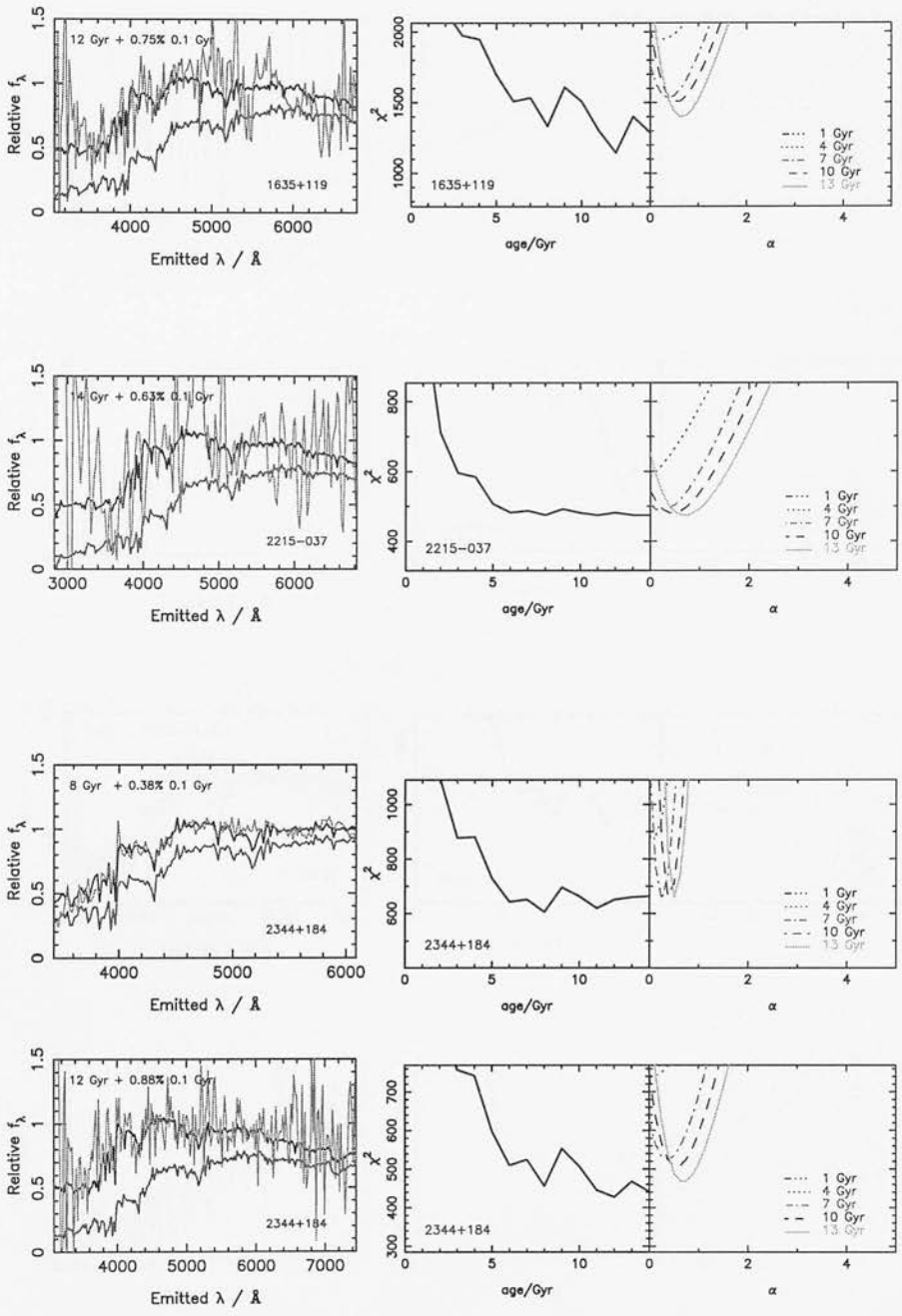

Figure A1 – *continued*

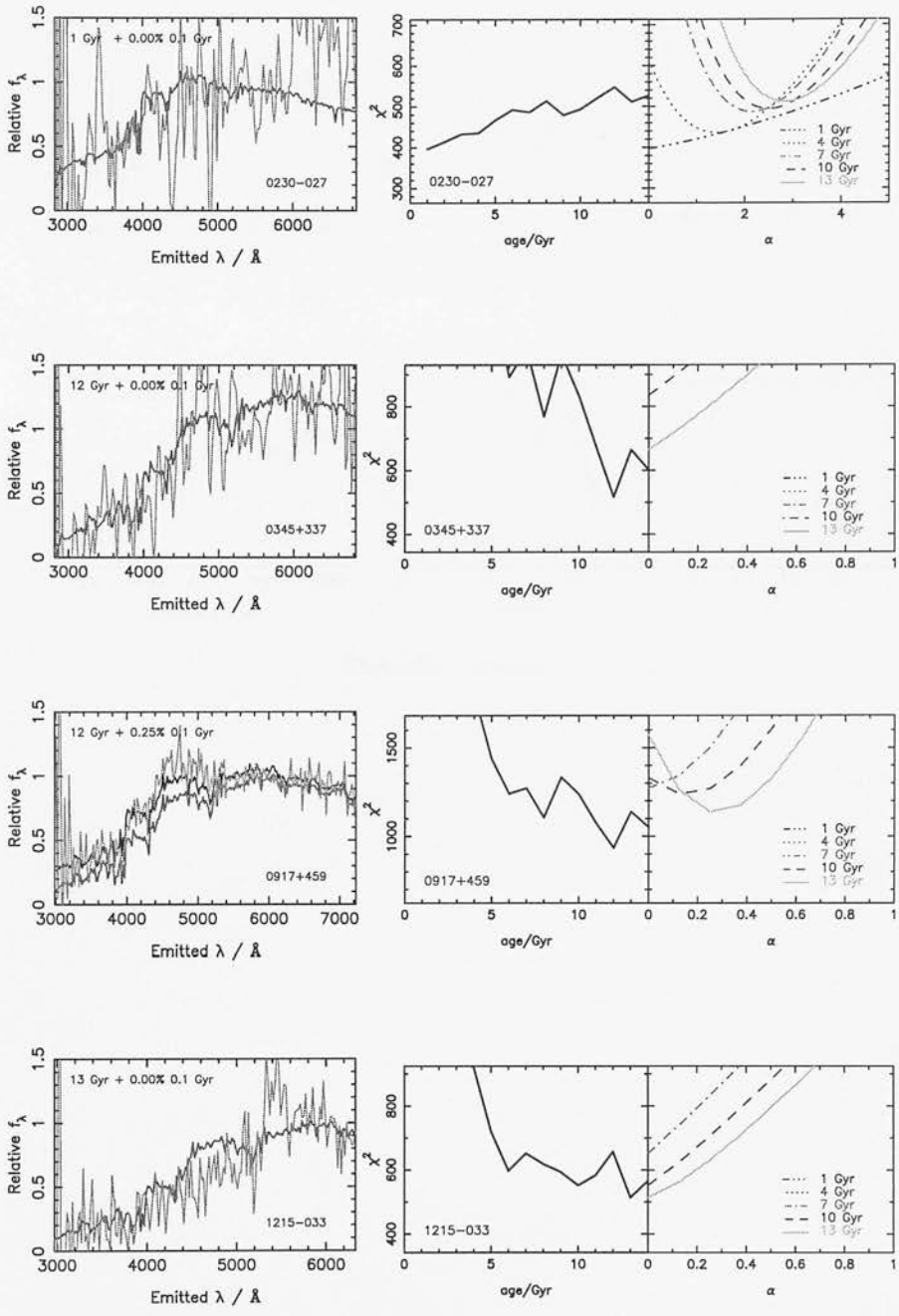

Figure A1 – *continued*

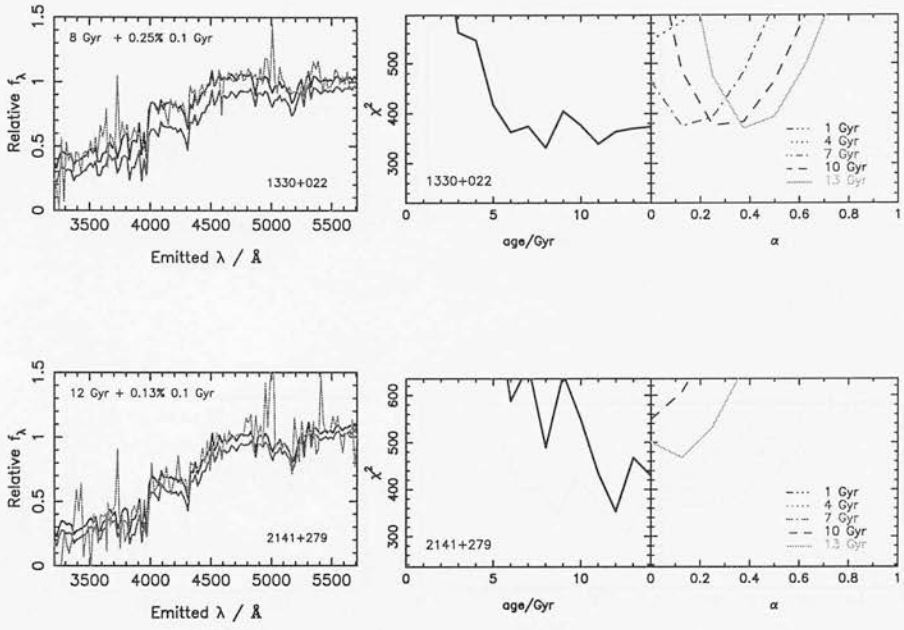

Figure A1 – *continued*

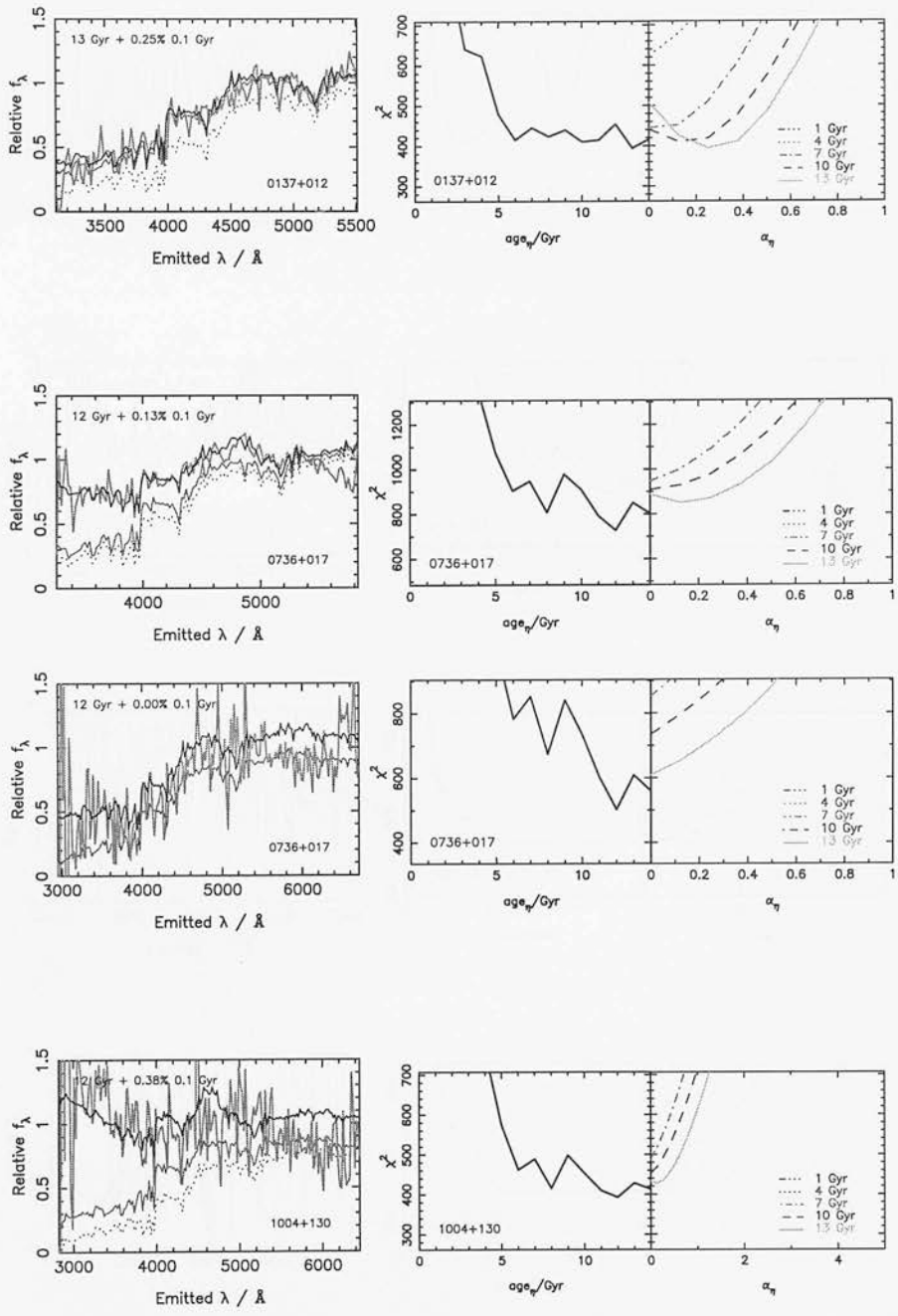

Figure A2. Model fits to the off-nuclear rest frame spectra, including the modelling of a nuclear contribution, for each object, with the corresponding χ^2 plots. The rest frame host galaxy spectra are in the first column (light grey), with the best-fitting two-component model flux plus the nuclear flux contribution (black) and the best-fitting two-component model spectra (Jimenez et al. 2000) superimposed (thin mid-grey). As in Fig. A1, the spectra of the single-aged old population (dotted line) is given for comparison. The second column shows the χ^2 evolution with age for the dominant older population and the third column shows the best-fitting χ^2 as a function of percentage young population, α, for fixed ages of the dominant component. The subscript η denotes results obtained by including the nuclear contribution. All models have solar metallicity. Where there are two spectra of the same object, the spectrum given first is that observed on the Mayall 4-m telescope, and the second is that observed using the William Herschel Telescope. The data for the following objects have been smoothed using a Hanning function: 2135+147 (RLQ), 2141+175 (RLQ), 0244+194 (RQQ), 0923+201 (RQQ), 1549+203 (RQQ), 2215−037 (RQQ), 0230−027 (RG) and 0345+337 (RG).

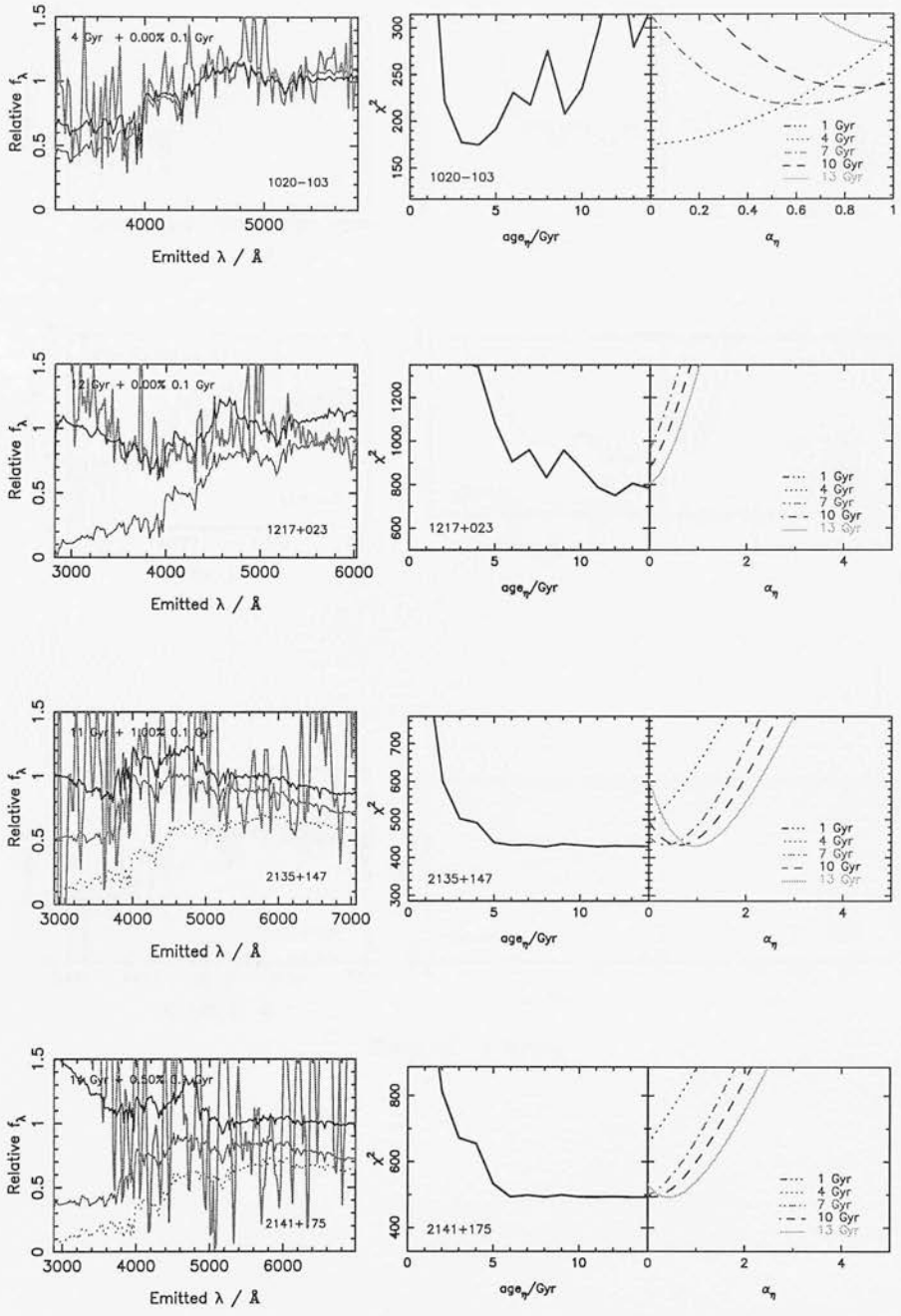

Figure A2 – *continued*

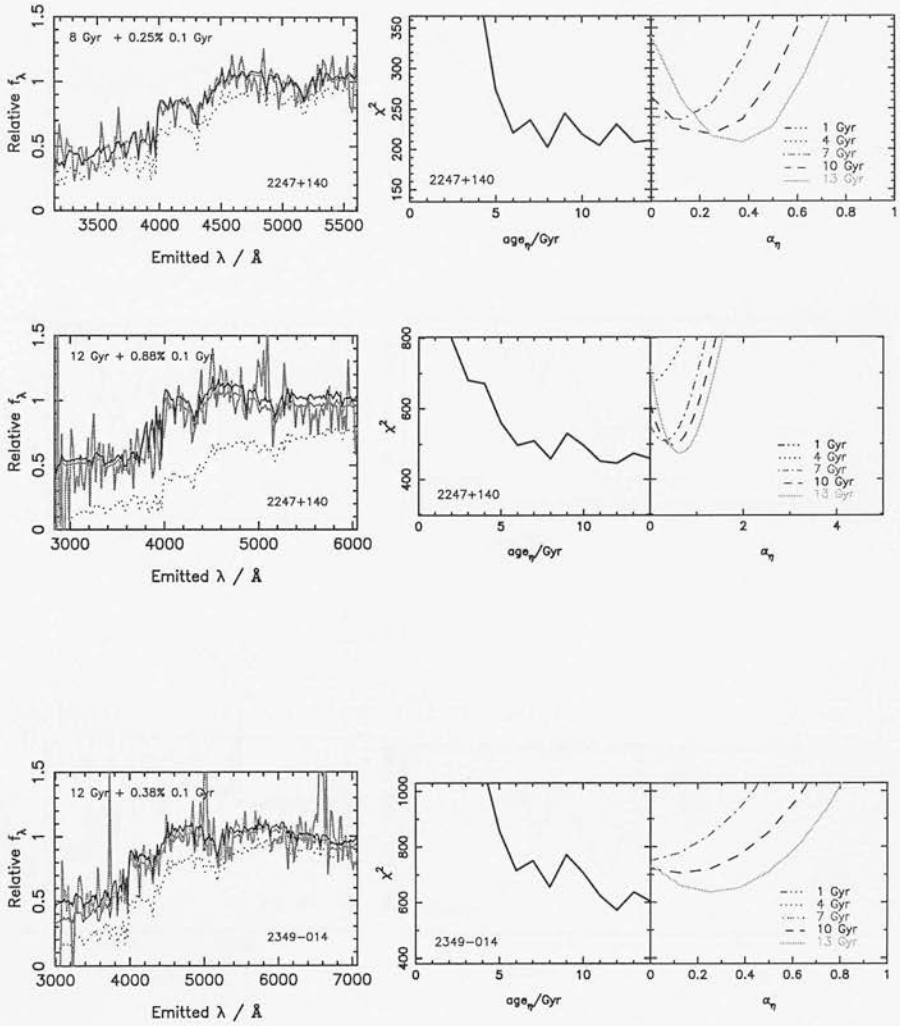

Figure A2 – *continued*

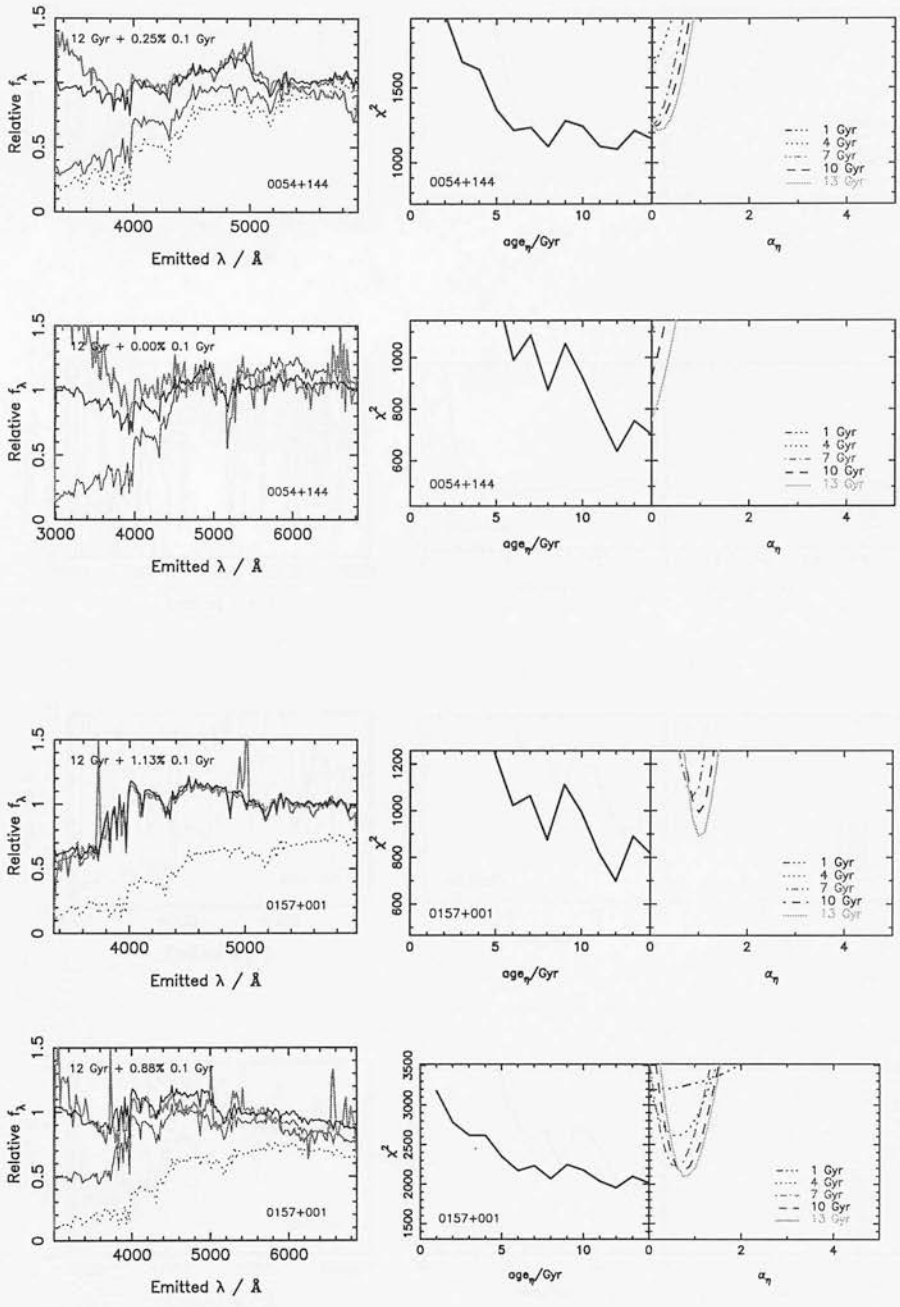

Figure A2 – *continued*

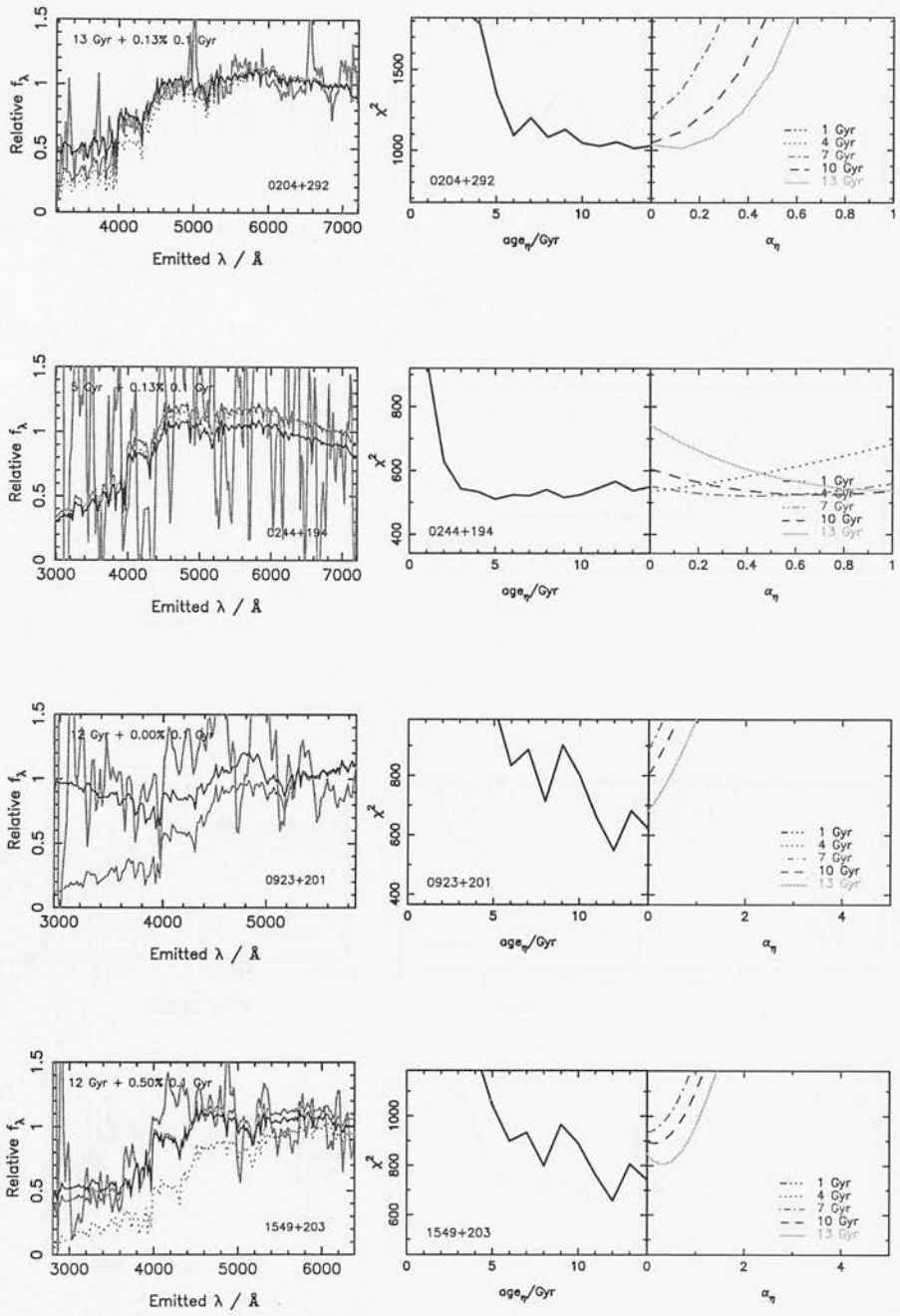

Figure A2 – *continued*

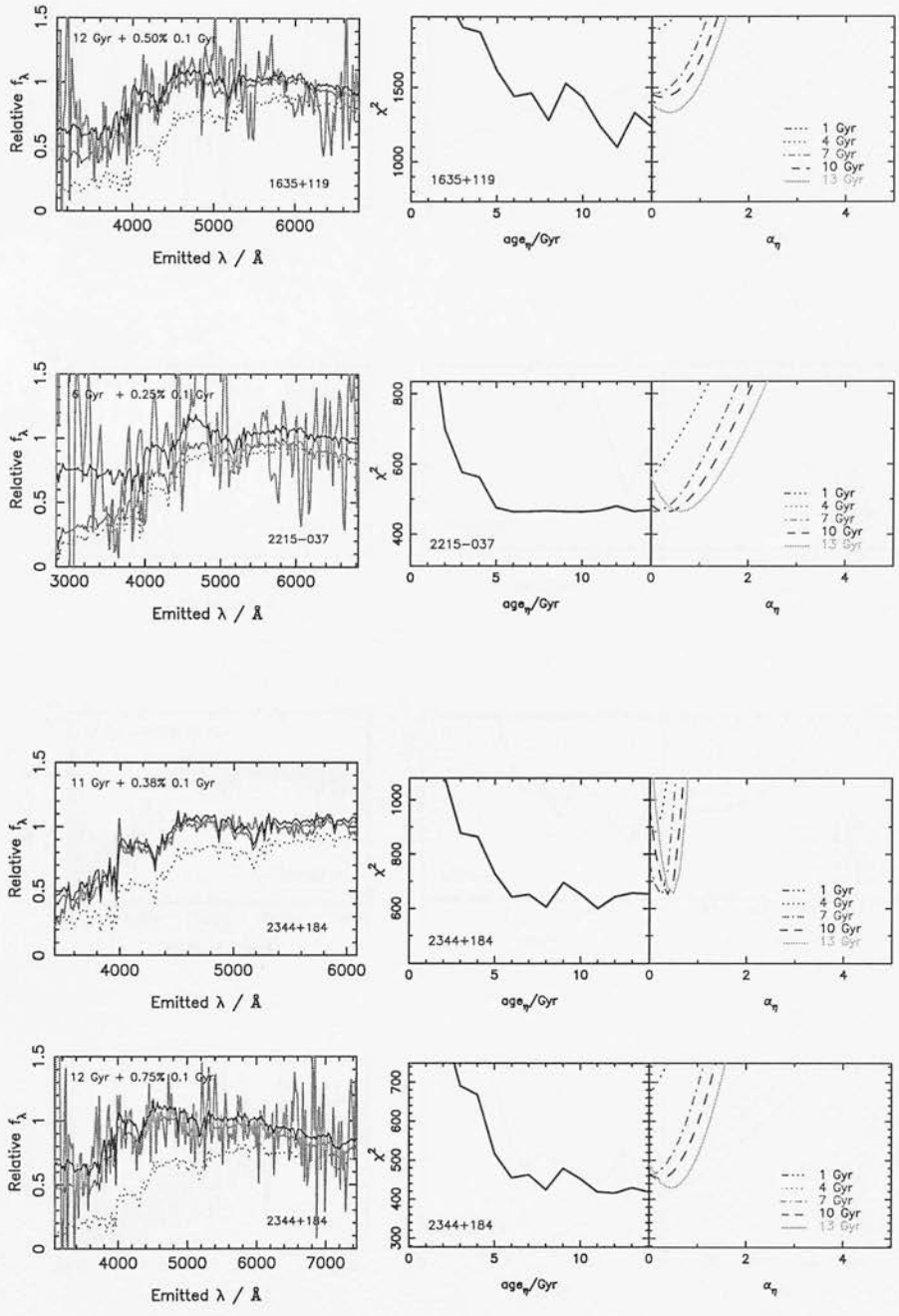

Figure A2 – *continued*

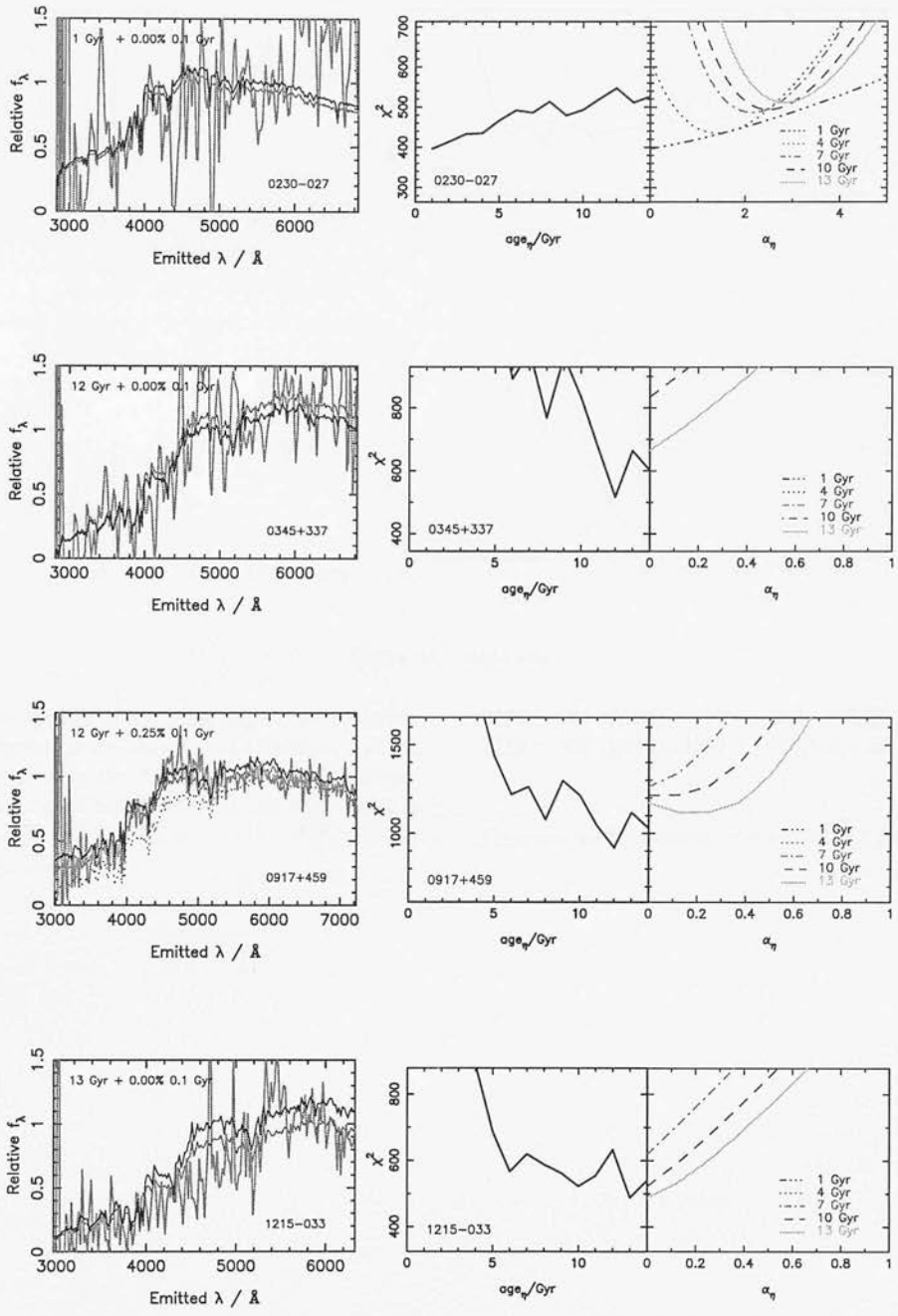

Figure A2 – *continued*

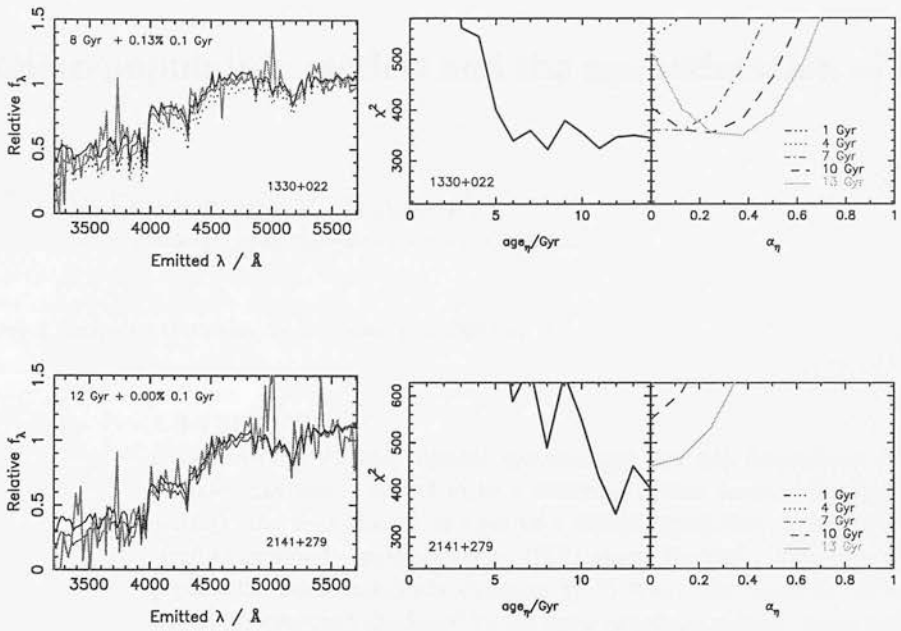

Figure A2 – *continued*

Where there are two spectra of the same object, the spectrum given first is that observed on the Mayall 4-m telescope, and the second is that observed using the William Herschel Telescope. The data for the following objects have been smoothed using a Hanning function: 2135 + 147 (RLQ), 2141 + 175 (RLQ), 0244 + 194 (RQQ), 0923 + 201 (RQQ), 1549 + 203 (RQQ), 2215 − 037 (RQQ), 0230 − 027 (RG) and 0345 + 337 (RG).

This paper has been typeset from a TEX/LATEX file prepared by the author.

Mon. Not. R. Astron. Soc. **323**, 385–390 (2001)

The Sun, stellar-population models and the age estimation of high-redshift galaxies

L. A. Nolan,* J. S. Dunlop and R. Jimenez†
Institute for Astronomy, University of Edinburgh, Royal Observatory, Edinburgh EH9 3HJ

Accepted 2000 November 3. Received 2000 October 25; in original form 2000 May 19

ABSTRACT

Given sufficiently deep optical spectroscopy, the age estimation of high-redshift ($z > 1$) galaxies has been claimed to be a relatively robust process due to the fact that, for ages <5 Gyr, the near-ultraviolet light of a stellar population is expected to be dominated by 'well-understood' main-sequence (MS) stars. Recently, however, the reliability of this process has been called into question by Yi et al., who claim to have developed models in which the spectrum produced by the main sequence reddens much more rapidly than in the models of Jimenez et al., leading to much lower age estimates for the reddest known high-redshift ellipticals. In support of their revised age estimates, Yi et al. cite the fact that their models can reproduce the spectrum of the Sun at an age of 5 Gyr, whereas the solar spectrum is not reproduced by the Jimenez et al. models until $\simeq$10 Gyr. Here we confirm this discrepancy, but point out that this is in fact a *strength* of the Jimenez et al. models and indicative of some flaw in the models of Yi et al. (which, in effect, imply that the Sun will turn into a red giant any minute now).

We have also explored the models of Worthey (which are known to differ greatly from those of Jimenez et al. in the treatment of post-MS evolution) and find that the main-sequence component of Worthey's models also cannot reproduce the solar spectrum until an age of 9–10 Gyr. We conclude that either the models of Yi et al. are not as main-sequence dominated at 4–5 Gyr as claimed, or the stellar evolutionary time-scale in these models is in error by a factor possibly as high as two. Our current best estimate of the age of the oldest galaxies at $z \simeq 1.5$ thus remains 3–4 Gyr, as we confirm with a new analysis of the existing data using the updated solar-metallicity models of both Jimenez et al. and Worthey.

Finally, by fitting a mixed metallicity model to the Sun, we demonstrate that, given rest-frame ultraviolet data of sufficient quality, it should be possible to break the age–metallicity degeneracy when analysing the spectra of high-redshift galaxies.

Key words: Sun: general – galaxies: high-redshift – galaxies: stellar content.

1 INTRODUCTION

For over a decade now, astronomers have attempted to estimate the ages of high-redshift galaxies using broad-band optical–infrared photometry (e.g. Lilly 1988; Dunlop et al. 1989; Chambers & Charlot 1990). Unfortunately, however, the derived ages have been rendered virtually meaningless by disagreements between modellers over post main-sequence evolution (e.g. Charlot, Worthey & Bressan 1996), and by the extreme susceptibility of such relatively crude broad-band data to dust reddening, emission-line contamination, etc.

In contrast, it has long been anticipated that relatively robust age constraints for high-redshift galaxies could be derived given rest-frame near-ultraviolet spectra of sufficient quality. This is because, for the potential ages of interest at $z > 1$ (i.e. ages <5 Gyr), the ultraviolet light of a stellar population is expected to be dominated by stars close to the turn-off point of the 'well-understood' main sequence (MS) (e.g. Magris & Bruzual 1993).

With the advent of deep optical spectroscopy on 10-m class telescopes, it has now proved possible to put this technique into practice. In particular, Dunlop et al. (1996) were able to use a deep Keck spectrum of the $z = 1.5$ radio galaxy LBDS 53W091 to first confirm that its near-ultraviolet spectrum was indeed dominated by starlight, and then to extract an age constraint of >3Gyr based primarily on comparison with a main-sequence only model of an evolving stellar population. Spinrad et al. (1997) explored further the reliability of this age estimate, and confirmed that the best agreement between ages derived using alternative evolutionary

* E-mail: lan@roe.ac.uk
† Present address: Physics and Astronomy Department, Rutgers University, Piscataway, NJ 08854-8019, USA.

synthesis models was obtained if fitting was confined to the detailed shape of the near-ultraviolet spectral energy distribution.

Not surprisingly, given its implications for cosmology (for $H_0 = 70\,\mathrm{km\,s^{-1}\,Mpc^{-1}}$, the age of an Einstein–de Sitter universe at $z = 1.5$ is only 2.3 Gyr), this result has been the subject of subsequent close scrutiny, and claims that 53W091 is in fact less than 2 Gyr old have been put forward by, for example, Bruzual & Magris (1997). However, Dunlop (1999) has argued that such low ages are only deduced using some models if the near-infrared photometry is also included in the fitting process, once again placing undesirable emphasis on the reliability of the modelling of post main-sequence evolution (a point previously also explored by Spinrad et al., 1997). Moreover, Dunlop (1999) has shown that, certainly for the slightly redder $z = 1.43$ galaxy 53W069, if fitting is confined to the Keck spectroscopic data (Dunlop 1999), the models of Bruzual & Charlot (1993), Worthey (1994) and Jimenez et al. (1998) *all* lead to the conclusion that its stellar population is >3 Gyr old (assuming solar metallicity).

Most recently, however, the reliability of even this near-ultraviolet spectroscopic age-dating has been called into question by Yi et al. (2000). Yi et al. (2000), claim to have derived a much lower age for 53W091, but also claim that this age is not due to differences in post-MS evolution, but rather to the fact that the spectrum produced by the main sequence in their models reddens much more rapidly than in the models of Jimenez et al. (1998). In support of their revised age estimates, Yi et al. cite the fact that their models can reproduce the spectrum of the Sun at an age of 5 Gyr, whereas the solar spectrum is not reproduced by the Jimenez et al. models until 8–10 Gyr. It is unclear to us why a stellar population should be expected to mimic the spectrum of the Sun at its current age (≃5 Gyr); even if the light from the stellar population is dominated by stars near the main-sequence turn-off the Sun is not expected to leave the main sequence until an age of ≃10 Gyr (Jorgensen 1991). Nevertheless this claim has motivated us to explicitly check the calibration of the main-sequence evolution in alternative evolutionary synthesis models of galaxy evolution.

This is the main subject of the present paper. What we have done is to take the three alternative and independent models of galaxy evolution developed by Yi et al. (2000), Jimenez et al. (1998) and Worthey (1994), and to check how rapidly they evolve to mimic the solar spectrum with and (more importantly) without inclusion of their post-MS components. The models are summarized in Section 2, and the results of comparison with the solar near-ultraviolet spectrum are presented in Section 3. We then proceed, in Section 4, to use these models (again with and without post-MS components) to check explicitly the extent to which the age estimates of 53W091 and 53W069 really are affected by different approaches to modelling post-MS evolution. The main remaining uncertainty is the impact of having to assume a value for the metallicity of the stellar population, and in Section 5 we explore whether, given near-ultraviolet data of sufficient quality, it may be possible to break the well-known age–metallicity degeneracy. Finally, our conclusions are summarized in Section 6.

2 THE MODELS

2.1 The models

This study was motivated by the apparent disagreement reported by Yi et al. (2000) between their own models and those of Jimenez et al. (1998). We are able to perform our own comparison of these models because Sukyoung Yi has kindly supplied us with his model spectral energy distributions (SEDs) up to an age of 5 Gyr (Yi, private communication). We also wanted to compare the predictions of a third independent set of evolutionary synthesis models, and have chosen the models of Worthey (1994) for this purpose. The reason for this choice was that we already knew, from our previous modelling of 53W091 (Dunlop et al. 1996; Spinrad et al. 1997) that the models of Worthey (1994) also appear to yield lower ages than those of Jimenez et al. (1998), but for reasons which we suspected were primarily as a result of a different treatment of post-MS evolution (see Charlot et al. 1996).

Since the primary objective in this paper is to check the calibration of MS evolution using the Sun, we have confined our attention only to models that assume solar metallicity. However, we *are* interested in removing any potential confusion introduced by different treatments of post-MS evolution, because it is hard to be sure that the UV spectrum of an instantaneous starburst really is completely dominated by MS stars in all alternative models beyond an age of 2–3 Gyr (and beyond 5 Gyr it is not expected to be). We have therefore constructed a MS-only version of the models of Jimenez et al. (1998), and have also been supplied with a MS-only version of the models of Worthey (1994) (Worthey, private communication). In both the Jimenez and the Worthey models the isochrones have been cut off at the same point (corresponding to point 55 in the Vandenberg grid in the case of Worthey's models). A pure MS-only version of the Yi et al. models was not available to us, but we do have access to a main-sequence + giant branch (MSGB) version, which is stripped of horizontal branch and asymptotic giant branch contributions, and should be an excellent approximation to an MS-only model, at least in the near-ultraviolet for ages <5 Gyr, as Yi et al. themselves claim.

2.2 χ^2 minimization

Since our main aim in this work was to calibrate the age-dating of distant stellar populations based on the rest-frame near-ultraviolet spectra, fitting was deliberately restricted to the spectral range 2000–4000 Å. The best fit was determined by binning the data to the same spectral resolution as the model in question, and then varying the age and normalization as free parameters until χ^2 was minimized.

For the high-redshift galaxies 53W091 and 53W069, the error on each binned spectral data point was derived from propagation of the original errors in the Keck optical spectra (see Dunlop et al. 1996; Dunlop 1999). In the case of the Sun, we are using the theoretical spectrum of Kurucz as the best available representation of the true solar SED, and have simply assumed a constant flux-density error (i.e. independent of wavelength), adjusted in size until reduced chi-squared (χ^2_ν) equalled unity for the very best-fitting model. It is thus only possible to compare the relative (rather than absolute) ability of the different models to reproduce the solar ultraviolet spectrum as the age of each model is varied.

3 COMPARISON WITH THE SOLAR SPECTRUM

3.1 Full models

In Fig. 1(a) we show reduced χ^2 as a function of age for each of the full stellar population models when age is varied in an attempt to best reproduce the solar spectrum. The models of Yi et al.

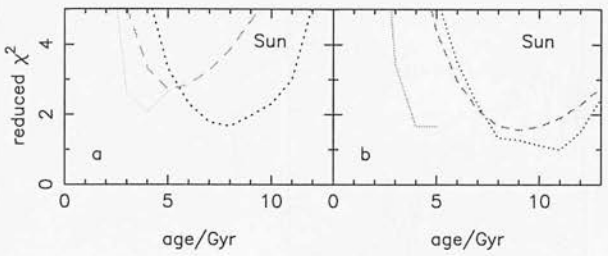

Figure 1. Reduced χ^2 as a function of age for the six alternative solar metallicity stellar population models fitted to the solar spectrum. On the left-hand panel are the results for the full stellar population models, and on the right-hand side are those for Worthey and Jimenez et al. main sequence (MS) only models and Yi et al. main sequence plus red giant branch (MSGB) models. Solid lines – Yi et al. (2000): dashed lines – Worthey (1994): dotted lines – Jimenez et al. (1998). The MS/MSGB models result in a better fit than the full models. The best-fitting age of Yi et al.'s MSGB models differ from the best-fitting ages of both Worthey's and Jimenez et al.'s MS only models by a factor of order two, implying a MS-turn-off age for the Sun of only 4–5 Gyr, compared with 9 or 11 Gyr implied by the MS-only models of Worthey and Jimenez et al. respectively.

predict the lowest age, indicating that the near-ultraviolet spectrum produced by these models best mimics that of the sun after an age of only 4 Gyr. The models of Worthey yield a best-fitting age of 5 Gyr, while those of Jimenez et al. predict an age of 8 Gyr. From this plot it might appear that it is the models of Jimenez et al. that are most unusual, but it is important to note that (i) it is the models of Jimenez et al. that yield the best quality of fit to the solar spectrum, and (ii) it is to be expected that the full stellar population models will *underestimate* the main-sequence turn-off (MSTO) age of the Sun, because of the inclusion of post-MS stars. Moreover, from this plot it is completely unclear how much of the (substantial) difference between the derived best-fitting ages can be attributed to differing contributions of post-MS stars to the galaxy ultraviolet SEDs.

3.2 Main-sequence only models

For a meaningful comparison between galaxy synthesis models and the expected MS turn-off age of the Sun, we really require to ensure that the ultraviolet spectra produced by the models are completely MS dominated. Therefore, in Fig. 1(b) we show reduced χ^2 as a function of age in an analogous way to Fig. 1(a), but this time using models, stripped as far as possible of post-MS contributions. This allows not only a sensible comparison with the Sun, but also makes it possible to assess the relative impact of post-MS contributions to the full model fits shown in Fig. 1(a).

This plot makes it clear that it is the models of Yi et al. that are unusual, and apparently in error by a factor of two in terms of rate of MS evolution. Stripped of HB and AGB contributions the predictions of the Yi et al. models are little changed, indicating a best-fitting age of 4–5 Gyr. In contrast, stripped of post-MS evolution the models of Worthey and Jimenez et al. appear to be in good agreement not only with each other (9 and 11 Gyr respectively) but also with the generally accepted MS turn-off age of the Sun (10.5 Gyr – Jorgensen 1991).

It is hard to assess the likely impact on the predictions of the Yi et al. models if the GB was also removed, but the lack of any dramatic change upon removal of HB and AGB contributions does tend to support their own claim that their models are already highly MS dominated at ages <5 Gyr. In contrast the contribution of post-MS stars in the models of Worthey must be relatively strong, even at 5 Gyr, because removal of HB+AGB moves the derived age from 5 to 7 Gyr, and subsequent removal of remaining post-MS stars completes the shift to 9 Gyr as shown in Fig. 1(b). This therefore backs up the suggestion made in Jimenez et al. (1998) that the main difference between the models of Jimenez et al. and Worthey lies in the strength of the AGB and RGB, but that the MS evolution in both models is very similar, and yields sensible values for the turn-off age of the Sun.

Table 1. A summary of the best-fitting ages produced by fitting the six alternative models discussed in the text to the near-ultraviolet spectral energy distribution of (i) the Sun (see Figs 1 and 2), (ii) the $z = 1.55$ galaxy 53W091 (see Fig. 3), and (iii) the $z = 1.43$ galaxy 53W069 (see Fig. 4). In the case of the Sun, the result of fitting the mixed-metallicity model discussed in Section 5 is also given (see Fig. 5). The value of reduced χ^2 is also given in each case, although in the case of the fits to the Sun, the values of reduced χ^2 can only be used to judge the relative quality of the alternative model fits.

object	model	best-fitting age/Gyr	reduced χ^2
Sun	J Full	8	1.67
	J MS	11	1.00
	W Full	5	2.72
	W MS	9	1.57
	Y Full	4	2.06
	Y MSGB	4	1.67
	J 3Z	8	1.37
LBDS 53W091	J Full	3	1.25
	J MS	3	1.22
	W Full	2	1.38
	W MS	3	1.22
	Y Full	2	1.30
	Y MSGB	2	1.25
LBDS 53W069	J Full	5	1.63
	J MS	6	1.72
	W Full	3	1.54
	W MS	4	1.78
	Y Full	2	1.63
	Y MSGB	3	1.69

These results are tabulated in Table 1, and in Fig. 2 we show the best-fitting model spectra superimposed on the solar spectrum. It is worth noting (from both Figs 2 and 1) that, as one would hope, the MS-only models in every case yield a better *quality* of fit to the solar spectrum than do the full models which include some contribution from more evolved stars. Interestingly, the MS-only models of Jimenez et al. yield both the best overall fit in terms of reduced χ^2, and a MS-turn-off age which most closely matches the accepted value of 10.5 Gyr (Jorgensen 1991).

In summary, either the time-scale of MS evolution in the models of Yi et al. is too short by a factor $\simeq$2, or the GB contribution to the ultraviolet spectrum at an age of 4 Gyr is unexpectedly large, in which case these models would again be extremely unusual and the comparison with the age of the Sun as suggested by Yi et al. must inevitably be meaningless.

4 COMPARISON WITH THE SPECTRA OF RED GALAXIES AT $z \simeq 1.5$

4.1 LBDS 53W091

The age implications of the deep Keck optical spectrum of the red mJy radio galaxy 53W091 have been previously discussed in some detail by Dunlop et al. (1996) and Spinrad et al. (1997). However

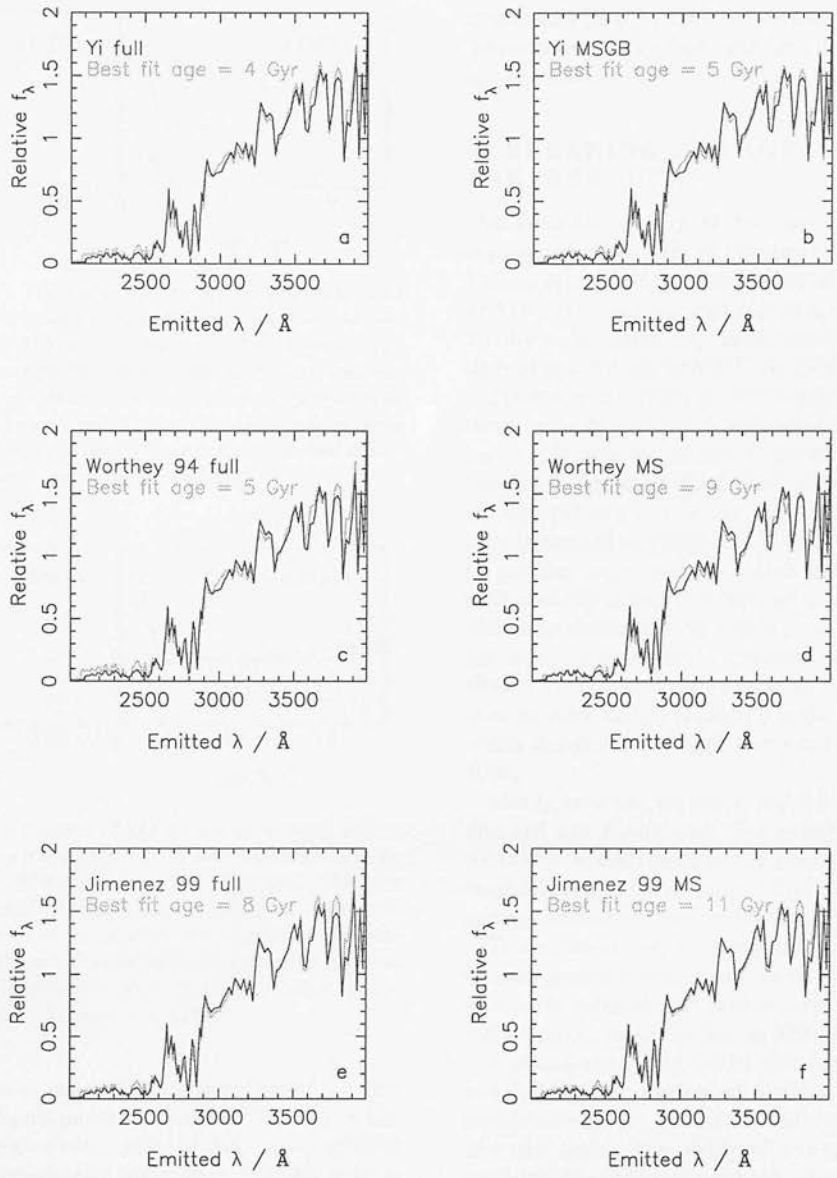

Figure 2. Best fits to the solar spectrum (black lines) for the various solar metallicity models (grey lines).

it is interesting and important to revisit the age-determination of this object for a number of reasons. First, the models of Jimenez et al. have been updated in the intervening years. Secondly, the Yi et al. models did not exist in 1996/1997. Thirdly, we have only recently obtained the MS-only versions of the Worthey models. We also felt it was important to re-analyse this spectrum given the claims made by Bruzual & Margris (1997) and Yi et al. (2000) that the most recent models yield best-fit ages for the stellar population in 53W091 of less than 2 Gyr.

Therefore in Fig. 3 we show the results of fitting the same six models (as fitted to the Sun above), to the rest-frame near-ultraviolet SED of 53W091. The results, summarized in Table 1, are that both the Jimenez et al. (1998) models (full and MS only) yield a best-fitting age of 3 Gyr (with ages as low as 2 Gyr formally excluded), both the Yi et al. models (full and MSGB) yield a best-fitting age of 2 Gyr, while the best-fitting age yielded by the Worthey models changes from 2 to 3 Gyr if post-MS contributions are excluded. Given the fact that we have already shown that the MS clock in the Yi et al. models appears to be running up to a factor of 2 too fast, this means that the argument over whether the age of 53W091 can or cannot be younger than 3 Gyr comes down to a debate over the validity of the stronger AGB and GB contributions in the Worthey models compared with the more MS-dominated Jimenez et al. models. Jimenez et al. (1998) argue that their models include a better treatment of mass-loss in evolved stars which results in less luminous RGB and AGB contributions. In summary, the available evidence still appears to favour a minimum age of 3 Gyr for this galaxy, subject to remaining uncertainties over the impact of possible non-solar metallicity (see Section 5).

4.2 LBDS 53W069

As discussed by Dunlop (1999), the Keck spectrum of the even redder mJy radio galaxy 53W069 ($z = 1.43$; Dey et al. 2000)

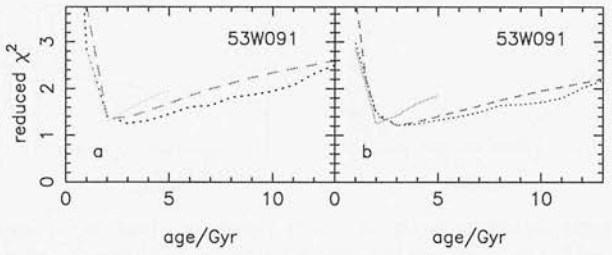

Figure 3. Reduced χ^2 as a function of age for the six alternative solar metallicity stellar population models fitted to the near-ultraviolet spectrum of the z=1.55 radio galaxy 53W091 (Dunlop et al. 1996; Spinrad et al. 1997). On the left-hand panel are the results for the full stellar population models, and on the right-hand side are those for Worthey and Jimenez et la. main-sequence (MS) only models and Yi et al. main-sequence plus red giant branch (MSGB) models. Solid lines – Yi et al. (2000): dashed lines – Worthey (1994): dotted lines – Jimenez et al. (1998).

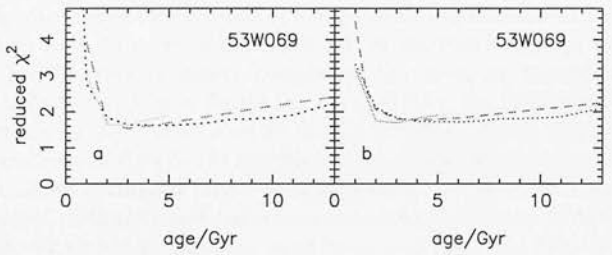

Figure 4. Reduced χ^2 as a function of age for the six alternative solar metallicity stellar population models fitted to the near-ultraviolet spectrum of the $z = 1.43$ radio galaxy 53W069 (Dunlop 1999; Dey et al., 2000). On the left-hand panel are the results for the full stellar population models, and on the right-hand side are those for Worthey and Jimenez et al. main-sequence (MS) only models and Yi et al. main-sequence plus red giant branch (MSGB) models. Solid lines – Yi et al. (2000): dashed lines – Worthey (1994): dotted lines – Jimenez et al. (1998).

appears to offer the best example discovered to date of a highly evolved coeval stellar population at a redshift as high as $z \simeq 1.5$. Dunlop (1999) found, from a comparison of their near-ultraviolet SEDs, that 53W069 is significantly redder than 53W091, and that the SED of the latter galaxy can be decomposed into that of 53W069 plus a low-level blue component that is approximately flat in f_λ. It is therefore to be expected that model-fitting to the near-ultraviolet SED of 53W069 might yield even higher age limits than those derived above for 53W091.

In Fig. 4 we show the results of fitting the same six models as before to the near-ultraviolet SED of 53W069. The results can again be found in tabulated form in Table 1. In summary, for this object five out of the six models yield a minimum age > 3 Gyr, with only the Yi et al. full models allowing an age as low as 2 Gyr. Since these models appear flawed based on the solar comparison discussed in Section 3, we conclude that it is extremely hard to escape the conclusion that 53W069 is at least 3 Gyr old. For this object the debate over whether the post-MS treatment of Jimenez et al. (1998) is to be preferred over that of Worthey (1994) translates into an uncertainty over whether the best-fitting age is in fact >3 or >4 Gyr (see Table 1).

For $H_0 = 70\,\mathrm{km\,s^{-1}\,Mpc^{-1}}$, the age of an Einstein–de Sitter universe at $z = 1.43$ is only 2.5 Gyr. Therefore, given the apparently flawed nature of the Yi et al. models, we conclude that the only way that the age of 53W069 at $z = 1.43$ can be contained within an Einstein–de Sitter universe is if varying the assumed metallicity from solar can in fact reduce the best-fitting age to <2.5 Gyr.

5 BREAKING THE AGE–METALLICITY DEGENERACY

The potential severity of the age–metallicity degeneracy was highlighted in the work of Worthey (1994), and acknowledged by Dunlop et al. (1996) in their original attempts to determine the age of 53W091. It is clear that assuming a metallicity of twice solar for the entire stellar population results in the lower limit to the derived age of both 53W091 and 53W069 falling below 2.5 Gyr.

Spinrad et al. (1997) presented arguments that, even assuming these galaxies possess a high-metallicity core, adoption of a universally high metallicity is inappropriate when analysing the integrated light from the central $\simeq$10 kpc of an elliptical galaxy (as sampled at $z > 1$ by the Keck spectroscopic slit). Moreover, both Jimenez et al. (2000) and Yi et al. (2000) have now attempted to produce more realistic mixed metallicity models and have independently found that such mixed-metallicity models in fact yield very similar ages to simple *solar* metallicity models (despite the basic disagreement between model time-scales detailed above). This appears to be true, even when the average metallicity is twice solar, simply because it is the low metallicity component which dominates the light shortward of 3000 Å (Jimenez et al. 2000).

Ideally, however, we would like to be able to fit both metallicity mix and age to the data. The extent to which this is possible obviously depends both on the quality of the spectroscopic data available, and on the presence of (primarily) metallicity dependent and age-dependent features within the available spectral range.

This approach will be explored further in a separate paper, but here we present evidence that the age–metallicity degeneracy can, at least in principle, be broken with data in the spectral range 2000–4000 Å, using the Sun as a test case.

A mixed-metallicity model was constructed from the 0.2-, 1- and 2.5-$Z_\odot$ full models of Jimenez et al., with the relative contributions of the different metallicity models allowed to vary as free parameters. The ability of this mixed-metallicity model to reproduce the metallicity and MSTO age of the sun is a test of the ability of stellar population synthesis models to break the age–metallicity degeneracy given data in this near-ultraviolet spectral range.

The solar spectrum was rebinned in the same way as for the solar-metallicity only fitting process. The mixed-metallicity model flux was built from normalized SEDs, so that

$$F_{3Z,\lambda,age} = X_{0.2Z_\odot} f_{0.2Z_\odot,\lambda,age} + X_{Z_\odot} f_{Z_\odot,\lambda,age} + X_{2.5Z_\odot} f_{2.5Z_\odot,\lambda,age}$$

where $F_{3Z,\lambda,age}$ is the mixed metallicity flux per unit wavelength in the bin centred on wavelength λ at *age* Gyr, $f_{Z,\lambda,age}$ is the flux per unit wavelength in the bin centred on wavelength λ of the model at *age* Gyr, and metallicity Z, and $X_{0.2Z}$ is the fractional contribution to $F_{3Z,age}$ by $f_{Z,age}$.

A χ^2 fit was used to determine the best-fitting age, total normalization, and values of $X_{0.2Z_\odot}$, $X_{Z_\odot}$ and $X_{2.5Z_\odot}$.

In Fig. 5 we show the results of this mixed-metallicity fitting procedure. Comparison of the left-hand plot with the dotted line in Fig. 1(a) demonstrates the extent to which allowing metallicity to vary has weakened the constraint on age. However, the best-fitting age is still 8 Gyr, as for the full solar-metallicity only models.

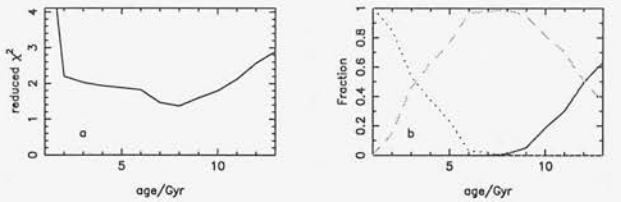

Figure 5. Left-hand side: reduced χ^2 as a function of age for the mixed metallicity model (see Section 5 for details). The best-fitting age is 8 Gyr, just as for the full solar-metallicity models of Jimenez et al. (2000). Right-hand side: fractional contributions to the mixed metallicity model of the different metallicity components as a function of age, i.e. $0.2\,Z_\odot$ (solid line), $Z_\odot$ (dashed line) and $2.5\,Z_\odot$ (dotted line). The large contribution of the super-solar component at lower ages, and the large contribution of the sub-solar component at high ages reflects the well-known age–metallicity degeneracy. However, at the best-fitting age of 8 Gyr, the mean metallicity is $0.99\,Z_\odot$, with the solar metallicity contribution completely dominating the model.

Fig. 5(b) shows the evolution of the fractional contributions to the flux of the different metallicity SEDs. At the best-fitting age of 8 Gyr, the flux is clearly completely dominated by the solar metallicity SED, as it should be. $X_{0.2\,Z_\odot}$ is 0.01, $X_{Z_\odot}$ is 0.99 and there is no contribution from the 2.5-$Z_\odot$ model. This gives a mean metallicity of $0.99\,Z_\odot$. In summary, given data of this (obviously excellent) quality, the mixed-metallicity model can return both the correct metallicity and the correct age to high accuracy (where here the correct age does not mean the turn-off age of the Sun, but rather the age of 8 Gyr which was returned using the full model with the correct metallicity).

6 CONCLUSION

In this paper we have not attempted a model-maker's comparison of different evolutionary synthesis models, deliberately not entering into the debate over which model uses the most trustworthy components, such as isochrones, stellar atmospheres, etc. These issues will be addressed in a future paper (Jimenez et al. in preparation). Instead, we have addressed the simple issue of whether the near-ultraviolet spectral energy distribution of the Sun is reproduced by the main-sequence only components of three independent models at an age commensurate with current estimates of the MS-turn-off age of the Sun. This test was suggested by Yi et al. (2000), but in fact leads us to the conclusion that the evolutionary time-scale of the main sequence in the Yi et al. models is anomalous when compared with the either the models of Worthey (1994), Jimenez et al. (1998) or the current best estimate of the MS turn-off age of the Sun.

We have also re-addressed the issue of the extent to which varying contributions from post-MS phases of stellar evolution can affect the age estimation of galaxies at $z \simeq 1.5$ from rest-frame ultraviolet spectra. We find that (assuming solar metallicity) the minimum age of the dominant stellar population in the $z = 1.55$ radio galaxy 53W091 is 2 Gyr if one invokes the relatively strong AGB/RGB components included in the models of Worthey (1994), and 3 Gyr is one adopts the weaker post-MS contributions included in the models of Jimenez et al. (1998). In the case of the even more passive $z = 1.43$ radio galaxy 53W069, these numbers become 3 and 4 Gyr respectively.

Finally, as stated above, these figures are derived on the assumption of approximately solar metallicity. Yi et al. (2000) and Jimenez et al. (2000) have in fact shown that the age metallicity degeneracy in a realistic mixed-metallicity population is probably not nearly as severe as previously feared. Nevertheless, ideally it is clearly desirable to determine both age and metallicity directly from the observations. Using the spectrum of the Sun, we have shown that, given data of sufficient quality, it should in principle be possible to break the well-known age–metallicity degeneracy using data covering only the near-ultraviolet spectral range which is accessible when observing galaxies at $z > 1$ with optical spectrographs. The possibility of breaking the age–metallicity degeneracy will be explored further in a subsequent paper.

ACKNOWLEDGMENTS

We would especially like to thank Sukyoung Yi for making his models available to us in exchange for the Jimenez models, and also Guy Worthey for the willingness and speed with which he supplied us with specific versions of his model predictions, customized to meet our specific requirements. LAN acknowledges the support of a PPARC studentship, and RJ acknowledges the support of a PPARC Advanced Fellowship.

REFERENCES

Bruzual G., Charlot S., 1993, ApJ, 405, 538
Bruzual G. A., Magris G. C., 1997, in Waller W. H. et al., eds, Proc. AIP Conf. Vol. 408, The Ultraviolet Universe at Low and High Redshift. Am. Inst. Phys., New York, p. 291
Chambers K. C., Charlot S., 1990, ApJ, 348, L1
Charlot S., Worthey G., Bressan A., 1996, ApJ, 457, 626
Dunlop J. S., 1999, in Rottgering H. J. A., Best P., Lehnert M. D., eds, The Most Distant Radio Galaxies. KNAW Colloq. Amsterdam. Kluwer, Dordrecht, p. 71
Dunlop J. S., Guiderdoni B., Rocca-Volmerange B., Peacock J. A., Longair M. S., 1989, MNRAS, 240, 257
Dunlop J., Peacock J., Spinrad H., Dey A., Jimenez R., Stern D., Windhorst R., 1996, Nat, 381, 581
Jimenez R., Padoan P., Matteucci F., Heavens A. F., 1998, MNRAS, 299, 123
Jimenez R., Padoan P., Juvela M., Bowen D. V., Dunlop J. S., Matteucci F., 2000, ApJ, 532, 152
Lilly S. J., 1988, ApJ, 333, 161
Jorgensen U. G., 1991, A&A, 246, 118
Magris G. C., Bruzual G. B., 1993, ApJ, 417, 102
Spinrad H., Dey A., Stern D., Dunlop J. S., Peacock J., Jimenez R., Windhorst R., 1997, ApJ, 484, 581
Worthey G., 1994, ApJS, 95, 107
Yi S., Brown T. M., Heap S., Hubeny I., Landsman W., Lanz T., Sweigart A., 2000, ApJ, 533, 670

This paper has been typeset from a TEX/LATEX file prepared by the author.